Using spontaneous and evoked activity to identify subregional specialisations of corticorecipient areas

Roberto Montanari

Thesis director

Dr. Ramón Reig García

University Miguel Hernández de Elche

- 2022 -

INSTITUTO DE NEUROCIENCIAS

1999 - 2019
AÑOS
INSTITUTO DE NEUROCIENCIAS

EXCELENCIA
SEVERO
OCHOA

Sant Joan d'Alacant, de 2022

To whom it may concern,

This doctoral thesis entitled "Using spontaneous and evoked activity to identify subregional specialisations of corticorecipient areas" have been developed by myself, Roberto Montanari, with the help of La Caixa-Severo Ochoa fellowship (2016/00006/001) and PROMETEO/2019/20, that have founded me during this work.

Sincerely,

Sant Joan d'Alacant, de 2022

Dr. D. Ramón Reig Garcia, Director of the doctoral thesis entitled **"Using spontaneous and evoked activity to identify subregional specialisations of corticorecipient areas"**

CERTIFIES:

That Mr *Roberto Montanari* has carried out under our supervision the work entitled **" Using spontaneous and evoked activity to identify subregional specialisations of corticorecipient areas "** in accordance with the terms and conditions defined in his/her Research Plan and in accordance with the Code of Good Practice of the University Miguel Hernández of Elche, satisfactorily fulfilling the objectives foreseen for its public defence as a doctoral thesis.

I sign for appropriate purposes, at San Joan d'Alacant, 14th of January of 2022

Thesis director

Dr. D. Ramón Reig Garcia

Sant Joan d'Alacant, de 2022

Ms. Elvira de la Peña García, Coordinator of the Neurosciences PhD programme at the Institute of Neurosciences in Alicante, a joint centre of the Miguel Hernández University (UMH) and the Spanish National Research Council (CSIC),

INFORMS:

That Mr Roberto Montanari has carried out under the supervision of our PhD Programme the work entitled "Using spontaneous and evoked activity to identify subregional specialisations of corticorecipient areas" in accordance with the terms and conditions defined in its Research Plan and in accordance with the Code of Good Practice of the University Miguel Hernández de Elche, fulfilling the objectives satisfactorily for its public defence as a doctoral thesis.

Which I sign for the appropriate purposes, in Sant Joan d'Alacant, 14 January 2022

Dr Elvira de la Peña García

Coordinator of the PhD Programme in Neurosciences

E-mail: elvirap@umh.es
www.in.umh.es

Tel: +34 965 919533
Fax: +34 965 919549

Av Ramón y Cajal s/n
SANT JOAN CAMPUS
03550 SANT JOAN D'ALACANT- SPAIN

This Doctoral Thesis, entitled "Using spontaneous and evoked activity to identify subregional specialisations of corticorecipient areas" is presented under the conventional thesis form with the following quality indicator:

Alegre-Cortés, J., Sáez, M., **Montanari, R**., & Reig, R. (2021). Medium spiny neurons activity reveals the discrete segregation of mouse dorsal striatum. *Elife*, *10*, e60580.
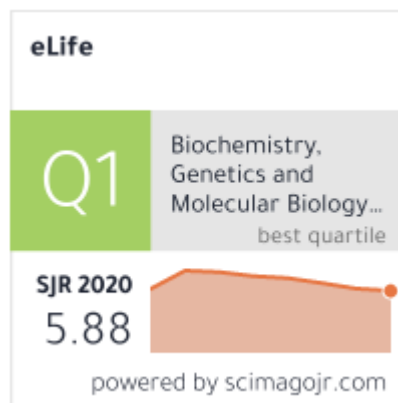
Al Mister De Celis e al Capitano Angioletto

che per primi mi hanno mostrato

come la grinta fosse la mia miglior dote

Index

List of abbreviations

AP, anteroposterior

amBC, anteromedial barrel cortex

BC, barrel cortex

BC_{deaff}, deafferentiated barrel cortex

BL, bilateral lidocaine

ChI, cholinergic interneuron

CC, corpus callosum

DCS, dorsocentral striatum

DLS, dorsolateral striatum

DMS, dorsomedial striatum

DS, dorsal striatum

FrA, frontal association area

GABA, gamma-amminobutirric acid

GPe, globus pallidus pars externa

GPi, globus pallidus pars interna

IW, intact whiskers

L1, cortical layer 1

L2/3, cortical layer 2/3

L4, cortical layer 4

L5, cortical layer 5

L6, cortical layer 6

LFP, local-field potential

LTS, low-threshold spiking

M1, primary motor cortex

ML, mediolateral

MSN, medium-spiny neuron

NPY^+, neuropeptide-Y positive

plBC, posterolateral barrel cortex

PPT, posterior parietal cortex

PV$^+$, parvalbumin positive

RFE, recurrent feature elimination

S1, primary somatosensory cortex

SNc, substantia nigra pars compacta

SNr, substantia nigra pars reticulata

STN, nucleus subthalamicus

SVM, support vector machine

TW, trimmed whiskers

V1, primary visual cortex

VGlut2, Vescicular Glutamate transporter 2

Vm, membrane potential

Abstract/ Resumen

The brain can continuously generate activity, both in a spontaneous manner and in response to sensory events. Such activity, in turn, can propagate across connected areas, establishing an association in their functioning. The study of functional connectivity is one of the main goals of the neurophysiology. This Doctoral Thesis focus on two systems, the corticostriatal and the interhemispheric, and describes local functional subregions individuated by cortical afferents based on the analysis of neural activity.

The first part focuses on the study of synaptic transmission between cortical areas and the dorsal striatum, the corticostriatal system. Behavioural studies divided the rodent dorsal striatum in two functionally different regions, the medial and the lateral. However, much anatomical evidence would suggest that the dorsal striatum is a single structure. To understand the functions of the dorsal striatum, it is essential to clarify first what is the most accurate interpretation between the two. In this work, we demonstrate that the dorsal striatum can be best understood as divided in two functional circuits, the dorsolateral and the dorsomedial one. This separation is based on the different porperties of the neurons involved and how they integrate the spontaneous slow wave. To realise this investigation, we combined the use of whole-cell patch-clamp in medial and lateral dorsal striatal regions and LFP recordings in many cortical areas *in vivo*. We have found that the dorsomedial striatum is more strongly modulated by the primary visual cortex than by the frontal association area, while the opposite relation holds for the dorsolateral striatum. Moreover, the primary motor and somatosensory cortex more tightly modulate the dorsolateral striatum than the dorsomedial one. Thus, thanks to their relationship with specific parts of the neocortex, the dorsolateral and dorsomedial striatum can be considered two separate, non-overlapped circuits. These results favour the homology between the primate putamen and the mouse dorsolateral striatum, and the primate caudate nucleus with the mouse dorsomedial striatum, respectively.

The second part of this Thesis studies the synaptic transmission mediated by the corpus callosum and, more specifically, how different regions of the barrel cortex of both hemispheres exchange information in the mouse. Rodents move the whiskers on both sides of their snout to palpate and explore the surrounding space. Whiskers are organised dorsoventrally in 5 longitudinal rows: from the row A, next to the dorsal facial midline, to the row E, just above the buccal opening. The barrel cortex contains a somatotopic representation of these whiskers. Each barrel column primarily responds to the stimulation of the corresponding contralateral whisker through well characterised brainstem-to-thalamus-to-cortex pathways. In addition, the barrel cortex receives callosal afferent axons from the opposite one. The callosal innervation is distributed heterogeneously: it is sparse in most of the barrel cortex, but very dense in a subregion (posterolateral aspect) bordering with the secondary somatosensory cortex and containing the representation of row A-whiskers. Despite these well-known subregional differences, no study so far has characterised the sensory responses mediated by the corpus callosum in relation to the distinct innervation patterns.

To study the callosal contribution in sparsely (anteromedial) and densely (posterolateral) innervated subregions of the barrel cortex, we used: c-Fos immunoessays, whole-cell

patch-clamp in the anaesthetised mouse coupled with contra- and ipsilateral whiskers stimulation (row A and row E), optogenetics and pharmacological techniques. We have found that the callosal contribution to the barrel cortex activity is stronger in the posterolateral than in the anteromedial subregion. In the former, synaptic recruitment upon homotopic whiskers displacement is so vigorous that a proportion of neurons responds almost identically to contra- and ipsilateral stimulation of the row A. Overlapping contra- and ipsilateral receptive fields are typical of body parts (axial and para-axial) dedicated to the midline of the sensory space, thus also the whiskers conform to this general rule as opposed to what was believed so far. In addition, we demonstrate that ipsilateral whiskers stimulation recruits feed-forward inhibition in the barrel cortex, and that barrel columns of the same identity in the two hemispheres are more tightly coupled than barrels with different identity through the corpus callosum.

––––––––––––––––––––

El cerebro genera actividad continuamente, tanto producida de forma espontánea como en respuesta a estímulos sensoriales. Esta actividad puede propagarse a otras áreas cerebrales, estableciendo una asociación en su funcionamiento. El estudio de dicha conectividad funcional es uno de los principales objetivos de la neurofisiología. Esta Tesis Doctoral se centra en dos sistemas, el corticoestriatal y el interhemisférico, y describe subregiones locales funcionales individualizadas por aferentes corticales en base al análisis de la actividad neuronal.

La primera parte está centrada en el estudio de la transmisión sináptica entre varias áreas de la corteza cerebral y el estriado dorsal, el sistema corticoestriatal. Estudios conductuales han dividido el estriado dorsal de los roedores en dos regiones funcionalmente diferenciadas, lateral y medial. Sin embargo, la mayoría de la evidencia anatómica sugiere que el estriado dorsal está formado por una estructura única. Para comprender las funciones del cuerpo estriado dorsal, es fundamental aclarar cuál es la interpretación más precisa. En este trabajo, demostramos que el estriado dorsal puede entenderse mejor dividido en dos circuitos funcionales, el dorsolateral y el dorsomedial. Dicha separación se basa en las diferentes propiedades de las neuronas que los forman y en cómo integran la actividad espontanea de onda lenta. Para realizar esta investigación, combinamos el uso de registros de *whole-cell patch-clamp* en las regiones lateral y medial del estriado dorsal y LFP en varias áreas corticales *in vivo*. Hemos encontrado que el cuerpo estriado dorsomedial está más fuertemente modulado por la corteza visual primaria que por el área de asociación frontal, mientras que la relación opuesta se mantiene para el cuerpo estriado dorsolateral. Además, la corteza motora primaria y la somatosensorial modulan más estrechamente el cuerpo estriado dorsolateral que el dorsomedial. Así, gracias a su relación con partes específicas de la neocorteza, el estriado dorsolateral y dorsomedial pueden considerarse dos circuitos separados, no superpuestos. Nuestros resultados favorecen la homología entre el putamen y caudado de primates con el estriado dorsolateral y dorsomedial del ratón respectivamente.

La segunda parte de esta tesis estudia la transmisión sináptica mediada por el cuerpo calloso y más concretamente, cómo diferentes regiones de la corteza de barriles de ambos hemisferios cerebrales intercambian información en el ratón. Los roedores mueven los bigotes de ambos lados de su hocico para palpar y explorar el espacio circundante. Los

bigotes se organizan dorsoventralmente en 5 filas longitudinales: desde la fila A, junto a la línea media dorsal facial, hasta la fila E, justo encima de la abertura bucal. La corteza de barriles contiene una representación somatotópica de estos bigotes. Cada columna de barriles responde principalmente a la estimulación del bigote contralateral correspondiente a través de vías bien caracterizadas del tronco del encéfalo al tálamo y, finalmente, a la corteza. Además, la corteza de barriles recibe axones aferentes callosos de la contralateral. La inervación callosa se distribuye de forma heterogénea: es escasa en la mayor parte de la corteza de barriles, pero muy densa en una subregión (coordenada posterolateral) que es adyacente a la corteza somatosensorial secundaria y que contiene la representación de la fila A de los bigotes. A pesar de estas diferencias conocidas entre subregiones, hasta ahora ningún estudio ha caracterizado las respuestas sensoriales mediadas por el cuerpo calloso en relación con los distintos patrones de inervación. Para estudiar la contribución callosa en subregiones de la corteza de barriles con inervación escasa (anteromedial) y densa (posterolateral), utilizamos: inmunoensayos de c-Fos, whole-cell patch-clamp en el ratón anestesiado junto con estimulación de bigotes contra- e ipsilaterales (fila A y fila E), optogenética y técnicas farmacológicas. Hemos encontrado que la contribución callosa a la actividad de la corteza de barriles es mayor en la subregión posterolateral que en la anteromedial. En la primera, el reclutamiento sináptico tras el desplazamiento de los bigotes homotopicos es tan vigoroso que una gran proporción de neuronas responde de manera casi idéntica a la estimulación contra- e ipsilateral de la fila A. Los campos receptivos contralaterales e ipsolaterales superpuestos son típicos de las partes del cuerpo (axiales y para-axiales) dedicadas a la línea media del espacio sensorial, por lo que también los bigotes se ajustan a esta regla general en oposición a lo que se creía hasta ahora. Además, demostramos que la estimulación ipsilateral de los bigotes recluta la inhibición de tipo *feed-forward* en la corteza de barriles, y que las columnas de barriles de la misma identidad en los dos hemisferios están más estrechamente acopladas que los barriles con identidad diferente a través del cuerpo calloso.

1. Introduction

1.1 An anatomical and functional overview of the basal ganglia

The basal ganglia are a group of subcortical nuclei involved in many aspects of movement production and cognitive and emotional processes in the vertebrate brain (Kandel et al., 2003). They are formed by telencephalic and mesencephalic structures anatomically and functionally interconnected: the striatum (dorsal and ventral), the substantia nigra (pars compacta and reticulata), the nucleus subthalamicus, and the globus pallidus (pars interna and externa). The striatum is composed by three important subdivisions in the primate: the caudate nucleus, the putamen and the ventral striatum (or nucleus accumbens). The caudate nucleus and the putamen are separated by the internal capsule, a portion of white matter interposed between neocortex and thalamus. The striatum receives input from neocortex, thalamus and brainstem. Globus pallidus and substantia nigra receive afferents from the striatum The globus pallidus is disposed medial to the putamen and lateral to the internal capsule. Its internal segment (GPi) is the source of the basal ganglia output and is similar to the substantia nigra pars reticulata (SNr) in that both are formed by GABAergic neurons. The substantia nigra pars compacta (SNc) instead contains dopaminergic neurons. The SN is disposed ventral to nucleus subthalamicus (STN), the only basal ganglia nucleus containing glutamatergic neurons.

The striatum receives glutamatergic input from the L5 of the neocortex and from the intralaminar nuclei of the thalamus (Doig et al., 2010), mesencephalic dopaminergic inputs (SNc and ventral tegmental area), and serotoninergic ones from the raphe nuclei of the brainstem (Kandel et al., 2003). The basal ganglia can exert an effect on the neocortex by contacting back the thalamus, and on the spinal cord by modulating the activity of the pedunculopontine nucleus. The most represented neurotransmitter in the brain is the GABA (Hynd and Bloom, 2005), and the basal ganglia certainly contribute to it. In fact, 90-95% of striatal neurons are GABAergic projection neurons of medium body size, with dendrites rich in spines, thus called medium-spiny neurons (MSNs). These are one of the principal targets of glutamatergic cortical afferents and the only source of efferent projections. Moreover, their spiking activity shows low frequency and can be triggered at the onset/offset of, and during, body movements. For this, in the classical view (Steiner and Tseng, 2016), basal ganglia are thought to control the selection and initiation of motor actions through two parallel circuits: the direct and the indirect. SNr and GPi tonically inhibit their thalamic and brainstem targets. Thus, when an excitatory signal activates the MSN of the direct pathway (dMSN), they release GABA onto GPi inhibitory neurons, which will stop to exert their tonic inhibition onto the thalamus and the pedunculopontine nucleus, releasing body movements. On the contrary, the activation of the indirect pathway through the engagement of iMSNs, will inhibit through GABA release the external GP (GPe), that will release its inhibition on the STN, which in turn will excite the GPi suppressing thalamic and pedunculopontine nucleus activity, blocking body movements.

18

Thus, iMSNs and dMSNs participate in two parallel and antagonist circuits and form distinct molecular classes of neurons (Steiner and Tseng, 2016). iMSNs express enkephalin and neurotensin, with the D2 dopamine receptor. dMSNs express substance-P and dynorphin, with the D1 dopamine receptor. Thanks to this, the two striatal classes are differently influenced by the release of dopamine from the SNc. D1 receptors are thought to facilitate synaptic transmission when activated by the neurotransmitter, while D2 receptors reduce it. In this manner, a release of dopamine in the striatum will result in the facilitation of movements thought to be initiated by motor and premotor cortices. Another basal ganglia pathway that can be more directly regulated by cortical afferents is the hyperdirect pathway. Here, cortical glutamatergic excitation is delivered onto the STN, promoting its excitation of the GPi and thus the inhibition of improper actions (Chen et al., 2020).

1.2 The dorsal striatum of the rodents

So far, we mentioned that 95% of the striatum is composed of iMSNs and dMSNs. The remaining cell classes are local interneurons: Parvalbumin$^+$ fast-spiking interneurons (PV$^+$), cholinergic interneurons (ChIs), low-threshold spiking interneurons (LTS), neuropopeptide-Y$^+$ interneurons (NPY$^+$), and others less characterised (Silberberg and Bolam, 2015). PV$^+$ are the 0.7% of the striatum, they receive direct excitation from the cortex and perform feed-forward inhibition onto MSNs with perisomatic synapses by releasing GABA (Tepper et al., 2008). Their presence concentrates in the dorsolateral striatum (DLS) (Gerfen et al., 1985). ChIs have a large body size (around 40μm) and aspiny dendrites and form the 1-2% of the striatum (Kawaguchi, 1993). Thanks to Na$^+$ and hyperpolarisation-activated cation channels they tonically fire *in vivo* with a frequency of 2-10Hz. They receive direct excitation from the thalamus (less from the cortex) and perform disynaptic inhibition onto MSNs through a not-yet characterised circuit motif (Silberberg and Bolam, 2015). Moreover, they are more active in the dorsomedial striatum (DMS) (Abudukeyoumu et al., 2019). LTS neurons are easily driven to fire by cortical monosynaptic contact, thus performing feed-forward inhibition onto MSNs contacting their distal dendrites. They express somatostatin, neuropeptide Y and nitric oxide synthase, yet no gradient in their distribution has been reported. NPY$^+$ interneurons instead are more concentrated in the ventral (i.e., nucleus accumbens) than in the dorsal striatum. They receive cholinergic, dopaminergic and cortical glutamatergic inputs. Since the IPSCs that they can exert on MSNs' distal dendrites are generally weak, a modulatory role has been attributed to them.

To the local circuits formed by the interneurons and their innervation of the MSNs, long-range afferents add. For example, thalamostriatal afferents depart from the median/parafascicular nuclei complex to target the dendritic shaft of MSNs in the striatum (Shepherd, 2013). However, the most prominent innervation is the one conveyed by the neocortex. Both pyramidal tract (PT) and intratelenchephalic (IT) cortical neurons can monosynaptically contact MSNs (Cowan and Wilson, 1994). Normally, IT neurons soma occupies the superficial half of the cortical L5, but some of them are found in L2/3 as well. Their axons are directed towards other cortical targets, but they branch into the

striatum. PT neurons occupy the deep L5 and direct their axons towards the thalamus, the STN and the brainstem, leaving collaterals in the striatum.
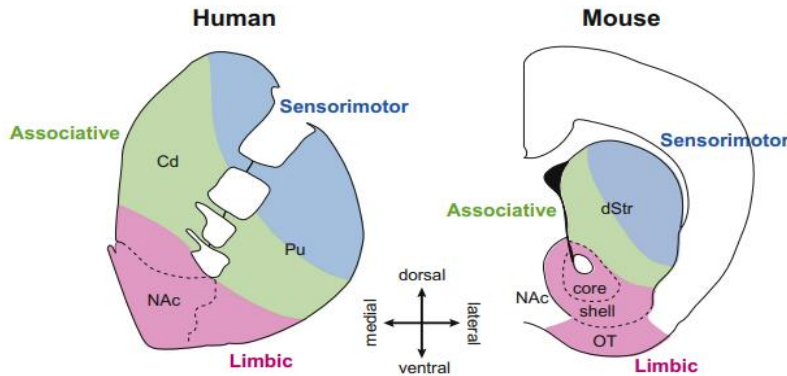
Fig I1 Functional subdivisions of the striatum in human (left) and mouse (right). Adapted from Chuhma et al., 2017.

The cortical input received by the MSNs has its origin in many different cortical areas, from primary sensory cortices to higher order association areas (Shepherd, 2013). In these projections the cortical topography is only loosely maintained (Hinitiryan et al., 2016). Moreover, different cortical areas target the striatum with a certain degree of specificity (Fig I1). The DLS receive afferents from frontal and parietal areas related with body representations (somatosensory cortex) and movements (premotor and motor cortices), thus it has been related to motor learning, planning and execution. The DMS receive afferents from the associative frontal cortices and occipital cortex (Hunnicutt et al., 2016), thus it has been related to higher cognitive behaviours such as reward prediction, but also to vision. Finally, the ventral part of the striatum receives afferents from to limbic cortices and amygdala, thus it has been related to the processing of emotions and gratification (Everitt et al., 1999).

Nevertheless, as apparent in Figure I1 (Chuhma et al., 2017), the rodent striatum does not form separated cytoarchitectonic nuclei as the case of caudate nucleus and putamen in primates, partially segregated by the internal capsule. In the current view, the putamen is homologous of the DLS while the caudate nucleus of the DMS. This is because DMS is thought to regulate actions directed towards a goal and the flexibility of strategy shifts, while the DLS is thought to regulate stimulus-response association and a navigation system (Gremel and Costa, 2013). This position is taken by a crescent number of behavioural studies (Graybiel, 2008; Bellaine et al., 2010). However, axonal connections from multiple cortical areas overlap extensively in the striatum (Kincaid et al., 1998; Hoffer et al., 2001; Hoover et al., 2003; Hooks et al., 2018), and some behaviour attributed to one dorsal subregion is also found in the other (e.g., action selection) (Klaus et al., 2017). These observations lead to the problem: are the primate putamen/rodent DLS and primate caudate/rodent DMS correct homologies?

The first part of this work is dedicated to respond to this question (see **2**) through the study of corticostriatal connectivity via slow wave activity propagation in subregions of the dorsal striatum.

1.3 The slow wave oscillatory activity

A concise review of what we currently know about the spontaneous slow wave oscillation is provided by Sanchez-Vives (2020). Slow oscillation of the electrical activity is a bistable dynamic brain state in which large neuronal populations become synchronously active (up state) and then silent (down state), this cycle repeating with a frequency of ~1Hz. Such oscillations characterise the membrane potential of cortical neurons, which hyperpolarises in the down state when all the synaptic input ceases, and depolarises in up state through barrages of excitatory and inhibitory synaptic inputs. If a piece of neocortex is physically disconnected, its activity falls in this slow oscillatory regime. Also, cortical slabs can oscillate spontaneously with this rhythm in vitro (Sanchez-Vives and McCormick, 2000). These characteristics suggest that the slow oscillation is the default activity pattern of the neocortex and that it has a cortical origin from which it spreads to almost the entire brain (Sanchez-Vives et al., 2017). This brain state is typical of slow-wave sleep and deep anaesthesia. In these circumstances, even if the oscillation can start in random points of the cortical mantle, it tends to originate in the prefrontal cortex and then to propagate (Massimini et al., 2004). In this sense, it behaves as a wave, whose front is led by infragranular neurons, especially the ones located in L5 (Sanchez-Vives and McCormick, 2000). The propagation is continuous along the cerebral cortex, and it shows varying velocities dependent on the species analysed. For example, the velocity of propagation has been estimated (via EEG, slow-wave sleep) in humans as fast as 1.2-7 m/s, while it is much reduced in the mouse (under anaesthesia), whose estimate is 30 mm/s.

When we talk about propagation of the slow wave oscillation, we refer to the initiation of an up state along a trajectory in the brain. Spontaneous up state initiation is often localised in L5 neurons (Sanchez-Vives and McCormick, 2000). As a confirmation of this phenomenon, optogenetic stimulation of L5 neurons, but not L2/3, can lead to up state initiation (Beltramo et al., 2013). Probably, when spontaneous, the up state initiation is due to large intrinsic excitability of L5 neurons that leads them to fire during down state (Sanchez-Vives, 2020). Both NMDA and non-NMDA channel receptors participate in the initial phase of an up state. During this state, both inhibitory and excitatory neurons fire action potentials, balancing their relative weights onto postsynaptic neurons. Nested within the up state, there are faster oscillations of the membrane potential, for example the beta (15-30 Hz) and the gamma (30-90 Hz). The reverberatory activity at synapses that gives origin and sculpts the up states is terminated by the transition into the down state. The up-to-down state transition may occur through different mechanisms (e.g. synaptic depression, dysfacilitation, fast inhibition, K^+ currents, extracellular K^+ dynamics and the likes) which lead the neuron to fall in a hyperpolarized state until the next synaptic barrage arrives (Sanchez-Vives, 2020).

The slow wave can propagate along a cortical column (i.e., from deep to superficial layers) but also subcortically (i.e., from the neocortex to connected areas). This is the case of the corticostriatal slow wave propagation (Wilson and Kawaguchi, 1996). MSNs possess the Kir2 K^+ channel, which tends to hyperpolarise the neuron near the reversal potential of the K^+. However, when the cortical glutamatergic input is so abundant to

overload the action of this species of channel, MSNs are led to the generation of an up state. In this case, AMPA and Kainate receptors permeable to Ca^{2+} initiate the state transition, which is later dominated by NMDA currents during the up state (Carter and Sabatini, 2004).

Conversely to the first part of the work, which is centred in the propagation of this kind of activity and less on the evoked one, the second will analyse in detail the evoked activity and will use the spontaneous as a confirmatory instance. Below, it follows an introduction to the barrel cortex and its callosal system to provide enough instruments for the interpretation of the results presented later.

1.4 An introductory note to the corpus callosum and the barrel cortex

Vertebrates have a bilateral nervous system. Therefore, drawing an imaginary longitudinal line splits the neural axis in two mirror halves. The two halves are not isolated from each other. Axons can depart from neurons on one side of the neural axis to reach neurons on the opposite side. In a decussation, axons terminate on the opposite side in a level of the axis *distinct* from the one of origin. In a commissure, axons terminate on the opposite side in a level of the axis *equivalent* to the one of origin. By means of these connectional motifs the two, otherwise separate, nervous systems promote unitary organismic functions.

The corpus callosum is a commissure. There are other commissures in the brain of placental mammals but the corpus callosum is the widest. Indeed, its dimensions are at odds with the effects one can provoke to behaviour by severing it: none. Or at least, this was the predominant view until the mid-fifties. Until that time, in fact, no one knew that one hemisphere can build up a memory of what it has experienced in the second hemisphere through the corpus callosum (Myers, 1955; Myers and Sperry, 1958). This copy is a bit deteriorated, thus it has been named "a weak carbon copy" (Sperry, 1961). Yet, even if weak, its presence has promoted a multitude of neuroscientific research. Investigators asked, for example, what is the process that generates the copy. Discovering how the two hemispheres are able to inter-communicate experiences, or how a brain talks to another brain, was seen as the key to understanding the neural code.

Even if, so far, the neural code has remained elusive, the efforts made generated much more details about interhemispheric communication. Indeed, the study of the electrophysiology of neurons and their circuits has provided us with tons of concepts on brain functioning. In this respect, one of the most studied parts of the brain is the neocortex. The neocortex is thought to be organised in functional columns spanning the dorsoventral layered aspect of the neocortical mantles. Such an organisation is anatomically visible in the layer 4 of the barrel cortex of the mouse. Each functional column, or barrel column [~6500 neurons, contained in approx. 200 μm x 300 μm x 1200 μm; (Petersen, 2019)], represents a single whisker on the animal snout. This system has been largely investigated for its relation to cortical and subcortical centres in the *home*

hemisphere. But the fact that it receives callosal innervation from the *opposite* hemisphere has been known since long (Wise and Jones, 1976). Yet, the effects of callosal innervation to the function of the contralateral barrel columns has received far less attention. Therefore, in this part of the thesis, we explored the contribution of the callosal innervation to the mouse barrel cortex by recording electrical responses emitted by the neurons when whiskers are displaced. This work is different from previous ones because we studied such responses in their subthreshold components rather than suprathreshold, and because it compares the response profiles evoked in subregions of the barrel cortex known to be differently innervated by the corpus callosum, an aspect neglected insofar.

In this part of the Introduction, we will describe what is the corpus callosum, its phylogenesis in mammals and development in the mouse. Next, we will have a brief look at the theories promoted by neuropsychology to explain its function, ending up with a description of the midline fusion theory, a theory inspired by electrophysiological and anatomical animal research. Then, we will introduce the barrel cortex with a particular focus on its anatomy and flow of activity. Finally, we will briefly review the literature about the corpus callosum in the barrel cortex to introduce the Objectives of this and the corticostriatal study.

1.5 Anatomical composition of the corpus callosum

The corpus callosum (CC) is a set of axons originating in projection neurons whose soma reside within the right or left neocortex. The human CC can be divided into different zones along the anteroposterior axis of the brain (van der Knaap and van der Ham, 2011). The most anterior portion, or rostrum, interconnects the frontal lobes. Posterior to it, the genu interconnects the prefrontal cortices. It follows the truncus that interconnects pre-central cortices such as pre- and supplementary-motor, insular and cingulate areas. More posteriorly, the CC becomes thinner and for this is called isthmus. The isthmus interconnects pre- and post-central gyri plus the auditory cortex. Since the primary somatosensory cortex (S1) is contained in the post-central gyrus, in this thesis we have studied the electrophysiology of the homologue of the human isthmus in the mouse. The isthmus is followed by the most caudal part of the CC, the splenium, which interconnects posterior parietal, medial temporal, and occipital areas. The excellent book chapter of Innocenti (1986) collects fundamental information about the CC in different non-human species, providing a comparative approach which is able to identify common principles of organisation. For example, neurons' somas participating in this structure have most commonly a pyramidal morphology, albeit inverted pyramids have been found in layer (L) 6 and, limited to cat V1, spiny-stellate cells in L4. Across cortical areas and species, they always reside in L3. As the L4 of cat V1, species-specific traits add to this general rule. The second largest fraction of callosal neurons reside in the infragranular layers of the cat and rodents, but in the monkey it is found only in somatosensory and motor cortices, thus in the homologous of the human isthmus. Callosal neurons can be contacted by thalamic afferents through asymmetric synapses in the spines of basal dendrites and axon initial segment. They can be also contacted by interneurons through symmetric

synapses in the soma, basal dendrites and axon initial segment. The axon emitted by callosal neurons varies in size, myelination and conduction velocity within an individual and across different species. For example, estimates of the fraction of myelinated axons reported in Innocenti (1986) runs from 43 to 69%, considering rat, cat, rabbit, monkey and man. However, Sturrock (1980) found only 28% of myelinated axons in the mouse. Furthermore, more recent data on S1 found myelination to increase with cortical depth, and different neurons can exhibit different myelination gradients and patterns along the axon, so that the opposition between myelinated *vs* unmyelinated may be too simplistic (Fig I1, right; Tomassy et al., 2014). In the same species of above, axonal diameter varies widely and, together with it, the conduction velocities. Diameters may be as thin as 0.08 μm or as thick as 5 μm, but on average they do not exceed 1 μm. In the cat, conduction velocity of somatosensory callosal axons can vary by an order of magnitude, ranging from 1 m/s to 10 m/s. In the parietal area 5 of the cat, antidromic action potentials can be evoked in callosal neurons with a latency varying between 1.3 and 20 ms (Cissé et al., 2004). All this variation in characteristics across species, across cortical areas and within a given individual, makes it clear that we are in front of a highly variable neural structure. In the case of the individual, probably this huge diversity can be attributed to the early experiences, which are able to sculpt the CC. Indeed, the CC is a remarkably plastic structure (for example, see Suarez et al., 2014a) that undergoes a dramatic developmental pruning. If orchestrated by a changing environment, such a pruning may lead ultimately to a corresponding phenotypic variety. Indeed, the CC completes its development in postnatal days of the animal when the individual is already in contact with the exterior world (see **1.7**). Moreover, the CC is not essential to living functions (Sperry 1961), a characteristic that may allow this kind of neural/natural selection to explore different phenotypic landscapes.
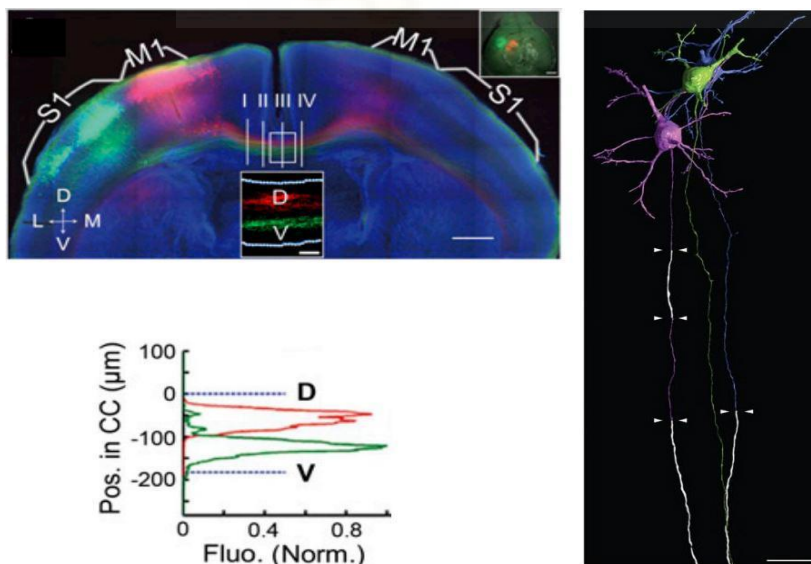
Figure I2 Anatomical disposition of callosal fibres and patterns of myelination. Left top: Arrangement of callosal axons departed from M1 (tdTomato, red) and S1 (GFP, green) and after having crossed the midline in the mouse. Note the orderly DV fashion. Scale bar 500 μm. Modified from Zhuo et al., 2013. Left bottom: Quantification of fluorescence inside the CC. TdTomato[+] axons from M1 lay dorsally to GFP[+] axons from S1. Modified from Zhuo et al., 2013. Right: 3D rendering of 3 neighbouring projection neurons traced in mouse S1 which show different patterns of myelination along the axon (white segments). Note the central axon completely lacks myelination at this level. Scale bar 20 μm. Modified from Tomassy et al., 2014.

Whether or not the arrangement of callosal fibres follows a topography seems controversial. Innocenti (1986) reported for monkey and cat that, while the anteroposterior aspect of the CC follows the topography of the cortex, the dorsoventral aspect does not, probably for the presence of heterotopic tracts mixed to the homotopic ones. However, Zhuo and associates (2013) clearly showed that the mediolateral topography of callosal neurons within the cortex constrains the dorsoventral position of their axon in the CC, at least in the mouse (Fig 1I, left). In turn, such topography within the CC determines the terminal location of the axon in the contralateral hemisphere. Thus, homotopy is maintained because more medial areas enter the CC more dorsally and terminate more medially in the contralateral hemisphere. On the contrary, more lateral areas enter the CC more ventrally and terminate more laterally in the contralateral hemisphere. This also constitutes evidence that most of the connections running through the CC are homotopic, thus they interconnect mirror-symmetric cortical areas in the two hemispheres (Innocenti, 1986). Yet, there exists a minority of heterotopic ones (for example, Fenlon et al., 2017).

The laminar distribution of callosal terminals also vary across species and cortical domains. In this thesis, we will focus only on the callosal innervation of the barrel cortex (see **1.7**). In addition, it is important to note that the great majority of callosal neurons in the neocortex is pyramidal, glutamatergic (with some evidence for the release of zinc) and form asymmetrical synapses on spines of basal and apical dendrites of contralateral neurons (Conti and Manzoni, 1994), with just a few cases of direct synapse on cell bodies (Innocenti, 1986). Lastly, their postsynaptic effect is mainly mediated by NMDA receptors, with a late non-NMDA component (Kawaguchi 1992).

1.6 Phylogenesis of the corpus callosum

The CC is only present in eutherian (placental) mammals where it interconnects the isocortex of the two hemispheres (see above). Probably it derives from the fasciculation during development of the dorsal part of the hippocampal commissure that separated, in the course of evolution, to form an independent commissure (Suarez et al., 2014b). Fossils indicate that early placental mammals, probably insectivores, relied much on olfaction, with subpallial and olfactory-recipient regions in communication through a conspicuous anterior commissure. Big olfactory structures, such as the olfactory nucleus and piriform cortex, corresponded in these animals to a relatively small isocortex. The insightful review of Suárez and associates (2014b) describes the evolution of the system of commissures of the vertebrate brain. It reports that a small isocortex/piriform cortex ratio is present today in hedgehogs and bats, accompanied by a very small CC, possibly reflecting the conditions of an early eutherian. Instead, a big isocortex/piriform cortex ratio, present in rodents and monkeys for example, is accompanied by a large CC. Consequently, this suggests that the isocortical expansion increased the size of the CC. Note that the CC originated in placental mammals, the eutherian order. Hence, it is no coincidence if this event co-occurred in the same order with the differentiation of a primary motor cortex from a pre-eutherian somatosensory territory (or 'sensorimotor amalgam') around 100 million years ago (Kaas, 2004). Today M1 is densely connected

through the CC, thus it may testify to the joint isocortical-callosal expansion. Finally, it is thought that mammalian species lacking a CC (marsupials and egg-laying monotremes) rely more on the anterior and hippocampal commissure to coordinate bilaterally the pallial activity.

1.7 Development of the corpus callosum in the somatosensory cortex with a focus on the barrel cortex

It is important to note that the callosal circuit we are characterising through electrophysiology is increasingly becoming a model circuit to study the development of the corpus callosum (Wang et al., 2007; Suárez et al., 2014; Fenlon et al., 2019; Zhuo et al., 2021). Thus, our data may supplement such literature in the effort to understand this structure under different perspectives.

First studies on callosal innervation of rodents S1 described a scant innervation pattern in the region of the long whiskers containing a recognisable granular layer (Wise and Jones 1976). In such a pattern, axons avoided the, but interdigitated with, L4 barrels. Subsequently, though, by means of tangential sections in flatten cortical preparations, a dense innervation has been observed to concentrate in septal areas and in the most lateral aspect of the barrel cortex (BC) (Olavarria et al., 1984; Koralek et al.,1990; Sehara et al., 2010).

Since this question remained unasked in recent developmental studies, here we ask: What is represented in the S1/S2 callosum-recipient border? The callosally-innervated area includes the representation of row A-whiskers and extends more laterally to invade S2 (Fig I2). The innervation extends also more anteromedially, invading the barrel representation of little whiskers in the upper and lower jaw (Hayama and Ogawa, 1997). According to Nussbaumer and Van der Loos (1985), the representation of the common fur between the whiskers overlaps with the one of the whiskers for more rostral, shorter whiskers. However, it does not overlap with more caudal, longer whiskers. In fact, the fur is represented medially and laterally to the BC in this case. Thus, it is likely that within the distance between the representation of row A/jaw whiskers and S2 there is a stripe densely innervated by the CC representing the fur present between the two sets of row A-whiskers, the area of fur precisely falling on top of the facial midline.

By *in utero* electroporation at embryonic day 15.5 of L2/3 progenitors with an EGFP-expressing plasmid the callosal innervation of S1 has been observed at different postnatal days (PD) (Wang et al., 2007; Zhuo et al., 2021). At PD2, L2/3 callosal axons appear in the white matter underneath the electroporated side. At PD3, they cross the midline. They reach the contralateral white matter by PD5. From PD6 to PD11, axons invade the contralateral S1 and arborise mainly in L1, L2/3 and L5. At PD12, these axons undergo a dramatic pruning in most of S1, limiting the innervation pattern to a narrow stripe at the S1/S2 border (Fig I2). The latter is the condition observable also in the adult. Such a wide pruning of the axons has been quantified in developing cats to be around 70% of the original quantity, with negligible cellular death (Innocenti, 1986). This means that some cortical neuron sends a transitory axon that will be later eliminated, likely through

macrophage phagocytosis. The pruning is preceded by a simultaneous fibres myelination and synaptogenesis (Innocenti, 1986). These are fundamental properties for neuronal communication and are established at PD12, when the animal's interactions with the exterior world become more complex. For example, at PD12 hearing onset occurs (Sonntag et al., 2009), and pups produce hormones and their receptors, acquiring the ability to respond to novelty-induced stress (Shmidt et al., 2003). Furthermore, in early postnatal days, if stress is induced by pups' manipulation, a bigger CC is developed in the adult (Denenberg et al., 1991). Thus, it seems clear that early experiences in a more 'stimulating' world can contribute to selecting the enormous diversity in characteristics of callosal neurons. If this is the case then, we should expect even a wider diversity in humans, where CC myelination occurs slowly during the lifespan to terminate only in puberty (Bloom and Hynd, 2005). A big phenotypic variation is expressed also between individuals belonging to a species. Indeed, in rats and monkeys CC size does not correlate with fibres number (Bloom and Hynd, 2005). This means that, for example, an equivalent callosal size can be obtained in an individual of the same species by a higher number of smaller diameter axons or by a smaller number of larger diameter axons.
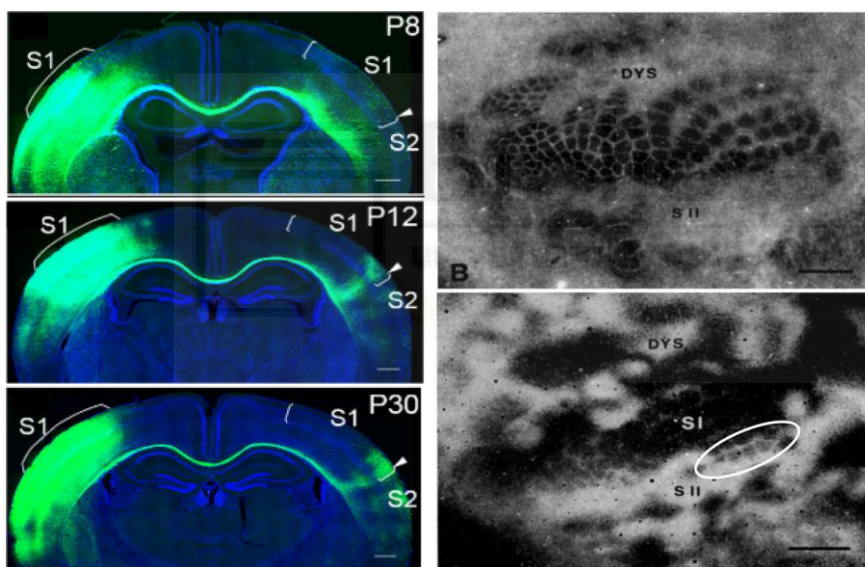
Figure I3 Developmental and adult pattern of callosal innervation of S1 and barrel cortex. Left column: Developmental course of CC formation in mouse S1 at PD8, PD12 and PD30 (from top to bottom). Note the dramatic axonal pruning occurred at PD12 (center) compared to PD8 (top). Modified from Zhuo et al., 2021. Right column: Flatten preparation of adult rat S1 cortex. Top: cytochrome oxidase reaction staining barrel hollows. Bottom: same cortex of Top under dark field illumination showing degenerating tissue (white zones) upon contralateral horseradish peroxidase injection. The white ellipse is drawn by us around row A-whiskers, the only one receiving callosal innervation (degenerated tissue). Modified from Koralek et al., 1990.

In addition, there are many evidence indicating that the correct development of the rodent callosal axon requires intact somatic activity (Koralek and Killackey 1990; Wang et al., 2007). However, the activity must show another characteristic to promote a correct development of the CC. Suárez and associates (2014a) demonstrated that a crucial factor is the presence of a *balanced* activity amid the two hemispheres during development. Indeed, cauterising whiskers in early postnatal days on one side of the snout resulted in

the lack of contralateral BC formation and of the callosal innervation at the S1/S2 border. However, the bilateral cauterisation partially recovered the phenotype: the S1/S2 border innervation pattern, even if thinned, could be observed again. This led the authors to conclude that the thalamocortical feeding of S1 is important, but one critical aspect for the formation of this structure is a balanced interhemispheric activity.

To sum up, the callosal innervation of the mouse BC is refined at PD12 and constituted by scant innervation mostly contained in septal columns but with dense innervation of row A-whiskers representation. In the coronal view, callosal axons terminate mostly in L1, L2/3 and L5a with a minor involvement of L5b and L6.

1.8 Functions of the corpus callosum and the midline fusion theory

To sketch an overview of the CC functions we need to leave the BC for a moment and dig deeper into the neuropsychological literature. Indeed, most of the theories that have been proposed for the function of the CC come from this field, sometimes inspired by neurological patients and psychophysical experiments. Here, we will report only some salient aspects of this approach. On the other hand, non-human research has been instrumental in discovering more basic operations of the CC. These are integrated in the midline fusion theory (Manzoni et al., 1989) and its refinement (Iwamura, 2000).

In the 'Introductory note', we have already attributed some function to the CC. We reported that the first impulse to the functional exploration of this structure can be traced back to the fifties and sixties. At that time, Myers and Sperry found interocular transfer in split-chiasm cats (Myers, 1955; Myers and Sperry 1958). Callosal resection prevented interocular transfer, thus they concluded that the CC was instrumental in laying down a copy of the information contained in the trained hemisphere into the untrained one (for more details see **5.10**). Subsequent research in split-brain patients provided additional, very interesting data. In the majority of right-handed humans, the cortical areas for language processing and production (Wernicke's and Broca's areas, respectively) are lateralised because they are contained in the left hemisphere. Thus, if split-brain patients are asked to verbally recognise an object presented only to the right hemisphere (via the right temporal hemiretina), they are not able to do so. Yet, when presented to the left hemisphere, recognition is not compromised. Moreover, if patients are asked to recognise the object presented to the right hemisphere by indicating or grabbing it among a pool of objects, also in this case recognition is accurate (Gazzaniga, 2000). This indicates that, contrary to the left, the right hemisphere is largely non-verbal but can perform recognition by other means. This and other discoveries motivated studies on hemispheric functional and anatomical asymmetries. Those studies promoted two mutually exclusive models of callosal functioning: excitatory *vs* inhibitory (Bloom and Hynd, 2005). It is important to note that excitation and inhibition here is not referred to as a neural mechanism of interaction, but as a functional one. In this optic, they are defined as when processing that involves a certain region in one hemisphere tends to activate (excitatory) or suppress (inhibitory) processing in a similar region of the opposite hemisphere (Bloom and Hynd, 2005). Excitatory and inhibitory models make opposite predictions on callosal size to

explain functional asymmetries. In the excitatory view, the two hemispheres integrate their activity working in a bilateral coordinated fashion, so that the activation of one is replicated into the other. Thus, hemispheric specialisation (i.e., asymmetry of function) is explained by a decreased contribution of the CC that, consequently, is predicted to be smaller. Instead, in the inhibitory view, one hemisphere inhibits homotopic spots in the opposite hemisphere. Thus, hemispheric dominance for a given function is obtained through a stronger inhibition delivered by the anatomically bigger area to the homotopic smaller contralateral one. Therefore, the stronger the lateralisation of function the bigger the CC. Such can be the case for language areas for which a more detailed inhibitory model has been proposed (Cook, 1984).

There are many experimental proofs for both theories produced in the nineties. However, as noted by Bloom and Hynd (2005), this literature is limited by the fact that callosal size does not correlate with the number of fibres (see **1.7**). Thus, if the strength of the callosal action depends on this number, magnetic resonance research correlating CC size to psychophysical performance may be seriously compromised. To date, even if more experimental data would favour the excitatory one, none of the models has defeated the other and possibly both can apply in different CC regions or tasks (Bloom and Hynd 2005).

Son of the excitatory view of the CC is the midline fusion theory (Manzoni et al., 1989). It is excitatory because it predicts that the activity of one hemisphere is duplicated in the contralateral one (and not suppressed in it). Cook (1984) reports that the excitatory view has been originally conceptualised by Sperry in 1962 (i.e., supplemental complementarity principle) and later refined by his disciple, Berlucchi, in the eighties. The midline fusion theory has been originally proposed to explain neural data in the visual system. Berlucchi and Rizzolatti (1968) found that "A recorded neuron in the right visual cortex of a split-chiasm cat can be activated by both eyes by a visual stimulus crossing the vertical meridian of the visual field. [...]". Recordings were obtained from the border between area 17 (V1) and 18 (V2), where callosal innervation is denser and a magnified representation of the fovea is present. Since the response of these neurons do not depend on which one of the right and left eye is stimulated, they are said to be endowed with a side-invariant representation of the visual field. Thanks to this, the visual scene can be experienced without interruption from one side to the other. Investigations in the somatosensory system followed. Across many placental mammals (tree shrews, rats, mice, squirrels, rabbits etc.), researchers found common characteristics of the somatosensory callosal organisation and similarities with the visual system appeared (Manzoni et al., 1989). In these animals, axial (i.e., midline) and para-axial (i.e., proximal to the midline) surfaces of the body are callosally connected in S1. Denser callosal innervation can be found in the representation of nose, central part of upper and lower lips, chin, intraoral surfaces, and dorsal and ventral midline of the trunk. Also, in the case of the trunk for example, homotopic callosal projection and recipient neurons were found at cytoarchitectonic borders of early cortical areas, similarly to the V1/V2 boundary. Such observations promoted the extension of the midline fusion theory to the somatosensory domain. In addition, callosal neurons were sparser in the representation of more lateralised parts of the face and head and, generally, even less pronounced in distal parts of the limbs and rodents' whiskers, that are para-axial organs. This last observation led Manzoni and associates (1989) to infer that body parts functioning as specialised

detectors seemed to preserve the "purity" of the sensory information and were not following the midline rule. This would also include the digits of primates. However, Iwamura (2000) reports that many S1 neurons representing the monkey's digits can be callosally activated, thus he proposes an extension of the midline fusion theory. He observes that the high spatial resolution of rodent's whiskers and primates' digits can be the analogue of the eyes' foveae in vision, where cells sensitive to light show the densest spatial distribution. Hence, the assumption made in the midline fusion theory for specialised detectors cannot explain the data. Instead, he suggests that callosally connected body parts are those that are recruited bilaterally when participating in a similar behavioural context. For example, shoulders, even being far from the geometrical body midline, are represented by neurons endowed with bilateral receptive fields. For Iwamura (2000), this can be explained because shoulders work or move together to adjust body position. Of course, the case is clearer for a central organ such as the tongue, heavily interconnected through the callosum. Yet, this must not exclude less evident cases in which a bilateral integration of distant body parts would be much needed. Such can be the case for laterally placed specialised detectors working at the vertical meridian of the sensory space (see also **5.5**).

The barrel cortex (BC; originally, the posteromedial barrel subfield) is an example of cortical representation of specialised detectors. It is a neocortical territory present only in whisking mammals, namely those mammals which can move whiskers back and forth. It is a region of S1 involved in the perception of whiskers-mediated touch and whiskers motor control. In order to perform these functions, the BC receives and/or sends afferents to cortical, striatal, tectal and brainstem areas. In the next sections, we will describe the main afferent and efferent pathways, we will briefly focus on the interlaminar flow of activity and terminate this overview by describing the major finding attributed to the physiology of CC in the BC.

1.9 Afferent and efferent pathways of the barrel cortex

There are three afferent pathways to the BC: the lemniscal, the paralemniscal and the extralemniscal one (Diamond et al., 2008). Each of these pathways starts with a first order (pseudo-unipolar) sensory neuron whose body resides in the trigeminal ganglion and whose myelinated process takes part to the infraorbital branch of the trigeminal ganglion. These neurons possess six to seven different kinds of free-endings in the whisker follicle which are excited by distinct forms of mechanical stress provoked by the whisker's vibrations (Takatoh et al., 2018), thus signalled in the brainstem. In the lemniscal pathway, whiskers-related primary afferents synapse in the brainstem onto neurons of the ventral portion of the principal nucleus (PrV) in an orderly fashion, individuating dense clusters of cells organised in cytoarchitectonic rectangles called barrelettes, each of which receives excitation from a single whisker (Erzurumlu et al., 2010). Second order neurons project their axons into the opposite side of the neural axis. This decussation terminates in the dorsomedial part of the ventroposteromedial nucleus of the thalamus (VPMdm). The axons remain ordered and distinguish discrete areas called barreloids for each of the whiskers. Barreloids neurons send their axon in the ipsilateral BC. In L4, they individuate

again discrete areas (200 μm x 300 μm) called barrels. Other projections reach the L5/6 border. Barrels predominantly contain spiny stellate and star pyramidal neurons. Given their small size and shape, they give a 'granular' aspect to the layer, thus called the granular layer (Ahissar and Staiger, 2010). Barrels are embedded in a less compact matrix without granular aspect, which delineates septal areas around the barrels, and a dysgranular cortex all around the barrels subfield within S1 (DYS in Fig I2, right column). The extralemniscal pathway has been discovered more recently, hence is less characterised (Diamond et al., 2008). However, it is known that second order neurons innervate the contralateral thalamus in the ventrolateral part of the ventroposteromedial nucleus (VPMvl). Its cortical afferents seem to innervate equally all the layers but avoid L1 and they are more septum- rather than barrel-aligned (Ahissar and Staiger, 2010). The paralemniscal pathway originates in the spinal nucleus (SpV) of the brainstem where it collects trigeminal primary sensory afferents, which however do not show discernible cytoarchitectonic clusters (Erzurumlu et al., 2010). Axons of second order neurons decussate and synapse onto the medial portion of the thalamic posterior nucleus (POm). POm innervates the ipsilateral S1 and S2. In S1, POm axons reach L1 and L5a but do not show preference for barrel or septal regions.

Prominent cortical input to the BC comes from M1 and S2 mostly in infragranular layers, and largely separated populations from L2/3 of the BC contact back either S2 or M1 (Yamashita el al., 2013). Bidirectional cortical connections also exist with the orbitofrontal cortex, posterior parietal cortex, dysgranular zone and the contralateral BC (Petersen, 2019). Connections to the contralateral BC travel through the CC and have been described in previous sections. Also the whisker representation in putative mouse M2 is reciprocally connected with the BC in the home hemisphere. Infragranular neurons are the main source of subcortical output of the BC. Conspicuous output projections invade the dorsolateral striatum and, to a lesser extent, the dorsomedial part (Reig and Silberberg, 2014; Alegre-Cortes et al., 2021). Another important projection reaches the somatosensory lamina of the superior colliculus (Petersen, 2019). From L6, axons project back into the thalamus where they are thought to deliver a feed-back to modulate the gain of incoming sensory inputs. Through its projection into the facial nucleus of the brainstem, the BC is thought to control the retraction phase within the whisking cycle of contralateral whiskers. The protraction phase relies on M1 instead (Sreenivasan et al., 2015).

1.10 The interlaminar flow of activity in the barrel cortex

In the canonical circuit, upon whisker stimulation, the VPMdm of the thalamus would activate L4 and jointly, at least in the rat, the L5/6 border (Constantinople and Bruno, 2013). This activation subsequently feeds L2/3 where it is projected to surrounding barrel columns and distant cortices, as for example the contralateral BC, ipsilateral M1 and S2 (Petersen, 2019). Gamma activity evoked in L2/3 is able to suppress the activity of surrounding columns in superficial layers but exciting deep ones, accentuating in this manner the activation of the whisker-related barrel and its control over the motor output (Adesnik and Scanziani, 2010). L2/3 also project to L5 of the home column and of the

contralateral hemisphere (Petreanu et al., 2007). Hence, L4‣ L2/3‣L5 constitutes the 'canonical' interlaminar pathway activated by the VPMdm. As can be noted, this activation will spread horizontally in other barrel columns and across cortical related areas. Such activity spread relies on intratelenchephalic projections from L2/3 and a subpopulation of L5 and L6. In parallel, precortical centres can be reached by pyramidal tract neurons contained in L5 (Petersen, 2019). Together with the canonical circuit, other circuit motives can be observed. Among them, direct activation of L5 and L6 from L4 (that bypass L2/3), the one of L6 from L5, the one of L2 from L5A that, in turn, can be activated directly by L6 by the same neurons that feed back to the thalamus (Petersen, 2019). Given this complex circuitry and the possibility of the BC to process sensory input, to be contacted by S2, M1 and M2, and to have direct access to the motor output, this area can be better conceived as a higher-order association area rather than a pure primary sensory cortex (Petersen, 2019).

1.11 Electrophysiological studies on the corpus callosum of the rodent barrel cortex

A systematic exploration of the interaction between the response of the two BCs is provided by Shuler and associates (2001). This work showed the first evidence that the activation of one BC affects the subsequent activation of the opposite one, which they recognise as a form of bilateral integration. In the anaesthetised rat, they recorded suprathreshold responses of L5 neurons in the BC at unspecified coordinates, while delivering ipsi- and contralateral stimulation jointly to 1, 2, 3 or 4 whiskers belonging to a column, either in rostral or caudal position. They found that previous ipsi- and contralateral stimulation diminish the spiking response to a subsequent ipsi- or contralateral stimulation. The results suggested that the two BCs are homotopically connected and that rostral whiskers are better callosally-connected than caudal ones. Notably, in this study row A-whiskers were the only ones to not have been stimulated, likely due to technical difficulties given by their position on the snout and the setup used. This work and a later one in the awake, head-restrained rat (Wiest et al., 2005), found a similar percentage of single units representing both the contra- and the ipsilateral whiskers. The Nicolelis' group thus sustained that a callosal representation of the whiskers is pervasive and this testifies the importance of considering each of the BC jointly representing the arrays of whiskers on both sides of the snout (Shuler et al., 2001; Wiest et al., 2005). Ipsilaterally-evoked subthreshold responses were first recorded in L5a and L5b of the anaesthetised rat's BC (Manns et al., 2004). The ipsilateral responses were 34% smaller than contralateral ones and lagged them by 22 ms on average. Yet, they were present in most of the cells of the study. However, the analysis did not separate between responses evoked in up and down states, with the resulting amplitude likely being severely underestimated. Indeed, in another work in which the ipsilateral response to whiskers stimulation has been estimated for different brain states (Reig and Silberberg, 2014), amplitude is much bigger, but still smaller than that evoked through contralateral stimulation, although the number of whiskers stimulated is much higher in the latter than in the former study. Probably for the same reasons (i.e., few whiskers stimulated, and

waveforms averaged from both up and down states) the same group was not able to find an ipsilateral response in L4 and L2/3 (Brecht et al., 2002, 2003). At least in anaesthetised animal preparations, the longer delay and lower amplitude thus distinguish the ipsi- from the contralateral response. Neurons that respond to thalamocortical volleys often respond also to ipsilateral stimulation of the whiskers, and this kind of activation is thought to rely on the corpus callosum. However, more recent evidence seems to depict a different role for the CC in the awake animal. Oran and associates (2021) used *in vivo* calcium imaging over callosal axons invading the BC from the contralateral one. Surprisingly, as visualised through calcium transients, callosal axons were not active during bilateral whisking in the free air. Instead, their activity was concentrated in epochs of behavioural quiescence and absence of whisking. This could explain the bilateral desynchronisation of spiking and subthreshold activity also recorded in the study during whisking. The authors propose a fascinating view for the interhemispheric correlations brought about by the CC in the BCs: "[...] interhemispheric correlations during quiet wakefulness enhance activity-dependent mechanisms that maintain the homoeostasis of synaptic and intrinsic excitability, and thus equalizing the sensitivity of homotopic cortical areas to sensory processing and other high brain functions. This process might be needed since during exploration sensory circuits on both sides are not necessarily activated at either the same rate or intensity, potentially leading to a drift in their set-points of sensitivity". Unfortunately, again, the axons invading the row A representation in the posterolateral aspect of the BC (or S1/S2 border) have not been imaged and whether or not this 'resetting' of the sensitivity occurs remains to be tested.

1.12 An overview on corpus callosum-mediated inhibition and the case of the barrel cortex

Another aspect remained unexplored in the BC, as opposed to other cortical areas, is whether or not callosal axons can recruit feed-forward inhibition in the contralateral hemisphere (Naka and Adesnik, 2016). Conti and Manzoni (1994) reported that a commonly observed callosal activation consisted in an excitatory postsynaptic potential followed by a prolonged inhibitory one (i.e., sequence EPSP-IPSP). In the cat V1, their onset is separated by circa 1 ms and the IPSP is attributed to a disynaptic feed-forward inhibition onto the directly excited neuron (Conti and Manzoni, 1994). Kawaguchi (1992) found, in the rat prefrontal cortex, that IPSPs had two components, one depending on GABA-A receptors, the other on GABA-B receptors. However, the callosally-evoked IPSP can also result from another mechanism, different from disynaptic inhibition. Indeed, cortical inhibitory cells can also be activated by axon collaterals of pyramidal cells excited monosynaptically by the CC. Presumably, some late hyperpolarising component sometimes reported has this origin (Conti and Manzoni, 1994). Favouring the widespread presence of the first mechanism, in the mouse prefrontal cortex, Anastimades and associates (2018) found callosal axons activating monosynaptically different kinds of interneurons. Excited by callosal afferents, Parvalbumin- and Somatostatin-positive cells could exert their inhibition onto prefrontal cortico-thalamic and cortico-cortical projection neurons. These two types of inhibitory interneurons are excited by the

thalamus in the BC as well (Tan et al., 2008). Since it has been observed that thalamic and callosal IPSPs rely on the same interneuron (Conti and Manzoni, 1994), it is possible that also in the BC callosal IPSPs can be evoked by Parvalbumin- and Somatostatin-positive interneuron types. Similarly, in the mouse primary auditory cortex, fast-spiking Parvalbumin-positive neurons have been found to mediate feed-forward inhibition through their excitation exerted by callosal fibres (Rock and Apicella, 2015; Slander and Isaacson, 2020). Once again, this suggests that Parvalbumin-positive interneuron may have the same role in the BC. One last form of inhibition, named "silent inhibition", is known to act at the callosal synapsis and does not rely on IPSPs (Palmer et al., 2012; but likely also present in the work of Shuler et al., 2001). Silent inhibition affects the firing, but not the subthreshold activity, of L5 neurons in S1 through a mechanism acting on their apical dendrites. Palmer and associates (2012) found that the suprathreshold response to a contralateral stimulation produces less spikes if preceded by an ipsilateral one. This effect relies on the activation of L1 inhibitory interneurons by the callosal afferents, which release GABA onto L5 neurons apical dendrites. The postsynaptic activation of the GABA-B1a receptor activates inward-rectifying K^+ channels and inactivates voltage-sensitive Ca^{2+} channels in this subcellular location of the pyramidal neuron. Spiking activity in the normal contralateral response is produced by concurrent excitation of the soma and backpropagating action potentials from the apical dendrite. However, when callosal afferents are activated 200-400 ms before contralateral stimulation, the long lasting recruitment of the GABA-B1a-mediated mechanisms at the apical dendrite blocks the generation of backpropagating action potentials, resulting in a net reduction of the spiking activity. Curiously, in rat L6 of frontal areas 1 and 2, even if pyramidal neurons and Parvalbumin-positive interneurons are contacted by the CC monosynaptically, feed-forward inhibition in both neuronal types seems to be the exception rather than the rule (Karayannis et al., 2006). Hence, the case of the BC cannot be taken for granted.

2. Objectives

The study on the corticostriatal pathway has the main objective of testing whether two functionally separated circuits and subregions can be discerned in the anatomically homogeneous dorsal striatum of the mouse. Answering this question would help understanding the primate/rodent homology of this brain structure and validate a method for functional mapping of the brain. Similarly, the study on the callosal pathway between the two BCs has the main objective of characterising subregional differences supported by different callosal innervation. Specifically, we wanted to compare *in vivo* the activity evoked in the ipsilateral hemisphere by whisker stimulation in the BC, by focusing on subthreshold receptive fields. If differences were to be found across the BC, their dependence on callosal afferents would have been determined through perturbation studies pointing at either imposing or suppressing the activity in the opposite hemisphere. Moreover, the totality of these experiments on the BC would have allowed us to test the midline fusion theory of the CC in the mouse whiskers system.

Below, we list the single objectives for both the studies:

1) Establish whether the DMS and the DLS MSNs differently integrate the slow wave oscillation as recorded in their membrane potential.

2) If differences are found in 1), establish whether or not they depend on different subregional functional connectivity to distinct cortical areas.

3) If differences are found in 1), establish whether there are more than two subregions (e.g. DMS *vs* DLS), focusing on the anatomical space between the two (dorsocentral striatum, DCS).

4) If differences are found in 1), test whether sensory stimulation can further refine the dorsal striatal boundaries obtained with spontaneous activity.

5) If differences are found in 1), test whether MSNs participating in the direct or indirect pathway differently integrate the incoming slow wave oscillation in the two subregions.

6) Observing the presence and anatomical location of the BC activity elicited by the use of ipsilateral whiskers during a period of spontaneous exploration by the mouse.

7) Characterising contra- and ipsilateral subthreshold whisker responses in the BC subregions that were either active or inactive in 6).

8) Testing the presence of feed-forward inhibition evoked by ipsilateral whiskers stimulation and characterising it in the BC subregions that were either active or inactive in 6).

9) Testing the presence of midline fusion in the whiskers system of the mouse for whiskers belonging to row A.

10) Testing the dependence on the CC of the responses evoked through ipsilateral whiskers stimulation by pharmacologically silencing the activity of the opposite hemisphere, recording only in the BC subregion that was active in 6).

11) Testing the dependence on the CC of the responses evoked through ipsilateral whiskers stimulation by homotopic optogenetics activation of the opposite hemisphere, recording in the BC subregions that were either active or inactive in 6).

12) Testing the presence and contribution of heterotopic callosal connectivity by optogenetics activation of the opposite hemisphere, recording in the BC subregions that were either active or inactive in 6).

3. Materials and Methods

3.1 Ethical approval

All the experimental procedures were in conformity with the directive 2010/63/EU of the European Parliament and of the Council, and the RD 53/2013 Spanish regulation on the protection of animals use for scientific purposes, approved by the government of the Autonomous Community of Valencia, under the supervision of the *Consejo Superior de Investigaciones Científicas* and the Miguel Hernandez University Committee for Animal use in Laboratory.

3.2 Mouse lines for dorsal striatum experiments

We crossed the D2-Cre mouse line (ER44 line, GENSAT) with a Cre-dependent Channelrhodopsin2-EYFP mouse line (Ai32, the Jackson laboratory) to selectively induce the expression of the depolarising exogenous channel in iMSNs. Together with the use of an optopatcher, this allowed the online classification of light-responding iMSNs and non-light-responding dMSNs (Ketzef et al., 2017) in n=36 mice. Further C57BL6 mice (n= 9) have been used for electrophysiological-only experiments.

3.3 Striatal and cortical recordings

For electrophysiological recordings, we used 20 male and 27 female mice aged between 12 and 44 weeks. We induced deep anaesthesia by i.p. injection of a mixture of ketamine (75 mg/kg) and medetomidine (1 mg/kg) in 0.9% NaCl. Anaesthesia level was constantly monitored and a fraction of the initial dose of the mix was administered in case of paw reflex recovery or sign of awakening in the cortical LFP signal. To prevent mechanical instability, experiments were performed on top of a vibration-cancellation table (CleanBench, TMC). For decreasing instability due to respiration, we performed a tracheotomy where we inserted a cannula. Ear- bars were used to fix the animal to a stereotaxic apparatus. A tube blowing oxygen-enriched air was placed 1 cm in front of the cannula. Core body temperature was controlled by a thermostat and maintained at $36.5 \pm 0.5°C$ on top of a heating pad. A total of 7 different craniotomies were performed according to the experimental demand, from Bregma: AP 0 mm, ML 2.5 mm (DMS); AP 0 mm, ML 4 mm (DLS); AP 0 mm, ML 3.25 mm (DCS); AP 2.7 mm, ML 1 mm (FrA); AP 1.5 mm, ML 2.0 mm (M1); AP 1.5 mm, ML 3.25 mm (BC); AP 3.5 mm, ML 2.5 mm (V1) (following Paxinos and Franklin, 2001). At the end of each experiment, mice were sacrificed by lethal i.p. injection of sodium pentobarbital (200 mg/kg).

Whole-cell recordings were obtained between 2013 and 2647 μm depth from 77 DLS (dMSNs= 49, iMSNs= 34), 91 DMS (dMSNs= 65, iMSNs= 32), 17 DCS (dMSNs= 10, iMSNs= 7), in total n=126; and between 675–926 μm depth (cortical layer 5) from 8 FrA, 6 M1, 6 BC and 6 V1 neurons, in total n=26. Pair recordings of MSNs (n= 6) were performed with two micromanipulators (Luigs and Neumann, MRE/MLE Mini 25). DLS and DMS were targeted with a penetration angle

of ~ 30°, while DCS with ~20°. Exposed brain surface was constantly kept wet with 0.9% NaCl solution. Signals were amplified by using a MultiClamp 700B amplifier (Molecular Devices) and digitized at 20 kHz with a CED acquisition board and Spike two software (Cambridge Electronic Design). Borosilicate patch pipettes (1B150F-4, WPI) were pulled with a Flaming/Brown micropipette puller P-1000 (Sutter Instruments) and had an initial resistance of 6–12 MΩ. Pipettes were back-filled with an intracellular solution containing: 125 mM K-gluconate, 10 mM KCl, 10 mM Na-Phosphocreatine, 10 mM HEPES, 4 mM ATP-Mg and 0.3 mM GTP-Na. pH and osmolality were adjusted to ~7.4 and ~280 mOsm/L respectively. Biocytin (0.2–0.4%, Sigma Aldrich) was then added to the intracellular solution to perform cell reconstruction after the experiment.

100 s of spontaneous activity were used for the analysis. We measured input resistance (MΩ) as the slope of a linear fit between injected depolarizing and hyperpolarizing current steps and membrane potential, and separately for up and down states. Membrane time constant (tau) was computed as the time to reach 63% of the voltage increment in response to a current pulse. Capacitance was obtained by dividing the tau for the input resistance. Electrical properties and morphological aspects after reconstruction (e.g., aspiny dendrites) we used to exclude 2 putative fast-spiking and 3 putative cholinergic interneurons from the pool. Thus, only MSNs and cortical neurons were included in the data set.

Tungsten electrodes (1-2 MΩ) were used for extracellular recordings targeting infragranular layers (1000 μm depth, angle 15°-25°) of the cortex. A pair of the abovementioned cortical areas was targeted in each experimental session and accompanied by a joint intracellular recording. Extracellular recordings were amplified using a differential AC Amplifier model 1700 (A-M Systems) and digitized at 20 KHz with CED and Spike-2.

3.4 Eye stimulation for dorsal striatum experiments

A white LED (contralateral eye distance= 0.5 cm) was used to evoke visual responses upon a 15 ms light flash every 5 s. Associated with this protocol, we recorded 17 MSNs in DCS and 10 MSNs in DMS. Optic gel (Viscotears) applied to the eyes prevented corneal desiccation.

3.5 Online identification of medium-spiny neurons

In D2-Cre x Ai32 mice, we used an optopatcher (Katz et al., 2019; Katz et al., 2013; Ketzef et al., 2017; A-M systems, WA USA) to identify optogenetics-responding neurons as iMSNs and non-responding as putative dMSNs. To this end, controlled pulses (SLA-1000–2, two channel universal LED driver, Mightex systems) of blue light (Fibre-coupled LED light source FCS-0470–000, 470 nm, Mightex systems) through an optic fibre (200 mm diameter, handmade) inserted in the patch pipette were delivered (Spike2 custom script) when the neurons displayed broad amplitude spontaneous activity. One or two serial pulses with five light steps of 500 ms each were delivered every 2 s with increasing intensity from 20% to 100% of full LED power (minimal light intensity was 0.166 mW,

maximal intensity was 0.83 mW measured at the fibre's tip). Light power was measured with a power meter console (PM100D, Thorlabs). ChR2$^+$-iMSNs responded with depolarising events (13.3 ± 8.28 mV) within 2.69 ± 1.37 ms, while non-responding cells were classified as putative dMSNs.

3.6 Morphological reconstruction for dorsal striatum experiments

After sacrificing, mice were transcardially perfused with 4% paraformaldehyde in 0.1 M phosphate buffer (PB, pH 7.4), the brain extracted and stored in PBS with 30% sucrose at 4°C. In order to contain the entire striatum, 25 μm thick coronal slices were collected from AP 1.4 mm to AP -1.3 mm relative to Bregma (Paxinos and Franklin, 2001) in order to contain the entire striatum and cutted through a digital automatic cryotome. To label intracellularly recorded neurons filled with biocytin, sections were incubated overnight with Cy3-conjugated streptavidin (Jackson ImmunoResearch Laboratories) diluted (1:1000) in 1% BSA, 0.3% Triton-X 100 in 0.1 M PBS. After application of mowiol (Calbiochem), they were coverslipped and imaged using a fluorescence microscope (DM6000B, Leica), then processed in ImageJ.

3.7 Characterisation of the slow wave oscillation in dorsal striatum experiment

Membrane potential (Vm) was smoothed (200 ms time window) and a threshold (mean Vm + 0.5 times its standard deviation) was applied to it in order to isolate up and down states. Events detected as up states but shorter than 200 ms were discarded. Up states recorded in the cortical LFPs were considered to propagate in MSNs only if the latter lagged the former within 500 ms. 13 parameters were extracted from the MSNs trace after subtraction of IMFs faster than 50 Hz for spike removal. After dividing the resulting trace in up and down time windows, we extracted the following Vm features during up states: 1) mean Vm; 2) Vm standard deviation; 3) Vm most hyperpolarised values (minimum); 4) Vm most depolarised values (maximum); 12) their difference (peak to peak); 6) maximum of the Vm derivative; 7) minimum of the Vm derivative; 11) number of peaks (Matlab function *findpeaks*)- intended as wide voltage excursions internal to the up states separated at least by 160 ms and surpassing 0.3 standard deviations of the Vm; 13) up state length; 5) mean Vm, averaged between up and down states; 8) transition speed from down to up and 9) from up to down states; 10) their ratio- slope transition down-to-up over up-to-down. In the latter case, the slope was obtained in a 300 ms time window centered at the detected onset of the transitions, smoothed (100 ms), and the derivative extracted. The mean plus 0.3 times the standard deviation of the derivative individuated a time segment on the Vm at which we fitted a first polynomial degree, whose angular coefficient was the speed of transition.

To classify MSNs as belonging to the DLS or DMS based on the above features, we used a Support Vector Machine (SVM; Cortes and Vapnik, 1995) with a linear kernel. This is a method of supervised classification that uses a hyperplane to separate the data. After 10 cross-validation of the classification, we used a Recursive Feature Elimination procedure

to understand which were the single features, or their combination, yielding the highest accuracy.

To classify MSNs along the theoretical striatal boundary, we evaluated the DCS-MSNs distribution in the previous classification space with respect to the DLS/DMS classification boundary. This procedure allowed us to discriminate between hypothesis 1 and 2 (see **4.3**). Thus, previous coefficients and intersection values of the SVM relative to DLS and DMS distributions were used to project the newly acquired data (DCS) against this hypervector. Since all the multivariate data were now distributed along a single hypervector, we could compute the probability density functions along the DLS/DMS classification boundary for the three MSNs distributions (i.e., DLS, DMS and DCS).

3.8 Extraction of the slow wave oscillation using NA-MEMD for both studies

In order to extract the slow wave oscillation vector from our recordings, we applied Noise-Assisted Multivariate Empirical Mode Decomposition (NA-MEMD; Ur Rehman and Mandic, 2011) to the row data downsampled to 1KHz. Since neural oscillations are non-linear, non-stationary signals they are difficult to capture with fixed, linear templates (e.g., wavelets) (Alegre-Cortés et al., 2017). Since the NA-MEMD method is a data-driven algorithm, it is more suitable for this objective. In fact, it decomposes the row signal in a set of constituent oscillatory modes (intrinsic mode functions, IMFs), each containing an oscillation in a certain frequency range. The instantaneous frequency and amplitude of these IMFs can be identified with the Hilbert transform. Since the row signals of LFPs and membrane potential are jointly input and that the NA-MEMD is computed simultaneously in all signal dimensions, a same number of IMFs is obtained for LFPs and membrane potential, each one carrying a specific frequency simultaneously recorded in the two signals. This procedure guarantees an enriched Time-Frequency spectrum when compared to traditional linear tools (Alegre-Cortés et al., 2016). Having the same number of IMFs per signal, allowed us the direct comparison of the IMF carrying the slow wave oscillation in the LFPs and membrane potential. The NA-MEMD has been applied to the data with the MEMD Matlab package (http://www.commsp.ee.ic.ac.uk/mandic/research/emd.htm), with the addition of a withe-noise signal. Once we isolated the slow wave oscillation in this manner, we stored it for further analysis. For the analysis and additional results on faster IMFs (e.g, theta, beta and gamma frequency) and more details on the methods, see the annexed article (Alegre-Cortés et al., 2021). Such procedure was applied for spontaneous activity data of the corticostriatal and barrel cortex data.

3.9 Mouse lines for barrel cortex experiments

For c-Fos experiments, we used wild-type C57BL6 mice (n= 16) of either sex between 2 and 3 months of age. For electrophysiological experiments we used wild-type C57BL6 mice (n= 23), and the transgenic lines NEX-Cre (Goebbels et al., 2006) (n= 23; generously donated from Dr. Klaus-Armin Nave and Dr. Victor Borrell) and Parvalbumin-Cre (n= 8; generously donated from Prof. Eduardo de Puelles), of either sex

and aged between 2 and 6 months. All animals were housed preferentially with cage-mates at T= 24 C° in our institution's animal facility with 12h daily illumination and food and water *ad libitum*.

3.10 c-Fos experiments

On the first day, in order to habituate mice to the environment, they were exposed to a covered empty arena (black PVC material; 50 x 50 x 70 cm) in complete darkness for ~1 hour. The following day, they were briefly (~15 min) anaesthetised with 2-4% isoflurane in oxygen (0.8 L/min) to allow interventions on whiskers pads. In trimmed whiskers condition, whiskers were trimmed bilaterally, paying attention to reach the very base of the whiskers. For bi- and unilateral lidocaine conditions, lidocaine (150-200 µL) was injected subcutaneously, with the volume subdivided in one to two injections in order to cover the entire whisker pad. We waited 90-120 min for the anaesthesia to fade completely before testing the mice in the arena in presence of new objects of various size and shape. To ensure the success of lidocaine injections, mice were visually checked to assess the inability to whisk prior to test. After 45 min of free exploration, mice were sacrificed by lethal injection of sodium Pentobarbital, transcardially perfused with 4% paraformaldehyde in 0.1 M phosphate buffer (pH 7.4), decapitated and their brain was extracted. After tangential brain sectioning and c-Fos immunostaining, images were acquired with a confocal microscope (Leica SPEII) with 10 µm step-size using a 20x immersion objective. Data from images were quantified using the Fiji software. Area and disposition of ROIs from barrels and septa were recognised by VGlut2 immunostaining, extracted and then projected onto the respective image showing the c-Fos channel. In this manner, we could assign the count of immunopositive nuclei to their area of origin. By dividing the nuclei count for the area, we obtained a measure of c-Fos$^+$ nuclei density (#nuclei/ 0.1 mm^2) in target barrels and septa. For bilateral interventions on the whiskers pads, we counted c-Fos$^+$ nuclei in the BC of both hemispheres, while for the unilateral injection of lidocaine only the hemisphere contralateral to the injection side was used for the count. In the lidocaine cohort, if the contralateral BC showed c-Fos expression clearly resembling the one of thalamocortical activation (i.e., c-Fos very dense and confined within barrel hollows), the lidocaine effect was considered faded prior to sacrifice and mice were excluded from the analysis.

3.11 Viral injections in the barrel cortex

To impose the activation of callosal-projection neurons, we infected pyramidal cells of the right BC. Anaesthesia (2-4% isoflurane in oxygen, 0.8 L/min) was induced and maintained for the course of the surgery in NEX-Cre mice immobilised in a stereotaxic apparatus (Kopf Instrument). Lidocaine cream was applied to the skin over the skull prior to opening and eyes were covered with ophthalmic gel (Viscotears 2mg/g) to prevent corneal desiccation. Analgesic (Metacam, 0.4 mL) was delivered by intraperitoneal injection. In order to reach the highest expression of virus in target areas, the craniotomy was drilled either at coordinates AP -2 ML -3.8 (plBC) or AP -1 ML -3.2 (amBC) from bregma, exposing the dura mater. The ssAAV-5/2-hEF1α-dlox-hChR2(H134R)

_EYFP(rev)-dlox-WPRE-hGHp(A) viral construct (ETH Zurich) was injected in small volumes (100-200 nL) at 0.7 mm depth with a precision injector (Nanoliter, WPI). Skin was then closed with surgical glue and animals rested in a recovery chamber until restoration of normal locomotor activity.

3.12 Histology and Immunohistochemistry for barrel cortex experiments

After their extraction, brains were post-fixed in PFA 4% for 2h at room temperature and then stored at 4 °C in PBS with 30% sucrose plus 0.1% sodium azide before their use. For flattened preparations of the cortex, the entire cortical mantle was isolated from the brain and pressed overnight in a custom-made, plastic press-and-hold apparatus of 1 mm depth in a PFA 4% bath prior to sectioning. Tangential slices 80 µm thick from flattened cortex and coronal slices 50 µm thick from intact brains were cut with a digital cryotome (Microm HM450; ThermoFisher). After washing with PBS, sections were exposed to a blocking solution of 0.1M PBS with 1% BSA and 0.5% Tryton-X 100 for 2h at room temperature. Next, they were incubated overnight with primary antibodies (4 °C) diluted in blocking solution. To target thalamocortical afferents for recognising L4 barrels, we used guinea pig anti-VGlut2 (1:5000; Synaptic Systems). For targeting c-Fos expressing nuclei, we used rabbit anti-cFos (1:700; Synaptic Systems). Mouse anti-NeuN (1:250; Sigma Aldrich) was used for neural somas membranes. The following day, sections were washed and incubated for 2h at room temperature in blocking solution with secondary antibodies, and adding streptavidin for tissue previously used in electrophysiological experiments (see below). Once this time was elapsed, they were mounted on microscope slides (Menzel-Gläser Superfrost Plus; ThermoFisher), covered with mowiol (Calbiochem) and coverslipped (Menzel-Gläser; ThermoFisher). To reconstruct biocytin-filled neurons from electrophysiological experiments, we used Cy2- or Cy3-conjugated streptavidin (Jackson ImmunoResearch Laboratories), diluted, respectively, 1:500 and 1:1000 in blocking solution. As secondary antibodies, we used goat anti-guinea pig Alexa fluor 568 and 633 (ThermoFisher), both with 1:500 dilutions, and donkey anti-rabbit Alexa fluor 488 (ThermoFisher), dilution 1:500. For staining somas' membrane, we used NeuroTrace™ 435/455 Blue Fluorescent Nissl Stain (ThermoFisher), dilution 1:250, and DAPI (ThermoFisher) for nuclei. For cell reconstruction of recordings in amBC, coronal sections were collected from bregma AP -0.58 to AP -1.58, while for plBC, from bregma AP -1.82 to AP -2.30 (following Paxinos and Franklin, 2001).

3.13 Whiskers and optogenetic stimulation

With the exception of the pairs A2-A3 and E2-E3, whiskers were trimmed bilaterally at their base to avoid any unintended stimulation accompanying the one of target whiskers. Spared whiskers, separately for each row (i.e., A and E), were glued together with super glue along their length. Then, they were attached to the tip of Teflon-coated stainless wire of a custom-made solenoid puller (see **3.16**) with super glue. In this manner, and depending on the target cortical area (i.e., plBC or amBC), mirror whiskers of both sides of the snout were connected to the solenoid puller. Whiskers displacement consisted in

fast caudo-rostral pulling (~3.5 mm) lasting 15 ms, delivered every 3 or 5 s, contra- and ipsilateral to the patch-clamp recording electrode.

For optogenetics experiments in NEX-Cre mice, step-like photo-stimulations lasting 5 or 10 ms were delivered with an optic fiber (400 µm diameter) connected to a blue light source (Prizmatix LED, 453 nm wavelength, 3.76 mW light power) and governed by the CED1401 (Power3) through a custom-made program (Spike2). Two craniotomies were drilled. The fibre tip was positioned perpendicular to the surface of the brain within the craniotomy used for delivering the viral construct, either at plBC or amBC coordinates. A micro-holding device (Sáez et al., 2018) was used to keep in the same coordinate the borosilicate capillary (1B150F-4, WPI) containing the LFP electrode and the optic fibre, except that the tip of the electrode was deepened 1 mm into the cortex, while the optic fibre rested on the brain surface. In the second, fibre-free craniotomy, another LFP electrode (0.9-1.2 MΩ) was placed at 1 mm depth into the cortex to check for the anatomical specificity of the optogenetic activation.

3.14 Electrophysiological recordings in the barrel cortex

Similarly to the corticostriatal experiments, electrophysiological recordings were performed on top of a laboratory table for vibration cancellation (CleanBench, TMC). Mice were head-fixed in a stereotaxic apparatus with ear-bars. We induced anaesthesia by i.p. injection of ketamine (75 mg/kg) and medetomidine (1 mg/kg) diluted in 0.9% NaCl saline solution. One third of the original dose was injected intramuscularly to maintain the level of anaesthesia once paw reflex could be evoked or the LFP trace exhibited signatures of awakening. To avoid mechanical instability during neural recordings due to respiration, a tracheotomy was performed prior to animal immobilisation in a customised stereotaxic apparatus (Stoelting). A tube blowing oxygen-enriched air was placed around 1 cm in front of the cannula, previously inserted in the trachea. The animal rested over a heating-pad governed by a thermostat (FHC Inc.) to maintain core body temperature at $36.5 \pm 0.5°C$.

Depending on the experiment, 2 to 3 circular craniotomies were drilled over the BCs, with an approximate diameter of 0.5 mm. Typically, they were one per hemisphere at mirror symmetric coordinates (reported in the main text), plus another in the right hemisphere when required to host a second LFP at non-mirror symmetric coordinates with respect to the contralateral (i.e., left hemisphere) patch–clamp electrode. Drilled holes were constantly kept wet by application of 0.9% NaCl saline solution for the entire duration of the recordings. In the craniotomy for patch-clamp recordings, we gently removed the dura with a syringe needle bent at the tip and stopped eventual bleeding with cotton sticks.

To approach the cortical representation of target whiskers (i.e., row A and row E) within plBC or amBC craniotomies, we delivered contralateral stimulations of the whiskers group matching its cortical representation, respectively, row A for plBC and row E for amBC. A borosilicate capillary filled with 0.9% NaCl saline solution contained an LFP electrode. We used this to navigate the craniotomy through a digital micromanipulator (Luigs & Neumann, set at 1 µm precision) for sampling cortical responses to whiskers'

stimulations on the dura's surface. After that the average of 10-20 LFP responses was displayed and calculated online by the software (Spike2), the electrode was moved to a new position within the craniotomy, and the process repeated. Normally, after 3-6 loci sampled, by visually comparing the averages obtained, the one with the strongest initial negative deflection was chosen to be the location for patch-clamp recordings. Especially in younger animals (PD ~60), these loci could be also recognised on the brain surface with reference to brain vessels.

For patch-clamp recordings, we used an angle of ~60°. Cortical depth of the recording was collected through display reading of the micromanipulator. By comparing our histological preparations with display readings and the bibliography (especially Petreanu et al., 2007), we considered as *supragranular* below L1 neurons recorded between 101 and 300 μm from the pia, as *granular* the ones recorded between 301 and 500 μm from the pia, and finally *infragranular* neurons below 501 μm and until the white matter, at approximately 1100 μm. After anatomical reconstruction of biocytin-filled neurons, these coordinates associated with the penetration angle showed to be optimal for neurons recorded in plBC. However, for recordings in amBC a more perpendicular angle would have been required. In order to correct the depth of these recordings to match their anatomical reconstruction, we applied the formula:

$$D = d*\cos(30°)$$

where D is the adjusted depth and d is the depth given by the display reading. Since in this manner we could minimally reduce the discrepancy of recording depth in 6 randomly chosen brains with reconstructed neurons in amBC (Fig M1), we applied this correction to all the remaining amBC neurons.
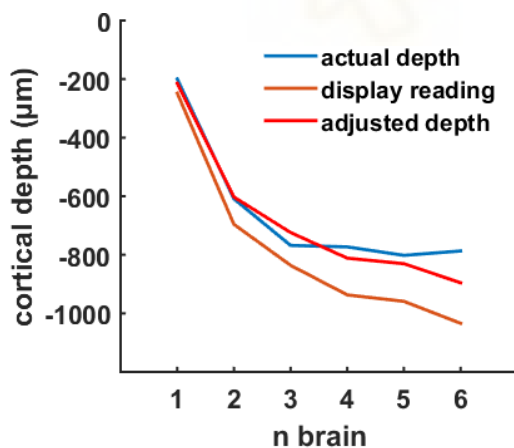
Fig M1 Correction of depth for recordings in anteromedial barrel cortex. Six randomly chosen brains with histologically reconstructed cortical depth of the neurons were used to extract the actual depth (blue line). This was compared to the display reading from the micromanipulator (d, brown line) and adjusted (D, red line) through a formula (provided in the text) to match the actual depth, further applied to remaining recordings in the same condition.

Pipettes for patch-clamp recordings (7-11 MΩ), were back-filled with intracellular solution containing: 125 mM K-gluconate, 10 mM KCl, 10 mM Na-Phosphocreatine, 10 mM HEPES, 4 mM ATP-Mg and 0.3 mM GTP-Na. pH and osmolarity were adjusted to ~7.4 and ~280 mOsm/L, respectively. Biocytin (0.2-0.4%, Sigma Aldrich) was then added to the intracellular solution to reconstruct the recorded cell after every experiment (Fig 2B and 5A). Borosilicate capillaries, both used for LFP or patch-clamp recordings, were pulled with a micropipette puller (Flaming/Brown P-1000, Sutter Instrument).

Recorded signals were amplified with MultiClamp 700B (Molecular Devices), converted to digital with a CED 1401 (Power 3) acquisition board at 20 KHz, and streamed to a laptop (Windows 10) running Spike2 software (Cambridge Electronics Design). At the end of each experiment, mice were sacrificed with a lethal i.p. injection of Pentobarbital, perfused transcardially with 4% paraformaldehyde in 0.1M phosphate buffer (pH 7.4), decapitated, their brain extracted and post-fixed overnight in 4% paraformaldehyde. Thus, brains were maintained in 30% sucrose solution with sodium azide at 4 °C until the sectioning day. In this study, we recorded intracellularly a total of 106 left-BC neurons (n= 62 plBC, n= 44 amBC) from 54 mice (~2 neurons/mouse). Of this pool, data on sensory stimulations (excitatory and/or inhibitory responses) were obtained from 81 neurons. Data on optogenetic stimulation were obtained from 47 neurons, 22 of which also underwent sensory stimulation. The number of neurons used for statistical comparisons and their layer distribution is reported in the main text.

3.15 Data analysis for barrel cortex experiments

We analysed data with Matlab 2015a (Mathworks). First, we downsampled acquired signals to 10 KHz. Then, we isolated spontaneous up and down network states in intracellular currents through a moving average window, considering up state values of membrane potential exceeding the threshold given by the sum of the mean membrane potential within such time window (i.e., one tenth of the signal length) with 0.4 times its standard deviation, and down states the values below this threshold (Fig M2). BC up states often display complex shapes (Fig M2), characterised by 2 or more peaks (Alegre-Cortés et al., 2021). Thus, short hyperpolarising events (< 150 ms) falling down the threshold and thus classified as brief down states (Fig M2, azure line), were elided and considered voltage excursions within up states (Fig M2, red line). Analogously, too short depolarising events (< 15 ms) misclassified as up state were reclassified as down state (not shown).
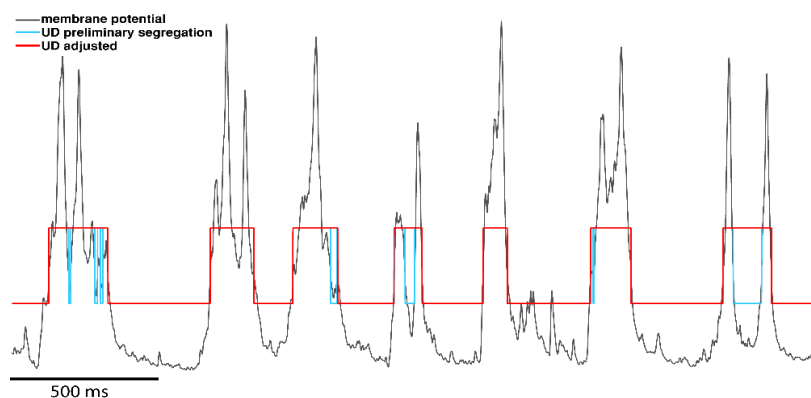
Fig M2 Segregation algorithm of spontaneously occurring up and down states in the membrane potential (gray line). A first up/down (UD) preliminary segregation (azure line), that misclassified hyperpolarising events internal to up states, is adjusted (red line) to consider those activity segments as up state.

Neural responses to whiskers and optogenetic stimulations were isolated from 200 ms before to 500 ms after the trigger associated with the stimulation. We selected responses in down state only for stimulations falling 100 ms after the end of an up state, and

separated from the ones occurring during up state. Both kinds of responses were spike-filtered. For each response of a single neuron, we used a median filter from the Matlab function *medfilt1,* setting n =70 (Fig M3; sampling resolution: 10 kHz). To smooth the output vector to assume a more physiological aspect after the spike removal (Fig M3), we used the Savitzky-Golay filter implemented in the Matlab function *sgolayfilt*, setting polynomial order k =2 and the odd frame size f =51.
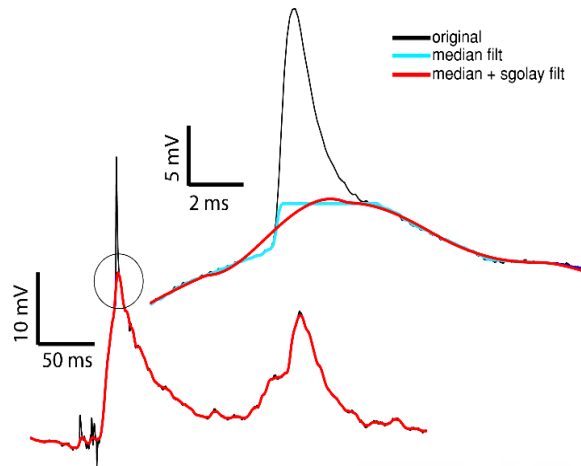
Fig M3 Spikes removal algorithm for intracellularly recorded neuronal responses. Lower in the image a neuron from posterolateral BC responding to contralateral stimulations of row A-whiskers by emitting a spike (black line, 'original'). The region in the black circle is zoomed-in upper in the image to show the algorithm performance. Median filter correctly removes the spike (azure line, 'median filt') but distorts the trace. Adding the smoothing with Savitzky-Golay filter (red line, 'median+sgolay filt') provides a more physiological aspect to the trace.

Next, we obtained the waveform average for each neuron through the mean of their spike-filtered responses. In order to characterise waveform averages, we extracted their onset delay, peak delay, amplitude and slope. In down state responses, for extracting the onset, the mean membrane potential of the down state in the 50 ms preceding the stimulation was taken as baseline and it was multiplied by 50 times its standard deviation to obtain a threshold value. The onset delay was defined as the difference in time between stimulation delivery (digital trigger) and threshold crossing by the membrane potential. For extracting the peak delay, we considered a time window of 300 ms after stimulation. The peak delay was defined as the difference in time between stimulation delivery and reaching the maximal amplitude of the response within such a time window. The amplitude was defined as the difference in membrane potential between the peak of the spike-filtered response and the pre-stimulus baseline (i.e., the down state potential). The slope was defined as the angular coefficient of the first degree polynomial fitted to the waveform average in the time between onset and peak delay (Matlab function: *fit*). These measures were visually assessed on the waveform averages and manually adjusted when needed. For responses falling in up state, we followed the same approach except that the onset delays were manually extracted. For experiments with TTX, in order to extract the amplitude of downward deflections of the signal (i.e., spontaneous up states), we smoothed the signal and used the Matlab function *findpeaks*. Hence, we averaged the voltage values associated with the peaks, separately for each recording in CTRL and TTX.

Peak delay, amplitude and slope were used to measure the Mahalanobis distance between homotopic ipsi- and contralateral responses in plBC or amBC, both for excitatory and inhibitory components. The Mahalanobis distance (d) between each observation in Y and the reference sample in matrix X is defined by the formula:

$$d(I) = (Y(I, m)-\mu)^* (s)^{-1}*(Y(I, m)- \mu)'$$

where I is a single observation in the dimension m (i.e., one of our parameters associated with a neuron), and μ and *s* are the sample mean and covariance of the data in X (Matlab function: *mahal*). We used this measure because it allowed us to extract a unidimensional distance in a multidimensional space, that in this case considers as a dimension each of the neuronal parameters. Before computing the Mahalanobis distance, parameters were normalised in the z- distribution. Distance from contralateral response was obtained by taking the contralateral parameters as reference sample, whose distribution centre was compared against the values in single neurons of contra- and ipsilateral responses. The same procedure was applied to compute the distance from ipsilateral response, but this time by using ipsilateral parameters as reference sample. The operation was applied separately for plBC and amBC data. Mahalanobis distance values are provided as the square root of the Matlab function output (given in squared values).

To further compare the responses, we used the Matlab function *xcorr* to calculate the cross-correlation coefficients between ipsi- and contralateral responses recorded from a given neuron. We selected the time window starting with stimulus delivery and ending after 400 ms, limiting the lag range to ±50 ms. Passive properties were calculated from negative and positive injection currents (i.e., from -100 to 100 nA, by 14 increasingly positive steps) delivered to neurons during spontaneous activity, separately for up and down states. We calculated the membrane constant τ (ms) as the time at which the membrane potential reached the 37% of its resting value upon current injection, averaged through negative and positive current steps. We obtained the resistance (MΩ) through the angular coefficient of the first degree polynomial fitted to membrane potential values receiving current injections at the different intensities, and separately calculated the values for up (R_{up}) and down (R_{down}) states. Finally, we measured the cells' capacitance (pF) by dividing τ for the resistance in up (C_{up}) and down states (C_{down}).

For modelling the estimate of linear summation in optogenetics experiments involving the joint activation of contralateral homo- and heterotopic BC territories, we summed the mean membrane potential of the homo- and heterotopic response distributions centred around the median peak delay (form -5 to + 5 ms) of the distribution of responses obtained upon BC-wide activations. To calculate the error of this sum due to chance scatter, the squared standard error of the mean of homo- and heterotopic distributions was summed and then square-rooted, thus applied symmetrically to the mean. The estimation of the linear sum with the relative error was then compared to the mean (± S.E.M) membrane potential of homo-, heterotopic and wide responses extracted in the same time window. This procedure was done separately for plBC and amBC neurons.

3.16 Whiskers' stimulator

In order to displace the whiskers to record evoked sensory responses in the BC, we built a solenoid-based whiskers puller inspired by the work of Krupa et al., 2000. The system is composed of mechanical and electrical components governed by an Arduino. Figure M4 shows the system's assemblies at the end of a stimulation (i.e., retracted position). Mechanical stimuli for whiskers displacement are obtained through 2 to 4 miniature

solenoids (5V, 3.5 mm travel) of the pull type (ROB-11015, Electrónica Embajadores), that pull a Teflon-coated, 3-stranded, stainless steel wire (152 µm outer diameter; 3SS-2T, Science Products GmbH), glued to target whiskers at the opposite end. Such wire slides back and forth inside a guiding polyethylene tube (279 µm inner diameter, 609 µm outer diameter; 800700, Science Products GmbH). At each end of the polyethylene tube is inserted by the tip a stainless steel guide tube (191 µm inner diameter, 404 µm outer diameter; 833200, Science Products GmbH) to confer rigidity at the endings and allowing to block all the tubing complex containing the sliding wire.
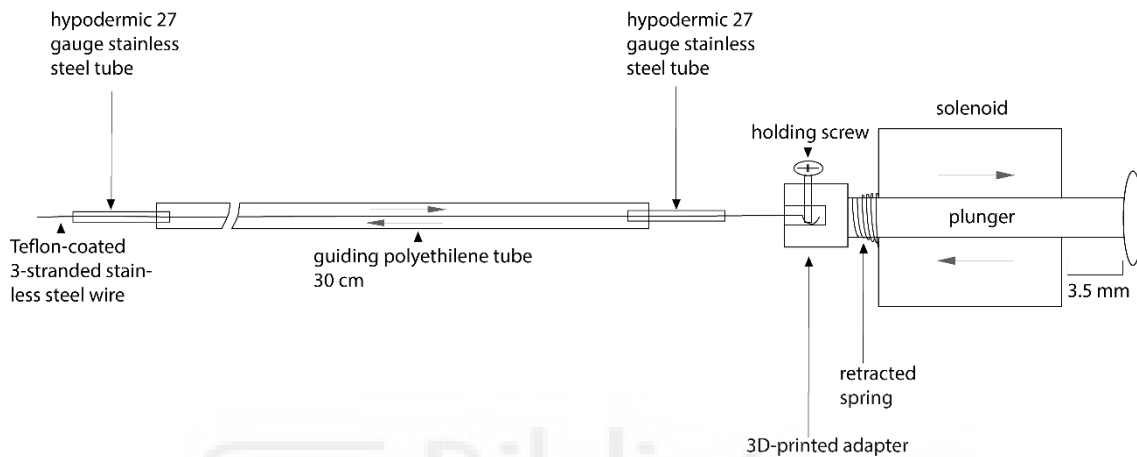
Fig M4 Retracted whiskers puller. Electrified miniature solenoid at the end of a whiskers stimulation and tubing components of the system.

Miniature solenoids were mounted on a 3D-printed support platform where the stainless steel guide tube lying in front of the head of the plunger was clamped. Here, also the body of the miniature solenoid was completely blocked inside a hard-plastic pocket. Another plastic platform was mounted on the anti-vibration table used for electrophysiological recordings, just in front of, but not in contact with, the stereotaxic apparatus hosting the mouse. From this platform, two to four columns emerged perpendicularly to the table's surface, each of which carrying a movable metal arm parallel to the table's surface and ending just in front of the animal's snout. These arms were used to clamp the second stainless steel guiding tube next to the stimulating end of the wire and could be manually aligned and fixed in register with the whiskers. As aforementioned, the tip of a single wire was glued to the target whiskers group. Thus, electrifying the miniature solenoid provoked the retraction of the plunger that consequently pulled the whiskers group. In this manner, and differently from the stimulating apparatus of Krupa et al., 2000, our stimulation was grossly caudo-rostral instead of ventro-dorsal. Thanks to the spring between the moving head and the fixed body of the miniature solenoid, de-electrifying it provoked the elastic return of the plunger and of the whiskers group to their resting position.

Electrical and hardware components serving the mechanics were an Ardunio board (Genuino Uno), a variable power supplier (0-15 V, 0-3 A; LABPS1503, VALLEMAN), 2 dual motor drivers (TB6612FNG, Sparkfun), and 4 relays (5 V; G46, FINDER). Each

of the motor drivers could electrify up to 2 miniature solenoids (for a maximum of 4 usable), and their standby state together with the selection of the active solenoid were controlled by Arduino. When active (standby off), the motor drivers allowed a 15 ms passage of current from the power supply directed in parallel towards the solenoid and its associated relay. The relays were used to collect the triggers accompanying the stimulation through the CED1401, thus aligned to the ongoing neural activity in Spike2. To end the stimulation, the passage of current was interrupted by deactivating the motor driver (standby on). In each experiment, the current was fixed at 7.3 V to obtain the maximal performance of the miniature solenoids. At this voltage and measured via a digital force gauge (resolution 0.001 N; FH2, SAUTER GmbH), the solenoids could exert a longitudinal pulling force of 7.4 $\pm$ 1.8 mN (mean $\pm$ std) on the whiskers group, provoking an abrupt displacement. To compensate for light differences in pulling force and possible ringing across solenoids, they were routinely and randomly assigned to different whiskers groups (i.e., contra- or ipsilateral, row A or row E stimulations) across experiments.

3.17 Statistics for dorsal striatum experiments

For comparing data distributions, we used Wilcoxon rank sum test (Matlab). When required, alpha values for multiple comparisons were corrected using Holm-Bonferroni correction. Error bars presented in the graphs as whiskers of the mean represent the standard deviation, unless stated otherwise. In hypothesis testing, we set alpha at 0.05.

3.18 Statistics for barrel cortex experiments

Graphs, quantification and statistical tests have been performed in Matlab R2015a (Mathworks). Values are expressed as median [25th-75th quantiles], with the median graphically represented by a red dot. Mean is graphically represented by a black square $\pm$ S.E.M. (whiskers). We used a two-sided Wilcoxon rank sum test for statistical comparison of unmatched samples and two-sided Wilcoxon sign rank test for matched samples. To test the homogeneity of distributions we used the $\chi 2$ –test and the tabulated values to infer statistical significance. For comparisons involving more than two sample distributions, we used Kruskal-Wallis test with Fisher's Least Square Difference (LSD) post-hoc test to infer statistical significance of pairwise comparisons. For all statistical tests, the null hypothesis was rejected at the 5% significance level. Symbols: * indicates $p< 0.05$, ** indicates $p< 0.01$ and *** indicates $p< 0.001$.

4. Results

4.1 Slow wave oscillation in dorsomedial and dorsolateral medium-spiny neurons shows different characteristics

An important aim of systems neuroscience is to understand how brain areas interact. One way to shed light on this aspect is to study their functional connectivity. By embracing the definition given by Getting (1989), here functional connectivity is intended as: "[…] the effect of one cell upon another by whatever pathways, monosynaptic or polysynaptic, interconnect the two cells". The spontaneous slow wave activity is generated in deep layers of the neocortex (Sanchez-Vives and McCormick, 2000) and it propagates to other cortical (*via* intratelencephalic neurons) and subcortical (*via* pyramidal tract and some intratelencephalic neurons) areas. Thus, by assuming that the pre-existing circuits will be maintained in the network when it falls in the slow wave oscillation regime, studying the slow wave propagation may reveal functional connectivity between the cortex and target areas. These concepts inspired our work aimed at understanding corticostriatal functional connectivity (Alegre-Cortes et al., 2021; Annexed article), and the corticocallosal functional connectivity between the two barrel cortices (see **4.13**). Here, we asked whether or not the homogeneous anatomical appearance of the mouse dorsal striatum (DS) masks a sharp functional boundary between its subregions, often reported as showing overlapped cortical innervation (Kincaid et al., 1998; Hoffer et al., 2001; Hoover et al., 2003; Hooks et al., 2018).

By whole-cell patch-clamp recording of medium-spiny neurons (MSNs) in the dorsolateral (DLS) and dorsomedial striatum (DMS), in conjunction with 1 to 2 LFPs from different cortical areas (Fig 1A-B), we studied the slow wave propagation in anaesthetised mice. In the dorsal striatum, state transitions of the MSNs membrane potential are triggered by the cortex (Wilson and Kawaguchi, 1996), likely with a marginal contribution from the thalamus. During up states and network transitions (i.e., up-to-down and down-to-up), DMS (n= 91) and DLS (n= 77) neurons differ in many features (11 out of 13 measured) of their slow oscillatory activity (Fig 1C). More specifically, in the up states, the average membrane potential, its standard deviation, its minimum and maximum value, and the depolarisation amplitude were significantly higher in DMS- than in DLS-MSNs. In addition, state transitions were more abrupt in the former, showing a significantly steeper slope from down-to-up and from up-to-down states. As further distinctions between the two populations, DLS-MSNs showed a higher number of peaks within their up states, and a higher peak-to-peak amplitude, all contained in up states of significantly longer duration than in DMS-MSNs. These differences in the integration of the slow wave, propagating in the DS from the cortex (Wilson and Kawaguchi, 1996), may reflect the distinct pattern of excitatory and inhibitory inputs they receive (Reig and Silberberg, 2014), the latter depending upon the cortical recruitment of the local inhibitory network.

By using the Support Vector Machine (SVM), a supervised machine-learning technique, we performed a Recursive Feature Elimination analysis on the slow wave parameters. This method allows one to obtain the importance relative to each of, or a combination of, the features to the classification of MSNs as DMS or DLS by recursively removing parameters and testing the classification accuracy (see **3.7** and the annexed article). In this manner, the number of peaks within up states (means: 1.09 in DMS *vs* 1.38 in DLS), their amplitude (means: 16.9 mV in DMS *vs* 12.6 mV in DLS), and the slope from the up to the down states (means: 630 mV/s in DMS *vs* 570 mV/s in DLS) were selected, in this order, as the most discriminative features, yielding to 88.56 ± 0.57 % classification accuracy. Figure 1D shows the clear separation of DMS and DLS MSNs populations in the 3-D space formed by the above (z-scored) parameters.
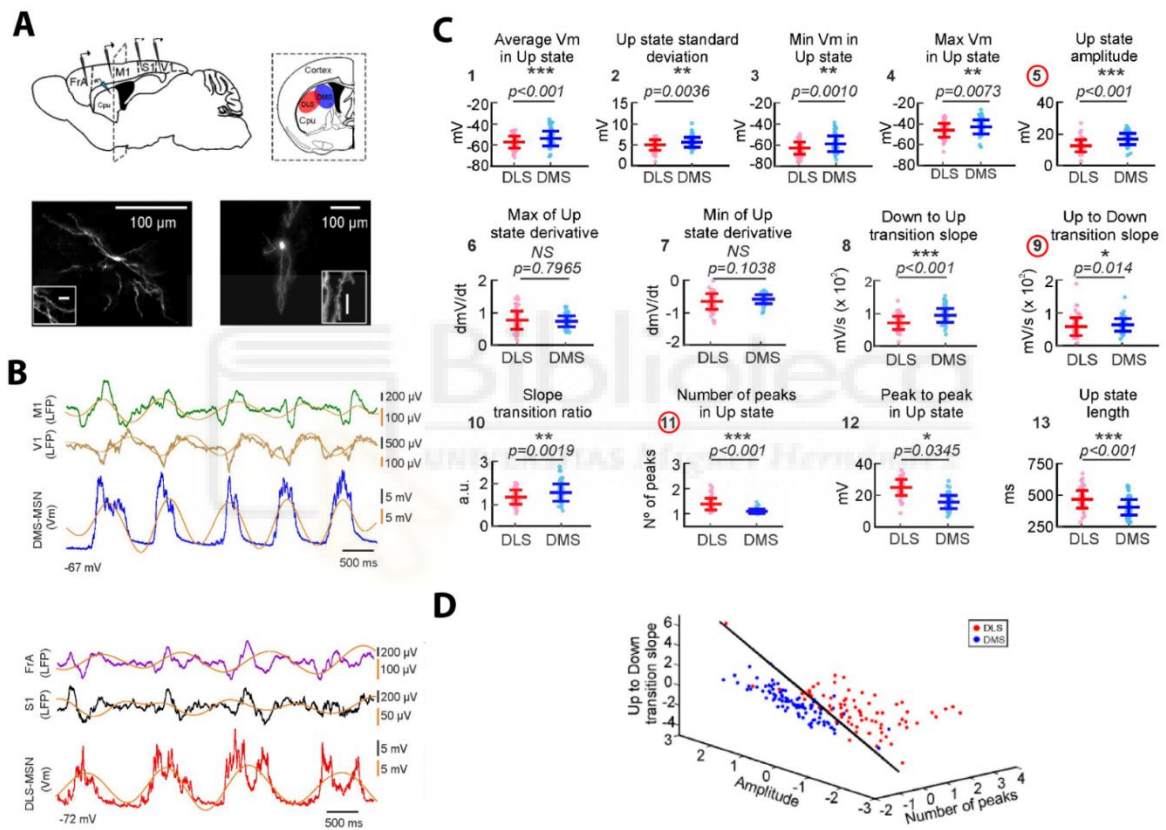
Fig 1 Slow wave oscillatory activity in the corticostriatal system. (A) Top: schematic of extra- and intracellular recording's locations. Bottom: biocytin-filled MSN reconstruction. (B) Representative example of MSNs intracellularly recorded in conjunction with two LFPs (green, brown, purple and black lines) in distinct cortical areas and relative IMFs (orange lines) carrying the slow wave oscillation. (C) Statistical comparison of up state features between the DS subregions. (D) Subspace of classification based on the RFE results (select features: red circles in C). Dots represent individual MSNs recorded in DLS (red) or DMS (blue). Classification hyperplane obtained after training the SVM with linear kernel in black.

4.2 Dorsomedial and dorsolateral medium-spiny neurons differ in their coupling to neocortical areas

DLS-MSNs displayed a characteristic high number of peaks (Fig 2A), to the extent that, the net bimodal distribution of membrane potential values (i.e., hyperpolarised in down states and depolarised in up states) found in DMS-MSNs, it was replaced by a high proportion of transition values in DLS-MSNs (Fig 2B). Since striatal oscillations rely on the cortical ones (Kasanetz et al., 2002), and *in vitro* striatal preparations lacks the spontaneous slow wave (Planert et al., 2013) that instead can be found in neocortical slabs (Sanchez-Vives and McCormick, 2000), we suspected a cortical contribution to the number of peaks during up state in MSNs. If this hypothesis was correct, then DS subregions more strongly connected to given cortical areas should exhibit features of the slow oscillations similar to those areas (e.g., number of peaks). Hence, we directed whole-cell patch-clamp recording in cortical areas connected to the DS: frontal associative cortex (FrA), M1, S1 and V1. We recorded in this manner 21 cortical neurons from L5 during spontaneously occurring up and down states (Fig 2C). M1 and S1 neurons showed on average a significantly higher number of peaks than FrA and V1 during up states (Fig 2C). Together with the known anatomy (Alloway et al., 2006), this suggested that the propensity to exhibit up state peaks in DLS-MSNs could be explained by the strong afferent connections received from M1 and S1, which impose their peaks onto this MSNs population.
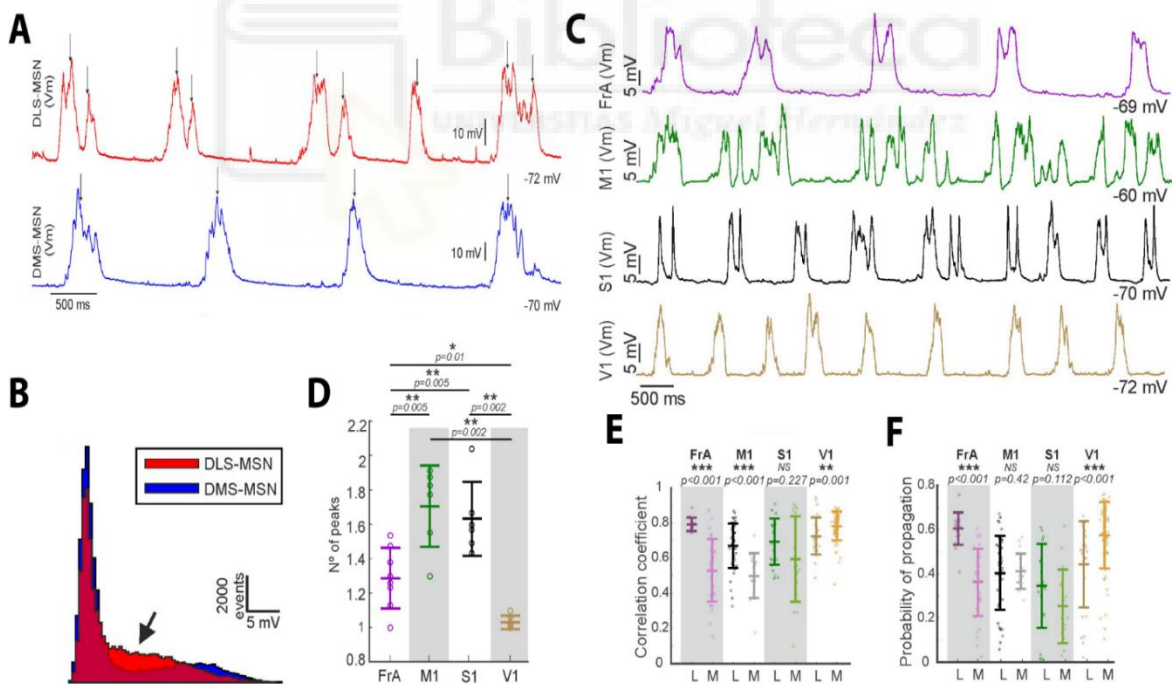
Fig 2 Slow wave characteristics in the DS subregions are due to their different cortical coupling. (A) Peaks individuation in DLS- and DMS-MSNs. (B) Representative example of Vm values distribution during slow wave oscillation of a DMS- and a DLS-MSN. Black arrow indicates transitions values of the Vm (i.e., after-peak valleys) nested in the up state. (C) Membrane potential during slow wave oscillation in distinct cortical areas. (D) Comparison of the number of peaks during up state in the membrane potential of cortical areas in C. (E) Comparison of IMFs' cross-correlation coefficients between LFPs and MSNs membrane potential

in DLS and DMS (respectively, L and M). (F) Probability of up state occurrence in the membrane potential after its detection in the cortical LFP (x-axis labels as in E).

Propagating from the neocortex, the slow wave activates MSNs (Wilson and Kawaguchi, 1996) and interneurons (Reig and Silberberg, 2014) in the DS. If differences between DLS and DMS-MSNs were due to distinct relationships with cortical areas, then the slow wave cycle had to reflect such differences. By using a noise-assisted multivariate empirical mode decomposition algorithm (NA-MEMD; see **3.8**), we decomposed cortical LFPs and MSNs membrane potential slow wave activity in its oscillatory constituents, and selected the mode (IMF) carrying only the slow wave oscillation (Fig 1B). LFPs and membrane potential IMFs were compared with respect to their cross-correlation during joint recordings. DLS- correlated more than DMS-MSNs with FrA and M1 (Fig 2E). Conversely, DLS- were less correlated than DMS-MSNs to V1. Associated with this measure, we computed the probability that the network transition from down to up states in the different LFPs is followed by the same transitions in the two MSNs populations, namely the probability of corticostriatal up states propagation. DLS- and DMS-MSNs did not differ with respect to M1 and S1 in this measure (Fig 2F), but in DLS-MSNs there was a significantly higher probability of propagation from the FrA than in DMS-MSNs, while the opposite relationship hold for the V1. Since the FrA produces significantly more peaks than V1, these results further confirmed their different coupling to DLS- and DMS-MSNs.

In summary, the activity from frontal (FrA) and sensorimotor regions (M1 and S1) is more tightly coupled to the DLS-MSNs, while the occipital region (V1) with DMS-MSNs.

4.3 Functional connectivity segregates dorsomedial and dorsolateral medium-spiny neurons with a sharp boundary

So far, in order to evaluate the homology between primate and rodent DS, we explored the latter by referring to two different subregions: DLS in homology to the putamen and DMS in homology to the caudate nucleus. However, in the mouse the two DS subregions are not anatomically distinguishable as in the primate, leaving the possibility that, by transition from one to the other along the DS mediolateral axis, we could meet a third population (dorsocentral, DCS) of MSNs, whose slow wave oscillation and cortical coupling would differ from the remaining and be absent in the primate. In Figure 3A, we represent this as our hypothesis number 2 (Hyp 2). The first (Hyp 1), would see a continuous and gradual change in MSNs cortical coupling, in which transition values would occupy the space between the two extremes (i.e., DMS and DLS). A third, last hypothesis (Hyp 3), would see DSL and DMS as the only two subregions in homology

with the primate. However, in the mouse they would be individuated just by the cortical functional connectivity and not by the DS macro-anatomy.

In order to select among these three possibilities, we intracellularly recorded MSNs at DCS coordinates (see **3.3**) and extracted the 13 features of above expressed by their slow wave oscillation. Each of these neurons was then projected in the standardised space used to classify DLS- and DMS-MSNs (Fig 3B). To understand which was the valid hypothesis among the suggested ones, the projection of the distribution of these data was evaluated with respect to the hypervector obtained with the SVM for the DMS/DLS classification (Fig 3A). If the DCS distribution would peak along the hypervector between (Hyp 1) or outside the previous two (Hyp 2), then the DCS would be a further specialised subregion with a characteristic cortical coupling. On the contrary, if the DMS and DLS are the only two identifiable subregions, then the DCS distribution should contain MSNs that belong to one of the former populations (Hyp 3). Our results show that the DCS distribution is composed of MSNs that either belongs to the DMS or to the DLS categories, supporting Hyp 3. Indeed, the probability density distribution of DCS (Fig 3C) was different from either the DMS and DLS taken alone ($p < 0.01$) because it was statistically equivalent to their combination ($p = 0.685$). Thus, DLS- and DMS-MSNs are separated by a sharp boundary and form two discrete populations in their functional connectivity to the neocortical areas examined.
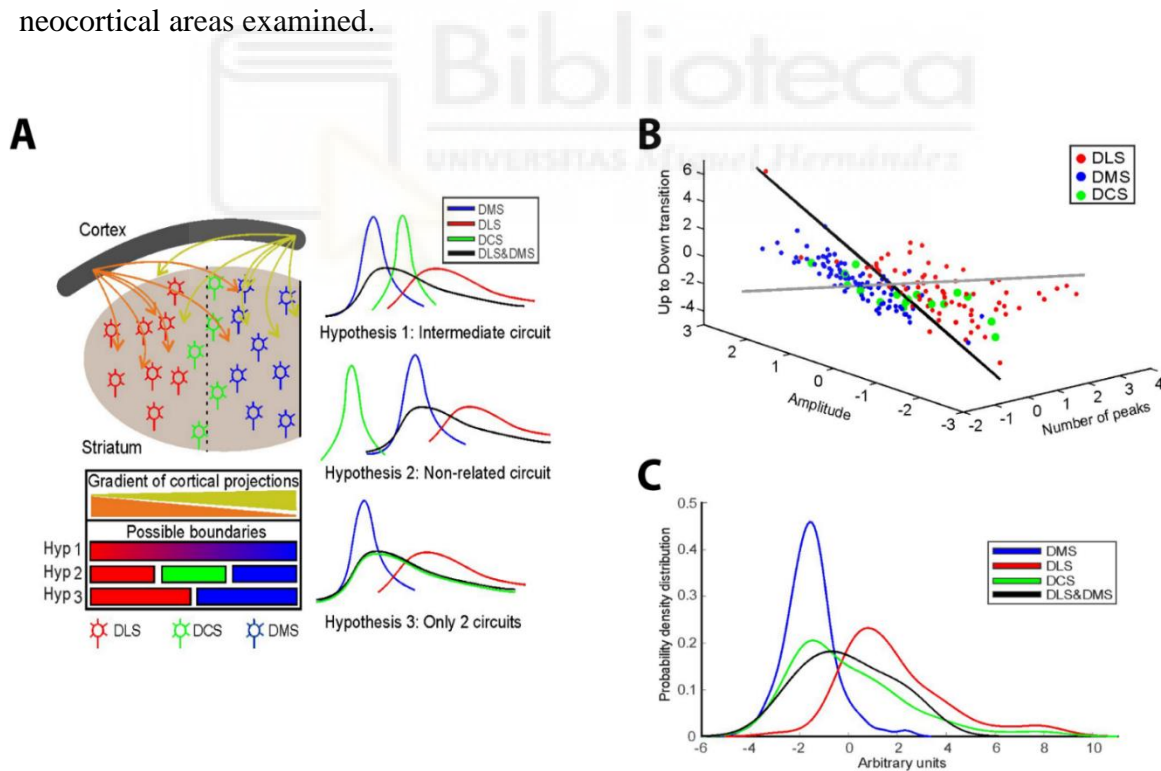
Fig 3 Determination of the functional boundaries in the dorsal striatum. (A) Graphical representation of the three-hypotheses scenario for the dorsal striatal segregation. (B) RFE classification space for DLS-, DMS- and DCS-MSNs. Classification plane in black and orthogonal hypervector for data projection in grey. (C) Probability density distributions projected onto the orthogonal hypervector of B. Empirical DCS-MSNs distribution (green) overlaps the theoretical mean distribution between DMS- and DLS-MSNs (black).

4.4 Visual response at the circuits' boundary

In order to confirm the results obtained through the spontaneous slow wave oscillatory activity, we wanted to explore the DS sensory evoked activity. While both DSL- and DMS-MSNs respond to contra- and ipsilateral whiskers stimuli, visual responses evoked through the stimulation of the contralateral eye are confined to DMS-MSNs (Reig and Silberberg, 2014). Since the visual stimulation is the most discriminative between DLS and DMS, we used it to test the visual responses in the DCS (n= 17), with the expectation of finding responding DMS-MSNs and non-responding DLS-MSNs.

We found 8 DCS-MSNs (47%) responding to visual stimulation (Fig 4A). Surprisingly, 3 of them (17.3%) were classified as DLS-MSNs by our classifier based on spontaneous activity (against 29.4% of DLS expected to not respond, thus correctly classified). Since the classifiers' accuracy is around 88.6%, this means that it can make a wrong guess in 11.4% of cases. Because the proportion of responding DLS-MSNs was higher than such error rate, we could not entirely explain the discrepancy based only on a misclassification. Hintiryan and colleagues (2016) have found that, while the visual axons from V1 are mostly concentrated in the DMS next to the brain ventricle, more laterally, at our DCS coordinates, visual axons come from anteromedial (AM) and anterolateral (AL) visual cortical areas. Hence, we recorded the visual response of 10 additional DMS-MSNs and compared it to the DCS ones. If a different visual response was detected between responding DCS- (n= 8) and DMS-MSNs (n= 10), then we could explain it by the innervation of different neocortical visual afferents.
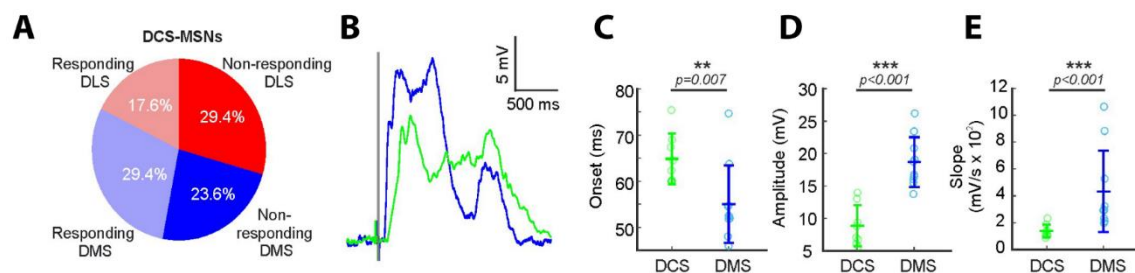
Fig 4 Visual response in the dorsal striatum to the stimulation of the contralateral eye. (A) Proportion of responding and non-responding DCS-MSNs classified as DLS- or DMS-MSNs. (B) Representative example of the waveform average visual response of a DMS-MSN (blue) and a DCS-MSN (green) aligned at stimulus onset (grey line). (C-E) Statistical comparison of the waveforms' parameters.

We found that DMS-MSNs respond more abruptly than DCS-MSNs (Fig 4B). Indeed (Fig 4C-E), the former population shows significantly bigger amplitude and steeper slope in the visual response (amplitudes DCS = 8.84 ± 3.15 mV, DMS = 18.67 ± 3.86 mV, p= 0.00009; slopes DCS = 139 ± 48.1 mV/s, DMS = 432 ± 302.9 mV/s, p= 0.0003). Importantly, as a strong discriminant between the different cortical origins of the two

responses (Fig 4C), the average onset delay of DCS-MSNs responses lagged by ~9 ms the DMS one (DCS = 64.84 ± 5.49 ms; DMS = 55.02 ± 8.37 ms, p=0.007). This suggested that, coherently with the AL and AM visual innervation of the DS (Hintiryan et al., 2016), DCS-MSNs responses were not mediated directly by V1.

Thus, there is the possibility that a small proportion of the MSNs originally classified as DLS for the up state characteristics, may receive a contribution from higher order visual areas fed by V1 (AL and AM). This suggests that considering additional areas of the neocortex may add further boundaries to the DS. Thus, complementing the spontaneous activity approach with cortically evoked activity (e.g., via sensory or electrical/optogenetic stimulation) may help in increasing the level of detail in identifying subregional functional specialisations of the DS.

4.5 Direct and indirect medium-spiny neurons differently integrate the slow wave oscillation in the dorsolateral striatum

In order to evaluate whether the participation in the direct or indirect pathway (see **1.1**) would affect the integration of the slow wave oscillation in MSNs, they were optogenetically identified as belonging to one pathway or the other (Fig 5A; see **3.5**) and their activity features analysed.

Significant differences in maximum and minimum membrane potential and its average value within up states were detected between iMSNs and dMSNs exclusively in DLS, showing always more positive values in iMSNs than dMSNs (Fig 5B). These results may reflect a difference in the engagement of hyperpolarising currents in the two DLS subpopulations during up states, with a higher drive in dMSNs than in iMSNs. Moreover, if our classifier is asked to classify iMSNs and dMSNs separately in DLS and DMS, it would fail in both cases (accuracy: 50% for DMS, 64% for DLS).

Taken together, these results suggest that the participation to the direct or indirect pathway can have some effect in corticostriatal functional connectivity only in the DSL. Yet, differently from the DLS/DMS marked segregation, such characteristics are not enough for our classifier to discriminate between the two pathways based solely on the up state fluctuations of the membrane potential.
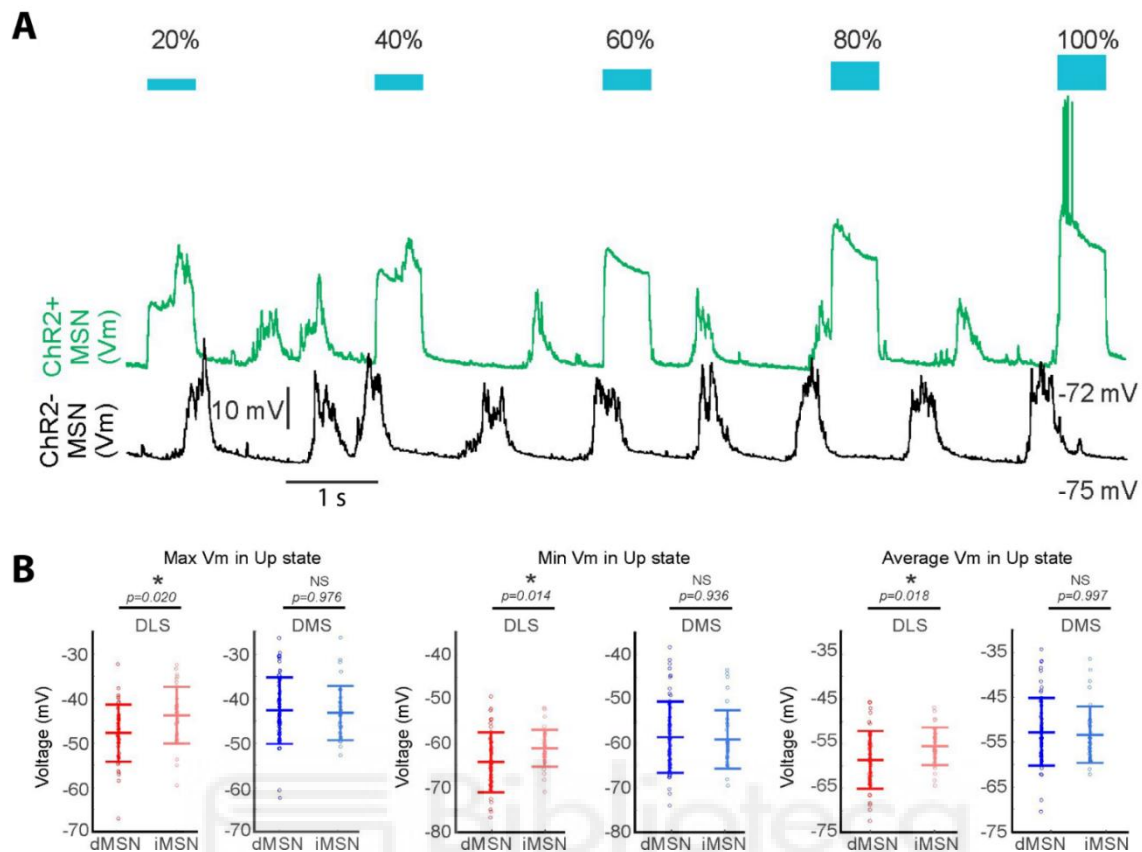
Fig 5 Slow wave oscillation in direct and indirect medium-spiny neurons. (A) Online identification of indirect (top, responding) and direct (bottom, non-responding) MSNs by opto-patch illumination. (B) Statistical comparison of slow wave oscillation parameters between direct and indirect MSNs in DLS and DMS.

Both DLS- and DMS-MSNs can respond to whiskers stimulation delivered either contra- or ipsilaterally (Reig and Silberberg, 2014). This means that the cortical area representing the whiskers (barrel cortex), is connected with the DS. Since it gets lost upon contralateral injection of TTX in the barrel cortex, it is thought that the ipsilateral response recorded in MSNs is mediated by corticostriatal fibres whose soma is excited by callosal afferents (Reig and Silberberg, 2016). In order to directly observe what is occurring in this area upstream to the DS, in the next part of the study, we will focus on the barrel cortex and characterise the propagation of activity through the corpus callosum.

4.6 The posterolateral barrel cortex is the main cortical recipient of the ipsilateral whiskers system activity.

Whiskers-mediated active exploration drives c-Fos expression in the barrel cortex (BC) (Staiger, 2006). Classically, experiments focused on trimming all the whiskers except one found staining of c-Fos$^+$ nuclei in the representing barrel of the hemisphere contralateral to the spared whisker (Reiner et al., 2017, Antón-Bolaños et al., 2019). This indicated the activation of somatotopic thalamocortical synapses promoting the metabolic activity in post-synaptic neurons. The BC can be also activated by ipsilateral whiskers, most likely through its callosal innervation (Shuler et al., 2001; Reig and Silberberg, 2016; Petreanu et al., 2007). However, to our knowledge, the pattern of c-Fos expression induced by the use of ipsilateral whiskers during active exploration has never been described. In the attempt to isolate such a pattern, we wanted to find a method to completely suppress the metabolic activity recruited by the sensory periphery in the BC which follows the thalamocortical pathway. Once obtained, if c-Fos$^+$ nuclei would have been present in the deafferentiated BC (BC$_{deaff}$), we would have been able to suspect a callosal origin of this activity, recruited by the active contralateral BC. Since the flattened preparation of the cortex allows the visualisation of the BC somatotopic cytoarchitecture through tangential slices, we used such preparation to study the distribution of c-Fos$^+$ nuclei.

For their habituation, mice were free to explore an empty arena (size: 50 x 50 x 70 cm) in the dark. The following day, in the same arena, they were exposed to newly placed objects for 45 minutes and then sacrificed for follow-up histology of the brains and c-Fos immunostaining (see **3.10**). In order to answer our question, we manipulated their whiskers differently before placing them in the arena this second time.

In one condition, we bilaterally trimmed the whiskers (TW, n$_{hemisphere}$= 10, 5 mice; Fig 6B). Thus, we compared the density of c-Fos$^+$ barrel nuclei of TW mice with the one of mice with intact whiskers (IW, n$_{hemisphere}$= 6, 3 mice; Fig 6A), and found no statistical difference (Fig 6E; density (#nuclei/ 0.1 mm^2): IW= 141.8 [69.0-202.4], TW= 167.3 [98.7-274.2], p= 0.3132), suggesting that BCs were still active despite the complete whiskers trim.

In order to completely deafferentiate the BCs we needed to avoid this phenotype. Thus, we subcutaneously injected lidocaine bilaterally in the whiskers-pads (BL, n$_{hemisphere}$= 8, 4 mice; Fig 6C) as this method is capable of blocking whiskers-evoked activity in BC neurons in a complete and long-lasting manner (Gener et al. 2009). Hemispheres collected from mice under bilateral lidocaine resulted in an extremely lower density of c-Fos$^+$ barrel nuclei when compared to hemispheres of the trimmed whiskers mice (Fig 6E; density (#nuclei/ 0.1 mm^2): BL= 8.2 [3.6-22.9], TW= 167.3 [98.7-274.2], p= 4.5 x10^{-5}). In contrast with previous conditions, this indicated that the two BCs were strongly deafferentiated from the whiskers and that, most importantly, other possible cortico-cortical or subcortical activity recruitment of the BC originating in the home hemisphere was not enough to trigger the expression of c-Fos in barrels' columns.

Thus, the unilateral subcutaneous injection of lidocaine in one whiskers pad (UL, $n_{hemisphere}$= 4, 4 mice; Fig 6D) was expected to block the thalamocortical input to the contralateral BC, enabling us to check for the presence of activity related to the use of ipsilateral whiskers (Fig 6D, schema). Indeed, c-Fos$^+$ barrel nuclei density was clearly higher in the deafferentiated BC (BC$_{deaff}$) upon unilateral lidocaine injection when compared to the bilateral cohort (Fig 6E; density (#nuclei/ 0.1 mm^2): UL= 80.2 [40.3-100.1], BL= 8.2 [3.6-22.9], p= 0.0162). This strongly suggests that, under unilateral injection of lidocaine, the active BC triggered activity in the BC$_{deaff}$. To further explore this result, we computed the density of c-Fos$^+$ barrel nuclei separately for the five rows (i.e., from A to E) and normalised for the maximal density across rows for each BC$_{deaff}$. We found that the density of c-Fos$^+$ nuclei was differently distributed across rows (Kruskal-Wallis test: p= 0.0021, df= 4, χ^2 = 16.86; Fig 6F). Specifically, density in row A was significantly higher than in both row D and row E (Fisher's LSD test: p_{AvsD} = 0.0030; p_{AvsE} = 7.0 x10^{-4}) similarly to the one of row B (p_{BvsD} = 0.0209; p_{BvsE} = 0.0063), with the rest of comparisons being statistically not significant (p_{AvsB} = 0.5093; p_{AvsC} = 0.0673; p_{BvsC} = 0.2421; p_{CvsD} = 0.2544; p_{CvsE} = 0.1188; p_{DvsE} = 0.6746). In addition, we ran a separate analysis on the septal territories comprised between barrel rows (i.e., A/B, B/C, C/D and D/E septal areas). The analysis revealed a homogeneous distribution of immunopositive nuclei (Kruskal-Wallis test: p= 0.0507, df = 3, χ^2 =7.79; Fig 6G), which still tended to peak in the posterolateral region of the BC (i.e., A/B septa), albeit not significantly.

These physiological data are coherent with anatomical ones of prominent callosal innervation of septal agranular areas, especially row A barrel columns and their immediate agranular surroundings (Olvarria et al., 1984, Koralek et al., 1990) with some involvement of the row B. Thus, we concluded that the latter, posterolateral portion of the BC is the main recipient of the activity generated by the use of ipsilateral whiskers during novel-objects exploratory behaviour, and that this relationship is likely mediated by callosal afferents at the cortical level.
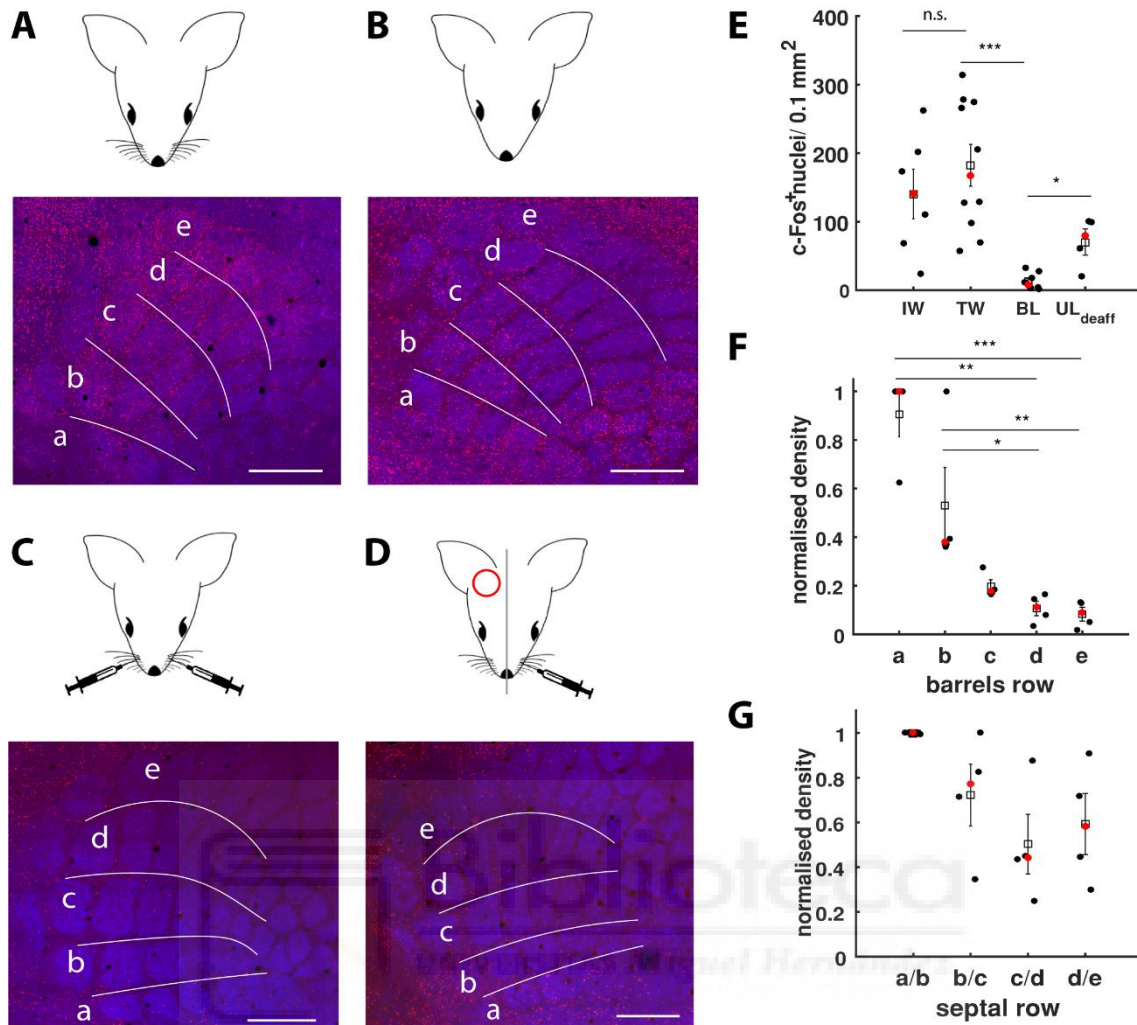
Figure 6 Isolation of the callosal recruitment of the barrel cortex observed through c-Fos immunostaining. (A) Widespread expression of c-Fos (anti-c-cFos, red channel) in the barrel cortex (anti-VGlut2, blue channel) of mice carrying intact arrays of whiskers after a period of exploration. (B) Same of A but upon trimming of the whiskers. The c-Fos expression shows that the barrel cortex was still active despite the intervention. (C) Bilateral subcutaneous injection of lidocaine in the whisker pads abolished the barrel cortex activity resulting in the almost complete absence of c-Fos expression. (D) Unilateral injection of lidocaine results in some expression of c-Fos in the barrel cortex. Letters indicate the identity of the rows. (E) Quantification of c-Fos$^+$ nuclei in the 4 conditions of A,B,C and D; respectively: intact whiskers (IW), trimmed whiskers (TW), bilateral injection of lidocaine (BL), unilateral deafferentation through lidocaine (UL$_{deaff}$). (F) Statistical comparisons of c-Fos$^+$ nuclei density normalised for the maximum across barrel rows of the UL$_{deaff}$ barrel cortex. (G) Statistical comparisons of c-Fos$^+$ nuclei density normalised for the maximum across septal rows of the UL$_{deaff}$ barrel cortex. Scale bars are 400 μm.

4.7 Contra- and ipsilateral subthreshold responses evoked by whisker stimulation in the barrel cortex and its subregions.

The c-Fos essays allowed us to obtain a functional and topographic overview at once of the cortical relationship between the two whiskers systems that are activated during the exploratory behaviour of the mice. However, synaptic transmission mechanisms

underlying this relationship were still unknown. To study such mechanisms, we recorded neurons by *in vivo* whole-cell patch-clamp in anaesthetised mice.

c-Fos$^+$ nuclei in the BC$_{deaff}$ distributed heterogeneously, by increasing from row E to row A territory. Hence, our objective was to compare subthreshold whiskers-mediated responses of single neurons belonging to 1) the BC area densely innervated by callosal axons and metabolically active despite peripheral deafferentation with 2) a sparsely innervated, less active one. To satisfy the first prerequisite, we targeted the posterolateral aspect of the BC, while for the second we directed our recordings towards its anteromedial aspect (Fig 7A). To perform well placed craniotomies for such a task, we used coordinates derived from the average BC map obtained through intrinsic optical imaging in Knutsen et al., (2016), ideally pointing to the representation of the row A (from bregma: AP -2, ML -3.8) and row E (from bregma: AP -1, ML -3.2) or within their immediate proximity. Further, to increase the precision of sampling from these two sites prior to whole-cell recordings, we assessed the whiskers-to-barrels mapping by means of contralateral stimulations of the target whiskers coupled with LFP recordings over the exposed dura (see **3.14**). Finally, patch pipettes were loaded with biocytin to allow the anatomical localisation of pipettes penetrations and streptavidin-labelled neurons, both for cortical depth and BC area (Fig 7B), and we also included cases in which we were not able to align recorded neurons with the BC geometry. Hence, to admit some anatomical uncertainty, we refer to the area of sampling containing the row A representation as to the posterolateral BC (plBC) and to the one containing the row E representation as to the anteromedial BC (amBC). For sensory stimulations, target whiskers (i.e., A2+ A3 and E2+ E3) were glued together separately for each row (Fig 2A). Next, they were fixed to a custom-made whiskers-puller stimulator (see **3.16**). Once a cell was patched, caudo-rostral pull stimulations of the whiskers' groups lasting 15 ms were delivered every 3 or 5 s.

In order to study the dynamics of subthreshold synaptic recruitment in the neurons, we anaesthetised the mice. Under deep anaesthesia, membrane potential of cortical neurons oscillates periodically at ~1 Hz (Fig 7C). A period of synaptically active state characterised by membrane depolarisation (up state) alternates with a period of synaptically inactive state characterised by membrane hyperpolarisation (down state). Because the spontaneous up and down states have a strong impact on whisker responses (Petersen et al., 2003; Reig and Sanchez-Vives, 2007) we analysed stimulations-responses falling only in down state (see **3.15**), including cases in which sensory stimulation triggered state transitions.
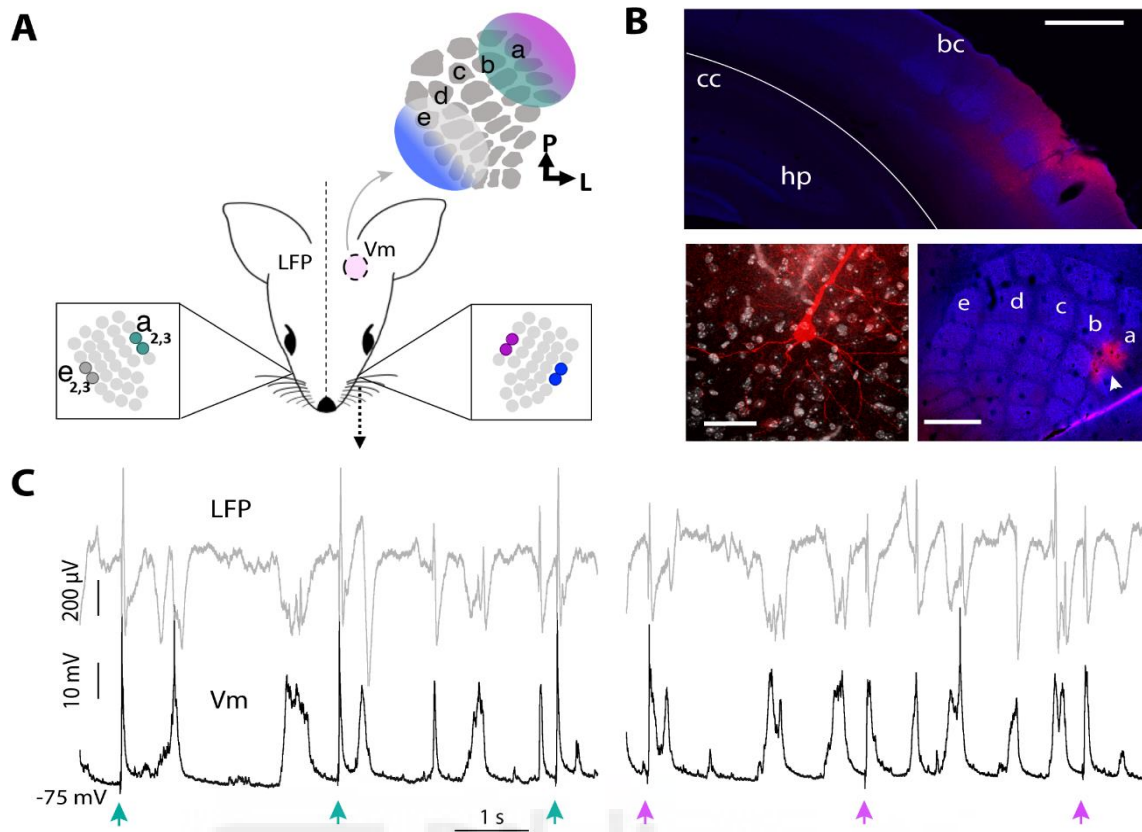
Figure 7 Experimental protocol. (A) Schematic drawing indicating the groups of whiskers stimulated within the whiskers arrays (boxes on the two sides of the mouse face) and the BC subregions targeted by the recordings (top right corner). Whiskers groups and BC subregions are colour-coded: purple and green indicate the rows A (respectively, ipsi- and contralateral) and the targeting of their representation in the plBC; blue and grey indicate the rows E (respectively, ipsi- and contralateral) and the targeting of their representation in the amBC. Membrane potential (Vm) was recorded in the left hemisphere, while collecting the homotopic local field potential (LFP) in the right. The black arrow indicates the direction of the pull stimulation. (B) Top: coronal section of the BC showing the targeting of the posterolateral aspect through biocytin-streptavidin staining (red) and thalamocortical afferents individuating the barrels (VGlut2, blue). The staining is concentrated towards the last, more ventral barrels, indicating that the recordings were centred in the plBC. Scale bar 400 μm; bc= barrel cortex, cc= corpus callosum, hp= hippocampus. Bottom left: recorded neuron filled with biocytin surrounded by nuclei of neighbouring cells (streptavidin, red; DAPI, grey). Scale bar 40 μm. Bottom right: flatten preparation of the BC (barrels: VGlut2, blue) representative of recordings in the plBC (arrowhead: streptavidin, red). Scale bar 400 μm. (C) Representative intracellular (bottom) and simultaneous contralateral LFP (top) recording during sensory stimulation. The same neuron responded to contralateral (left, green arrows) and ipsilateral (right, purple arrows) stimulation of row A in the plBC.

In the whiskers system, ascending axons from barrelettes in the brainstem trigeminal complex cross the midline before feeding the contralateral thalamocortical pathway. For this reason, whiskers stimulation in one side of the snout primarily evokes a response in the contralateral BC of thalamic origin (Fig 8A, 8C-E). Instead, a response detectable in the BC ipsilaterally to the stimulation side (Fig 8B, 38F-H) is supposedly conveyed by callosal innervation (Shuler et al., 2001; Reig and Silberberg 2014, 2016). Since thalamocortical afferents in the BC are somatotopically arranged, we refer to homotopic stimulation as to when the row of stimulated whiskers matches their representation in the BC area of recording.

We sampled both contralateral and ipsilateral homotopic whiskers-evoked responses from 18 supragranular (L2/3, 24.7%), 18 granular (L4, 24.7%) and 37 infragranular neurons (L5, 30.1%; L6, 20.5%), for a total of 73 neurons. Moreover, two neurons from this pool in which the spike shape could be characterised, showed a remarkably short spike half-width ($<$ 0.7 ms; population median: 1.15 ms), thus we considered them as putative fast-spiking neurons, but we included them in the analysis because their subthreshold responses did not seem to differ from the general population (not shown). Since we wanted to focus on the synaptic recruitment exerted more directly by the afferent pathways, we restricted our analysis to the first components of the evoked postsynaptic potentials (PSPs). Thus, we analysed the response latency (i.e., onset delay), the delay to the highest peak within the first 300 ms, response amplitude, and the speed of its onset-to-peak rising phase (i.e., slope).

In down state, firm pull of the whiskers groups robustly evoked postsynaptic potentials in all layers, that were dominated by an excitatory component (EPSPs). We found that contralateral EPSPs of supra-, granular and infragranular neurons did not differ statistically for all the parameters considered (Fig 8A and Tab 1). Hence, we could activate the entire cortical column similarly. This indicated that we could reliably recruit supra- and infragranular layers which contain callosal-projection neurons (Wise and Jones, 1976), a fundamental aspect to test the callosal contribution in response to ipsilateral stimulations.

Congruently with other works (Reig and Silberberg, 2014; Manns et al., 2004), homotopic ipsilateral responses appeared generally weaker than the contralateral counterpart (Fig 8B), but they revealed a difference in the timing of layer excitation (Tab1; Kruskal-Wallis test on onset delay: χ^2= 6.92, df= 2, p= 0.0314). Indeed, while depolarisations occurred with comparable amplitude and similar speed of the rising phase (i.e., slope) across layers, infragranular neurons responded significantly faster than granular and supragranular ones (Fisher's LSD test on onset delay: p_{IvsG}= 0.0401; p_{IvsS}= 0.0260), confirming similar findings on suprathreshold activity (Plomp et al., 2017). Instead, onset delay of supra- and granular neurons did not differ (p_{SvsG}= 0.8813).

Overall, the thalamocortical excitation provoked by contralateral whiskers (row) displacement was able to recruit activity comparably across BC layers. Ipsilateral stimulations provoked responses with similar dynamics across layers too, except that they recruited infragranular layers more rapidly (3-4 ms) than upper ones.

stimulation side	parameter	cortical layers			Kruskal-Wallis test	
		supragranular	granular	infragranular	χ2 (df=2)	p
contralateral	onset delay (ms)	12,6 [11,1-14,5]	11 [9,8-12,8]	13,1 [8,8-14,7]	2,3	0,3151
	peak delay (ms)	27 [24,7-41]	28,7 [22,2-35,3]	28,8 [23-39,9]	0,05	0,9723
	amplitude (mV)	22,1 [18,4-27,5]	20 [18,1-27]	19,2 [15,4-24,5]	0,53	0,7659
	slope (mV/s)	1938 [862-2402]	1309 [903-2199]	1562 [823-2450]	0,54	0,7615
ipsilateral	onset delay (ms)	19,6 [16,6-32,7]	20,6 [17-25]	16,5 [14,5-20,7]	6,92	0,0314*
	peak delay (ms)	74 [48,6-140,5]	84,3 [49,6-151,5]	49,6 [37,9-104,5]	3,57	0,1673
	amplitude (mV)	13,2 [9,5-23]	15,6 [11,7-20,5]	15,9 [11,1-22,1]	4,1	0,8028
	slope (mV/s)	284 [62-1017]	348 [87-702]	528 [152-997]	2,7	0,2587

Tab 1 Statistical comparisons of response parameters between cortical layers to contra- and ipsilateral whiskers stimulation. Infragranular neurons showed a significantly faster onset of the response to ipsilateral stimulation compared to more superficial layers. Data are reported as median [25th-75th quantile].

Next, we separated homotopic contralateral responses belonging to the two BC subregions in down state (plBC *vs* amBC) and we compared them with respect to onset delay, peak delay, amplitude and slope (Fig 8C-E). None of the parameters differed statistically between plBC and amBC for supra-, granular and infragranular layers (Tab 2). However, a slightly stronger response was apparent in the grand averages of plBC neurons, especially in supragranular layers (Fig 8C). Indeed, when the cortical column was considered altogether by pooling the data across layers, the amplitude of the response to contralateral stimulation resulted significantly stronger (medians' difference= 3.5 mV) in plBC than amBC neurons (plBC: 21.9 [18.1-26.8] mV, amBC: 18.4 [15.1-23] mV; p= 0.0414).

Then, in the same pool of neurons, we compared the responses evoked through the homotopic ipsilateral stimulation (Fig 8F-H). This time, differences in the grand averages between plBC and amBC neurons were evident (Fig 8F-H, left), and more obvious in supra- and infragranular layers than in the granular one. Indeed, in supragranular layers, the amplitude's peak was reached earlier, accompanied by wider amplitude and a much steeper slope in plBC than in amBC neurons (Tab 2). In infragranular layers, the two populations differed in the same parameters. In addition, a much faster onset delay characterised responses in plBC compared to amBC ones (medians' difference= 5.7 ms; Tab 2). In the granular layer, instead, the onset delay did not differ between plBC and amBC responses, but we detected faster peak delay, wider amplitude, and a statistical tendency to show faster slope (p= 0.0529) in the former than in the latter BC subregion (Tab 2). These results demonstrate that plBC neurons respond to homotopic ipsilateral stimulation much more vigorously than amBC ones.
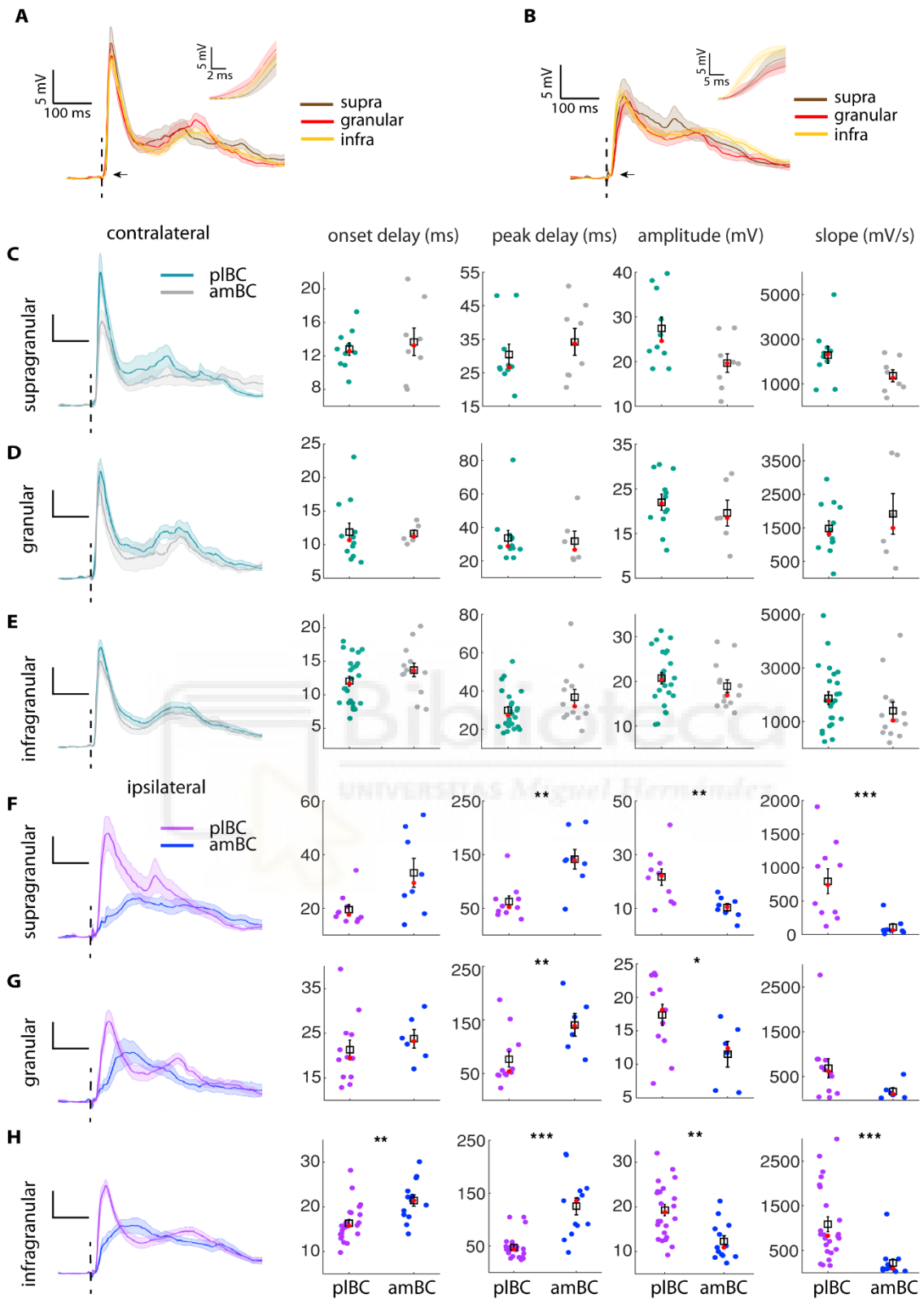
Fig 8 Grand average of sensory responses. (A) Grand average of sensory responses upon homotopic contralateral stimulation in the different cortical layers pooled across BC subregions. Responses are aligned at the stimulation onset (black dashed line). Inset: magnification of the waveforms at response onset (black arrow). (B) Same of A for ipsilateral responses. (C-E) Left: same of (A) for responses recorded in plBC and amBC. Black solid lines: vertical= 5 mV, horizontal= 100 ms. Right: statistical comparison of response parameters. (F-H) Left: same of (A) for ipsilateral responses recorded in plBC and amBC. Black solid lines: vertical= 5 mV, horizontal= 100 ms. Right: statistical comparison of response parameters. Shaded areas= ±S.E.M.

stimulation side	layer	onset delay (ms) plBC	amBC	p	peak delay (ms) plBC	amBC	p
contralateral	supragranular	12,6 [11,1-14,2]	13,2 [10,1-16,8]	0,8286	26,6 [25,9-32,1]	33,7 [24,3-43]	0,7618
	granular	10,6 [8,6-13,9]	11,2 [10,7-12,8]	0,5532	28,7 [27,1-34,5]	26,8 [21,5-37,8]	0,6165
	infragranular	11,6 [8,7-14,7]	13,6 [12,3-15,4]	0,2935	27,1 [21,5-35,3]	31,9 [27,1-43,2]	0,1267
ipsilateral	supragranular	17,6 [16-20,7]	29,5 [21,4-47,6]	0,0545	52,5 [41,6-67,3]	139,5 [121,9-174,4]	**0,0085**
	granular	19,5 [15,2-24,8]	23,2 [20-28,1]	0,2831	52,7 [47,7-75,9]	138,8 [100,3-173,9]	**0,0069**
	infragranular	15,7 [13,9-18,5]	21,4 [18,1-24,2]	**0,0017**	44 [29,9-49,2]	135,7 [85,1-155,8]	**0,0001**

stimulation side	layer	amplitude (mV) plBC	amBC	p	slope (mV/s) plBC	amBC	p
contralateral	supragranular	24,5 [21,9-36,4]	19,6 [15,3-24,4]	0,0545	2303 [1866-2629]	1267 [779-2019]	0,0676
	granular	21,7 [18,4-27,1]	18,4 [15,1-27]	0,3845	1310 [987-2159]	1501 [783-3681]	0,8201
	infragranular	20,3 [16,7-26,4]	16,9 [15-21]	0,3012	1769 [1000-2642]	1044 [581-1789]	0,1569
ipsilateral	supragranular	22,1 [12,5-26,7]	10,3 [8-13,2]	**0,0085**	741 [328-1140]	60,9 [45,4-116]	**0,0009**
	granular	18 [13,8-22,2]	12,4 [6,1-15,1]	**0,032**	616 [149-874]	111 [29-194]	0,0529
	infragranular	18,7 [13,7-23,8]	10,9 [9-15,2]	**0,001**	830 [501-1716]	93,5 [55,9-219]	**>0.00001**

Tab 2 Statistical comparison of the parameters of contra- and ipsilateral sensory responses shown in Fig 3 between plBC and amBC neurons, separated for cortical layer. Significant p-values are in bold.

Moreover, in response to ipsilateral stimulation, significant interlaminar differences were not detected in either BC subregions (not shown). Yet, onset delays strongly tended to differ across layers in plBC (Kruskal-Wallis test on onset delay: χ^2= 5.75, df= 2, p= 0.0562), where infragranular layers showed the fastest response onset (~16 ms; Tab 2).

Given the unusual properties of the ipsilateral plBC response, we wondered whether it could be the outcome of an increased intrinsic excitability of the neurons rather than of a distinct synaptic recruitment. In order to distinguish between the two possibilities, we compared intrinsic membrane properties between plBC and amBC neurons (i.e., membrane time constant, input resistance and capacitance), separately for up and down states (Tab 3). Because no statistical differences were detected, the ipsilateral responses were the outcome of a distinct synaptic recruitment in plBC compared to amBC.

parameter	BC territory plBC	amBC	Wilcoxon rank sum test p
τ (ms)	7.0 [2.3-10.9]	7.1 [4.8-15.7]	0.2896
R_{down} (MΩ)	51.0 [42.0-65.7]	49.9 [39.6-70.9]	0.9867
R_{up} (MΩ)	49.9 [44.3-61.7]	47.8 [38.4-67.3]	0.6477
C_{down} (pF)	133.4 [55.1-221.5]	136.0 [93.0-210.5]	0.5435
C_{up} (pF)	134.0 [51.3-220.7]	144.5 [106.1-226.5]	0.3294

Tab 3 Statistical comparisons of intrinsic membrane properties between neurons sampled in the two barrel cortex subregions. No statistical difference can be detected in relevant membrane properties across network states for the two pools of neurons, suggesting that differences in whiskers-mediated responses only depend on a different synaptic recruitment. Data are reported as median [25th-75th quantile].

Since 1) the plBC is known to receive the widest callosal innervation (Ivy and Killackey 1981; Olavarria et al., 1984; Koralek et al., 1990; Wang et al. 2007; Suarez et al., 2014a; Fenlon et al., 2017; Zhuo et al., 2021), 2) the membrane properties of plBC and amBC neurons did not differ (Tab 3), and 3) the plBC (i.e., row A and, to a lesser extent, row B) remained active despite the block of the contralateral peripheral input (Fig 6D-G), differences in whiskers-mediated responses point to a stronger callosal recruitment in plBC than in amBC.

Likely, the stronger activation of the cortical column in plBC of the opposite hemisphere, in particular the supragranular callosally-projecting layer (Fig 8A), may contribute to such subregional differences. Yet, disregarding the underlying synaptic pathway, the above results add fundamental aspects to the physiology of the BC, posing plBC neurons as exquisitely sensitive detectors of ipsilateral row A-whiskers displacement.

4.8 Ipsilateral stimulation recruits feed-forward inhibition in the barrel cortex

In order to better characterise these responses for their dependence on callosal afferents, we tested the presence of feed-forward inhibition. This operation has been found to be exerted by callosal axons in the mouse primary auditory cortex (Slander and Isaacson 2020, Rock and Apicella 2015) and prefrontal cortex (Anastasiades et al., 2018), in the cat primary visual cortex (Conti and Manzoni, 1994), but more rarely in the rat frontal cortex (Karayannis et al., 2006; but see Kawaguchi, 1992). In the BC, feed-forward inhibition on projection neurons is normally disynaptic and it is well known to operate at least in the thalamocortical circuit. For example, in the thalamorecipient granular layer, feed-forward inhibition relies on GABAergic Parvalbumin- and Somatostatin-positive interneurons (Staiger et al., 1996; Tan et al., 2008). Acting on projection neurons, this circuit motif can modulate the time window for the integration of thalamic inputs (Gabernet et al., 2005) and be modulated by the direction of whiskers deflection (Wilent and Contreras, 2005). However, IPSPs evoked through ipsilateral whiskers stimulation have not been yet characterised for the BC (Naka and Adesnik, 2016).

In order to decompose the excitatory and inhibitory response components induced by ipsilateral stimulation, we filled the pipettes with low chloride intracellular solution and injected positive current into the neurons, depolarising them close to their excitatory reversal potential (~ 5 mV). Then, we delivered contra- and/or ipsilateral homotopic stimulations. Contralateral responses were sampled in 4 plBC and 2 amBC infragranular neurons plus 1 amBC granular neuron (subregions and laminae pooled: n= 7). Ipsilateral responses were sampled in 8 plBC and 5 amBC infragranular neurons, 1 granular neuron in both subregions, and 1 plBC and 3 amBC supragranular neurons (laminae pooled plBC: n= 10; laminae pooled amBC: n= 9).

We found that that both contra- and ipsilateral stimulations could reliably evoke feed-forward inhibition in the BC. Figure 9A shows the grand average obtained for contra- (n= 7) and ipsilateral (n= 19) inhibitory responses, together with the excitatory counterpart (n= 73 neurons), both averaged disregarding cortical layers and BC subregion. We found that the median peak delay of excitation and inhibition was statistically equivalent in

contra- and in ipsilateral responses, suggesting that on average inhibitory and excitatory potentials peak simultaneously in both cases (contra $_{exc\ vs\ inh}$: 28.2 [24.2-38.8] *vs* 30.2 [29.2-36.7], p= 0.3360; ipsi $_{exc\ vs\ inh}$: 61.8 [44.8-136.3] *vs* 62.9 [38.9-99.5], p= 0.4724). In the same pool of contralateral responses, we compared the EPSPs and IPSPs onsets. IPSPs lagged EPSPs median onset by 4 ms (EPSP= 12.4[9.6-14.5] ms, IPSP= 16.4[11.5-19.5] ms) but, likely due to the small sample size of IPSPs or the scarcity of fast-responding thalamorecipient granular samples (n= 1), onsets were not statistically distinct (p= 0.1731). Yet, we were interested in this estimate of the EPSP-IPSP onsets sequence as a means of comparison while looking at the ipsilateral one.

The differences in the excitatory PSPs components in the two BC subregions were suggestive of parallel differences in the inhibitory ones. Hence, we compared the onset delay of excitation and inhibition separately in plBC and amBC neurons. In amBC, onset of the IPSP (n= 9) was severely delayed (almost 12 ms) compared to the EPSP (n= 27) (EPSP= 22.6 [18.5-27.7] ms, IPSP= 34.3[32.9-44.1] ms, p= 1.06×10^{-5}). In plBC, instead, IPSPs lagged EPSPs onset by only 4.9 ms (EPSP= 16.4[15-20], IPSP= 21.3[19.3-27.8], p= 0.0028). Thus, in plBC the EPSP-IPSP onsets sequence shared similarities in timing with the contralateral estimate (4 ms).

These results suggested that the ipsilaterally-evoked feed-forward inhibition had different characteristics across the BC. To confirm it, we statistically compare them. In line with the expectations (Fig 9B-C), the ipsilateral whiskers stimulation induced inhibitory responses with earlier onset and peak in plBC than in amBC neurons (onset delay: plBC= 21.3 [19.3-27.8] ms, amBC= 34.3 [32.9-44.1] ms, p= 0.0054; peak delay: plBC= 39.2 [38.1-55.0] ms, amBC= 79.4 [74.4-134.0] ms, p=6.5×10^{-4}). In addition, strictly following the excitation profile (Fig 8F-H), response amplitude in plBC was stronger than the amBC one (amplitude: plBC= 13.5 [11.6-14.3] mV, amBC= 6.0 [5.1-7.6] mV, p=0.0350), and exhibited a much steeper rise (slope: plBC= 765.2 [459.9-1.7 $\times 10^3$] mV/s, amBC= 141.1 [49.8-218.1] mV/s, p=0.0041).
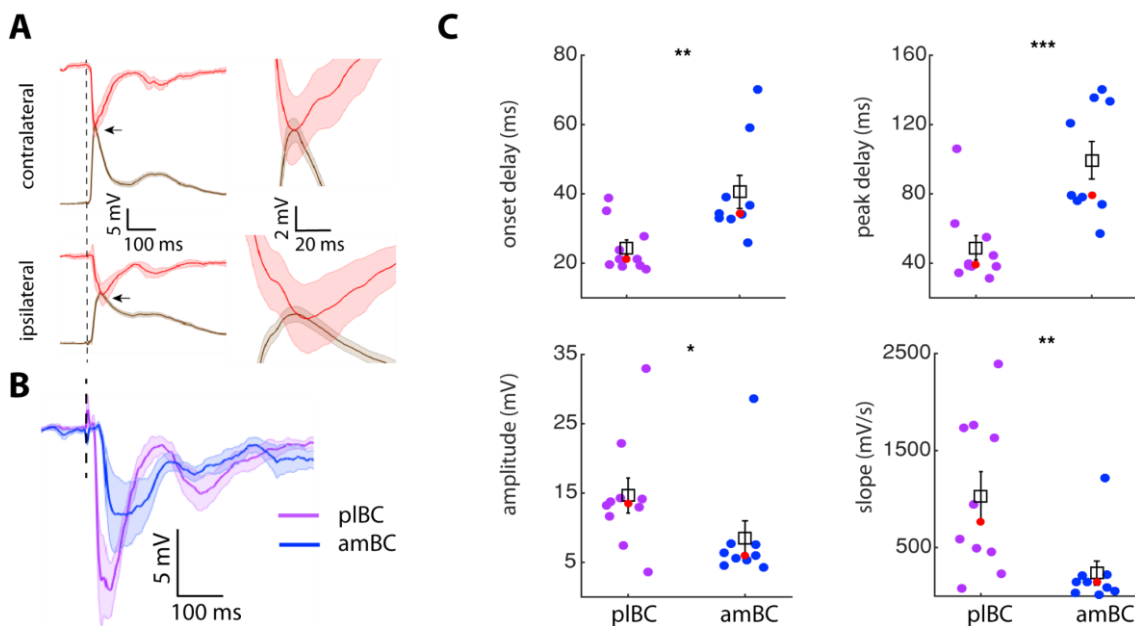
Fig 9 Inhibitory postsynaptic potentials evoked through ipsilateral whiskers stimulation. (A) Left: grand average of postsynaptic potentials evoked in down state at baseline (brown) and depolarised (red) membrane potential and aligned at stimulation onset. Right: insets showing the peak of the responses (black arrow on the left). (B) Grand average of inhibitory postsynaptic potentials evoked in down state at depolarised membrane potential and aligned at stimulation onset in the two subregions of the BC. Shaded areas= ±S.E.M. (C) Comparisons between parameters of the responses in (B).

Hence, comparably to the action of callosal axons in other cortical areas (Slander and Isaacson 2020; Rock and Apicella 2015; Anastasiades et al., 2018; Karayannis et al., 2006; Kawaguchi, 1992), these results show that the ipsilateral stimulation could recruit feed-forward inhibition in the BC. Importantly, such circuit operation varies in the two BC subregions, likely as a result of their distinct callosal innervation. Moreover, in line with thalamocortical volleys where excitation is modulated by complementary inhibition (Fig 9A), the difference in strength and dynamics between ipsilateral IPSPs (Fig 9B) seems to reflect the difference of excitation received by amBC and plBC (Fig 8F-H).

4.9 Ipsilaterally-evoked responses mimic contralateral ones in the posterolateral barrel cortex

Differently from the weak ipsilateral response recorded in amBC, which may represent a typical response of callosally-poorer areas of the BC, the dynamics of ipsilateral responses in plBC neurons were more abrupt, almost resembling thalamocortical ones. Since they rise from the stimulation of row A-whiskers, which is the row that lay nearest to the facial midline, we suspected that there were neurons in the pool endowed with a side-invariant receptive field. Hence, we decided to quantify the similarity between ipsi- and contralateral responses evoked during down state in the two BC subregions.

To do this, we computed their Mahalanobis distance based on peak delay, amplitude and slope normalised in the z-score distribution (see **3.15**). In the three-dimensional space formed by the raw parameters, the cloud of ipsilateral responses tends to collapse onto the contralateral one in plBC but not in amBC (Fig 10A-B). Intriguingly, by measuring the Mahalanobis distance between contra- and ipsilateral responses, we found that the majority of plBC ipsilateral responses (23/46, 50%) rested within 2 arbitrary units of distance from both ipsi- and contralateral responses, overlapping with more than half of contralateral ones (26/46, 56%) (Fig 10C, inset). In the callosally-poorer amBC, contralateral responses falling in this range dropped to 14.8% (4/27) and just 3.7% was detected for ipsilateral responses (1/27) (Fig 10D, inset). This confirmed that, contrary to the amBC, in a great fraction of plBC neurons the two responses were remarkably similar. More in general, the distance of ipsi- from contralateral responses (Fig 10E, left) was very significantly smaller in plBC than amBC neurons (plBC= 1.7 [1.4-2.8], amBC= 10.4[5.2-12.6], p= 4.2 x10^{-7}). An analogous result was obtained for IPSPs (Fig 10E, right) when pooled contralateral (n= 7) and separated ipsilateral inhibitory responses from plBC (n= 10) and amBC (n= 9) were compared (plBC= 2.3[1.4-3.4], amBC= 9.2[8.1-21.1], p= 9.7 x10^{-4}), extending this similarity up to the pattern of inhibition.

At resting membrane potential, we were also able to compute the cross-correlation coefficient between contra- and ipsilateral responses for each neuron. Thus, we compared the values obtained in the two BC subregions (Fig 10F). Cross-correlation coefficient was significantly higher for plBC than amBC neurons (cc coeff. $_{contra-ipsi}$: plBC= 0.91 [0.88-0.96], amBC= 0.70 [0.56-0.83], p= 5.1 x10^{-8}). Notably, in almost one third of plBC neurons (32.6%, 15/46), the cross-correlation between contra- and ipsilateral responses exceeded 0.95, while in amBC was only 3.7%, namely 1 neuron out of 27. In order to better illustrate this phenomenon, we plotted the grand average response of such highly-correlating plBC neuronal population (Fig 10G). Except for the delayed onset, which suggests the presence of a higher number of synapses underlying ipsilateral responses, the two volleys of activity are almost identical. This behaviour derives from a variety of responding patterns across neurons (n= 15) that we have distinguished visually based on the amplitude of the first peak (Fig 10H). Some neurons emit stronger responses to contralateral stimulations (c > i, 60%), others to ipsilateral stimulations (c < i, 33.3%), and one of them could not be visually assigned to these categories, being contra- and ipsilateral responses fully overlapped (c $\approx$ i, 6.6%). Furthermore, we show the waveform averages of a neuron that belongs to this population (c< i type), in which we were able to record the ipsilateral IPSP in addition to contra- and ipsilateral EPSPs, and where the complementary timing of excitation and feed-forward inhibition is noteworthy (Fig 10I).
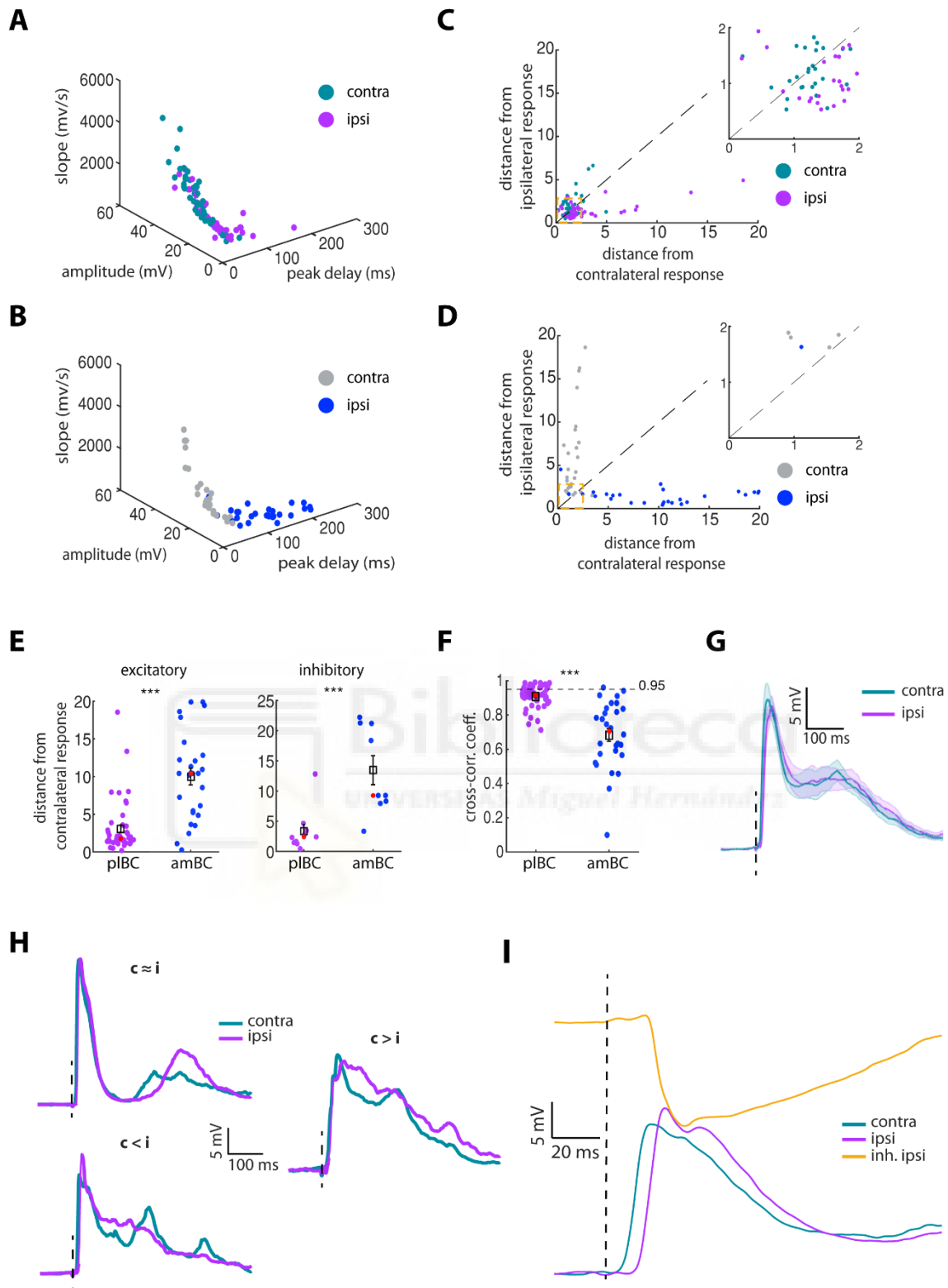
Fig 10 Side-invariant representation of row A-whiskers in the posterolateral barrel cortex. (A) Tridimensional plot of the parameters of sensory responses in plBC. (B) Same as A for amBC neurons. (C) Mahalanobis distance of each neuron from the centres of contra- and ipsilateral responses recorded in plBC. Inset: magnification at 2 a.u. of distance from both axes. (D) Same as C for amBC neurons. (E) Statistical comparison of the distance of ipsilateral responses from the contralateral counterpart in plBC and amBC neurons. (F) Statistical comparison of cross-correlation coefficients between contra- and ipsilateral responses. Dashed line marks the threshold at 0.95. (G) Grand average of plBC neurons' waveforms selected from above the threshold indicated in F and aligned at stimulation onset (black dashed line). Shaded

areas= ±S.E.M. (H) The three types of response in the pool of neurons composing the grand average of G aligned at stimulation onset (black dashed line). (I) Waveform averages of EPSPs accompanying ipsi- and contralateral stimulation from another neuron belonging to the grand average of G, and the waveform average of the IPSPs evoked by the ipsilateral stimulation at depolarised membrane potential.

Since such response could be evoked from row A-whiskers displacement of either side of the snout, the plBC possesses neurons with a subthreshold, side-invariant representation of these organs. Contrary to the amBC, and virtually to the rest of the BC representing long whiskers, this suggests that plBC neurons receive a mirror copy of the sensory event generated homotopically in the contralateral hemisphere, in line with other body representations in which the midline fusion theory applies (Manzoni et al., 1989; Iwamura, 2000).

4.10 Intact contralateral barrel cortex activity is required to observe the vigorous ipsilateral response.

What is the source of this vigorous ipsilateral receptive field? Is it really cortico-callosal or rather subcortical? Indeed, non-crossing axons innervating ipsilaterally the thalamus from the principal sensory nucleus (PrV) only depart from its dorsal aspect (Fukushima et al., 1979), where lips and lower jaw but not the long whiskers are represented (Erzurumlu et al., 2010). Yet, the possibility that ventral PrV-to-thalamus decussating axons establish *en passant*, functional synapses in the contralateral ventral PrV (i.e., ventral PrV-to-ventral PrV) had never been tested to our knowledge. Thus, we could not exclude a priori that an ipsilateral sensory event would feed the BC through a commissure in the neural axis earlier than the callosal one.

To confirm a cortical midline fusion phenomenon, we had to learn to what extent the vigorous response of plBC neurons depended on the callosal neurons resident in the contralateral BC. Hence, we suppressed its activity by applying TTX (1-1.5 μL, 100 μM) and recorded neurons in the BC ipsilateral to the stimulation side. Thus, for every neuron (n= 11; 1 neuron per mouse), we compared sensory responses upon ipsilateral homotopic stimulations before (CTRL) and after (TTX) the drug application, while maintaining neurons under whole-cell patch-clamp (Fig 11A).

Amplitude of LFP downward deflections (Fig 11B) in the injected BC greatly decreased upon TTX application, indicating a strong depression of its excitatory activity (LFP_{CTRL}= 463.0 [408.4-528.1] μV, LFP_{TTX}= 141.4 [130.7-152.6] μV, Wilcoxon signed rank test: p= 9.7 x10^{-4}).

Following the application of TTX, although a weak depolarisation of the membrane potential could be still evoked in the neurons upon whiskers' displacement (Fig 11C), the dynamics of the response were dramatically altered compared to the CTRL epoch (Fig 11D). Indeed, onset and peak delays elongated, amplitude was strongly decreased, and slope rose significantly slower upon TTX application (Wilcoxon signed rank test; onset delay: CTRL= 18.6 [15.7-19.4] ms, TTX= 21.3 [18.7-22.8] ms, p= 0.0313; peak delay: CTRL= 46.2 [42.8-49.1] ms, TTX= 94.5 [42.2-109.9] ms, p= 0.0137; amplitude: CTRL= 21.1 [12-23.3] mV, TTX= 8.3 [6.4-10.1] mV, p= 0.0010; slope: CTRL= 865 [538-985]

mV/s, TTX= 178 [67.1-320] mV/s, p= 0.0010). This indicated a sparser and weaker synaptic recruitment in TTX compared to CTRL.

In a subset of these neurons (n=10), we also recorded contralateral responses during CTRL. Hence, we were able to extract the Mahalanobis distance between ipsi- (in CTRL and TTX) and contralateral responses (in CTRL) based on their peak delay, amplitude and slope after z-score normalisation (Fig 11E). The distance between contra- and ipsilateral responses increased in TTX compared to CTRL (Wilcoxon signed rank test; Mahalanobis distance: CTRL= 2.7 [2.4-3.5], TTX= 14.8 [3.9-17.0], p= 0.0020), pointing to a loss of similarity between the two. Indeed, the cross-correlation coefficient between waveforms average of contra- and ipsilateral responses significantly diminished after TTX application (Fig 11F), confirming such observation (Wilcoxon signed rank test; cc coeff.: CTRL= 0.92 [0.90-0.96], TTX= 0.70 [0.62-0.83], p= 0.0020).
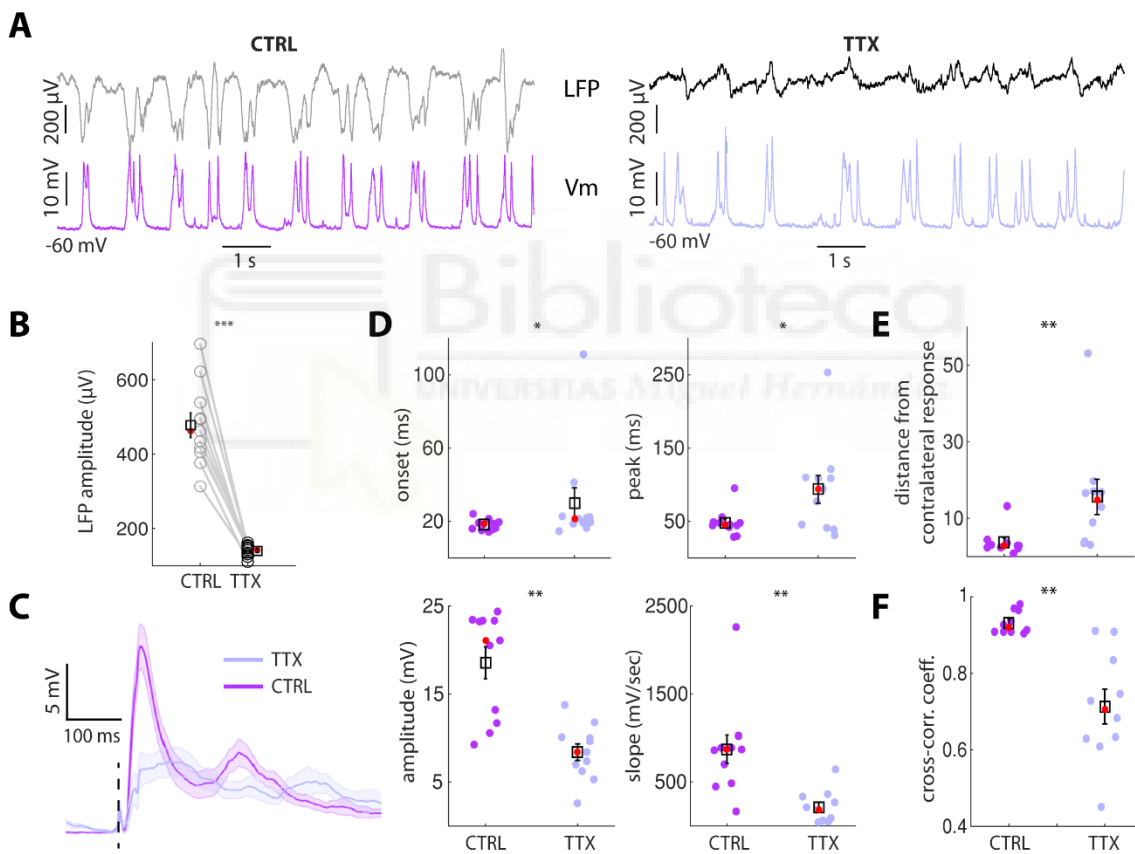
Fig 11 Ipsilateral response dynamics in the posterolateral barrel cortex depend on intact contralateral activity. (A) Simultaneous LFP (top) and membrane potential (V_m, bottom) recorded in homotopic spots (plBC) of the two hemispheres. Left: activity before TTX application (CTRL); Right: activity after TTX application (TTX) of the same neuron on the left. Note the drastic decrease of LFP downward (excitatory) deflections measured in B. (B) Statistical comparison of the amplitude of LFP downward deflections during spontaneous activity. (C) Grand averages of plBC neurons responding to the ipsilateral stimulation of row A-whiskers aligned at stimulation onset (black dashed line). Shaded areas= ±S.E.M. (D) Statistical comparison of the response parameters of the waveform averages composing the grand averages in C. (E) Statistical comparison of Mahalanobis distance of the parameters in D. (F) Statistical comparison of cross-correlation coefficients obtained from contra- (CTRL only) and ipsilateral (CTRL and TTX) waveform averages.

Because intact contralateral BC activity was required to shape the thalamocortical-likeness in the ipsilateral response of plBC neurons, we concluded that the dynamics so distinctive of these responses rely on contralateral callosal-projection neurons.

4.11 Responses evoked optogenetically at the cortical level recapitulate the ones evoked by whiskers stimulation.

Note that, even if we were able to clearly modify their dynamics by contralateral TTX application, we could not completely abolish ipsilateral responses. The residual depolarisation observed in plBC neurons could result either from 1) callosal neurons that did not intake enough TTX within the time of recordings, thus they were still able to excite the contralateral plBC, or 2) from the presence of an ipsilateral receptive field source in precortical centres that, alone or in combination with the callosal one, would build up ipsilateral responses. We excluded the involvement of S2 because in the studied placental mammals it does not project to contralateral S1 (Innocenti, 1986), moreover it could have intaken the TTX for anatomical vicinity, thus being equally affected.

To investigate the hypothesis that ipsilateral responses depended entirely on the corpus callosum and exclude the second possibility, we had to skip the sensory periphery and directly impose the activation of projection neurons in one BC while recording in the opposite one. If we could evoke responses similar to those evoked by sensory stimulations, and that differed between plBC and amBC in a comparable manner, we could infer a pure callosal origin for the sensory responses.

To this aim, we used the NEX-Cre mouse line in which projection neurons can be targeted with a Cre-dependent viral construct (Goebbels et al., 2006). We injected a Cre-dependent AVV-ChR2 carrying EYFP either in the plBC or amBC coordinates (100-200 nl; see **3.11**) to impose their excitation directly at the cortical level. Congruent with the expression of Nex gene in projection neurons (Goebbels at al., 2006), we could observe EYFP-labelled axons innervating the BC in the hemisphere opposite to the injected one (Fig 12A). As previously reported, BC received sparse callosal innervation (Wise and Jones 1976) which is mostly concentrated in septal areas (Olavarria et al., 1984). However, as seen through the flatten cortical preparation, a rich group of axons envelops barrels representing the row A-whiskers (Fig 12A, left), and innervates supra- and infragranular layers (Olavarria et al., 1984; Koralek et al., 1990; already visible in Ivy and Killackey 1981's Fig 7 and 11B). With the NEX-Cre mice expressing ChR2-EYFP, we performed homotopic experiments by shining blue light (i.e., 5 or 10 ms light-step, 400 µm diameter, 453 nm wavelength, 3.76 mW light power) over the injected hemisphere while recording intracellularly at mirror-symmetric coordinates in the contralateral BC in the supra-, infra- and granular layers (Fig 12B). In order to confirm the sole activation of homotopic areas of the injected BC, for most of the recorded neurons (20/24) we inserted two LFP electrodes, the first at the coordinates symmetrically mirroring the patch-clamp electrode, the second at non-mirror symmetric coordinates (either plBC or amBC). We recorded the activity of 12 neurons in plBC (4 supra-, 4 granular, 4 infra-) and 12 neurons in amBC (3

supra-, 2 granular, 7 infra-) in response to homotopic contralateral optogenetics illumination.

In these experiments, LFPs traces showed that the infected BC instantly and powerfully activated at the coordinates mirroring the contralateral recorded neuron, accompanied by a later and weaker depolarisation evoked at non-mirror symmetric coordinates (Fig 12C). Differently from sensory responses, the ones evoked directly from the cortex by optogenetic stimulation (Fig 12D-E) had statistically similar onset and peak delay in plBC and amBC neurons (onset delay: plBC= 8.8 [5.9-13.5] ms, amBC= 6.1 [5.0-12.5] ms, p= 0.4060; peak delay: plBC= 34.9 [28.1-59.0] ms, amBC= 71.1 [45.0-92.4] ms, p= 0.1029). However, by showing higher amplitude and faster slope compared to amBC neurons, plBC responding neurons emitted more vigorous responses (amplitude: plBC= 20.1 [13.0-22.8] mV, amBC= 9.0 [8.1-13.0] mV, p= 0.0089; slope: plBC= 561.4 [397.4-1.3 $\times 10^3$] mV/s, amBC= 152.1 [80.5-309.0] mV/s, p= 0.0062). Furthermore, the overall difference in shape of the two responses seemed to recapitulate with surprising fidelity the difference in shape amid ipsilateral sensory-evoked responses. Indeed, statistically comparing (Wilcoxon rank sum test) the waveforms between plBC and amBC neurons evoked by optogenetics and sensory stimulations pooled across layers and aligned at stimulus onset (Fig 12F), resulted in a similar pattern of significant (and non-significant) p-values over time, with the sensory p-value distribution being a 'stretched' version of the optogenetic one.
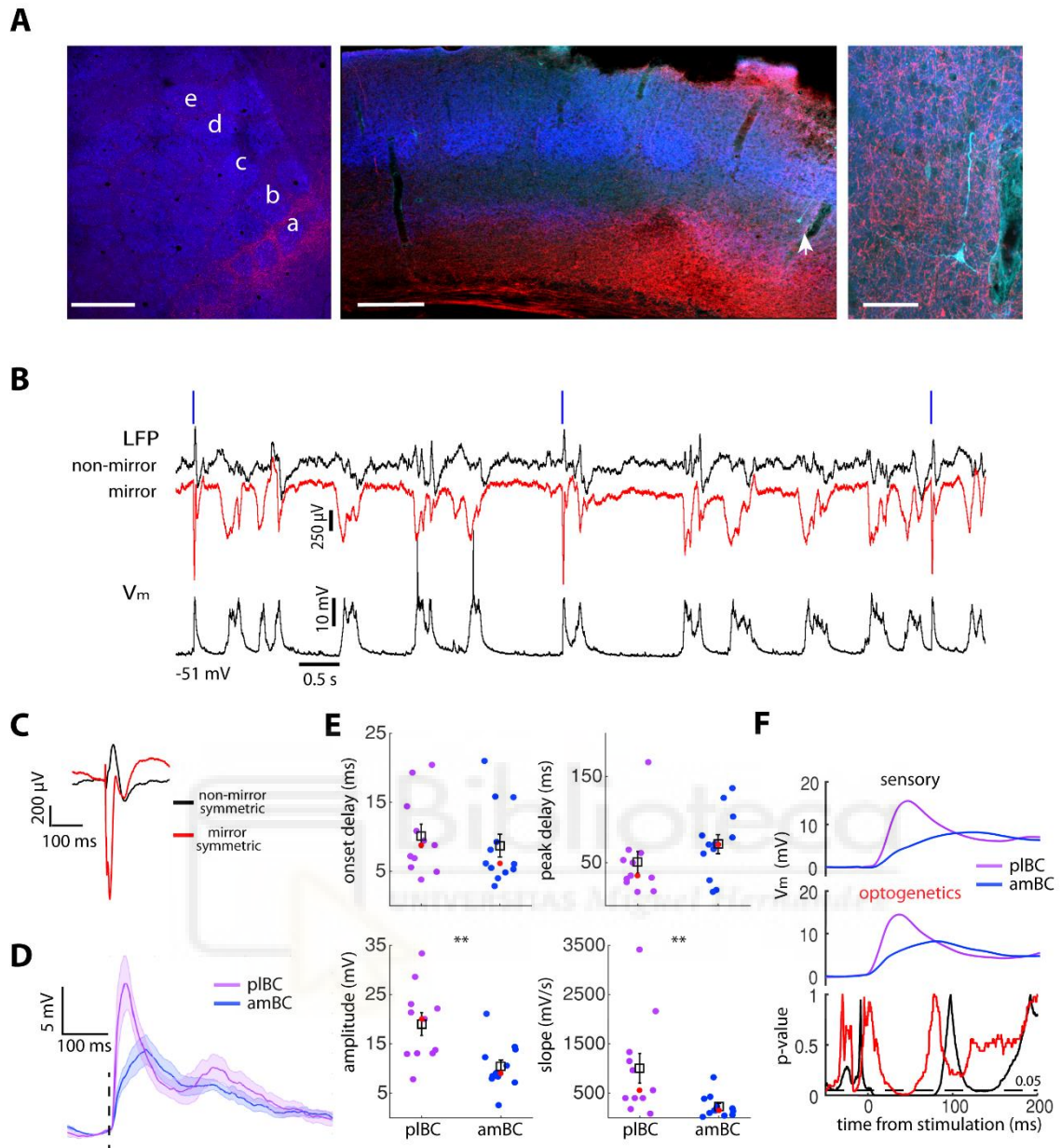
Fig 12 Neural responses to homotopic optogenetics stimulation recapitulate the responses to the homotopic sensory ones. (A) Left: flatten cortical preparation showing the callosal innervation (red) of the BC upon AVV-ChR2-EYFP injection in the opposite BC of a NEX-Cre mouse. Note the bulk of callosal axons enwrapping row A (labelled with 'a'). Scale bar= 500 μm. Middle: coronal section of a mouse preparation as in the left with a biocytin-filled recorded neurons in the plBC (white arrow) reached by EYFP-positive axons (red). Scale bar= 200 μm. Right: higher magnification of the infragranular pyramidal neuron from the middle panel. Scale bar= 50 μm. Red= ChR2-EYFP; blue= VGlut2; cyan= biocytin. (B) Synchronous recordings of membrane potential (V_m) and double LFPs in the two BCs. The neuron recorded in plBC responds to contralateral homotopic (i.e., mirror-symmetric) optogenetics stimulations. (C) Waveform average of the two LFPs shown in B. Note that the response to the light stimulation is confined to the extracellular electrode mirror-symmetric with the contralateral patch-clamp electrode. (D) Grand averages of homotopic optogenetic responses aligned at stimulation onset (black dashed bar). Shaded areas= ± S.E.M. (E) Statistical comparison of the response parameters from the waveform averages of the neural populations composing the grand average in D. (F) Smoothed sensory- and optogenetics-evoked grand average responses together with their statistical comparison in time. Red line= p-value distribution of the statistical comparison of optogenetics-evoked responses between plBC and amBC; Black line= p-value distribution of the statistical comparison of sensory-evoked responses between plBC and amBC. Black dashed line= threshold for significant p-values.

Since we assessed that 1) the sole activation of the contralateral BC is enough to generate a more vigorous response in plBC than amBC, and 2) optogenetics responses recapitulate in time the profile of the sensory ones, the involvement of the callosal trigger alone is sufficient to explain the average subregional differences related to ipsilateral sensory responses. By extension, these results strongly suggest that the origin of the receptive field in neurons responding side-invariantly to the displacement of the two rows A is the corpus callosum.

4.12 Homotopic transcallosal responses are stronger than heterotopic ones and can linearly sum up in single neurons.

BC suprathreshold responses can be modulated by ipsilateral heterotopic whiskers stimulations (Shuler et al., 2001). Moreover, bilaterally cauterising whiskers belonging to the row A and B during the mouse critical period, thus eliminating the relative cortical barrels, still allows the formation of the callosal tract innervating the BC in the adult (Suarez et al., 2014a), suggesting that not all the callosal afferents that invade the opposite plBC originate in cortical representation of row A. These physiological and anatomical observations led us to explore the presence of responses relying on heterotopic connectivity. With the NEX-Cre mouse line, we sought to characterise subthreshold responses in plBC and amBC neurons upon heterotopic (i.e., non-mirror symmetric) contralateral optogenetics stimulations. Furthermore, we explored the possibility of callosal synaptic integration evoked by wide (i.e., jointly homo- and heterotopic) BC activations of the opposite hemisphere. To this aim, we classified a given experiment as heterotopic when the activated LFP was in a non-mirror symmetric position (i.e., either plBC or amBC) with respect to the contralateral patch-clamp electrode (Fig 13E). Instead, when both mirror and non-mirror symmetric LFPs showed strong (> 400 μV) or comparable activation, we classified the experiment as virtually activating the entire BC (BC-wide; Fig 13F).

We found that both plBC and amBC neurons can respond to heterotopic stimulations of the contralateral BC (Fig 13A and 13C). Notably, while in plBC all the neurons tested could be excited (n= 4; 2 supra-, 1 granular, 1 infra-), in amBC this was more difficult since 3 neurons out of 7 (2 supra-, 3 granular, 2 infra-) did not respond to the stimulation (1 in each layer), thus such neurons were excluded from subsequent analyses. Instead, wide activations of the contralateral BC were able to evoke a response in all the neurons tested (n= 7 in plBC: 2 supra-, 1 granular, 4 infra-; n= 4 in amBC: 2 supra- and 2 infra-). Moreover, in plBC, responses to heterotopic stimulations where the weakest when compared to homotopic and BC-wide ones (Fig 13A-B). Indeed, while preserving a similar onset delay, they differed from the remainders in peak delay, amplitude and slope (Tab 4). Specifically, their maximal amplitude was reached later in time (Fisher's LSD; peak delay: p_{HEvsHO}= 0.0440, $p_{HEvsWIDE}$= 0.0045), it was significantly smaller (amplitude: p_{HEvsHO}= 0.0309, $p_{HEvsWIDE}$= 0.0085) and EPSPs rose on average more slowly (slope: p_{HEvsHO}= 0.0138, $p_{HEvsWIDE}$= 0.0016). No statistical difference was detected comparing homotopic with BC-wide stimulations (peak delay: $p_{WIDEvsHO}$= 0.2101; amplitude: $p_{WIDEvsHO}$= 0.4199; slope: $p_{WIDEvsHO}$= 0.2676), suggesting that most of the callosal input is

conveyed by homotopic fibres. Contrary to the plBC, in amBC (Fig 13C) we detected a significant difference exclusively in the onset of the responses (Fig 13D and Tab 4). In particular, homotopic stimulations clearly provoked faster responses than heterotopic ones (Fisher's LSD; onset delay: $p_{HEvsHO}= 0.0084$) and were similar to BC-wide activations in this respect ($p_{WIDEvsHO}= 0.3055$), suggesting that the underlying synaptic pathway sustaining heterotopic responses is less direct than the homotopic one in amBC. Visually (Fig 13C-D), earlier onset of BC-wide activations could be also appreciated when comparing them to heterotopic ones, but the statistics failed to reach significance likely due to the small sample size (n= 4 in both groups; onset delay: $p_{HEvsWIDE}= 0.1886$).
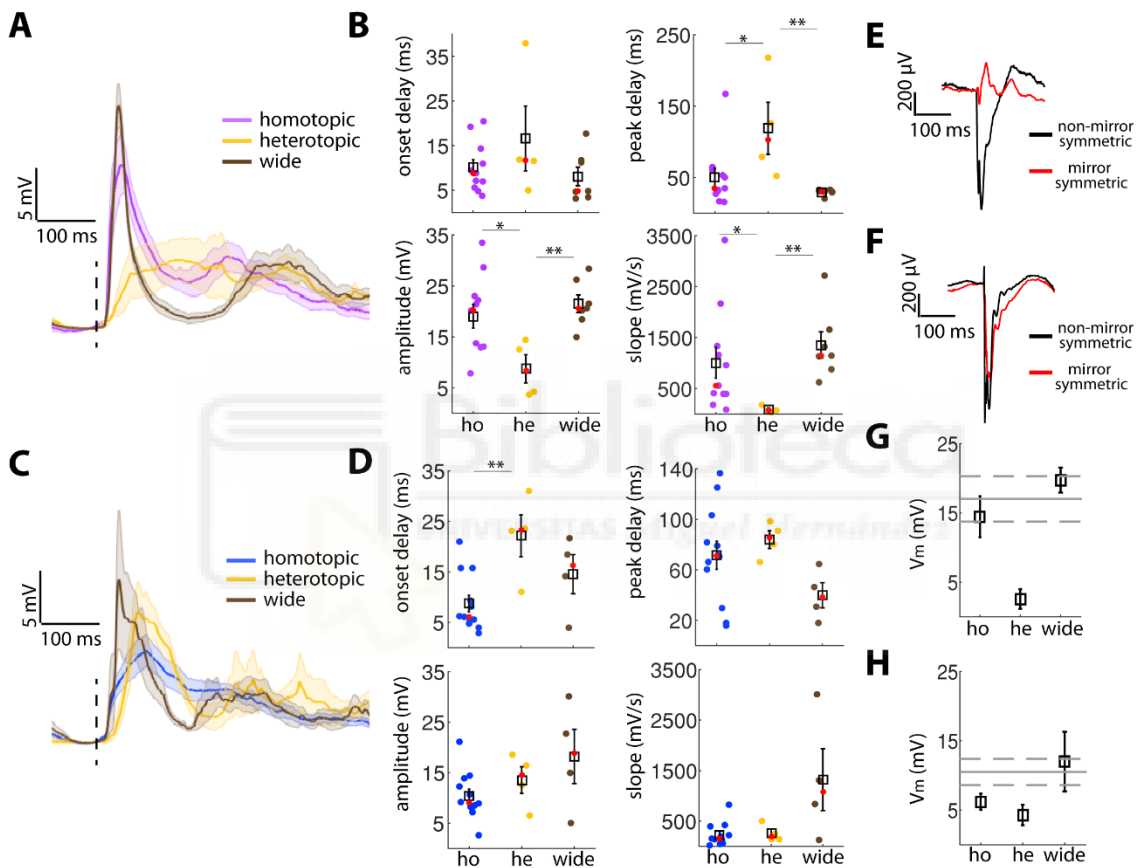
Fig 13 Homotopic, heterotopic and wide callosal activation of the barrel cortex subregions. (A) Grand averages of optogenetics-evoked responses in plBC aligned at stimulation onset. Shaded areas= ±S.E.M. (B) Statistical comparison of response parameters of plBC neurons. (C) Same as A for amBC neurons. (D) Same as B for amBC neurons. (E) Waveform average of LFPs response to illumination that shows the BC activation confined to a non-mirror symmetric subregion with respect to the contralateral patch-clamp electrode (heterotopic activation). (F) Waveform average of LFPs response to illumination involving mirror and non-mirror symmetric BC subregions (BC-wide activation) with respect to the contralateral patch-clamp electrode. (G) Visual comparison of response amplitude against a statistical model of homo- and heterotopic linear summation (grey solid line) with ±S.E.M. (dashed grey lines) for plBC neurons. (H) Same as G for amBC neurons. ho= homotopic stimulation; he= heterotopic stimulation; wide= BC-wide stimulation.

Either with an elongated onset delay and few responding neurons (amBC) or with an attenuated response (plBC), these data show that the two BCs preferentially operate via

homotopic (i.e., mirror-symmetric) transcallosal receptive fields rather than heterotopic ones, confirming previous results obtained with suprathreshold activity (Shuler et al., 2001), and more generally in line with the macroscopic homotopic organisation of the corpus callosum (Innocenti, 1986).

BC subregion	parameter	stimulation type			Kruskal-Wallis test	
		homotopic	heterotopic	wide	χ2 (df=2)	p
posterolateral	onset delay (ms)	8.8 [5.9-13.5]	11.7 [8.3-24.9]	4.8 [3.8-11.5]	2.67	0.2637
	peak delay (ms)	34.9 [28.1-59.0]	102.7 [65.9-172.1]	30.4 [29.1-32.6]	8.09	0.0175*
	amplitude (mV)	20.1 [13.0-22.8]	8.4 [3.9-13.5]	20.6 [18.8-25.0]	7.17	0.0277*
	slope (mV/s)	561 [397-1.3 x10³]	71.6 [50.8-126]	1.1 x10³ [944-1.5 x10³]	10.11	0.0064**
anteromedial	onset delay (ms)	6.1 [5.0-12.5]	23.3 [17.0-27.2]	16.3 [9.0-20.1]	7.09	0.0084*
	peak delay (ms)	71.1 [45-92.4]	85.7 [73.2-94.7]	38.5 [24.4-55.3]	4.68	0.0961
	amplitude (mV)	9.0 [8.1-13.0]	14.5 [9.5-17.5]	18.8 [9.9-26.4]	2.61	0.2712
	slope (mV/s)	152.1 [80.5-309.0]	193.3 [136.2-375.5]	1.0 x10³ [480.9-2.1 x10³]	3.81	0.1489

Tab 4 Statistical comparisons of response parameters to optogenetic illumination of the BC contralateral to the intracellular recorded neuron, separated for the two BC subregions. Data are presented as median [25th-75th] quantiles.

Yet, in both the subregions tested, we noted higher response amplitude upon contralateral BC-wide activations, likely as the result of a greater synaptic summation. To learn about the modality of such a summation, we selected the mean amplitude in homo- and heterotopic responses in the activity segment (10 ms) of the waveform centred around the mean peak amplitude of BC-wide evoked responses (see **3.15**). If homo- and heterotopic responses were integrated through a linear summation process, then the amplitude of BC-wide evoked responses selected in the same time window should fall within the range of the sampling error of their sum. We found that this was indeed the case for both plBC (Fig 13G) and amBC (Fig 13H) neurons and concluded that their subthreshold currents can linearly sum when contralateral homo- and heterotopic territories are jointly active.

This suggests that the integration of the widespread contralateral activity is partially independent from the different callosal innervation reaching the two subregions (amBC sparse *vs* plBC dense). More specifically, it is possible that through the intracortical circuitry activated by the callosal trigger in the home-hemisphere (likely septa-related), neurons in the amBC (both septa- and barrels-related) may compensate for the sparseness of direct callosal connections and be strongly recruited despite the involvment of a more indirect pathway.

4.13 Slow wave oscillation in the posterolateral barrel cortex reflects an increased afferent input

Importantly, such a use of the slow wave features to understand functional connectivity between subregions used for the corticostriatal circuitry, opened the way to apply the same methods in studying the callosal connectivity between the two BCs.

We recorded *in vivo* by whole-cell patch clamp the spontaneous activity (minimum: 60 sec) of plBC (n= 57) and amBC (n= 28) neurons sampled along the cortical depth, some of which belongs to the pool of neurons that subsequently received the sensory

stimulation, and that were the object of the previous thesis' paragraphs. Simultaneously, we recorded 2 LFPs, 1 in plBC and 1 in amBC of the contralateral hemisphere.

The frequency of the slow wave oscillation of the membrane potential was higher in plBC than amBC neurons (Fig 14A). This was attributable to the shorter time length of up states (circa 100 ms) in plBC than amBC neurons, while the down states had a statistically equivalent duration (Fig 14B). Thus, up states were of less duration but more in number in plBC than amBC neurons.

We reasoned that the increased number of network transitions (i.e., up states) in plBC could be explained by an increased afferent input and hypothesised that the denser callosal innervation of the plBC could contribute to it. Figure 14C shows homotopic and heterotopic comparisons of the probability of transition to the up state in the neuron following the detection of a transition in the contralateral LFPs. Both the probabilities were very significantly higher in plBC than amBC neurons, suggesting that the former neurons are more tightly coupled to the entire contralateral BC than the latter, thus receiving the afferent input from a broader contralateral territory.

To further test this possibility, by using the NA-MEMD algorithm (see **3.8**), we extracted the IMFs carrying only the slow wave in the LFPs (from both plBC and amBC) and in the jointly recorded membrane potential (either in plBC or amBC neurons) in the opposite hemisphere. Again, we measured the coupling to the slow wave oscillation for plBC and amBC neurons with homotopic and heterotopic contralateral BC territories, but this time for their cross-correlation with the LFPs (Fig 14D). plBC neurons had significantly higher coefficients of cross-correlation than amBC neurons for both the homo- and heterotopic comparisons.

As a last confirmation, we run the same comparisons between slow wave IMFs with respect to their coherence (Fig 14E). plBC neurons had higher coherence than amBC ones in the frequency of the slow wave (around 0.8-1.2 Hz) with both the homotopic and heterotopic LFPs.
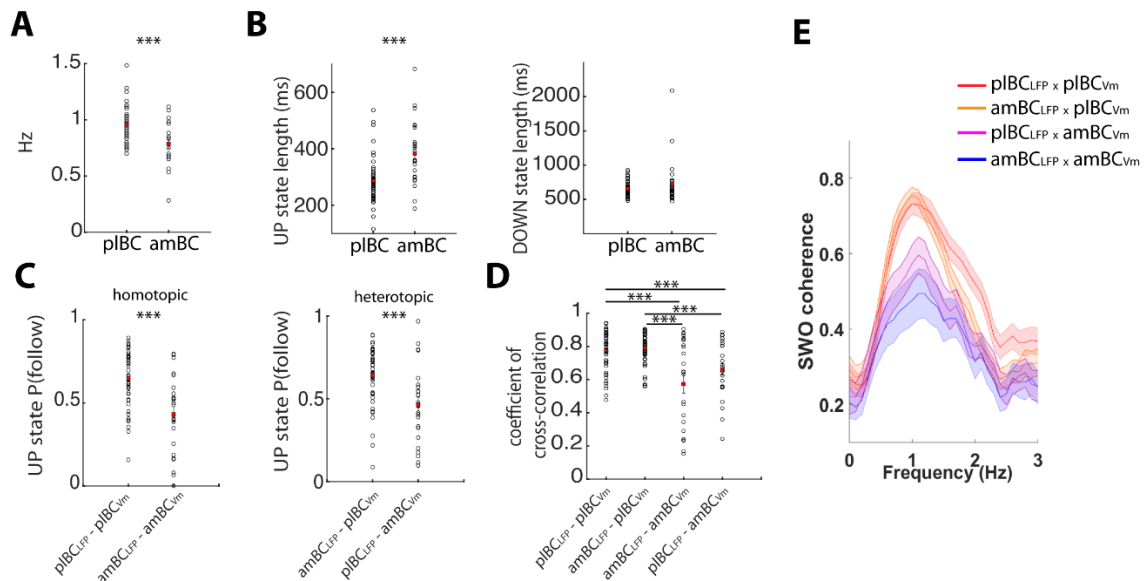
Fig 14 Subregional differences in the slow wave oscillation of the barrel cortex. (A) Frequency of the slow wave oscillation in the membrane potential. (B) Duration of up and down states. (C) Probability of up state occurrence in the membrane potential after detection in contralateral LFPs. (D) Cross-correlation coefficient between IMFs carrying the slow wave oscillation of the membrane potential and contralateral LFPs. (E) Coherence between IMFs carrying the slow wave oscillation of the membrane potential and contralateral LFPs.

Taken together, these results strongly suggest the presence of a greater functional connectivity of plBC neurons with the contralateral BC than amBC neurons, resulting in a more conspicuous afferent input in the former. This is coherent with the data on the optogenetics-evoked activity (Fig 13A-D), for which, contrary to the amBC, the callosally-recipient plBC is more directly connected to heterotopic contralateral territories.

4.14 Summary of the results

The row A-whiskers representation contained in the plBC is known to receive the densest callosal innervation departing from the contralateral BC, while in the remaining area the callosal innervation is sparse (Wise and Jones 1978; Olavarria et al., 1984; Koralek et al., 1990; Suarez et., 2014a; Fenlon et al., 2017; Zhuo et al., 2021). In this work, we have found that such subregional difference in innervation patterns profoundly affects the activity of the BC related with the ipsilateral whiskers system. That is, blocking the input from contralateral whiskers during objects exploration confines the activity (c-fos expression; Fig 6D, 6F) of the BC in its more callosal, posterolateral subregion (i.e., row A and, to a lesser extent, row B-whiskers representations). Furthermore, the plBC is much more sensitive than the amBC to the stimulation of homotopic ipsilateral whiskers (row A *vs* row E, respectively; Fig 8E-H and Tab 2) to the extent that, in some of the neurons (50% Mahalanobis distance estimate; ~33% ipsi-to-contra cross-corr. coeff. estimate), contra- and ipsilateral subthreshold responses are almost completely overlapped (Fig

10G-I). Practically absent in amBC (Fig 10B,10D,10F), this plBC feature demonstrates that a proportion of neurons is endowed with a side-invariant representation of the two rows A, congruently with other callosally-connected somatosensory body representations (Manzoni et al., 1989; Iwamura, 2000). The similarity of PSPs evoked by the displacement of either rows A extends also to the inhibitory components of the response (Fig 10E). Moreover, we have demonstrated that the strong ipsilateral sensitivity in the plBC is dramatically altered by contralateral TTX silencing (Fig 11C,11E-F), and that such a response, as well as the one in amBC, can be evoked directly at the cortical level via contralateral optogenetics (ChR2) stimulation (Fig 12D,12F). These data demonstrated that much, if not the totality, of the source of subregional differences in plBC and amBC neurons with respect to the ipsilateral whiskers' representation is the corpus callosum. In addition, we provide the first evidence for the presence of feed-forward inhibition in the BC evoked through ipsilateral whiskers stimulation (Fig 9A-C). Since the inhibitory potentials vary between amBC and plBC comparably to the excitatory ones, it is very likely that they also depend on the corpus callosum, as it is the case for other cortical areas (Rock and Apicella 2015; Anastasiades et al., 2018; Karayannis et al., 2006; Kawaguchi, 1992). Additionally, comparing heterotopic and homotopic optogenetics stimulations indicates a preferential homotopic relation between the two BCs, and suggests the presence of a different heterotopic circuitry reaching the two subregions. In fact, heterotopic responses have a delayed onset compared to homotopic ones only in amBC (Fig 13A-D). Likely in amBC, the circuitry underlying heterotopic responses is less direct than the one reaching plBC. Despite this, both subregions can linearly sum homo- and heterotopic joint activations of contralateral BC territories (Fig 13G-H). Lastly, the preference for heterotopic contacts towards the plBC is further confirmed by the propagation of the spontaneous slow wave oscillation, which tends to show a stronger coupling between plBC and homo- and heterotopic contralateral BC territories than the one of amBC (Fig 14C-E), reflecting an increased afferent input.

5. Discussion

5.1 The corticostriatal functional connectivity

Based on the integration of the spontaneous slow wave oscillation propagating from the neocortex, we identified two functional circuits in the DS separated by a sharp boundary. MSNs membrane potential during up states show different features in the DM and in the DL striatum (Fig 1). By recording membrane potential in many cortical areas of L5 neurons, we found that up states differences in DS subregions can be attributed to a distinct corticostriatal functional connectivity. Coherently with this, cortical LFPs jointly recorded with DLS and DMS-MSNs intracellular membrane potential, revealed a stronger slow wave coupling of M1, S1 and FrA with MSNs in the former subregion, and the one of V1 with MSNs in the latter (Fig 2). This analysis of functional connectivity (as defined in Getting, 1989), has been greatly helped by the use of NA-MEMD (ur Rehman and Mandic, 2011) and Hilbert transform for the detailed isolation of the slow wave oscillation with unprecedented resolution (Alegre-Cortés et al., 2017). Our data suggested that the lack of a local anatomical homology between the DS of rodents and primates, is compensated by the presence of a clear functional boundary with respect to DS subregional specialisations, in agreement with behavioural studies (Graybiel, 2008; Balleine et al., 2010). Thus, the data support the homology between DLS with putamen, and DMS with caudate nucleus. In addition, the methods presented open a way to study functional connectivity between brain areas that can be complemented by stimulation of upstream areas to increase the level of resolution (e.g., visual stimulation in DCS; Fig 4). Since the slow wave oscillation is present also in the awake animal (Poulet and Crochet, 2018; Vyazovskiy et al., 2011) and there are shared features between spontaneous and evoked brain activity (Luczak et al., 2015), functional connectivity mapped in this manner may have a predictive power on the awake state, when striatal activity is more desynchronised (Mahon et al., 2010), and the contributions from cortical areas are more difficult to assign.

5.2 The DLS and the DMS compose different functional circuits in the mouse

Despite the extensive overlap of cortical afferents along the mediolateral axis of the mouse DS coming from a great variety of cortical areas (Kincaid et al., 1998; Hoffer et al., 2001; Hoover et al., 2003; Hooks et al., 2018), we demonstrated that two different circuits can be identified based on the MSNs up state membrane potential. Their segregation depends on the relation to distinct neocortical areas. In addition, DLS and DMS are separated by a sharp transition because up state membrane potential in a putative central region of the DS belongs either to the DL or DM SVM-category, but not to a third one (Fig 3). Here we ask: What can be the origin of this sharp transition? The number of peaks inside the up states has been the major feature in MSNs classification, being higher in DLS than in DMS. In order to understand this result, we recorded L5 cortical neurons, and found that FrA, S1 and M1 neurons produce more peaks than V1 during up state. Together with the known anatomy (Alloway et al., 2006; Hoffer and Alloway, 2001), this

suggested that somatomotor cortices exert a sharper modulation onto DLS- than onto DMS-MSNs, which instead is more strongly connected to limbic, visual and associative cortical areas (Hinitiryan et al., 2016).

Associated with the cortical glutamatergic afferent input, local circuit components may have contributed to the sharp transition. Note that the slow wave oscillation propagates also to resident interneurons (Reig and Silberberg, 2014). One important species of DS interneuron is the PV^+ fast-spiking interneuron, which cortical axons recruit to provide strong feed-forward inhibition onto MSNs (Tepper et al., 2008). Our data on the barrel cortex indicated that this corticostriatal circuit motif is common also to corticocallosal and thalamocortical circuits, thus it may constitute a common, long-range solution to modulate local circuits in target areas through glutamatergic input. Notably, PV^+ fast-spiking interneurons show a heterogeneous distribution along the mediolateral axis of the DS (Gerfen et al., 1985) that can give rise to differential inhibitory inputs in DLS and DMS. Another interneuronal species showing a heterogeneous distribution in the DS is formed by cholinergic interneurons. Indeed, they exert disynaptic inhibition onto MSNs (English et al., 2012) and are more active in the DMS (Abudukeyoumu et al., 2019). However, at present the source of this sharp boundary despite the overlapping cortical innervation remains unknown. Future works may directly address the role of interneurons and neuromodulatory systems in generating the DLS/DMS functional boundary.

5.3 Slow wave propagation in the dorsal striatum

Confirming the results obtained with the evaluation of cortical and striatal up state features, we have found that the slow wave oscillation in DLS-MSNs has a higher correlation with FrA and M1 than DMS-MSNs, and that DMS-MSNs have a higher correlation with V1 than DLS-MSNs (Fig 2E). Also the probability of up state propagation followed a similar trend, in that FrA up states had more probability to be followed by DSL-MSNs than DMS-MSNs up states and, conversely, V1 up states had more probability to be followed by DMS-MSNs than DLS-MSNs up states (Fig 2F). These results parallel the underlying corticostriatal innervation that in this case is more divergent (Hinitiryan et al., 2016; Reig and Silberberg, 2014). Moreover, some attribute of the slow wave was useful to statistically distinguish iMSNs from dMSNs, but only in the DLS (Fig 5B) and not with our classifier. Thus, the slow wave recruitment of the local circuits is homogeneous among the two striatal pathways.

Yet, the different visual responses of DCS- and DMS-MSNs (Fig 4B-E) could not be anticipated by the study of the slow wave propagation. This suggests that the activation of upstream areas may complement our method of mapping functional connectivity by adding extra levels of detail.

5.4 The callosal action in the barrel cortex

The barrel cortex (or posteromedial barrel subfield) has historically been the focus of studies aimed at understanding the development and physiology of the neocortex. Thanks to the readily visible somatotopic organisation provided by the 'barrels', this area enabled

researchers to study in strict association anatomy with function, promoting the conceptualisation of the functional unit of the neocortex: the cortical column (Mountcastle, 1997). Indeed, what we know about cortical processing in general, and the one for the perception of touch in particular, largely derives from studies on the barrel cortex of mice and rats. We learned about the coding of touch (Knutsen and Ahissar, 2009), the characterisation of cortical interlaminar flow of activity and the roles of different cortical cell types during tactile tasks (Petersen, 2019). However, most of the studies focused on just one hemisphere at a time. As a consequence, callosal responses of the barrel cortex have received far less attention. Studies on this topic are few and mostly focused on suprathreshold activity, recorded either under anaesthesia (Shuler et al., 2001; Plomp et al., 2017) or in the awake animals (Wiest et al., 2005; Oran et al., 2021). Surprisingly, no work has explored systematically the ipsilateral receptive fields of the barrel cortex by relating subthreshold dynamics of sensory responses to the subregions individuated by its callosal innervation. An exception is the work of Petreanu and associates (2007), where the authors characterise responses in the representation of row A upon optogenetic stimulation of callosal fibres. However, they used an *in vitro* approach, thus they could not characterise sensory responses nor compare them between BC subregions to unveil their peculiarities.

In this study, we show that the callosal contribution to the evoked activity in the barrel cortex of the mouse is predominant in its posterolateral aspect (plBC). Here, neurons represent row A-whiskers, a para-axial row of whiskers which is the nearest to the geometrical facial midline. We interpreted this result in the light of the midline fusion theory (Manzoni et al., 1989; Iwamura, 2000). This theory states that somatosensory and visual cortical neurons, that are dedicated to the intersection at the midline of the right and left sensory hemi-spaces, are connected through the corpus callosum, and often reside in cytoarchitectonic borders of cortical areas. Here, they receive information from the two hemi-sensory periphery disregarding the side of its origin, thus producing a side-invariant representation of the sensory periphery. As mentioned above, in the mouse, the cytoarchitectonic border between area S1 and S2 is limited in S1 by the posterolateral aspect of the BC that contains the representation of the row A-whiskers (Olavarria et al., 1984; Koralek et al., 1990). In agreement with the theory, callosal afferents densely innervate this subregion (Ivy and Killackey 1981; Wang et al., 2007; Suarez et al., 2014; Fenlon et al., 2017; Zhuo et al., 2021), while sparsely innervating the rest of the whiskers' representation, with a preference for septal columns (Olavarria et al., 1984; Koralek et al., 1990; Sehara et al., 2010). By suppressing the thalamocortical excitation of the BC and using a c-Fos immunoessay at the end of a period of environmental exploration by the mouse, we found that the BC posterolateral aspect (i.e., the row A and, to a lesser extent, the row B) remains active, suggesting a callosal recruitment of this subregion. Whole-cell patch-clamp recordings here directed, revealed that neuronal receptive fields are more sensitive to the stimulation of homotopic ipsilateral whiskers than in the anteromedial aspect of the BC, emitting a much vigorous response in the former than in the latter case (i.e., row A- *vs* row E-whiskers stimulation), while contralateral responses were much more similar across layers. Through TTX activity suppression and ChR2 activity imposition of the opposite BC, we found that such a vigorous response is dependent on callosal-projection neurons. Furthermore, in the posterolateral BC we have found 32.7-50% of the neurons responding to contra- and ipsilateral stimulations with

remarkably similar dynamics. This unveiled the callosal-dependent, side-invariant representation of row A-whiskers.

5.5 The Iwamura's extension of the midline fusion theory

It may be recognised that the two rows A do not occupy the exact midline of the face, but they are some millimetres far from it, thus constitute para-axial organs. We want to remind here that the midline of the sensory space does not have to coincide with the geometrical midline of the body (Iwamura, 2000) as originally postulated by Manzoni et al., (1989). Conti and associates (1986) found that neurons representing the trunk had bilateral receptive fields spanning up to 5-6 cm far from the exact body midline. Moreover, other para-axial structures such as the shoulders have cortical representations densely interconnected through the corpus callosum (Iwamura, 2000). The separation between physiological (i.e., sensory) and anatomical midline is evident also in the visual domain. Indeed, the two eyes are fairly far from the exact midline of the face. However, a narrow strip crossing the two foveae is inter-hemispherically connected and dedicated to the vertical meridian of the visual space (Berlucchi and Rizzolatti 1968; Gazzaniga 2000). As described by Manzoni and associates (1989), in earlier studies, somatosensory bilateral receptive fields were attributed only to the geometrical body midline, involving the oral cavity, the head and the trunk. Thus, the distal parts of the extremities and the rodents' whiskers were excluded. This apparent absence of interhemispheric connections was explained by the need to preserve the purity of information processing of body parts with high spatial resolution, like the distal extremities of primates (Jones and Powdell, 1968) or rodents' whiskers (Manzoni et al., 1989). However, it was discovered that distal extremities with high spatial resolution, like monkeys' fingers, also have bilateral receptive fields in S1 (reviewed in Iwamura, 2000), and confirmed that row A receives callosal afferents (Koralek et al., 1990). Iwamura (2000) stressed the fact that also the two foveae, representing the peak of the eyes' spatial resolution, have bilateral receptive fields dependent on callosal innervation (Berlucchi and Rizzolatti 1968). Thus, the author proposed that the callosally-connected representations are not those that lie at the geometrical body midline but rather are those body parts that work bilaterally in a similar behavioural context. For example, an object can be explored bimanually at the unison, and it is in such a case that the sensory space would benefit from a continuum, or bilateral integration, between the two hemi-representations. This observation draws a net difference between the cortical representation of the map of the peripheral sensory array (i.e., whiskers) and the map of the external space constructed by the sensory array (Pluta et al., 2017). In the whiskers system, the neural substrate for the first may be recognised in the single-whisker representations of L4 barrels by the thalamocortical pathway, which are devoid of direct callosal input (Petreanu et al., 2007). Contrary to the first, the second needs the integration of information from multiple whiskers. Such an operation has been found to rely on the supragranular layers (Pluta et al., 2017), origin and target of callosal connections. Moreover, similar inter-barrels integration can be expressed by septal neurons (Brecht and Sackmann, 2002), another major component of the callosal system (Olavarria et al., 1984; Koralek et al., 1990). These features of the callosal circuitry suggest that it may be involved in the representation of the scanned, peripersonal space.

This extension of the midline fusion theory, that assigns more wight to the physiology (map of the scanned space) and less to the anatomy (body map of the sensory array), can also better include all the previous data on bilateral receptive fields on trunk, oral cavity, head and shoulders (Iwamura, 2000), and perfectly accommodate our results on row A-whiskers.

5.6 c-Fos expression in the barrel cortex

The production of c-Fos in the BC, and in the other whiskers' relay stations of the CNS (Staiger, 2006), can be induced by spontaneous but sustained tactile experience (Filipkowski et al., 2000). The nuclear protein c-Fos is produced upon expression of the *c-fos* immediate early gene. It is a general marker for cellular responses because it is a component of the transcription factor AP-1 (activator protein-1) which activates DNA expression upon different kinds of cellular stress, including neural activity (Kaczmarek 1993). By allowing the detection of functional pathways in the brain, the use of c-Fos mapping is widespread in developmental studies of the BC, where is often used to observe alterations of the whiskers' representation linked to genetic manipulations (Reiner et al., 2017; Antón-Bolaños et al., 2019). Since it enables one to associate neural activity with anatomical specificity, we used the c-Fos assay to characterise the callosal recruitment of the BC. Other studies applying the c-Fos assay in the same area, has normally reported the pattern of activation of the hemisphere contralateral to the stimulated whiskers and used the ipsilateral one as a control, finding far greater c-Fos production in the former (Mack and Mack 1992; Filipkowski et al., 2000). This is similar to our condition of intact whiskers (Fig 6A), with the exception that in our case the thalamocortical activation could be observed bilaterally, being both the whisker pads free to palpate objects. An unexpected result is that cutting the whiskers bilaterally did not abolish the c-Fos production (Fig 6B). Indeed, when one whisker/row is spared from the trim, the c-Fos is produced abundantly in the barrel/s representing the spared whisker/row, leaving the rest of the BC relatively free of c-Fos (Filipkowski et al., 2000; Antón-Bolaños et al., 2019). Instead, we could detect c-Fos[+] nuclei spanning the entire BC. This activity pattern can be explained by the observation that animals without whiskers tended to touch the walls of the home-cage directly with the snout. Since in the BC the representation of the common fur between the whiskers is partially overlapped with the one of the whiskers (Nussbaumer and Van der Loos 1985), the phenotype we observed could result from fur stimulation. Such a behaviour is probably not present in animals left with a single whisker because they can soon learn how to use it to maintain a proper distance between the snout and the surfaces. In this case then, the neural representation of the spared whisker attracts all the metabolic activity. Instead, such an activity is completely absent from both the BCs when we injected the lidocaine subcutaneously before the period of novel objects exploration (Fig 6C). This suppression of activity is consistent with the absence of whiskers-mediated responses in the BC of rats receiving the same peripheral treatment (Gener et al., 2009). The almost complete absence of c-Fos[+] nuclei also suggests that other cortices like M1, that can influence the activity of the BC in the home-hemisphere (Veinante and Deschenes, 2003; Zagha et al., 2013), could not significantly activate barrel cortical columns in this condition. For these reasons, and for the localisation of c-Fos[+] nuclei in the callosally-innervated subregion of the BC after contralateral sensory

90

deafferentation (Fig 6D-G), we attributed the origin of such activity to the opposite, active BC. Furthermore, in line with the possibility that callosal activity can induce c-Fos production, Kaczmarek (1993) reports that activation of the NMDA receptor is a major route for the *c-fos* expression *in vivo* as well as an important postsynaptic target of callosal glutamate release (Kawaguchi 1991). Importantly, with this work we provide evidence that the two BCs are jointly engaged by the use of whiskers belonging to only one side of the body during spontaneous exploration. This observation favours earlier proposals for considering the functional unit of the neocortex not the cortical column alone, but callosally-connected homologous columns of the two hemispheres (Berlucchi 1981b,1983; see also Shuler et al., 2001 and Wiest et al., 2005).

5.7 Ipsilateral responses are generally weaker than contralateral responses

Sometimes reported as a rule (Manzoni et al., 1989), ipsilateral responses produce less spikes than contralateral ones in the neocortex (Manzoni et al., 1980; Conti et al., 1986; Shuler et al., 2001; Wiest et al., 2005; Tutunculer et al., 2006). Congruently with this, in previous (Reig and Silberberg, 2014; Manns et al., 2004) and in the present work, subthreshold responses to ipsilateral stimulations rose slower and with a smaller amplitude than the contralateral counterpart (Fig 8 and Tab 2). This can likely result in a minor driving force for spiking. Many possible reasons can explain such a phenomenon. One of them may be the longer polysynaptic pathway that underlies ipsilateral responses. Indeed, a higher number of subsequent synapses involved, either intra- or interhemispherically, can introduce variability in the timing of incoming depolarising inputs. This would impede their synchronous summation to a larger extent than that of the contralateral responses, conveyed by the more direct thalamocortical pathway. Another reason with a similar outcome may be the heterogeneous axonal diameter and myelination of the corpus callosum which affect its conduction velocity. In line with this interpretation, early evidence suggests that in the adult mouse only 28% of the callosal fibres show myelination (Sturrock, 1980). Furthermore, in the BC, axons originating in the somas of infragranular layers are more extensively myelinated than the ones of supragranular layers (Tomassy et al., 2014), with both cortical laminae projecting to the opposite BC. This opens the possibility that the weaker response can result from relatively asynchronous depolarising inputs reaching postsynaptic neurons. Supporting this hypothesis, Petreanu and associates (2007) reported that *in vitro* stimulation of L2/3 callosal axons could result in the desynchronised summation of excitatory postsynaptic currents. Another aspect to consider in the BC is the 'sparse coding' of superficial layers, for which even in the awake animal, sensory responses produce very few action potentials (Ramirez et al., 2014), and 25% of superficial callosal projection neuron in rabbit S1 do not produce any (Swadlow and Hicks, 1997). Since one of the most prominent callosal tract departs from the contralateral supragranular layers of the BC (Petreanu et al., 2007; Suarez et al., 2014a), a reduced possibility of contralateral spiking can result in a weaker ipsilateral sub- and suprathreshold response.

However, sensory stimuli applied right on top, or slightly next, to the body midline evoke the strongest response in terms of spikes in neurons endowed with bilateral receptive

fields (Manzoni et al., 1989). This resembles our recordings in the plBC where subthreshold responses were the most vigorous despite the stimulation being delivered ipsilaterally. Indeed, some of them (n= 15) violated the rule mentioned above in terms of subthreshold potentials, showing comparable dynamics in response to ipsi- and contralateral stimulations (Fig 9G-I). Since the plBC is enriched in afferent callosal axons, likely their number compensate for the longer synaptic pathway, thus a faithful replica of the contralateral excitation can be here delivered.

5.8 Onset delay of callosal responses

As recorded through excitatory potentials in postsynaptic neurons, callosal conduction velocities may vary considerably. In the cat parietal cortex, homotopic contralateral electric stimulation evoked EPSPs with an onset varying between 1.3 to 20 ms (Cissé et al., 2003). This wide range was reported to not necessarily be due to an underlying polysynaptic pathway since antidromic response latencies in callosal neurons could be as slow as 18.5 ms. It is not surprising if one considers again the high variability in axonal calibre (from 0.08 to 5 μm, typical <1 μm) and degree of myelination (Innocenti, 1986). Similarly, we have found that onset delays vary in the same range (from 2 to 21 ms circa) across the BC when homotopic optogenetics stimuli are delivered (Fig 11E). However, it is unlikely that all the neurons we recorded were directly reached by callosal boutons, leaving the possibility that some of the responses were supported by local, intracortical connectivity. This can be the trend of amBC neurons, which emitted slowly rising ipsilateral responses with low amplitude and late peaks in a subregion of the cortex poorly innervated by the CC (Fig 8F-H). Such a response could be the result of sensory-induced local network activity, sharing characteristics with a spontaneously occurring up state. PSPs of this kind, either excitatory or inhibitory, may be conveyed by axonal branches of other of neurons monosynaptically contacted by the callosal afferents (Conti and Manzoni, 1994), which in turn contact amBC neurons. Extensive inter-barrels axonal arborisations and monosynaptic connections from the CC are characteristics of septal neurons (Olavarria, 1984; Koralek et al., 1990; Brecht et al., 2002, 2003), thus they are the possible candidate mediating slowly rising, low amplitude ipsilateral responses of our pool.

Despite the exact pathway connecting the two BCs, Plomp and associates (2017) found that, upon whiskers stimulation, infragranular spike responses in the BC had an earlier onset than the ones of upper layers in the ipsilateral hemisphere. Comparably, in our study, we have found that the response onset of infragranular neurons preceded by ~3 ms the one of supra- and granular layers (Fig 8B; Tab 1). This effect is markedly present in plBC, whose infragranular neurons display faster responses than the ones of amBC (Fig 8H and Tab 2). Since the phenomenon is more marked in the more densely innervated region by the corpus callosum, we suggest that infragranular neurons have a higher probability to be directly reached by callosal axons with respect to more superficial neurons. Even if this hypothesis remains untested directly, Petreanu and associates (2007) found in row A-whiskers representation contralateral L2/3 callosal axons contacting pyramidal cells in decreasing abundance from L5 to L2/3 to L6, endorsing this proposal.

As mentioned above, the callosal innervation of row A representation and the rest of the BC is markedly different (Fig 12A). Heterotopic (i.e., non-mirror symmetric) optogenetics stimulation could evoke a response (Fig 13A,13C) in the totality of plBC neurons (4/4, 100%) but only in a proportion of amBC neurons (4/7, 57%). In either case, they can linearly sum to homotopic ones (Fig 13G-H). Yet, while in plBC homo- and heterotopic responses have a similar onset delay (Fig 13B, Tab 4), in amBC heterotopic responses are more delayed (Fig 13D, Tab 4), suggesting the involvement of differences in the underlying synaptic pathways. One reason may be the lack of direct heterotopic callosal contacts in amBC, as opposed to their presence in plBC, thus heterotopic responses may be supported by local reverberation of the response conveyed by axonal branches of monosynaptically excited neurons (as above), or by the excitation of the contralateral S2 that is known to project to the ipsilateral BC (Petersen, 2019). An alternative yet less parsimonious reason may be the lower calibre or myelination of heterotopic axons reaching the amBC compared to plBC, which would slow down the triggering of the synaptic events in the amBC. Which one of the possible scenarios is at play in the BC subregions poorly and richly innervated by the CC requires further research.

5.9 Callosal recruitment of feed-forward inhibition in the barrel cortex

With this work we provide for the first time evidence that ipsilateral whiskers stimulation can recruit feed-forward inhibition in the BC (Fig 9A). We have reached this conclusion because the onset of IPSPs is consistently delayed with respect to the one of the EPSPs, both in plBC (medians' diff.= 4.9 ms) and amBC (medians' diff.=12 ms). Yet, in the plBC this mechanism is more abrupt than in amBC (Fig 9B-C), and its timing more closely resemble the feed-forward inhibition brought about by thalamocortical volleys, where the EPSPs-IPSPs onset sequence is separated by 4 ms (medians' diff.) in our pool. In the contralateral, thalamocortical pathway, this form of inhibition of projection neurons heavily relies on Parvalbumin$^+$ (PV$^+$) fast-spiking interneurons (Gabernet et al., 2005), but also Somatostatin$^+$ interneurons can perform it with distinct dynamics (Tan et al., 2008). In both cases, this process is typically disynaptic. Note that in a thalamocortical disynaptic inhibition, the pyramidal (or another inter-) neuron and the interneuron are supposed to receive excitatory inputs at roughly the same time from the thalamus. However, in order to observe the onset of inhibitory currents in the pyramidal neuron, the interneuron needs a time window for summing up the thalamic PSPs to reach its action potential (AP) threshold, plus another interval for the AP to propagate until the axon terminal and release GABA. This results in a net delay for the occurrence of IPSPs compared to EPSPs in the pyramidal neuron. In the BC, PV$^+$ fast-spiking interneurons are involved in this mechanism (Gabernet et al., 2005), and have a well myelinated axon with fast conduction velocity (Micheva et al., 2021). From the peak of an AP recorded at the soma, the latency for the onset of the first inhibitory postsynaptic current in a connected pyramidal neuron has a median of 1.27 ms (Micheva et al., 2021). Since we recorded IPSPs lagging EPSPs of 4 ms, putative contralateral PV$^+$ fast-spiking interneurons had on average only 2-3 ms to arrive at AP threshold upon thalamic trigger.

However, we do not know what basal membrane potential they rest at (i.e., their distance form AP threshold) nor their intrinsic excitability, thus is difficult to estimate with what speed they sum up thalamic EPSPs. Instead, what we can suspect is that this feed-forward inhibition was very likely disynaptic, because a higher number of consecutive synapses would further increase the delay for IPSPs occurrence and not fit the data. In the same manner, the very small delay present in the EPSPs-IPSPs onset sequence in response to the ipsilateral stimulation may indicate that a similar callosally-mediated disynaptic inhibition was taking place in plBC, as it has been demonstrated in the mouse primary auditory cortex (Rock and Apicella, 2015). This mechanism at the callosal synapse in the BC is plausible because, in L6, interneurons can be directly excited by callosal afferents in row A (Petreanu et al., 2007). However, to date, we do not know how relevant or widespread this connectional motif is.

5.10 Can callosal hubs mediate transhemispheric learning?

Once defined as the "riddle of the corpus callosum" (Sperry, 1961), the apparent lack of behavioural effects following rescission of the greatest cerebral commissure puzzled researchers for long. Cats and monkeys with callosum resection appeared "[...] virtually indistinguishable from their normal cage mates under most testing and training conditions" (Sperry, 1961). Remarkably, sectioning the totality of brain commissures (e.g., habenular, hippocampal, anterior etc.) through midline cuts would result in: "Aside from manifesting an initial tremor and unsteadiness when the cerebellum is bisected, monkeys recovered from such midline surgery show no disabling paralysis, ataxia, or spasticity. There is no forced circling, nor are there other asymmetries. The animals are not overly hyperactive or lethargic. Visceral and other homeostatic functions continue as before. The monkeys remain alert and curious and retain fair-to-good muscular coordination. They perceive, learn, and remember much as normal animals do" (Sperry, 1961). Probably, the "riddle of the *commissures*" would have been more appropriate in this case.

However, in 1955, Ronald Myers discovered something that would have attracted a great wealth of neuroscientific endeavour for more than half a century. He found that cats with corpus callosum and optic chiasm resection could not perform a visual discrimination task learned with one eye when tested on the untrained eye (Myers 1955; Myers and Sperry, 1958). Controls having only the optic chiasm resection but the callosum intact could instead perform well with the untrained eye. Also, after training with the corpus callosum intact, if one removes in these cats the hemisphere in the directly trained side (ipsilateral), they are able to perform the task by using the untrained eye. The authors conclude that "the corpus callosum is shown to be instrumental in laying down a second set of memory traces, or engrams, in the contralateral hemisphere - a mirror-image duplicate or weak carbon copy of the engram on the directly trained side [...]". The Nobel laureate also ascribes other two prominent functions to the corpus callosum. One is that this structure aids the visual use of both hands across the vertical midline of the visual space, somehow anticipating the midline fusion theory; the second is an interhemispheric general excitatory tonic effect (Sperry 1961).

Primary sensory cortices of placental mammals have sparser callosal innervation than higher cortical centres (Innocenti, 1986). In cats, monkeys and rodents visual callosal connections are concentrated in a strip between V1 (or area 17) and V2 (or area 18) called binocular or transition zone, allotted to the vertical meridian of the visual space (Berlucchi and Rizzolatti 1968). A similar pattern of callosal connections limited to a stripe at the border between S1 and S2 characterises the whiskers representation of mice and rats (Olavarria et al., 1984; Koralek et al.,1990). In the thesis, we have shown that also this stripe can be dedicated to the midline of the sensory space pertaining to the whiskers. Here we speculatively ask: Can such callosal hubs be the neuronal relays of the sensory transhemispheric learning described by Sperry and associates?

As mentioned above, the c-Fos is a component of the AP-1 transcription factor which activates DNA expression. In this manner, synaptic proteins may be produced which can potentiate or depress synapses. For this reason, c-Fos production has been linked to learning processes at the neural level (Kaczmarek 1993; Staiger, 2006). For example, Staiger (2006) reports that the same single whisker experience leading to c-Fos production can activate the calcium-calmodulin kinase IIα and cAMP-response element binding protein (CREB), widely known to be responsible for plastic changes in synaptic strength. Under this perspective, our result on UL_{deaff} mice showing c-Fos production in the plBC and septa (Fig 6D-G) may indicate that a certain learning process was taking place through the activation of callosal fibres. For example, the hypothesis that the circuit was re-adjusting to enable the mouse to palpate objects in the absence of half of the touch periphery cannot be ruled out.

Other evidence links the callosal activity to learning. Sleep is fundamental to memory formation and consolidation, especially its non-REM phase, or slow wave sleep (Stickgold 2005). A 10-100 Hz electrical stimulation of callosal fibres during sodium pentobarbital-induced slow wave activity enhances callosally-mediated EPSPs in neurons (Cissé et al., 2004), demonstrating that these fibres are capable of forms of plasticity linked to memory formation during slow wave activity. Moreover, early unilateral whiskers denervation, strengthen callosal activation of sensory-deprived L5 neurons (Petrus et al., 2019), a mechanism through which the spared whiskers acquire a bilateral representation, explaining certain symptoms in patients following amputation and demonstrating a high degree of callosal plasticity. Even more recent is the finding that calcium transients in afferent callosal fibres of the barrel cortex are mostly present during behavioural quiescence, that is when the animal is awake but quiet and does not whisk (Oran et al., 2021). Also in this state neurons can entrain in slow wave activity (Vyazovskiy et al., 2011). Oran and associates (2021) interpret the fact that the callosal activity is relegated to behaviourally inactive periods by invoking a callosal role in bilateral homeostasis. More specifically, they propose that callosal fibres may install a set-point of comparable sensitivity between the two hemispheres during quiescence that was lost during active behaviour for the largely asymmetric environmental recruitment of the two hemispheres. We add that, if confirmed, such a 're-setting' may be in itself how the transhemispheric learning process does occur. In this case, the cytoarchitectonic borders of primary visual and somatosensory cortices (i.e., areas 17/18 and S1/S2 border) may be the candidate centres mediating some of the transhemispheric exchange of experiences and skills, which would require slow wave activity during sleep. Favouring

this view, brainstem monoaminergic systems that innervate the cortex have important roles in slow wave activity (e.g., noradrenaline, Cirelli et al., 2005; Constantinople and Bruno, 2011) and induction of LTP gene expression (Cirelli et al., 2000). Importantly, precisely at the area 17/18 border of the monkey, monoaminergic innervation changes pattern: serotonin innervation of area 17 is gradually replaced in area 18 by noradrenaline and dopamine innervation (Parnavelas and Papadopoulos, 1989). Consequently, this pattern could have distinct effects on LTP gene expression. However, what is the functional role of this pattern's switch of monoaminergic innervation at the cytoarchitectonic border remains unknown.

What would happen if the split chiasm cats who learned visual discrimination with one eye are sleep-deprived before being tested on the untrained eye? Would transhemispheric learning still occur in the absence of slow wave activity? Would we find more c-Fos at the area 17/18 border after a session of training in the hemisphere contralateral to the trained eye, similarly to our results for the whiskers? And, lastly, what are the interactions between the brainstem monoaminergic system and the corpus callosum during the slow wave activity? Studies which directly address these questions are thus required to confirm such a hypothesis for callosal hubs in early sensory cortices.

As we explained along this thesis, most of the evidence about the functions of the CC were obtained from split-brain studies, together with other brain lesions and agenesis of the CC in patients and animals. These studies have reported extraordinarily valuable information to understand the function of the CC. However, it is known that brain lesions, or other types of long term functional changes, generate neuronal plasticity modifications (Baynes et al., 1995; Glickstein, 2009), allowing compensatory mechanisms that could mask relevant features of the underlying interhemispheric communication. This can be summed up in the sentence of Pascual-Leone and colleagues (2005): "symptoms are not the manifestation of the injured brain region, but rather the expression of plastic changes in the rest of the brain". For these reasons, in this thesis acute interhemispheric disconnection by TTX application (Fig 10) has been favoured to the classic approach of a chronic callosotomy.

5.11 Whiskers: functionally equivalent or distinct?

There is some evidence that assigns distinct roles to different whiskers rows. For example, row E whiskers (i.e., the most lateral row) have been found to encode locomotion speed, acceleration and head-turns in rats (Chorev et al., 2016). Furthermore, computer simulations assigned different functions to different rows of whiskers by virtue of their morphological trends and position in the whiskers array (Hobbs et al., 2016). In addition, during the whisking cycle, whiskers rotate around their axis. In this torsion, the upper rows (A and B) counter-rotate with respect to lower rows (C, D and E) (Knutsen et al., 2008). This is attributed to oblique intrinsic muscles which differently anchor to whiskers follicles in upper and lower rows, producing opposite torsional patterns (Haidarliu et al., 2017). Such a characteristic may be due to different roles in the whisking cycle. Our result of a favourite interhemispheric activity transmission between rows A adds evidence for functional grouping of different rows as well. However, behavioural experiments that investigated the capability of rats to discriminate the width of an aperture (Krupa et al.,

2001b) or the horizontal offset of two poles at the two sides of the snout (Knutsen and Ahissar 2006) found that cutting the whiskers either along an arc or a row affected the performance comparably. In general, they found that what is detrimental to task learning (Knutsen and Ahissar 2006) or execution (Krupa et al., 2001) is a reduced number of whiskers, independently of their identity (i.e., their belonging to a specific row or arc). Consequently, this suggested the whiskers are functionally equivalent (Krupa et al., 2001). Indeed, Chaudhary and Rema (2018) found that trimming unilaterally the array of whiskers deteriorated the performance of rats in a gap-crossing task. Yet, they also reported that the deficit was less important if a similar number of whiskers was removed from upper rows (A, B and C) bilaterally, thus sparing lower rows (E and D) bilaterally. They concluded that not only the number of whiskers is important for a good performance, but also their bilateral availability. Thus, whether whiskers are functionally equivalent or distinct is far from being clear. Likely, the different task demands involved in the diverse cases contributed to provoke a different strategy of whiskers use, rendering them more or less replaceable (Krupa et al., 2001; Knutsen and Ahissar 2006) but only if bilaterally balanced (Chaudhary and Rema 2018; Suarez et al., 2014a).

5.12 Beyond the midline rule in the whiskers system

By whisking, mice scan the peripersonal space to extract environmental information. Objects' properties and location may be encoded in the brain by different coding strategies exploiting a spatial frame of reference (Knutsen and Ahissar, 2009). A map of the scanned space is represented by L2/3 of the BC in mice whisking against a pole (Pluta et al., 2017). In other primary sensory systems, information relative to peripersonal space is known to be encoded with respect to an egocentric frame of reference, to possibly serve, in a second stage, a wider allocentric navigation system (Wang et al., 2020). This view is inspired by the associative parietal cortex of the primate, where egocentric neural representations for object reaching and grasping can be defined relative to head, eye or limb (Andersen and Buneo, 2002). Also the rat's posterior parietal cortex (PPC) contains cells signalling ego- and allocentric coordinates (Wilber et al., 2014) and it receives axonal connections from the BC (Petersen, 2019). In the BC, neurons representing the row E-whiskers have been found to encode egomotion and head-turns (Chorev et al., 2016). Moreover, a single touch of the C2 whisker provokes widespread cortical activity which reaches the PPC with bilateral symmetry within 100 ms (Aronoff et al., 2010), demonstrating that this area integrates whiskers information that can be relative to egomotion. Thus, it is possible that head direction cells, present in the rat PPC (Wilber et al., 2014), integrate information from the whiskers which track head position and, perhaps, the position of other face-related parts.

As noted, contrary to the amBC, the plBC receive heterotopic inputs as directly as homotopic ones because their onset does not differ in delay upon contralateral BC activation (Tab 4). Moreover, early symmetric upper (rows A, B, C) whiskers removal, do not abolish the formation of the callosal innervation of the plBC (S1/S2 border in Suarez et al., 2014a), suggesting that this region is invaded also from heterotopic (i.e., non-plBC) callosal axons. Since heavily callosal-connected body representations, as the plBC one, are thought to represent the midline of the tactile sensory space (Manzoni et

al., 1989; Iwamura, 2000), and that the two rows A are the ones that lay nearest to the facial midline, here we propose that such a circuit may be used by the animal to gather incoming sensory inputs from the two sides of the snout while organising them with reference to a sensory midline, roughly aligned with the facial one. During object scanning, this mechanism may help the mouse to point the centrally placed body parts, such as the nose and the mouth, towards touch-salient features. Indeed, in rodents, whisking and sniffing are tightly coupled (Deschenes et al., 2012). This phenomenon would not be so far from what happens in another, highly tactile species: the star-nosed mole. In order to align the mouth with a piece of food for its ingestion, this animal performs a 'tactile foveation' which is mediated by highly touch-sensitive midline appendages interposed between the two nostrils (11th appendages; Catania and Remple, 2003). Strikingly resembling the row A-whiskers representation in mice and rats, the 11th appendages have the densest callosal innervation among the peers which form the tactile 'star' (Catania and Khaas, 2001). Therefore, the row A-whiskers system may be used to align spatial coordinates of the scanned space between midline organs.

5.13 Possible significance of densely callosal cortical areas

Furthermore, here we propose that dense callosal reciprocal innervation of sensorimotor cortices may be a developmental strategy for cortical magnification. This is because a given organ's representation is doubled without subtracting cortical space in the home hemisphere. Thus, even if row A-whiskers, unlike the 11th appendage of the star-nosed mole, do not seem to have a more magnified representation in the home hemisphere than other whiskers, they can be considered instead *callosally* magnified. Consequently, the lack of efficiency in signalling from which side of the snout a given contact occurred (due to their largely side-invariant cortical representation), it may be compensated by the fact that, once their barrel columns are active, they may count on two hemispheres instead of one (as the case of the remaining rows) for downstream processing of the activity. With this mechanism, densely callosal areas may have a stronger weight on the behavioural output. If experimentally confirmed, this could contribute to explain why in the acute phase of a callosotomy, patients can lose control of body parts.

5.14 Limits of the study

Our results obtained through TTX and ChR2 demonstrate that the vigorous ipsilateral response depends on contralateral callosal-projection neurons. However, we should stress that this may not be valid for the totality of neurons. Indeed, our interpretation is based on the grand averages of the pool of neurons sampled, allowing us to describe the general, most common trend. However, we cannot ultimately exclude the presence of a minority of cases of neurons endowed with an ipsilateral receptive field originating in subcortical structures instead of the opposite hemisphere.

Moreover, we do not know the real proportion of sensory midline-representing neurons of row A. One problem is related to the method used to identify them. Indeed, we obtained different percentages using the Mahalanobis distance of the parameters, where the 50% of neurons resulted roughly equidistant between contra- and ipsilateral responses (Fig

10C), and the coefficient of cross-correlation of the two waveform averages, that indicated an almost complete overlap for contra- and ipsilateral responses in the 32.7% of the neurons (Fig 10F-G). In either case, a greater problem for their estimation are the blind patch-clamp recordings used in this study. These may have led us sometimes to record in the *proximity* instead of *in* the exact cortical representation intended, thus, in any case, our percentages are very likely an underestimation. Indeed, our onset of the subthreshold response in the granular layer (median= 11 ms) is delayed if compared to principal whisker stimulation estimate in the rat (from 6.6 to 9.4 ms) (Brecht et al., 2002). However, upon closer inspection, response in 4 granular neurons had an onset > 15 ms, well above what is reported for principal whisker response of thalamorecipient neurons (Brecht et al., 2002), suggesting that in these cases the recordings were out of the cortical representation of the stimulated whiskers. In fact, when these neurons were excluded from the interlaminar comparison of Tab1, the granular layer responded significantly faster (10.4 [9-11.3] ms) than supra- and infragranular layers (Kruskal-Wallis test on onset delay: χ^2= 7.53, df= 2, p= 0.0232; p_{IvsG}= 0.0166, p_{SvsG}= 0.0104), with a median onset delay within the range of principal whisker responses found in barrels and septa (6.6 - 13 ms; Brecht et al., 2002). The same exclusion criterion would be not possible to apply in supra- and infragranular layers since in L2/3 the onset to principal whisker stimulation in barrels and septa has a huge variability (5 - 39.8 ms; Brecht et al., 2003), and in L5 only the onset associated with barrels is known (9.6 - 10.6 ms; Manns et al., 2004) but not the one relative to septa (normally longer). To overcome these problems, next investigations may use intrinsic optical imaging as in Knutsen et al., 2016 prior to recordings.

Additionally, our protocol for whiskers' stimulation has been very useful for the objective of learning about peculiarities related to whiskers identity and their callosal representation. However, it remains to be discovered what kind of information was transmitted interhemispherically. It is well known that the BC neurons are sensitive to the identity of the whisker stimulated (principal *vs* surround; Brecht et al., 2002, 2003), their number (Mirabella et al., 2001), the direction of the stimulation and its speed (Bale and Maravall, 2018). Since we were focused only on the callosal mapping, we kept all of these aspects constant for the sensory stimulation. Future investigations may address such a topic by systematically varying the above parameters while recording ipsilateral responses. Some information about whiskers identity is present in Shuler et al., 2001, where the authors find that homologous whiskers are better connected than heterologous ones and that rostral whiskers are better connected than caudal ones via the corpus callosum. However, the anteroposterior and mediolateral coordinates of their electrode penetrations are not reported, thus we do not know in which barrel representation they were recording from. In the cat area 17/18 border, callosal-recipient neurons are normally complex cells which are sensitive to roughly the same visual features presented in either visual field (Berlucchi and Rizzolatti, 1968). However, we do not know yet if a similar scenario applies to the rodents' whiskers.

6. Conclusions/ Conclusiones

Here it follows a list of conclusions of both studies:

1) The difference in up state features of membrane potential in MSNs allows one to separate the DL and DM striatal subpopulations.

2) DS-MSNs' differences in up states can be attributed to different cortical couplings: frontoparietal areas (FrA, M1 and S1) with the dorsolateral striatum and V1 with the dorsomedial striatum, similarly to the condition in the primate.

3) The up state activity in the membrane potential of MSNs recorded at the DCS coordinates suggest that DLS and DMS-MSNs are discrete subpopulations in their relation to the propagating slow wave.

4) Integration of the slow wave oscillation from the neocortex differs between direct and indirect MSNs only in the DLS, while in DMS it is integrated homogeneously by the two pathways.

5) The use of whiskers during exploration can activate the production of c-Fos in the ipsilateral hemisphere, more abundantly in CC-recipient whiskers representations (plBC).

6) Whisker representations in the BC of the mouse preferentially activate homotopic subregions in the contralateral BC through the CC, reproducing in a smaller scale its macroscopic anatomical organisation.

7) Due to the strong callosal recruitment of the plBC (mostly homotopic), row A-whiskers have a side-invariant representation in a proportion of neurons. These neurons may contribute to fuse left and right sensory hemi-spaces at the facial midline.

8) The homotopic ipsilateral stimulation can recruit feed-forward inhibition in the BC. As it occurs in other cortical areas, this mechanism may be mediated by the CC.

9) The plBC integrates more directly activity from heterotopic contralateral BC subregions than the callosally-poor amBC.

A continuación, se muestra una lista de conclusiones de ambos los estudios:

1) La diferencia en las características del *up state* del potencial de membrana de las MSNs permite separar las subpoblaciones estriatales DL y DM.

2) Las diferencias entre DS-MSNs en *up state* se pueden atribuir a diferentes acoplamientos corticales: áreas frontoparietales (FrA, M1 y S1) con el estriado dorsolateral y V1 con el estriado dorsomedial, de manera similar a lo descrito en primates

3) La actividad durante los *up states* de las MSNs registradas en las coordenadas DCS sugiere que las DLS-MSNs y DMS-MSNs son subpoblaciones discretas,

4) La integración de la oscilación de onda lenta de la neocorteza difiere entre los MSN directas e indirectas solo en el DLS, mientras que en el DMS es integrada homogéneamente por las dos vías.

5) El uso de los bigotes durante la exploración puede activar la producción de c-Fos en el hemisferio ipsilateral, más abundantemente en las representaciones de bigotes que reciben mas axones desde el CC (plBC).

6) Las representaciones de bigotes en la corteza de barriles del ratón activan preferentemente subregiones homotópicas en la corteza de barriles contralateral a través del CC, reproduciendo en menor escala su organización anatómica macroscópica.

7) Debido al fuerte reclutamiento calloso de la plBC (principalmente homotópico), los bigotes de la fila A tienen una representación invariante con respecto al lado del cuerpo, en una proporción de neuronas. Estas neuronas pueden contribuir a fusionar los hemi-espacios sensoriales izquierdo y derecho de la línea media facial.

8) La estimulación ipsilateral homotópica puede reclutar inhibición de tipo feed-forward en la corteza de barriles. Como ocurre en otras áreas corticales, este mecanismo puede estar mediado por el CC.

9) La plBC integra más directamente la actividad de las subregiones BC contralaterales heterotópicas que la amBC, la cual recibe menor innervación callosa.

7. References

Abudukeyoumu, N., Hernandez-Flores, T., Garcia-Munoz, M., & Arbuthnott, G. W. (2019). Cholinergic modulation of striatal microcircuits. *European Journal of Neuroscience*, 49(5), 604-622.

Adesnik, H., & Scanziani, M. (2010). Lateral competition for cortical space by layer-specific horizontal circuits. *Nature*, *464*(7292), 1155-1160.

Ahissar, E., & Staiger, J. (2010). S1 laminar specialization. Scholarpedia, 5(8):7457.

Alegre-Cortés, J., Soto-Sánchez, C., Pizá, Á. G., Albarracín, A. L., Farfán, F. D., Felice, C. J., & Fernández, E. (2016). Time–frequency analysis of neuronal populations with instantaneous resolution based on noise-assisted multivariate empirical mode decomposition. *Journal of neuroscience methods*, *267*, 35-44.

Alegre-Cortés, J., Sáez, M., Montanari, R., & Reig, R. (2021). Medium spiny neurons activity reveals the discrete segregation of mouse dorsal striatum. *Elife*, *10*, e60580.

Alloway, K. D., Lou, L., Nwabueze-Ogbo, F., & Chakrabarti, S. (2006). Topography of cortical projections to the dorsolateral neostriatum in rats: multiple overlapping sensorimotor pathways. *Journal of Comparative Neurology*, *499*(1), 33-48.

Anastasiades, P. G., Marlin, J. J., & Carter, A. G. (2018). Cell-type specificity of callosally evoked excitation and feedforward inhibition in the prefrontal cortex. *Cell reports*, *22*(3), 679-692.

Andersen, R. A., & Buneo, C. A. (2002). Intentional maps in posterior parietal cortex. *Annual review of neuroscience*, *25*(1), 189-220.

Antón-Bolaños, N., Sempere-Ferràndez, A., Guillamón-Vivancos, T., Martini, F. J., Pérez-Saiz, L., Gezelius, H., ... & López-Bendito, G. (2019). Prenatal activity from thalamic neurons governs the emergence of functional cortical maps in mice. *Science*, *364*(6444), 987-990.

Aronoff, R., Matyas, F., Mateo, C., Ciron, C., Schneider, B., & Petersen, C. C. (2010). Long-range connectivity of mouse primary somatosensory barrel cortex. *European Journal of Neuroscience*, 31(12), 2221-2233.

Bale, M. R., & Maravall, M. (2018). Organization of sensory feature selectivity in the whisker system. *Neuroscience*, *368*, 70-80.

Balleine, B. W., & O'doherty, J. P. (2010). Human and rodent homologies in action control: corticostriatal determinants of goal-directed and habitual action. *Neuropsychopharmacology*, *35*(1), 48-69.

Baynes, K., & Gazzaniga, M. S. (2005). Lateralization of language: Toward a biologically based model of language. *Linguistic Review*, 22(2-4), 303-326.

Beltramo, R., D'urso, G., Dal Maschio, M., Farisello, P., Bovetti, S., Clovis, Y., ... & Fellin, T. (2013). Layer-specific excitatory circuits differentially control recurrent network dynamics in the neocortex. *Nature neuroscience*, *16*(2), 227-234.

Berlucchi, G., & Rizzolatti, G. (1968). Binocularly driven neurons in visual cortex of split-chiasm cats. *Science*, *159*(3812), 308-310.

Berlucchi, G. (1981). Una ipotesi neurofisiologica sulle asimmetrie funzionali degli emisferi cerebrali dell'uomo. *Ricerche di Psicologia*.

Berlucchi, G. (1983). Two hemispheres but one brain. *Behavioral and Brain Sciences*, *6*(1), 171-172.

Bloom, J. S., & Hynd, G. W. (2005). The role of the corpus callosum in interhemispheric transfer of information: excitation or inhibition? *Neuropsychology review*, *15*(2), 59-71.

Brecht, M., & Sakmann, B. (2002). Dynamic representation of whisker deflection by synaptic potentials in spiny stellate and pyramidal cells in the barrels and septa of layer 4 rat somatosensory cortex. *The Journal of physiology*, *543*(1), 49-70.

Brecht, M., Roth, A., & Sakmann, B. (2003). Dynamic receptive fields of reconstructed pyramidal cells in layers 3 and 2 of rat somatosensory barrel cortex. *The Journal of physiology*, *553*(1), 243-265.

Carter, A. G., & Sabatini, B. L. (2004). State-dependent calcium signaling in dendritic spines of striatal medium spiny neurons. *Neuron*, *44*(3), 483-493.

Catania, C. K., & Kaas, J.H. (2001). Areal and callosal connections in the somatosensory cortex of the star-nosed mole. *Somatosensory & motor research*, *18*(4), 303-311.

Catania, K. C., & Remple, F. E. (2004). Tactile foveation in the star-nosed mole. *Brain, behavior and evolution*, *63*(1), 1-12.

Chen, W., de Hemptinne, C., Miller, A. M., Leibbrand, M., Little, S. J., Lim, D. A., ... & Starr, P. A. (2020). Prefrontal-subthalamic hyperdirect pathway modulates movement inhibition in humans. *Neuron*, *106*(4), 579-588.

Chorev, E., Preston-Ferrer, P., & Brecht, M. (2016). Representation of egomotion in rat's trident and E-row whisker cortices. *Nature neuroscience*, *19*(10), 1367-1373.

Chaudhary, R., & Rema, V. (2018). Deficits in behavioral functions of intact barrel cortex following lesions of homotopic contralateral cortex. *Frontiers in systems neuroscience*, *12*, 57.

Chuhma, N., Mingote, S., Kalmbach, A., Yetnikoff, L., & Rayport, S. (2017). Heterogeneity in dopamine neuron synaptic actions across the striatum and its relevance for schizophrenia. *Biological psychiatry*, *81*(1), 43-51.

Cirelli, C., & Tononi, G. (2000). Differential expression of plasticity-related genes in waking and sleep and their regulation by the noradrenergic system. *Journal of Neuroscience*, *20*(24), 9187-9194.

Cirelli, C., Huber, R., Gopalakrishnan, A., Southard, T. L., & Tononi, G. (2005). Locus ceruleus control of slow-wave homeostasis. *Journal of Neuroscience*, *25*(18), 4503-4511.

Cissé, Y., Crochet, S., Timofeev, I., & Steriade, M. (2004). Synaptic enhancement induced through callosal pathways in cat association cortex. *Journal of neurophysiology*, *92*(6), 3221-3232.

Cissé, Y., Grenier, F., Timofeev, I., & Steriade, M. (2003). Electrophysiological properties and input-output organization of callosal neurons in cat association cortex. *Journal of neurophysiology*, *89*(3), 1402-1413.

Conti, F., & Manzoni, T. (1994). The neurotransmitters and postsynaptic actions of callosally projecting neurons. *Behavioural brain research*, *64*(1-2), 37-53.

Constantinople, C. M., & Bruno, R. M. (2011). Effects and mechanisms of wakefulness on local cortical networks. *Neuron*, *69*(6), 1061-1068.

Constantinople, C. M., & Bruno, R. M. (2013). Deep cortical layers are activated directly by thalamus. *Science*, *340*(6140), 1591-1594.

Cook, N. D. (1984). Homotopic callosal inhibition. *Brain and language*, *23*(1), 116-125.

Cowan, R. L., & Wilson, C. J. (1994). Spontaneous firing patterns and axonal projections of single corticostriatal neurons in the rat medial agranular cortex. *Journal of neurophysiology*, *71*(1), 17-32.

Denenberg, V. H., Fitch, R. H., Schrott, L. M., Cowell, P. E., & Waters, N. S. (1991). Corpus callosum: Interactive effects of infantile handling and testosterone in the rat. *Behavioral neuroscience*, *105*(4), 562.

Deschênes, M., Moore, J., & Kleinfeld, D. (2012). Sniffing and whisking in rodents. *Current opinion in neurobiology*, *22*(2), 243-250.

Diamond, M. E., Von Heimendahl, M., Knutsen, P. M., Kleinfeld, D., & Ahissar, E. (2008). 'Where' and 'what' in the whisker sensorimotor system. *Nature Reviews Neuroscience*, *9*(8), 601-612.

Doig, N. M., Moss, J., & Bolam, J. P. (2010). Cortical and thalamic innervation of direct and indirect pathway medium-sized spiny neurons in mouse striatum. *Journal of Neuroscience*, *30*(44), 14610-14618.

English, D. F., Ibanez-Sandoval, O., Stark, E., Tecuapetla, F., Buzsáki, G., Deisseroth, K., ... & Koos, T. (2012). GABAergic circuits mediate the reinforcement-related signals of striatal cholinergic interneurons. *Nature neuroscience*, *15*(1), 123-130.

Erzurumlu, R. S., Murakami, Y., & Rijli, F. M. (2010). Mapping the face in the somatosensory brainstem. *Nature Reviews Neuroscience*, *11*(4), 252-263.

Everitt, B. J., Parkinson, J. A., Olmstead, M. C., Arroyo, M., Robledo, P., & Robbins, T. W. (1999). Associative processes in addiction and reward the role of amygdala-ventral striatal subsystems. *Annals of the New York Academy of Sciences*, *877*(1), 412-438.

Fenlon, L. R., Suárez, R., & Richards, L. J. (2017). The anatomy, organisation and development of contralateral callosal projections of the mouse somatosensory cortex. *Brain and Neuroscience Advances*, *1*, 2398212817694888.

Filipkowski, R. K., Rydz, M., Berdel, B., Morys, J., & Kaczmarek, L. (2000). Tactile experience induces c-fos expression in rat barrel cortex. *Learning & Memory*, *7*(2), 116-122.

Fukushima, T., & Kerr, F. W. (1979). Organization of trigeminothalamic tracts and other thalamic afferent systems of the brainstem in the rat: presence of gelatinosa neurons with thalamic connections. *Journal of Comparative Neurology*, *183*(1), 169-184.

Gabernet, L., Jadhav, S. P., Feldman, D. E., Carandini, M., & Scanziani, M. (2005). Somatosensory integration controlled by dynamic thalamocortical feed-forward inhibition. *Neuron*, *48*(2), 315-327.

Gazzaniga, M. S. (2000). Cerebral specialization and interhemispheric communication: does the corpus callosum enable the human condition? *Brain*, *123*(7), 1293-1326.

Gener, T., Reig, R., & Sanchez-Vives, M. V. (2009). A new paradigm for the reversible blockage of whisker sensory transmission. *Journal of neuroscience methods*, *176*(2), 63-67.

Getting, P. A. (1989). Emerging principles governing the operation of neural networks. *Annual review of neuroscience*, *12*(1), 185-204.

Glickstein, M. (2009). Paradoxical inter-hemispheric transfer after section of the cerebral commissures. *Experimental brain research*, *192*(3), 425.

Goebbels, S., Bormuth, I., Bode, U., Hermanson, O., Schwab, M. H., & Nave, K. A. (2006). Genetic targeting of principal neurons in neocortex and hippocampus of NEX-Cre mice. *Genesis*, *44*(12), 611-621.

Getting, P. A. (1989). Emerging principles governing the operation of neural networks. *Annual review of neuroscience*, *12*(1), 185-204.

Haidarliu, S., Bagdasarian, K., Shinde, N., & Ahissar, E. (2017). Muscular basis of whisker torsion in mice and rats. *The Anatomical Record*, *300*(9), 1643-1653.

Hintiryan, H., Foster, N. N., Bowman, I., Bay, M., Song, M. Y., Gou, L., ... & Dong, H. W. (2016). The mouse cortico-striatal projectome. *Nature neuroscience*, *19*(8), 1100-1114.

Hayama, T., & Ogawa, H. (1997). Regional differences of callosal connections in the granular zones of the primary somatosensory cortex in rats. *Brain research bulletin*, *43*(3), 341-347.

Hobbs, J. A., Towal, R. B., & Hartmann, M. J. (2016). Evidence for functional groupings of vibrissae across the rodent mystacial pad. *PLoS computational biology*, 12(1), e1004109.

Hoffer, Z. S., & Alloway, K. D. (2001). Organization of corticostriatal projections from the vibrissal representations in the primary motor and somatosensory cortical areas of rodents. *Journal of Comparative Neurology*, *439*(1), 87-103.

Hooks, B. M., Papale, A. E., Paletzki, R. F., Feroze, M. W., Eastwood, B. S., Couey, J. J., ... & Gerfen, C. R. (2018). Topographic precision in sensory and motor corticostriatal projections varies across cell type and cortical area. *Nature communications*, *9*(1), 1-16.

Hoover, J. E., Hoffer, Z. S., & Alloway, K. D. (2003). Projections from primary somatosensory cortex to the neostriatum: the role of somatotopic continuity in corticostriatal convergence. *Journal of neurophysiology*, *89*(3), 1576-1587.

Innocenti, G. M. (1986). General organization of callosal connections in the cerebral cortex. In *Sensory-motor areas and aspects of cortical connectivity* (pp. 291-353). Springer, Boston, MA.

Ivy, G. O., & Killackey, H. P. (1981). The ontogeny of the distribution of callosal projection neurons in the rat parietal cortex. *Journal of Comparative Neurology*, *195*(3), 367-389.

Iwamura, Y. (2000). Bilateral receptive field neurons and callosal connections in the somatosensory cortex. *Philosophical Transactions of the Royal Society of London. Series B: Biological Sciences*, *355*(1394), 267-273.

Joel, D., & Weiner, I. (2000). The connections of the dopaminergic system with the striatum in rats and primates: an analysis with respect to the functional and compartmental organization of the striatum. *Neuroscience*, *96*(3), 451-474.

Jones, E. G., & Powell, T. P. (1968). The commissural connexions of the somatic sensory cortex in the cat. *Journal of Anatomy*, *103*(Pt 3), 433.

Kaas, J. H. (2004). Evolution of somatosensory and motor cortex in primates. *The Anatomical Record Part A: Discoveries in Molecular, Cellular, and Evolutionary Biology: An Official Publication of the American Association of Anatomists*, *281*(1), 1148-1156.

Kaczmarek, L. (1993). Molecular biology of vertebrate learning: is c-fos a new beginning? *Journal of neuroscience research*, *34*(4), 377-381.

Kandel, E. R., Schwartz, J. H., Jessell, T. M., Siegelbaum, S., Hudspeth, A. J., & Mack, S. (Eds.). (2003). *Principles of neural science*. New York: McGraw-hill.

Karayannis, T., Huerta-Ocampo, I., & Capogna, M. (2007). GABAergic and pyramidal neurons of deep cortical layers directly receive and differently integrate callosal input. *Cerebral Cortex*, *17*(5), 1213-1226.

Kasanetz, F., Riquelme, L. A., & Murer, M. G. (2002). Disruption of the two-state membrane potential of striatal neurones during cortical desynchronisation in anaesthetised rats. *The Journal of physiology*, *543*(2), 577-589.

Kawaguchi, Y. (1992). Receptor subtypes involved in callosally-induced postsynaptic potentials in rat frontal agranular cortex in vitro. *Experimental Brain Research*, *88*(1), 33-40.

Kawaguchi, Y. (1993). Physiological, morphological, and histochemical characterization of three classes of interneurons in rat neostriatum. *Journal of Neuroscience*, *13*(11), 4908-4923.

Kincaid, A. E., Zheng, T., & Wilson, C. J. (1998). Connectivity and convergence of single corticostriatal axons. *Journal of Neuroscience*, *18*(12), 4722-4731.

Klaus, A., Martins, G. J., Paixao, V. B., Zhou, P., Paninski, L., & Costa, R. M. (2017). The spatiotemporal organization of the striatum encodes action space. *Neuron*, *95*(5), 1171-1180.

Knutsen, P. M., Pietr, M., & Ahissar, E. (2006). Haptic object localization in the vibrissal system: behavior and performance. *Journal of Neuroscience*, *26*(33), 8451-8464.

Knutsen, P. M., Biess, A., & Ahissar, E. (2008). Vibrissal kinematics in 3D: tight coupling of azimuth, elevation, and torsion across different whisking modes. *Neuron*, *59*(1), 35-42.

Knutsen, P. M., & Ahissar, E. (2009). Orthogonal coding of object location. *Trends in neurosciences*, *32*(2), 101-109.

Knutsen, P. M., Mateo, C., & Kleinfeld, D. (2016). Precision mapping of the vibrissa representation within murine primary somatosensory cortex. *Philosophical Transactions of the Royal Society B: Biological Sciences*, *371*(1705), 20150351.

Koralek, K. A., Olavarria, J., & Kellackey, H. P. (1990). Areal and laminar organization of corticocortical projections in the rat somatosensory cortex. *Journal of Comparative Neurology*, *299*(2), 133-150.

Koralek, K. A., & Killackey, H. P. (1990). Callosal projections in rat somatosensory cortex are altered by early removal of afferent input. *Proceedings of the National Academy of Sciences*, *87*(4), 1396-1400.

Krupa, D. J., Brisben, A. J., & Nicolelis, M. A. (2001a). A multi-channel whisker stimulator for producing spatiotemporally complex tactile stimuli. *Journal of neuroscience methods*, *104*(2), 199-208.

Krupa, D. J., Matell, M. S., Brisben, A. J., Oliveira, L. M., & Nicolelis, M. A. (2001b). Behavioral properties of the trigeminal somatosensory system in rats performing whisker-dependent tactile discriminations. *Journal of Neuroscience*, *21*(15), 5752-5763.

Luczak, A., McNaughton, B. L., & Harris, K. D. (2015). Packet-based communication in the cortex. *Nature Reviews Neuroscience*, *16*(12), 745-755.

Mack, K. J., & Mack, P. A. (1992). Induction of transcription factors in somatosensory cortex after tactile stimulation. *Molecular Brain Research*, *12*(1-3), 141-147.

Mahon, S., Vautrelle, N., Pezard, L., Slaght, S. J., Deniau, J. M., Chouvet, G., & Charpier, S. (2006). Distinct patterns of striatal medium spiny neuron activity during the natural sleep–wake cycle. *Journal of Neuroscience*, *26*(48), 12587-12595.

Manzoni, T., Barbaresi, P., Conti, F., & Fabri, M. (1989). The callosal connections of the primary somatosensory cortex and the neural bases of midline fusion. *Experimental Brain Research*, *76*(2), 251-266.

Manns, I. D., Sakmann, B., & Brecht, M. (2004). Sub-and suprathreshold receptive field properties of pyramidal neurones in layers 5A and 5B of rat somatosensory barrel cortex. *The Journal of physiology*, *556*(2), 601-622.

Massimini M, Huber R, Ferrarelli F, Hill S, Tononi G. (2004). The sleep slow oscillation as a traveling wave. *The Journal of neuroscience* 24:6862–6870.

Mirabella, G., Battiston, S., & Diamond, M. E. (2001). Integration of multiple-whisker inputs in rat somatosensory cortex. *Cerebral Cortex*, *11*(2), 164-170.

Mountcastle, V. B. (1997). The columnar organization of the neocortex. *Brain: a journal of neurology*, 120(4), 701-722.

Myers, R. E. (1955). Interocular transfer of pattern discrimination in cats following section of crossed optic fibers. *Journal of Comparative and Physiological Psychology*, *48*(6), 470.

Myers, R. E., & Sperry, R. W. (1958). Interhemispheric communication through the corpus callosum: mnemonic carry-over between the hemispheres. *AMA Archives of Neurology & Psychiatry*, *80*(3), 298-303.

Naka, A., & Adesnik, H. (2016). Inhibitory circuits in cortical layer 5. *Frontiers in neural circuits*, *10*, 35.

Nussbaumer, J. C., & Van der Loos, H. (1985). An electrophysiological and anatomical study of projections to the mouse cortical barrelfield and its surroundings. *Journal of neurophysiology*, *53*(3), 686-698.

Olavarria, J., Van Sluyters, R. C., & Killackey, H. P. (1984). Evidence for the complementary organization of callosal and thalamic connections within rat somatosensory cortex. *Brain research*, *291*(2), 364-368.

Oran, Y., Katz, Y., Sokoletsky, M., Malina, K. C. K., & Lampl, I. (2021). Reduction of corpus callosum activity during whisking leads to interhemispheric decorrelation. *Nature communications*, *12*(1), 1-14.

Palmer, L. M., Schulz, J. M., Murphy, S. C., Ledergerber, D., Murayama, M., & Larkum, M. E. (2012). The cellular basis of GABAB-mediated interhemispheric inhibition. *Science*, *335*(6071), 989-993.

Parnavelas, J. G., & Papadopoulos, G. C. (1989). The monoaminergic innervation of the cerebral cortex is not diffuse and nonspecific. *Trends in neurosciences*, *12*(9), 315-319.

Pascual-Leone, A., Amedi, A., Fregni, F., & Merabet, L. B. (2005). The plastic human brain cortex. *Annu. Rev. Neurosci.*, *28*, 377-401.

Petersen, C. C., Hahn, T. T., Mehta, M., Grinvald, A., & Sakmann, B. (2003). Interaction of sensory responses with spontaneous depolarization in layer 2/3 barrel cortex. *Proceedings of the National Academy of Sciences*, *100*(23), 13638-13643.

Petersen, C. C. (2019). Sensorimotor processing in the rodent barrel cortex. *Nature Reviews Neuroscience*, *20*(9), 533-546.

Petreanu, L., Huber, D., Sobczyk, A., & Svoboda, K. (2007). Channelrhodopsin-2–assisted circuit mapping of long-range callosal projections. *Nature neuroscience*, *10*(5), 663-668.

Petrus, E., Saar, G., Ma, Z., Dodd, S., Isaac, J. T., & Koretsky, A. P. (2019). Interhemispheric plasticity is mediated by maximal potentiation of callosal inputs. *Proceedings of the National Academy of Sciences*, *116*(13), 6391-6396.

Planert, H., Berger, T. K., & Silberberg, G. (2013). Membrane properties of striatal direct and indirect pathway neurons in mouse and rat slices and their modulation by dopamine. *PloS one*, *8*(3), e57054.

Plomp, G., Michel, C. M., & Quairiaux, C. (2017). Systematic population spike delays across cortical layers within and between primary sensory areas. *Scientific reports*, *7*(1), 1-14.

Pluta, S. R., Lyall, E. H., Telian, G. I., Ryapolova-Webb, E., & Adesnik, H. (2017). Surround integration organizes a spatial map during active sensation. Neuron, 94(6), 1220-1233.

Poulet, J. F., & Crochet, S. (2019). The cortical states of wakefulness. *Frontiers in systems neuroscience*, *12*, 64.

Ramirez, A., Pnevmatikakis, E. A., Merel, J., Paninski, L., Miller, K. D., & Bruno, R. M. (2014). Spatiotemporal receptive fields of barrel cortex revealed by reverse correlation of synaptic input. *Nature neuroscience*, *17*(6), 866-875.

Reig, R., & Sanchez-Vives, M. V. (2007). Synaptic transmission and plasticity in an active cortical network. *PloS one*, *2*(8), e670.

Reig, R., & Silberberg, G. (2014). Multisensory integration in the mouse striatum. *Neuron*, *83*(5), 1200-1212.

Reig, R., & Silberberg, G. (2016). Distinct corticostriatal and intracortical pathways mediate bilateral sensory responses in the striatum. *Cerebral Cortex*, *26*(12), 4405-4415.

Renier, N., Dominici, C., Erzurumlu, R. S., Kratochwil, C. F., Rijli, F. M., Gaspar, P., & Chédotal, A. (2017). A mutant with bilateral whisker to barrel inputs unveils somatosensory mapping rules in the cerebral cortex. *Elife*, *6*, e23494.

Rock, C., & junior Apicella, A. (2015). Callosal projections drive neuronal-specific responses in the mouse auditory cortex. *Journal of Neuroscience*, *35*(17), 6703-6713.

Sáez, M., Ketzef, M., Alegre-Cortés, J., Reig, R., & Silberberg, G. (2018). A new Micro-holder device for local drug delivery during in vivo Whole-cell recordings. *Neuroscience*, *381*, 115-123.

Sanchez-Vives, M. V., & McCormick, D. A. (2000). Cellular and network mechanisms of rhythmic recurrent activity in neocortex. *Nature neuroscience*, *3*(10), 1027-1034.

Sanchez-Vives, M. V., Massimini, M., & Mattia, M. (2017). Shaping the default activity pattern of the cortical network. *Neuron*, *94*(5), 993-1001.

Sanchez-Vives, M. V. (2020). Origin and dynamics of cortical slow oscillations. *Current Opinion in Physiology*, *15*, 217-223.

Sehara, K., Toda, T., Iwai, L., Wakimoto, M., Tanno, K., Matsubayashi, Y., & Kawasaki, H. (2010). Whisker-related axonal patterns and plasticity of layer 2/3 neurons in the mouse barrel cortex. *Journal of Neuroscience*, *30*(8), 3082-3092.

Schmidt, M., Enthoven, L., Van Der Mark, M., Levine, S., De Kloet, E. R., & Oitzl, M. S. (2003). The postnatal development of the hypothalamic–pituitary–adrenal axis in the mouse. *International journal of developmental neuroscience*, *21*(3), 125-132.

Shepherd, G. M. (2013). Corticostriatal connectivity and its role in disease. *Nature Reviews Neuroscience*, *14*(4), 278-291.

Shuler, M. G., Krupa, D. J., & Nicolelis, M. A. (2001). Bilateral integration of whisker information in the primary somatosensory cortex of rats. *Journal of Neuroscience*, *21*(14), 5251-5261.

Slater, B. J., & Isaacson, J. S. (2020). Interhemispheric callosal projections sharpen frequency tuning and enforce response fidelity in primary auditory cortex. *Eneuro*, *7*(4).

Sonntag, M., Englitz, B., Kopp-Scheinpflug, C., & Rübsamen, R. (2009). Early postnatal development of spontaneous and acoustically evoked discharge activity of principal cells of the medial nucleus of the trapezoid body: an in vivo study in mice. *Journal of Neuroscience*, *29*(30), 9510-9520.

Sperry, R. W. (1961). Cerebral organization and behavior. *Science*, *133*(3466), 1749-1757.

Sperry, R. W. (1962). Orderly function with disordered structure. *Principles of self-organization*, 279-290.

Sreenivasan, V., Karmakar, K., Rijli, F. M., & Petersen, C. C. (2015). Parallel pathways from motor and somatosensory cortex for controlling whisker movements in mice. *European Journal of Neuroscience*, *41*(3), 354-367.

Staiger, J. F., Zilles, K., & Freund, T. F. (1996). Distribution of GABAergic elements postsynaptic to ventroposteromedial thalamic projections in layer IV of rat barrel cortex. *European Journal of Neuroscience*, *8*(11), 2273-2285.

Staiger, J. F. (2006). Immediate-early gene expression in the barrel cortex. *Somatosensory & motor research*, *23*(3-4), 135-146.

Steiner, H., & Tseng, K. Y. (Eds.). (2016). *Handbook of basal ganglia structure and function*. Academic Press.

Stickgold, R. (2005). Sleep-dependent memory consolidation. *Nature*, *437*(7063), 1272-1278.

Sturrock, R. R. (1980). Myelination of the mouse corpus callosum. *Neuropathology and applied neurobiology*, *6*(6), 415-420.

Suárez, R., Fenlon, L. R., Marek, R., Avitan, L., Sah, P., Goodhill, G. J., & Richards, L. J. (2014a). Balanced interhemispheric cortical activity is required for correct targeting of the corpus callosum. *Neuron*, *82*(6), 1289-1298.

Suárez, R., Gobius, I., & Richards, L. J. (2014b). Evolution and development of interhemispheric connections in the vertebrate forebrain. *Frontiers in human neuroscience*, *8*, 497.

Swadlow, H. A., & Hicks, T. P. (1997). Subthreshold receptive fields and baseline excitability of" silent" S1 callosal neurons in awake rabbits: contributions of AMPA/kainate and NMDA receptors. *Experimental brain research*, *115*(3), 403-409.

Takatoh, J., Prevosto, V., & Wang, F. (2018). Vibrissa sensory neurons: linking distinct morphology to specific physiology and function. *Neuroscience*, *368*, 109-114.

Tan, Z., Hu, H., Huang, Z. J., & Agmon, A. (2008). Robust but delayed thalamocortical activation of dendritic-targeting inhibitory interneurons. *Proceedings of the National Academy of Sciences*, *105*(6), 2187-2192.

Tepper, J. M., Wilson, C. J., & Koós, T. (2008). Feedforward and feedback inhibition in neostriatal GABAergic spiny neurons. *Brain research reviews*, *58*(2), 272-281.

Tomassy, G. S., Berger, D. R., Chen, H. H., Kasthuri, N., Hayworth, K. J., Vercelli, A., ... & Arlotta, P. (2014). Distinct profiles of myelin distribution along single axons of pyramidal neurons in the neocortex. *Science*, *344*(6181), 319-324.

Tutunculer, B., Foffani, G., Himes, B. T., & Moxon, K. A. (2006). Structure of the excitatory receptive fields of infragranular forelimb neurons in the rat primary somatosensory cortex responding to touch. *Cerebral Cortex*, *16*(6), 791-810.

Ur Rehman, N., & Mandic, D. P. (2011). Filter bank property of multivariate empirical mode decomposition. *IEEE transactions on signal processing*, *59*(5), 2421-2426.

van der Knaap, L. J., & van der Ham, I. J. (2011). How does the corpus callosum mediate interhemispheric transfer? A review. *Behavioural brain research*, *223*(1), 211-221.

Veinante, P., & Deschênes, M. (2003). Single-cell study of motor cortex projections to the barrel field in rats. *Journal of Comparative Neurology*, *464*(1), 98-103.

Vyazovskiy, V. V., Olcese, U., Hanlon, E. C., Nir, Y., Cirelli, C., & Tononi, G. (2011). Local sleep in awake rats. *Nature*, *472*(7344), 443-447.

Wang, C., Chen, X., & Knierim, J. J. (2020). Egocentric and allocentric representations of space in the rodent brain. *Current opinion in neurobiology*, *60*, 12-20.

Wang, C. L., Zhang, L., Zhou, Y., Zhou, J., Yang, X. J., Duan, S. M., ... & Ding, Y. Q. (2007). Activity-dependent development of callosal projections in the somatosensory cortex. *Journal of Neuroscience*, *27*(42), 11334-11342.

Wiest, M. C., Bentley, N., & Nicolelis, M. A. (2005). Heterogeneous integration of bilateral whisker signals by neurons in primary somatosensory cortex of awake rats. *Journal of neurophysiology*, *93*(5), 2966-2973.

Wilber, A. A., Clark, B. J., Forster, T. C., Tatsuno, M., & McNaughton, B. L. (2014). Interaction of egocentric and world-centered reference frames in the rat posterior parietal cortex. *Journal of Neuroscience*, *34*(16), 5431-5446.

Wilent, W. B., & Contreras, D. (2005). Dynamics of excitation and inhibition underlying stimulus selectivity in rat somatosensory cortex. *Nature neuroscience*, *8*(10), 1364-1370.

Wilson CJ, Kawaguchi Y. (1996). The origins of two-state spontaneous membrane potential fluctuations of neostriatal spiny neurons. *The Journal of neuroscience* 16:2397–2410.

Wise, S. P., & Jones, E. G. (1976). The organization and postnatal development of the commissural projection of the rat somatic sensory cortex. *Journal of Comparative Neurology*, *168*(3), 313-343.

Yamashita, T., Pala, A., Pedrido, L., Kremer, Y., Welker, E., & Petersen, C. C. (2013). Membrane potential dynamics of neocortical projection neurons driving target-specific signals. *Neuron*, *80*(6), 1477-1490.

Zagha, E., Casale, A. E., Sachdev, R. N., McGinley, M. J., & McCormick, D. A. (2013). Motor cortex feedback influences sensory processing by modulating network state. *Neuron*, *79*(3), 567-578.

Zhou, J., Wen, Y., She, L., Sui, Y. N., Liu, L., Richards, L. J., & Poo, M. M. (2013). Axon position within the corpus callosum determines contralateral cortical projection. *Proceedings of the National Academy of Sciences*, *110*(29), E2714-E2723.

Zhou, J., Lin, Y., Huynh, T., Noguchi, H., Bush, J. O., & Pleasure, S. J. (2021). NMDA receptors control development of somatosensory callosal axonal projections. *Elife*, *10*, e59612.

Annex I

Acknowledgments

Annex II

Medium spiny neurons activity reveals the discrete segregation of mouse dorsal striatum

Javier Alegre-Cortés[†], María Sáez[†], Roberto Montanari, Ramon Reig*

Instituto de Neurociencias CSIC-UMH, San Juan de Alicante, Spain

Abstract Behavioral studies differentiate the rodent dorsal striatum (DS) into lateral and medial regions; however, anatomical evidence suggests that it is a unified structure. To understand striatal dynamics and basal ganglia functions, it is essential to clarify the circuitry that supports this behavioral-based segregation. Here, we show that the mouse DS is made of two non-overlapping functional circuits divided by a boundary. Combining in vivo optopatch-clamp and extracellular recordings of spontaneous and evoked sensory activity, we demonstrate different coupling of lateral and medial striatum to the cortex together with an independent integration of the spontaneous activity, due to particular corticostriatal connectivity and local attributes of each region. Additionally, we show differences in slow and fast oscillations and in the electrophysiological properties between striatonigral and striatopallidal neurons. In summary, these results demonstrate that the rodent DS is segregated in two neuronal circuits, in homology with the caudate and putamen nuclei of primates.

***For correspondence:**
ramon.reig@umh.es

[†]These authors contributed equally to this work

Introduction

The basal ganglia are a group of subcortical nuclei involved in a diversity of functions including motor control, learning, decision making, and reward (*Packard and Knowlton, 2002*; *Schultz et al., 1997*; *Yin and Knowlton, 2006*). The striatum is the main input structure of the basal ganglia, receiving glutamatergic transmission from the cortex and the thalamus (*Alloway et al., 2009*; *Kincaid et al., 1998*; *Wilson, 1987*). In primates and other mammals, the dorsal part of the striatum is formed by the nuclei caudate and putamen, which are anatomically separated by the internal capsule. In contrast, rodent dorsal striatum (DS) is considered a homogeneous structure due to the absence of anatomical border and the copious presence of overlapping axonal connections (*Alloway et al., 2006*; *Hooks et al., 2018*; *Hoover et al., 2003*). However, some recent studies have divided the DS in two regions, dorsomedial (DMS) and dorsolateral (DLS) striatum, based on their behavioral roles (*Graybiel, 2008*; *Hauber and Schmidt, 1994*). While both regions participate in motor control, DLS is often related with habit, stimulus-response associations and navigation, whereas the DMS mediates action-outcome associations, goal-directed actions and flexible shifting between behavioral strategies, suggesting a role in higher cognitive functions (*Faure et al., 2005*; *Hilário and Costa, 2008*; *Lerner et al., 2015*; *Thorn et al., 2010*). In order to understand the basal ganglia circuits and their related behaviors, an essential question should be addressed: Is the functional segregation of the DS supported by two different circuits?

Cortex and thalamus project to the striatum, forming organized glutamatergic synapses along its mediolateral axis, and defining multiple striatal subregions (*Hintiryan et al., 2016*; *Hunnicutt et al., 2016*). This corticostriatal axonal innervation presents a high degree of convergence and divergence (*Flaherty and Graybiel, 1991*) and originates in both hemispheres from different subtypes of pyramidal neurons (*Cowan and Wilson, 1994*; *Hooks et al., 2018*; *Levesque et al., 1996*; *Reiner et al., 2003*; *Wilson, 1987*). Corticostriatal connections innervate both striatonigral and striatopallidal

medium-sized spiny neurons (direct and indirect MSNs, respectively) (*Doig et al., 2010*; *Wall et al., 2013*), which represent 95% of the neurons in the striatum (*Kita and Kitai, 1988*), and different types of interneurons (*Tepper et al., 2008*). The lateral region of the striatum is highly innervated by axons from somatosensory and motor related cortical areas, while the medial one receives cortical axons from visual, auditory, associative, limbic (*Hintiryan et al., 2016*; *Hunnicutt et al., 2016*) and with lower axonal density from somatosensory cortical regions (*Reig and Silberberg, 2014*).

In addition to the differences in cortical or thalamic axonal innervation, there are dissimilarities in the composition of the striatal microcircuits. The distribution of parvalbumin (PV) and cholinergic interneurons (ChIs) along the mediolateral axis of the DS is not homogeneous (*Gerfen et al., 1985*; *Kita et al., 1990*; *Matamales et al., 2016*; *Muñoz-Manchado et al., 2018*). Furthermore, dopaminergic projections from the lateral part of the substantia nigra massively innervate the DS (*Ikemoto, 2007*), with particular impact in the activity of ChIs along the DS (*Chuhma et al., 2018*). All these precise afferent connectivity, microcircuit interactions, and neuromodulation regulate the synaptic activity of DLS- and DMS-MSNs.

The activity of every neural circuit is limited by anatomical and functional constrains which will restrict the repertoire of spontaneous and evoked activity patterns, defining the functional connectivity of the brain (*Getting, 1989*; *Luczak et al., 2015*). In this work, we describe how MSNs of the lateral and medial regions of the DS integrate spontaneous and sensory evoked activity.

The slow wave oscillation (SWO) is characterized by periods of high spontaneous activity (Up states) intermingled with silent periods (Down states) at the frequency of ~ 1 Hz, which is originated in the cortex (*Sanchez-Vives and McCormick, 2000*; *Timofeev et al., 2000*) and propagates directly to the striatum, modulating the resting state of MSNs (*Sáez et al., 2018*; *Wilson and Kawaguchi, 1996*) and interneurons (*Reig and Silberberg, 2014*). Based in their heterogeneous activity, we found that DS is segregated in two circuits and propose a biological substrate that explains their differences.

Because MSNs recorded in vivo are known to fire scarcely (*Adler et al., 2012*; *Berke et al., 2004*; *Wilson, 1993*), we performed single and pairs of whole-cell patch-clamp recordings to analyze their subthreshold dynamics during spontaneous and evoke activity, identifying their specific pathways. Our findings show how the DS is divided in two non-overlapping circuits, based on the MSNs activity. DLS- and DMS-MSNs differ in the integration of the slow wave and beta oscillations, as well as in the functional coupling to multiple cortical regions. By means of double in vivo patch-clamp recordings, we demonstrate a sequential propagation of the cortical slow wave oscillation (SWO) along DS. In addition, we found that the evoked responses of MSNs to visual stimulation displayed different properties along the medio-lateral axis, that were consistent with cortical projections and independent of the circuit in which the MSN was embedded. MSNs close to the midline responded with shorter delays, bigger amplitudes and faster slopes than the ones placed in dorsocentral territories. Finally, we identified that the direct and indirect pathways MSNs have particular attributes in the DLS and DMS, displaying differences in their electrophysiological properties and synaptic integration.

In conclusion, consistent with previous behavioral studies, our results demonstrate that DS is divided in two functional circuits, separated by a sharp boundary, each of them with specific properties that are essential to understand the striatum and basal ganglia functions.

Results

MSNs in the DLS and DMS have different electrophysiological properties

We obtained in vivo whole-cell patch-clamp recordings from 223 neurons located in the DS (n = 197) and several cortical areas (n = 26). All of them displayed SWO with prominent Up and Down states (*Figures 1C*, *2A*, Figures 4A–B, D, 5A–B and 6A), at close frequency of ~ 0.7 Hz in both brain regions. The different types of striatal neurons were identified by their electrophysiological properties and morphology (*Figure 1B*, see Materials and methods). Direct and indirect pathway MSNs were determined by their responses to the light stimulation using the optopatcher (*Katz et al., 2019*; *Ketzef et al., 2017*; Figure 7A). All average graphs showed in this study represent the standard deviation unless stated otherwise.
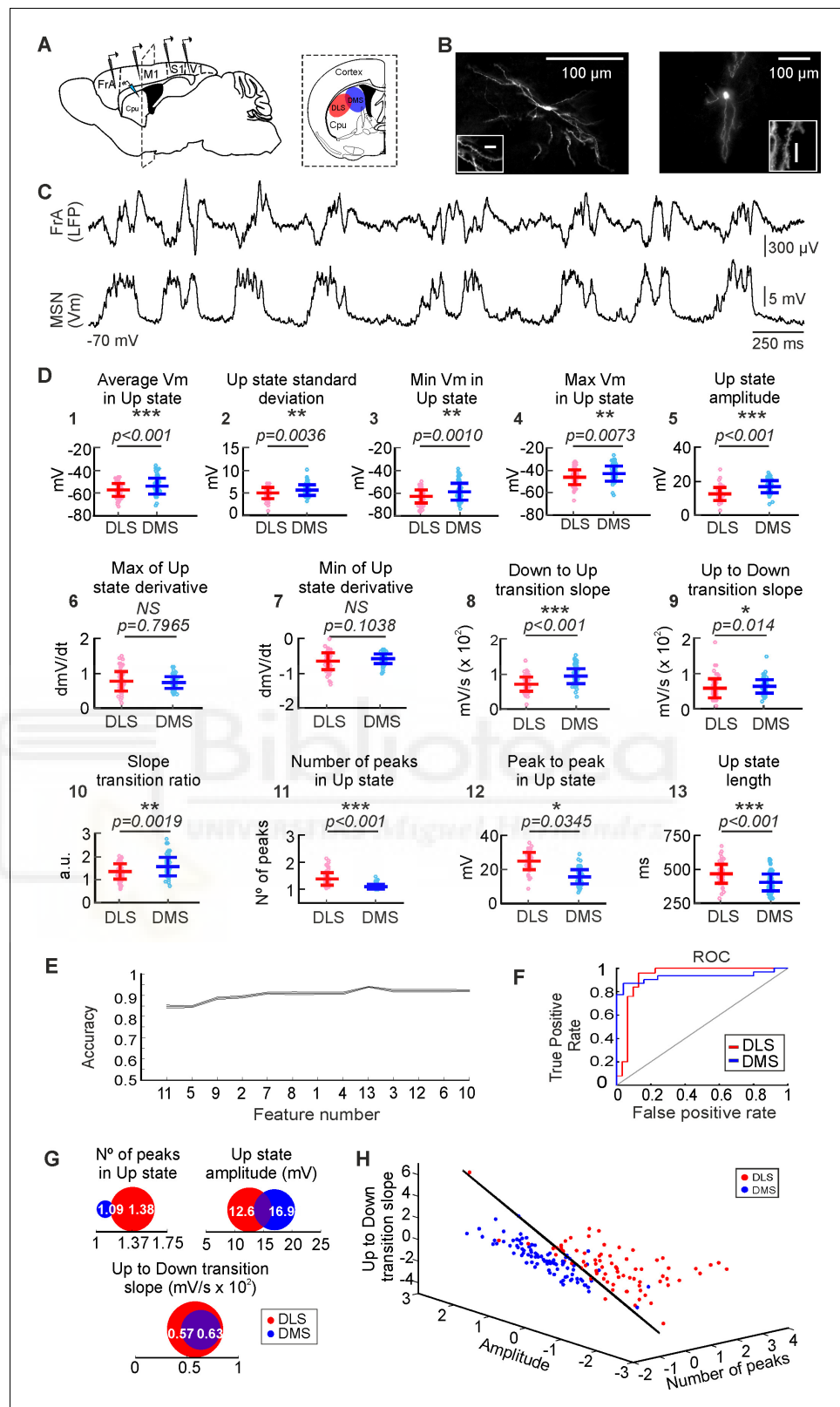
Figure 1. Analysis and classification of SWO in dorsal striatum. (**A**) Schematic representation of the in vivo recording setup. (**B**) Morphological reconstruction of DLS-MSN (left) and DMS-MSN (right). Different scales show neuron magnitude and its dendritic spines, confirming that the recorded neuron is a MSN. (**C**) Representative LFP (top) and whole-cell patch-clamp recording of a MSN (bottom). (**D**) Featurization of the SWO of DLS- and DMS-

Figure 1 continued on next page

Figure 1 continued

MSNs (see Materials and methods). (E) RFE of the computed features (feature number) to determine their order of relevance classifying DLS- and DMS-MSNs. A SVM with a linear kernel was selected as classification algorithm. (F) Example ROC curve of the DLS-DMS classification for one of the crossvalidations using the three most relevant features, illustrated in D. (G) Schematic representation of the data distribution of DLS and DMS groups for the most relevant features (numbers 11, 5, and 9, respectively). White number represent the mean; the radius of the circle represents the variance. (H) Subspace of classification based on the RFE results. Dots represent individual MSNs recorded in DLS (red) or DMS (blue). Classification hyperplane obtained after training the SVM with linear kernel in black. p Values obtained using the Wilcoxon Rank-sum test.

The online version of this article includes the following figure supplement(s) for figure 1:

Figure supplement 1. Classification of DLS- and DMS-MSNs at animal level.
Figure supplement 2. Correlation between the SWO features and electrophysiological properties of MSNs.

In order to study the circuit attributes that may characterize the DS, our initial approach was to compare the electrophysiological properties of striatal MSNs recorded in the lateral (DLS, n = 77) and medial (DMS, n = 91) regions of the DS in anesthetized mice. The membrane potential of the Down states was stable during the recordings with no differences between striatal regions (DLS-MSNs = −69.89 ± 5.79 Hz, DMS-MSNs = -69.867 ± 7.67 Hz, p=0.42). MSNs exhibited a rich sub-threshold activity during Up states; however, they displayed a very low rate of spontaneous action potentials with similar frequencies along DS (DLS-MSNs = 0.3 ± 0.95 Hz, DMS-MSNs = 0.24 ± 0.53 Hz, p=0.58). Input resistance was higher for DLS-MSNs (DLS-MSNs = 312 ± 25 MΩ, DMS-MSNs = 255 ± 16 MΩ, p=0.04). These changes in resistance could impact in the neuronal properties of synaptic integration, setting the gain and timing for their synaptic inputs. Thus, the integration of the spontaneous activity on DLS- and DMS-MSNs could be, at least partially, modulated by the cellular differences which underlie their intrinsic electrophysiological properties.

The spontaneous activity from DLS- and DMS-MSNs have different attributes

We first studied the properties of the SWO recorded in whole-cell from dorsal striatal MSNs. In order to obtain a quantitative description of the activity of the MSNs in this brain state, we computed 13 different features to characterize the magnitude (i.e mean and max membrane potential, amplitude) and shape (i.e. ratio between transitions, number of peaks) of the Up states (*Figure 1D*), from which 11 were statistically different between DLS- and DMS-MSNs (Ups extraction and all features are explained in methods section). The average membrane potential in the Up states was higher in the DMS-MSNs, as well as their standard deviation, minimum and maximum membrane potential and the total amplitude (*Figure 1D*, features n˚ 1–5). Their upward and downward transition slopes and its ratio were also higher in DMS-MSNs (*Figure 1D*, features n˚ 8–10). DLS-MSNs displayed higher number of peaks during the Up states and peak to peak amplitude, as well as longer Up states (*Figure 1D*, features n˚ 11–13). Similar to cortical neurons (*Sanchez-Vives and McCormick, 2000*), Up states in MSNs are comprised by a barrage of excitatory and inhibitory synaptic inputs (*Reig and Silberberg, 2014*). Therefore, these divergences in the integration of the spontaneous activity may reflect changes in the excitatory and inhibitory inputs that DLS- and DMS-MSNs receive.

Once we obtained a statistical prove of the differences in the SWO between DLS and DMS, we asked whether these differences were sufficient to define DLS- and DMS-MSNs as two different populations. More specifically, we asked which parameters, or combination of them, could be used to distinguish between DLS- and DMS SWO more accurately. To do so, we searched for those features of the Up states whose combination maximized the accuracy of classifying MSNs corresponding to DLS or DMS circuits. Using a supervised machine-learning technique, named Support Vector Machine (SVM) (*Cortes and Vapnik, 1995*) with a linear kernel, we performed a Recursive Feature Elimination (RFE) analysis to rank the 13 computed features of the Up states, according to their combined utility to classify DLS- or DMS-MSNs (*Figure 1E*). Therefore, starting from the whole set of parameters, they were recursively removed depending on their relevance for the classification of DLS- and DMS-MSNs (see Materials and methods); as a results of the RFE, we obtained a sorting of the features depending on their relevance for the classification. The most relevant features were: first, the number of peaks in the Up states and second, the amplitude inside the Up state, which
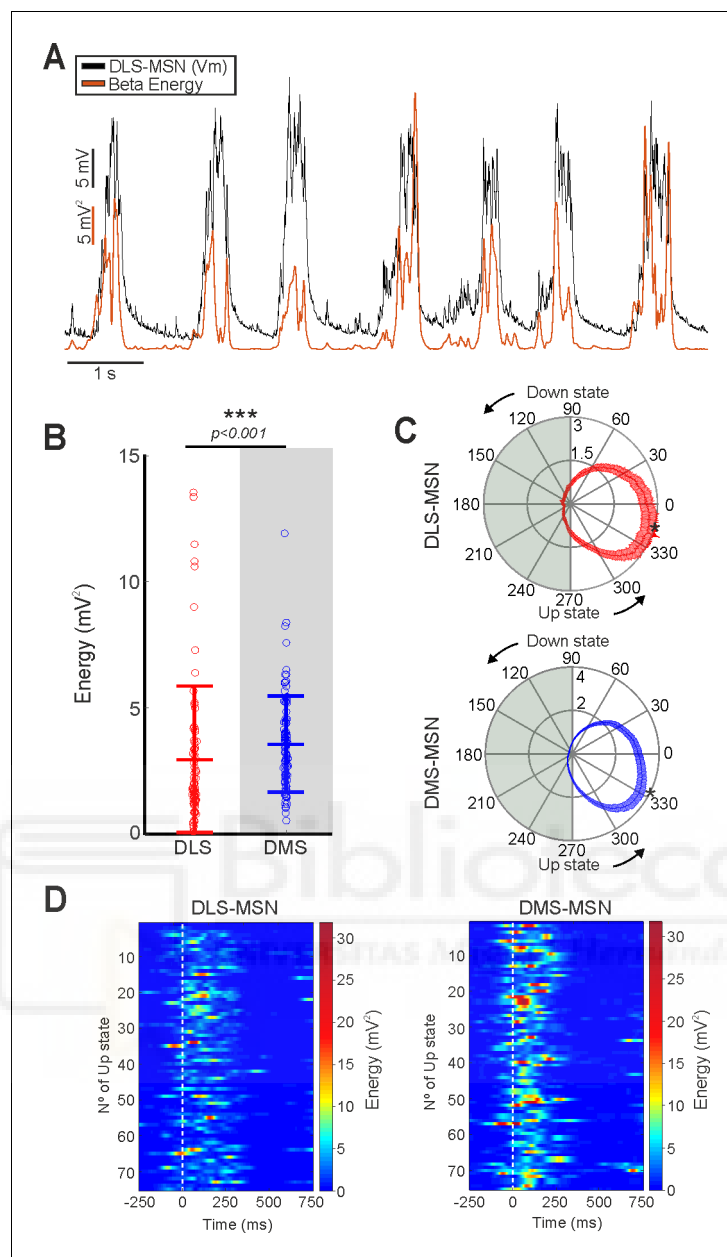
Figure 2. Beta band in membrane voltage of dorsal striatal MSNs. (**A**) Example of energy of the beta band (red trace) during the MSN SWO recorded in DMS. (**B**) Energy of the beta band of DLS- and DMS-MSNs. (**C**) Average of phase alignment of beta band to the SWO in DLS- (left) and DMS-MSNs (right) (Raylegh test, p<0.001 in both cases). Asterisk indicates the radial position of the beta peak. Beta peak occurs first in DMS-MSNs (p<0.001). (**D**) Representative examples of beta phase locking in DLS- (left) and DMS- MSNs (right). White line represents the beginning of each Up state. p Values in **B** obtained using the Wilcoxon Rank-sum test. p Values of the phase locking in **C** were computed using Rayleigh test.

The online version of this article includes the following figure supplement(s) for figure 2:

Figure supplement 1. Theta and Gamma band in membrane potential of dorsal striatum.

Figure supplement 2. Example of decomposition of different traces by the NA-MEMD.

resulted in an accuracy score of 84.61 ± 0.47%. When a third feature, the speed of transition from Up to Down states, was added, the accuracy increased to 88.56 ± 0.57%. The addition of new parameters increased the accuracy up to ~ 92%, value at which it remained stable (*Figure 1E*). In a compromise between accuracy and interpretability, we selected the space formed by the three most

relevant features for further analyses; number of peaks, amplitude and Up to Down transition slopes (*Figure 1H*).

Because multiple MSNs were recorded from the same animals (on average ~ 4 MSNs per mouse, *Supplementary file 1B*), and this could weigh the distributions and bias the result, we did an additional one-animal-out classification (*Figure 1—figure supplement 1*). In this analysis, all the MSNs recorded from one animal are excluded from the training phase of the classifier. Once trained, these MSNs are presented to the classifier in order to predict their position (see Materials and methods). By using this approach, we ensure that any bias that the animal may have introduced into the training phase of the classifier is removed. The result shows that the classification is present at the animal level (*Figure 1—figure supplement 1*), as well as the neuronal one (*Figure 1H*). In conclusion, our classifier based on the spontaneous activity integration of the MSNs indicates that DLS and DMS are identified as two distinct functional circuits.

In order to unravel the source of the Up states differences between DLS- and DMS-MSNs, we first computed the correlations of the intrinsic membrane properties, showed in *Table 1* and the Up state features of the MSNs; no comparison had an absolute correlation value over 0.3 (*Figure 1—figure supplement 2*). Therefore, it cannot be concluded that the intrinsic electrophysiological properties of MSNs are relevant to discriminate between striatal regions.

In the next step to further depict the differences between DLS and DMS, we characterized the fast oscillations that are phase locked to the Up state. High-frequency oscillations are prominent during wakefulness and during the Up states of the SWO (*Compte et al., 2008*; *Steriade et al., 1996*). In the cortico-basal ganglia-thalamic loop, high-frequency activity has been related with different functions and processes in health and disease (*Brown, 2003*; *Feingold et al., 2015*). For instance, exaggerated beta-band oscillations occur in Parkinson's disease. With the purpose to study possible differences in the high-frequency oscillations of DLS and DMS, we compared the energy in the theta (6–10 Hz), beta (10–20 Hz) and gamma (20–80 Hz) bands of DLS- and DMS-MSNs (*Figure 2—figure supplement 1*). To that end, we applied the Noise-Assisted Multivariate Empirical Mode Decomposition (NA-MEMD), extracting the Intrinsic Mode Functions (IMFs) (see Materials and methods) carrying the information of the different oscillatory activity bands. The NA-MEMD is a noise-assisted template-free technique for time frequency analysis of n-dimensional signals; it let us obtain an enriched decomposition of the spontaneous activity compared to traditional techniques (Fourier decomposition, wavelet, and others), due to the non-linear properties of neural oscillations (*Averbeck et al., 2006*; *Cole and Voytek, 2017*; *Laurent, 1996*; *Shamir and Sompolinsky, 2004*).

Our results show that the energy of the beta band was higher, and statistically different, in DMS-MSNs (*Figure 2B–D*). On average, the peak of beta energy occurs in the first third of the Up state in both striatal regions, but it is closer to the beginning of the Up state for DMS-MSNs (*Figure 2C*, DMS=-26.81±24.63°, DLS=-13.26±30.01°, p=0.0007). Following this divergence in beta band, we tested whether high-frequency oscillation contained enough information to classify DLS- and DMS-

Table 1. Intrinsic properties of DLS and DMS of direct and indirect MSNs.
Comparisons between DLS- and DMS-MSNs (p<0.05, *symbol). Comparisons between indirect DLS-MSNs and indirect DMS-MSNs (p<0.01, # symbol). All values are means ± SEM. p Values obtained using the Wilcoxon Rank-sum test.

	Input Resistance (MΩ)	Resistance Down state hyp. (MΩ)	Resistance Down state dep. (MΩ)	Resistance Up state hyp. (MΩ)	Resistance Up state dep. (MΩ)	Capacitance (pF)	Tau (ms)
DLS	312± 25 *	292± 24 *	313± 23 *	304± 23	315± 27	19.45± 1.52	4.57± 0.23
dMSNs	297± 33	279± 31	284± 28	289± 30	296± 35	20.72± 1.98	4.52± 0.29
iMSNs	338± 41 #	312± 36 #	355± 40 #	324± 37	342± 41	17.58± 2.35	4.63± 0.40
DMS	255± 16 *	241± 20 *	259± 17 *	262± 20	262± 17	21.68± 1.55	4.61± 0.15
dMSNs	260± 22	249± 28	265± 23	269± 28	267± 23	23.20± 2.21	4.77± 0.19
iMSNs	241± 18 #	223± 18 #	248± 16 #	248± 20	252± 20	18.43± 1.04	4.26± 0.24

MSNs. To that end, we trained an SVM with a linear kernel with the amplitude and position of the peak energy inside the Up state of each band. We obtained a classification accuracy of 70.61 ± 0.89% indicating that the high frequencies do not discriminate between DS regions as clearly as Up state properties. Moreover, the addition of the high-frequency properties as extra features to our previous classifier did not improve the level of discrimination obtained by the SWO features (*Figure 1E,F*). Therefore, we conclude that DLS- and DMS-MSNs can be identified as belonging two different circuits based on the features of the Up states during the SWO.

DLS and DMS are two non-overlapping functional circuits in mouse

Once it had been shown that DLS and DMS circuits could be separated based on their SWO, we studied the transition from one circuit to the other, exploring the properties of this brain state in dorsocentral striatum (DCS) (*Figure 3A*), a hypothetical third region between DLS and DMS (see Materials and methods). We considered three possible scenarios (*Figure 3A,B*): If the activity of both circuits is mostly driven by the afferent inputs, we should observe a gradient moving from one circuit to the other (Hypothesis 1), or alternatively a third type of circuit (Hypothesis 2). Whether other factors, either extrinsic or intrinsic to the DS, control the spontaneous activity of these circuits, we should observe a sharp transition from one circuit to the other (Hypothesis 3). To address this question, we recorded MSNs in the DCS (see Materials and methods) in whole-cell, extracting the previous 13 features of the SWO (*Supplementary file 1A*). Then, we projected the DCS-MSNs into the standardized space used for the classification of DLS- and DMS-MSNs (*Figure 3C*), containing the values of number of peaks in the Up state, Up state amplitude and Up to Down transition slopes (*Supplementary file 1A*, *Figure 3—figure supplement 1*). In order to study the distribution of DCS-MSN in the parameter space relative to the populations of DLS- and DMS-MSNs we used the SVM that had been used previously to classify these two populations. We wanted to understand if the DCS-MSNs created a continuum between the DLS- and DMS-MSNs populations along the decision axis or whether this separation remained after the addition of the new pool of MSNS. To answer this question, we used the hypervector computed by the SVM to perform the classification (*Figure 3C*, see Materials and methods). We projected the data onto this hypervector and compared the distribution of the MSNs recorded from DCS to determine whether they belonged to either DLS or DMS circuits, or whether they had different properties (*Figure 3D*). If a sharp functional boundary exists between DLS and DMS, we would have recorded an undetermined amount of MSNs belonging to both circuits (Hypothesis 3). Otherwise, it would appear a new cluster with an undescribed third functional type of MSN, with an unknown distribution along the hypervector (Hypothesis 2) or in between DLS and DMS-MSNs distributions (Hypothesis 1). The distribution of MSNs recorded in the DCS was consistent with a mixture of MSNs from DLS and DMS circuits supporting a sharp transition between DLS and DMS regions [see discussion]. DCS distribution (*Figure 3D*, green trace) was significantly different to either the DLS and DMS distributions (p<0.01, *Figure 3D*, red, blue, and black traces respectively) and equivalent to the combination of both (p=0.681, *Figure 3D*, green and black traces).

Thus, we conclude that all recorded MSNs in DS belong to the previously described DMS and DLS functional circuits and they are separated by a sharp functional boundary.

Sensory response in the boundary between circuits

MSNs in the DS integrate bilateral and multisensory information (*Reig and Silberberg, 2014*). This process is supported by an anatomically restricted distribution, depending on the recipient area of axons coming from cortical sensory regions. Bilateral tactile responses to whisker deflections can be recorded along the DS, from the most lateral territories to the border of the lateral ventricle in the DMS. On the other hand, visual responses seem enclosed to medial territories (*Reig and Silberberg, 2014*). Inspired by this description, we aimed to discern whether MSNs located in the anatomical region where the boundary between DLS and DMS was observed responded to visual stimulation and how they were related with our previous DLS- or DMS-MSNs classification. To this end, visual stimuli were presented to the contralateral eye as 15 milliseconds flashes from a white LED (see methods) during whole-cell recordings in the 17 MSNs located in the DCS. Our result shows that eight of them (47%) responded to the visual stimulation (*Figure 3E*). Then, we asked how these neurons were labeled by our classifier (*Figure 3C*): From nine neurons identified as DMS-MSNs, five of
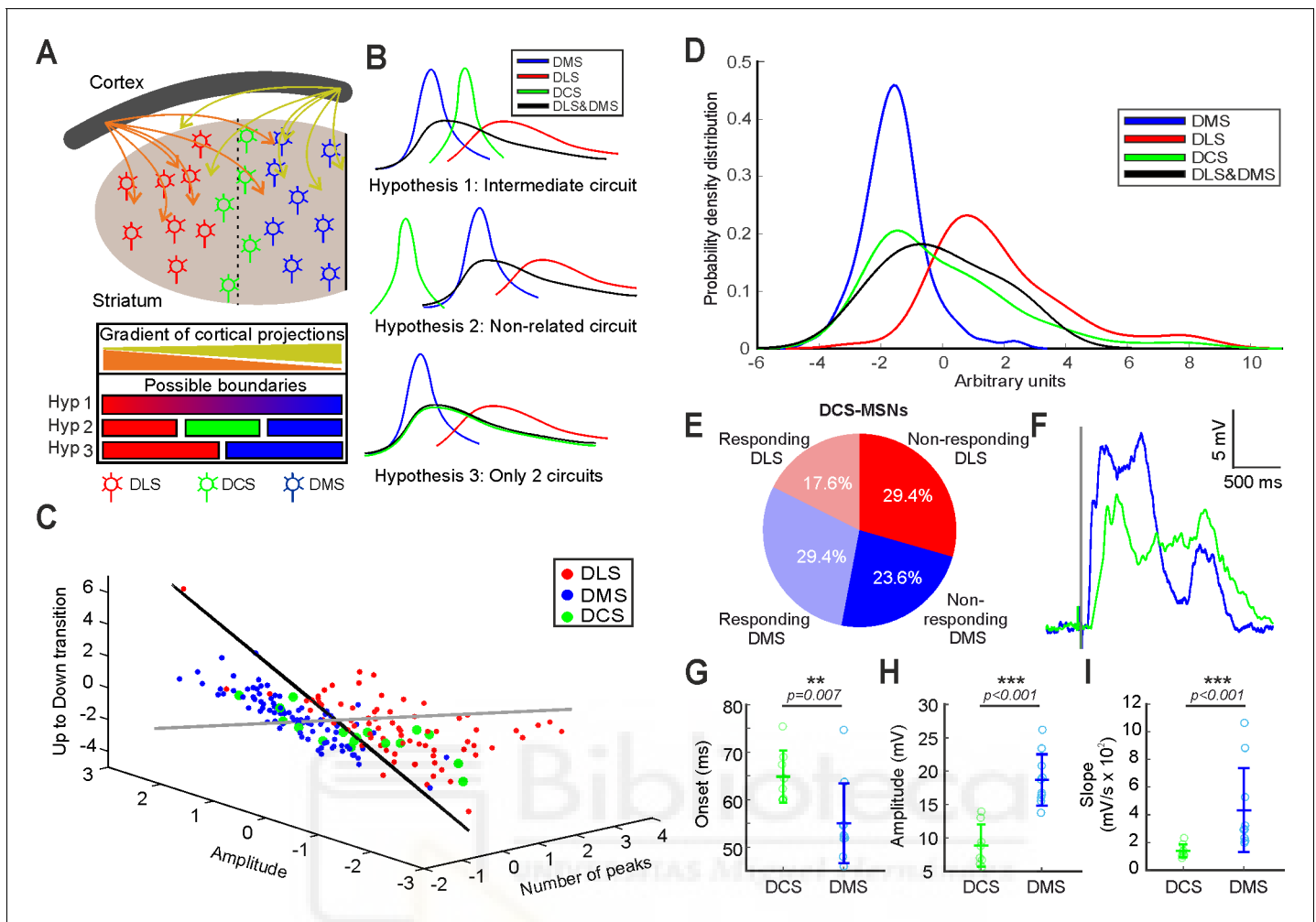
Figure 3. Study of the SWO in the DCS striatum and determination of the functional boundary between DLS and DMS. (**A**) Schematic representation of the 'boundary question'. (**B**) Three possible hypotheses about DCS-MSNs SWO. Hyp. 1: There is an intermediate distribution between DLS and DMS SWO (top); Hyp. 2: There is a different type of SWO distribution (middle); Hyp. 3: There is no specific DCS distribution of SWO and the MSNs recorded at DCS are a combination of DLS- and DMS-MSNs (bottom). The black line displays the distribution of the SWO combining both DLS and DMS. (**C**) Distribution of DLS-, DMS-, and DCS-MSNs in the subspace of classification determined by the RFE. Classification plane in black. Orthogonal hypervector to the classification plane in gray. (**D**) Distribution of dorsolateral, dorsomedial and dorsocentral MSNs and the combining DLS-DMS function along the orthogonal hypervector to the hyperplane classification. All comparison between distributions are significant (p<0.01) except for DCS with DMS-DLS (p=0.681). (**E**) Percentage of neurons recorded in the DCS coordinate, responding or not to visual stimulation and classified as DLS or DMS. (**F**) Waveform average of visual responses recorded in an MSN from DCS (green) and DMS (blue). (**G–I**) Averages of onset (**G**), amplitude (**H**), and slope (**I**) of the visual responses recorded in MSNs from DCS coordinate and DMS. p Values obtained using the Wilcoxon Rank-sum test.

The online version of this article includes the following figure supplement(s) for figure 3:

Figure supplement 1. Z-scoring of the SWO features.

them responded to the visual stimulus; and from eight neurons identified as DLS-MSNs, three of them responded as well (*Figure 3E*). Therefore, some neurons identified as DLS-MSNs responded to visual stimulation in the DCS coordinate.

Anatomically, it has been described that several visual areas project to the DS. For example, V1 projections are located in the most medial regions of the DS, while medial and lateral anterior visual cortical areas extend their projections to more lateral striatal territories (*Hintiryan et al., 2016*), including our DCS anatomical coordinate. This suggests that MSNs will respond to visual stimulation differently, depending on their position in the DS. Therefore, we recorded a new set of MSNs in the DMS responding to the same visual stimulation (n = 10) and compared them with respect to the MSNs with visual responses in the DCS coordinate (n = 8). The result (*Figure 3F–I*) shows that

amplitudes and slopes were statistically different and clearly higher in the DMS-MSNs (amplitudes DCS = 8.84 ± 3.15 mV, DMS = 18.67 ± 3.86 mV, p=0.00009; slopes DCS = 139 ± 48.1 mV/s, DMS = 432 ± 302.9 mV/s, p=0.0003). Importantly, the onset of the visual responses was nine milliseconds slower for the DCS-MSNs (DCS = 64.84 ± 5.49 ms; DMS = 55.02 ± 8.37 ms, p=0.007) (*Figure 3G*), suggesting that they receive inputs from different populations of neurons. This result is consistent with the difference in cortico-striatal projections from visual areas (*Hintiryan et al., 2016*), in which V1 axons project to the most medial region of the striatum, while they are absent in the DCS coordinate. On the other hand, axons from anterior medial (AM) and anterior lateral (AL) visual regions, related with other aspects of the visual processing (*Garrett et al., 2014*; *Marshel et al., 2012*) reach the central region of the DS with a smaller density of projections than V1 to DMS (*Hintiryan et al., 2016*). This is compatible with the smaller amplitudes and slower slopes (*Figure 3H,I*). Thus, we support that the differences in the visual response are due to the different visual regions that are projecting to those MSNs, independently of whether they belong to DLS or DMS circuitry.

DLS- and DMS-MSNs segregation is explained by their membrane potential transitions

To understand the main source of differences between the integration of the spontaneous activity in the DLS- and DMS-MSNs, we started by analyzing the first ranked feature: number of peaks during Up states (*Figure 1D–E*, feature n°11). We studied whether this difference occurred in cortical regions, from where they can be transmitted to the DS (*Figure 4A*). It is known that striatal oscillations depend on the cortical ones (*Kasanetz et al., 2002*; *Wilson, 1993*) and in vitro slices containing the striatum are absent of spontaneous oscillations (*Planert et al., 2013*).

We performed in vivo whole-cell recordings in Layer V of FrA (frontal associative cortex), M1 (primary motor cortex), S1 (primary visual cortex), and V1 (primary visual cortex) (*Figure 4B*). We found that S1 and M1 have significantly higher average number of peaks per Up state than FrA and V1 (*Figure 4C*). This result together with previous anatomical descriptions (*Alloway et al., 2006*; *Hoffer et al., 2003*; *Hooks et al., 2018*) strongly suggest that the membrane dynamics inside the Up state in the DLS are controlled by the sensory-motor cortical areas.

The main features for the classification of DLS- and DMS-MSNs (*Figure 1G*) were relative to state transitions (Up to Down transition) or intra-state transitions (number of peaks). In order to understand whether these differences may be caused by changes in the depolarizing and hyperpolarizing dynamics of MSNs, we studied the temporal properties of the membrane potential transitions. To analyze the convergence of synchronized hyper/depolarizing events onto MSNs that created detectable changes in the whole-cell recording, we first detected the sharp transitions of the voltage trace and phase locked them to the SWO cycle (*Figure 4D* [see Materials and methods]). Thus, we obtained a measure of the temporal dynamics of hyper/depolarizing events of the MSNs. Then, we computed their ratio for the DLS- and DMS-MSNs. We found differences in the depolarizing/hyperpolarizing ratio (DH ratio) of DLS- and DMS-MSNs aligned to the transitions between Up and Down states (*Figure 4E*). The DH ratio was significantly higher, implying that the total balance of inputs, onto DLS-MSNs was biased toward a bigger depolarization during the transition from the Down to the Up state and toward a larger hyperpolarization values during the transition from the Up to the Down state. This is consistent with the significant differences found for both Up states slopes (*Figures 1D* and *4F*, features 8–9).

In summary, our results show that the main differences between DLS- and DMS-MSNs spontaneous activity, selected by our classifier, are consistent with the number and the temporal distribution of the voltage fluctuations of the membrane potential during the Up states, suggesting that they are modulated by excitatory inputs from specific cortical areas and the striatal microcircuits interactions, mostly inhibitory.

Sequential propagation of the cortical Up states to the striatum

The SWO has a cortical origin, from where it propagates to the striatum activating MSNs (*Kasanetz et al., 2002*; *Ketzef et al., 2017*; *Reig and Silberberg, 2016*; *Sáez et al., 2018*; *Wilson and Kawaguchi, 1996*) and interneurons (*Reig and Silberberg, 2014*). In order to clarify how cortical activity is related with the DS, we studied the correlations of the Up states between
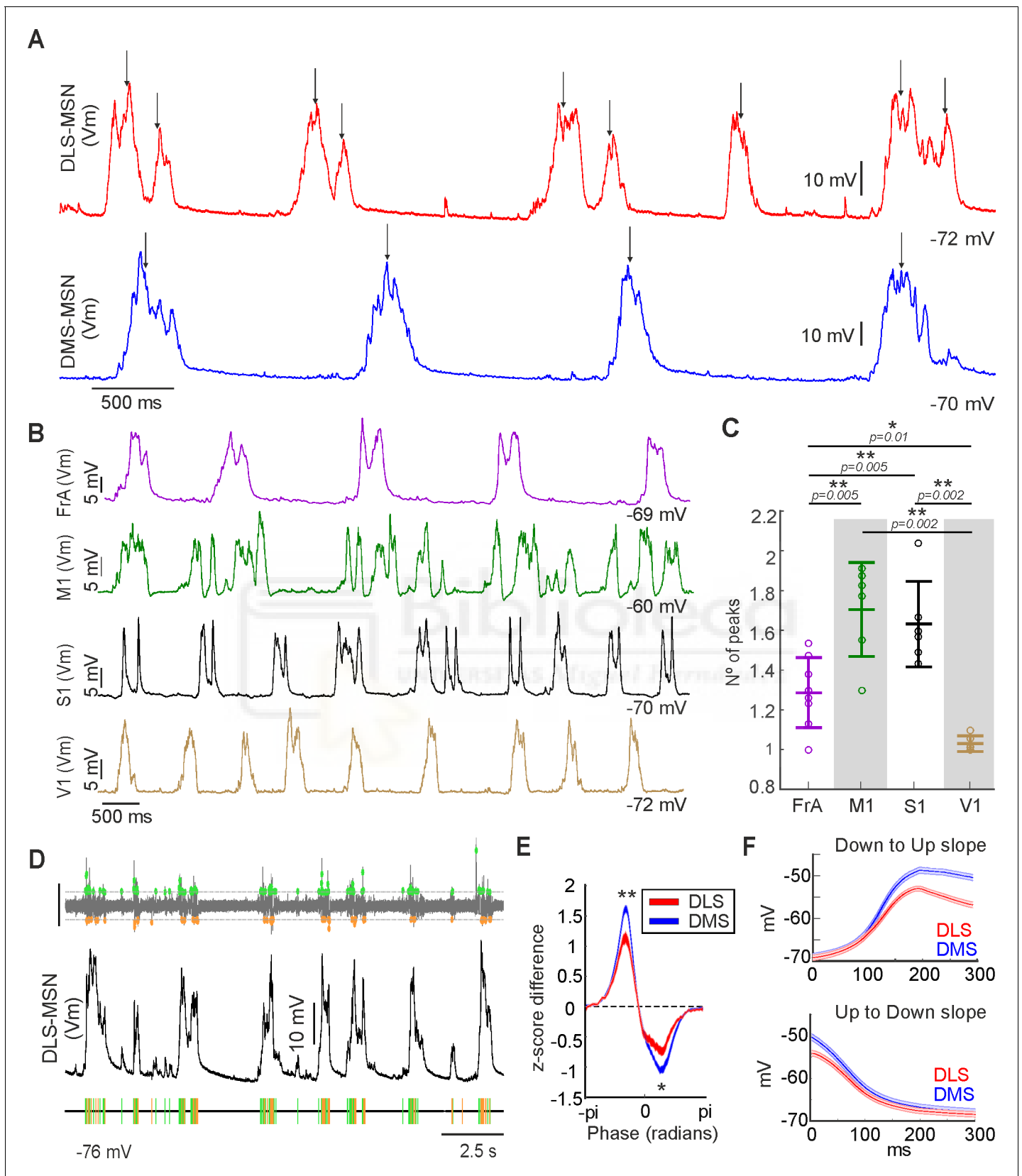
Figure 4. Number of peaks and depolarized/hyperpolarized ratio of the SWO in dorsal striatum. (**A**) Detection of peaks (black arrows) in the Up state in a DLS-MSN (red) and a DLS-MSN (blue) (see Materials and methods). (**B**) Representative examples of SWO in different cortical regions recorded. (**C**)

Figure 4 continued on next page

Number of peaks per Up state in the different cortical regions (left). Non-labeled comparisons are not significant. (**D**) Extraction of depolarized/hyperpolarized events by computational approach (see Materials and methods). Top: Detection of the events using a threshold in the first derivative of the Vm. Scale bar represents 0.1 dmV/dt. Bottom: Representation of the detected depolarized (green) and hyperpolarized (orange) events from whole-cell recording of a DLS-MSN (middle). (**E**) Average of the depolarized/hyperpolarized ratio aligned to the SWO cycle of DMS- and DLS-MSNs. Comparison of positive (p<0.0072) and negative (p<0.0398) values at peaks. (**F**) Grand average of the transitions from Down to Up (upper) and Up to Down (bottom). Shaded bars in E and F represent SEM. p Values obtained using the Wilcoxon Rank-sum test. In C, alpha values for multiple comparisons were corrected using Holm-Bonferroni correction.

several cortical areas and MSNs located in DLS and DMS (*Figure 5*). First, we applied the NA-MEMD algorithm to extract the IMF carrying the SWO (*Figure 5A–B*). Then, we used it to compute the cross-correlation between the whole-cell recordings of the MSNs in DLS or DMS with the pairs of simultaneous local field potentials (LFPs) recorded in FrA, M1, S1, and V1. We found that neuronal activity from DLS- and DMS-MSNs had different correlations with FrA, M1 and V1 LFPs (*Figure 5D*). Correlation with FrA and M1 activity was higher for DLS neurons, while correlation with V1 was higher for neurons recorded from DMS. When we represented correlation values with FrA and V1, two clusters were clearly distinguishable, corresponding to DMS- and DLS-MSNs (*Figure 5E*), suggesting specific functional coupling to the cortex for both striatal regions. It is important to note that we used this approach to understand the global correlation of the striatal SWO with different cortical areas, which does not have to be confused with the modulation of activity once the MSNs are in the active Up state (*Figure 1C*, see Discussion).
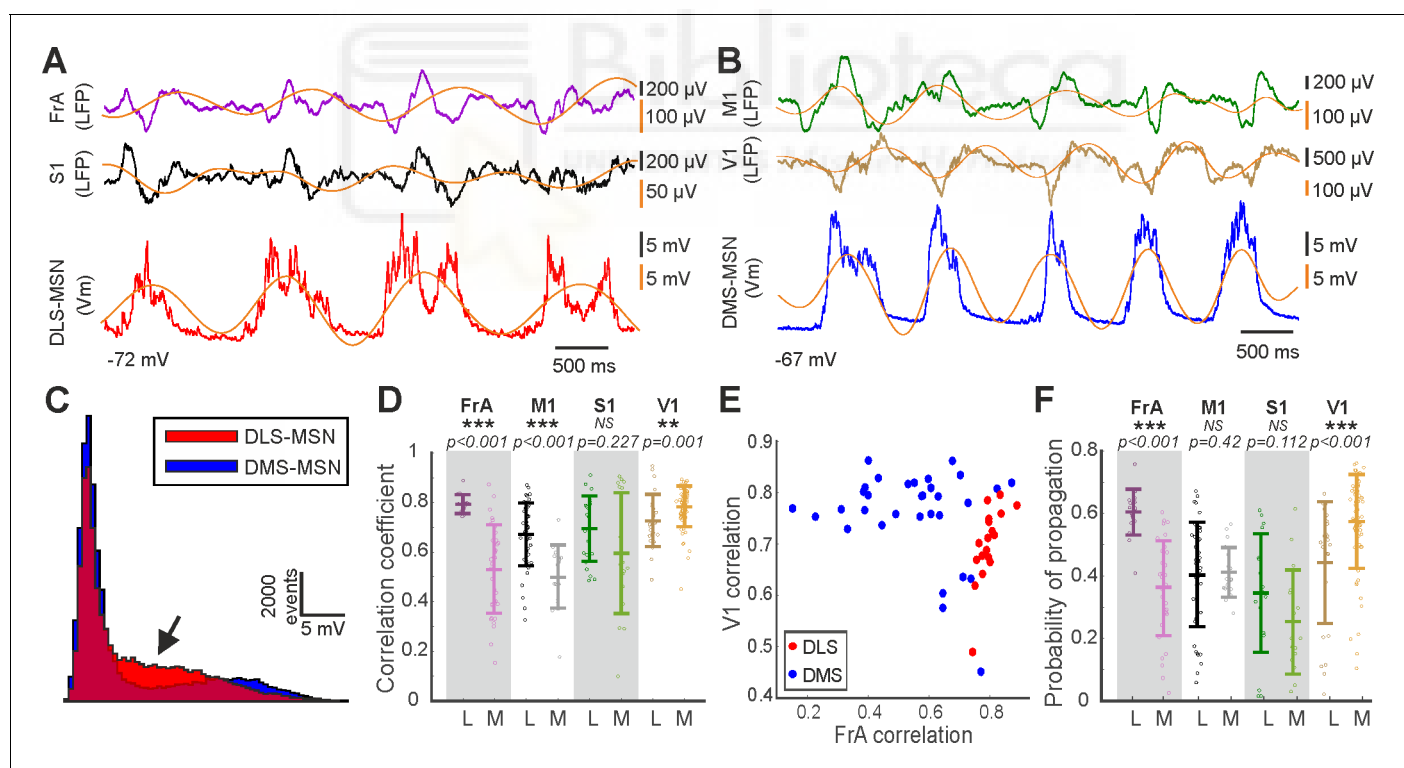
Figure 5. Integration of the cortical SWO in dorsal striatum. (**A**) Example of simultaneous recordings from a DLS-MSN (red) and double LFPs from FrA (purple) and S1 (black) together with SWO extraction by NA-MEMD (orange line). (**B**) Example of simultaneous recordings from a DMS-MSN (blue) and double LFP from M1 (green) and V1 (ochre) together with SWO extraction by NA-MEMD (orange line). (**C**) Histogram of the membrane potential values of the MSNs in A and B, the black arrow indicates the dissimilar shape of the bimodal distributions. (**D**) Correlation coefficient of different cortical regions to DLS- and DMS-MSNs. (**E**) Raster plot showing the correlation between all MSNs and the LFP from FrA and V1. (**F**) Probability of propagation of the Up state from different cortical regions to DLS- and DMS-MSNs. p Values obtained using the Wilcoxon Rank-sum test. In D and F, alpha values for multiple comparisons were corrected using Holm-Bonferroni correction.

Next, we used the IMF carrying the slow component of the SWO (*Figure 5A–B*, orange line) to analyze the probability of occurrence of an Up state recorded in an MSN, following the occurrence of a cortical Up state (*Figure 5F*). Consistent with the correlation results, the probability that an Up state in FrA is followed by an Up state in DLS was significantly higher than in DMS. Similarly, Up states in V1 had higher probability to be followed by an Up state in DMS than in DLS. In summary, the activity from FrA and sensory-motor cortical regions (M1 and S1) is strongly related with DLS-MSNs, while the activity in V1 does with DMS-MSNs.

These results predicted that, following the known propagation of the SWO across the cortex, with a predominant rostro-caudal direction (*Massimini et al., 2004*; *Ruiz-Mejias et al., 2011*), a sequential activation could be expected along the DS. In order to test this hypothesis, we first compared the order of transitions to an Up state recorded in both poles of the cortex by pairs of LFPs. We found an Up state in FrA preceding an Up state in V1 in the 71% of times (p value<0.0001, *Figure 6F*), demonstrating the preference of the rostro-caudal propagation of the SWO in cortex.

Finally, in order to test our prediction, we performed two simultaneous whole-cell patch-clamp recordings in two identified MSNs, located in the DLS and DMS (*Figure 6*). A representative example is shown in *Figure 6A–D*. In all six recorded pairs, the Up state in DLS-MSN preceded the one in DMS-MSN in 71.11 ± 9.37% of the times (*Figure 6E*, p=0.0313), with an average delay of
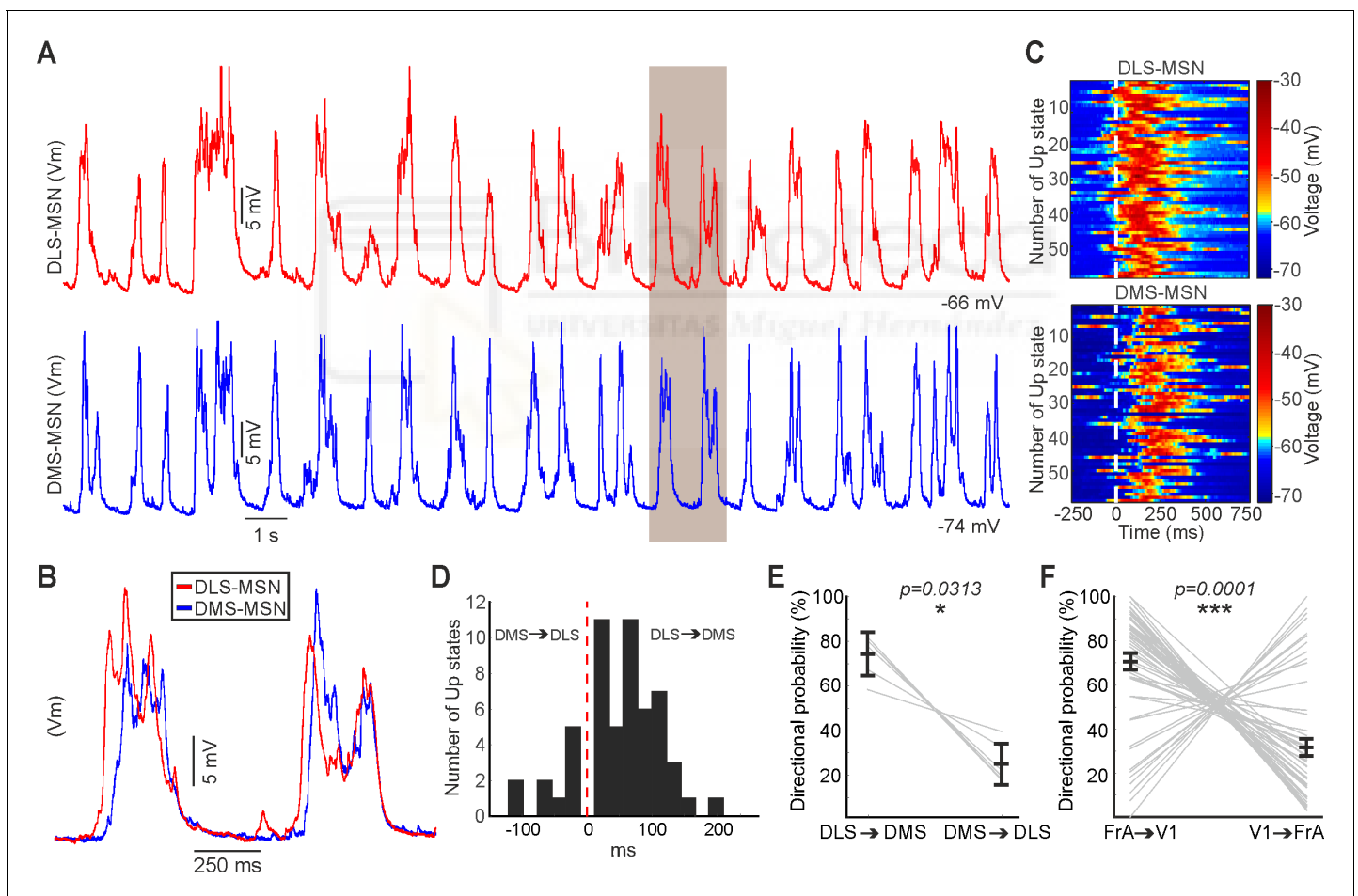
Figure 6. Sequential activation of the dorsal striatum during the SWO. (**A**) Representative example of simultaneous double in vivo whole-cell recordings in DLS (top, red) and DMS (bottom, blue). (**B**) Inset of the shaded part in **A**, showing two aligned membrane potential traces to their Down states. Notice that DLS-MSN onset is preceding the DMS-MSN. (**C**) Raster plot of the same example of a paired recording in DLS (top) and DMS (bottom) MSNs. Each line represents a 1 s time window aligned to the onset of each of the Up states of the DLS-MSN (white line). (**D**) Example of the distribution of delays between the onset of the Up state in the DMS- relative to the DLS-MSN. Positive values indicate that the Up state arrive later to the DMS-MSN. Same neuron in A, B, C, and D. (**E**) Directional probability of DS-MSNs, obtained from pairs of whole-cell recordings (N = 6). (**F**) Directional probability of V1 and FrA cortical areas, obtained from pairs of LFPs (N = 54). p Values obtained using the Wilcoxon Rank-sum test.

53.24 ± 32.16 ms. In the rest of the cases (28.62 ± 8.77%), in which DMS-MSN preceded the DLS-MSN, the delay was similar (average delay DLS-DMS = 51.91 ± 29.80 ms).

In conclusion, our results regarding the propagation of the cortical Up states to DS, confirm a stronger functional coupling of FrA to DLS and V1 to DMS. This generates a sequential activation of the DS, in which in most of the cases, DLS precedes DMS by tens of milliseconds.

Direct and indirect MSNs have distinct properties in DLS and DMS

In a final step to deconstruct DS circuitry, we studied the activity of MSNs corresponding to the direct or indirect pathway. To understand corticostriatal dynamics it is essential to apprehend how both pathways integrate the upstream cortical activity. To answer our question, we analyzed the whole-cell recoding of the DS that were optogenetically identified as direct and indirect MSNs through the optopatcher (*Figure 7A*, see Materials and methods). First, we analyzed whether the features that were previously used to describe the Up states (*Figure 1D*) allowed us to differentiate between the MSNs belonging to each pathway in DLS and DMS. Our results show differences in the integration of the spontaneous activity between direct and indirect pathways only in DLS. We found three features of the Up states that were significant different when comparing direct and indirect MSNs in DLS: maximum and minimum membrane potential value of the Up state and the average
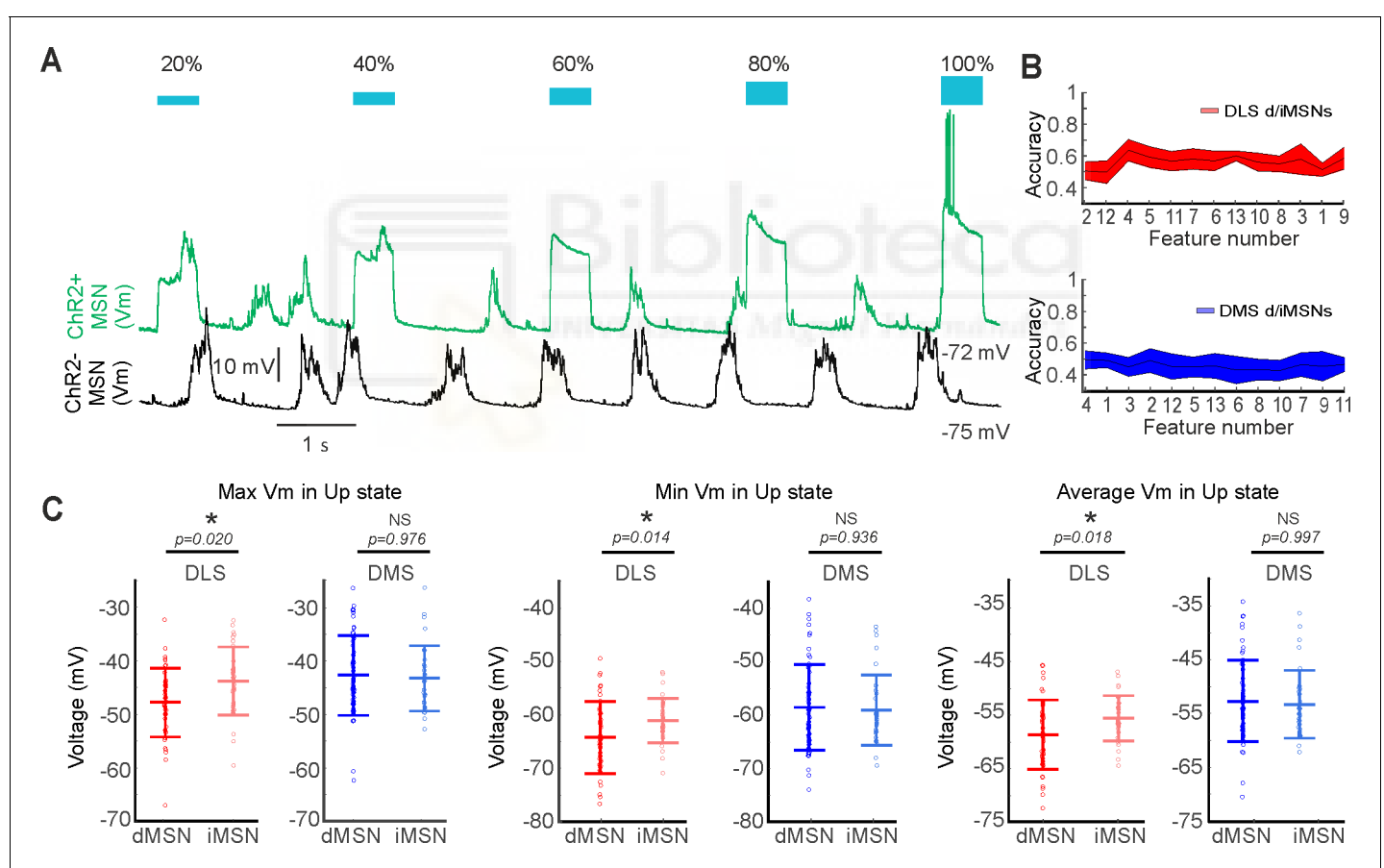
Figure 7. Differences between direct and indirect pathway MSNs in dorsal striatum. (**A**) Example showing an in vivo identification of an MSN using the optopatcher. Responses in D2-ChR2-YFP mice (top trace, ChR2$^+$, green) to light pulses, inducing depolarization in the MSN. Negative cells (bottom trace, ChR2$^-$, black) did not respond to light pulses. Blue squares indicate the intensity of the light pulse stimulation, from 20 to 100%. (**B**) RFE to optimize the classification of dMSNs and iMSNs in DLS (red) or DMS (blue). A SVM with a linear kernel was selected as classification algorithm. (**C**) Significant differences in three SWO features were found in DLS (red) between direct (dark) and indirect (light) pathways, but not in DMS (blue). p Values obtained using the Wilcoxon Rank-sum test.

The online version of this article includes the following figure supplement(s) for figure 7:

Figure supplement 1. Beta, Theta, and Gamma bands in membrane voltage of direct and indirect pathways in the DLS and DMS.

value of the Up state (*Figure 7C*). Then, we asked whether DLS- and DMS-MSNs could be subdivided in two additional populations corresponding with the direct or indirect MSNs in both striatal regions. The result did not yield separation, classification accuracy was 50% for DMS-MSNs and 64% for DLS-MSNs (*Figure 7B*). High-frequency oscillations were also similar between pathways in both striatal regions (*Figure 7—figure supplement 1*).

Finally, we studied whether the differences in the electrophysiological properties between DLS- and DMS-MSNs, described before (*Table 1*), were dependent on one of the two pathways. Resistance values, during Down states, were significantly higher for indirect DLS-MSNs compared to indirect DMS-MSNs, while no differences were found between direct DLS- and DMS-MSNs (*Table 1*).

In summary, our results show that DLS- and DMS-MSNs cannot be subdivided by the direct and indirect pathways. However, their differences in resistance and integration of the spontaneous activity demonstrate that direct and indirect MSNs have distinct properties in the DLS and DMS.

Discussion

Circuits are limited but not defined by their anatomy; different axonal projections, cell types and synaptic dynamics delimit their spontaneous and evoked activity patterns. In this study, we have described two functional circuits in the anatomically homogenous DS, covering the medial and lateral regions and separated by a sharp functional boundary. We discriminated DLS and DMS circuits based on different properties of their spontaneous activity recorded in MSNs by means of the in vivo whole-cell patch-clamp technique. The use of an anesthetized preparation was convenient for a number of reasons; first, it granted the mechanical stability that allowed the recording of our dataset that includes whole-cell patch clamp recordings in multiple cortical and striatal areas, specially the double patch-clamp recordings in the striatum. In addition, during anesthesia, as well as sleep and resting awake periods, the brain activity is in the SWO regime (*Poulet and Crochet, 2018*). This stereotyped brain state is highly characterized extra- and intracellularly (*Sanchez-Vives et al., 2017*), and consists on slow traveling waves of cortical origin that will propagate to multiple cortical and subcortical areas, including the striatum. This approach allows the study of the functional constrains in the striatum that will modulate this spontaneous activity and are still present during awake or evoked states (*Getting, 1989*; *Luczak et al., 2015*), when striatal activity is more desynchronized (*Mahon et al., 2006*). Thus, the SWO is an adequate brain state to understand the functional organization of the DS.

To analyze the oscillatory activity, we used NA-MEMD algorithm (*Rehman and Mandic, 2010*) together with Hilbert transform (*Huang et al., 1998*). This algorithm is suited to decompose nonlinear nonstationary signals (*Alegre-Cortés et al., 2017*; *Alegre-Cortés et al., 2016*; *Hu and Liang, 2014*; *Mandic et al., 2013*). Given the well-known nonlinear properties of neural oscillations (*Averbeck et al., 2006*; *Cole et al., 2017*; *Laurent, 1996*; *Shamir and Sompolinsky, 2004*), the use of NA-MEMD leads to an increased detail of description when compared with traditional techniques (*Alegre-Cortés et al., 2017*; *Hu and Liang, 2014*). In our knowledge is the first time that it is used to analyze membrane oscillations of single neurons.

In humans, the dynamics of the SWO have demonstrated to be highly reproducible within and across subjects, providing information about the general state of the cerebral cortex and suggesting its applicability as a method to unravel functional circuits (*Massimini et al., 2004*). The analysis of the SWO has been used to detect neurophysiological alterations in humans and in a mouse models of neurological disorders such as; Alzheimer's disease (*Busche et al., 2015*), Down syndrome (*Ruiz-Mejias et al., 2016*), or epilepsy (*Amiri et al., 2019*), among others. Here, we analyzed the electrophysiological properties of MSNs, their evoked visual responses and the slow and the fast components of their oscillatory activity, and we found that the Up states of the SWO are useful method to identify brain circuits. Therefore, we are extending the previous concept and proposing a methodology to study the brain functional connectivity.

DLS and DMS are two different functional circuits in mouse

We have shown that DS is divided in two different circuits, demonstrating the presence of a sharp functional transition from one circuit to another in the central region of the DS. This sharp transition is unexpected given the anatomical organization of corticostriatal projections, due to the profusion of axon terminals which provide overlapping inputs from multiple cortical areas to several regions of

the DS (*Alloway et al., 2006*; *Hintiryan et al., 2016*; *Hoffer et al., 2003*; *Hoover et al., 2003*). Hence, an essential question arises: why do we find a sharp boundary instead of a gradient transition between DLS- and DMS-MSNs? Our results show that the number of peaks during Up states is a critical feature to discriminate between DLS- and DMS-MSNs (*Figure 1E*), being higher in DLS-MSNs (*Figure 1D*, feature 11). In order to understand this result, we recorded layer V neurons in FrA, M1, S1, and V1, showing a larger number of peaks during Up states in FrA, M1, and S1 than in V1 (*Figure 4C*). This suggests that, in agreement with previous anatomical studies (*Alloway et al., 2006*; *Hoffer and Alloway, 2001*; *Hooks et al., 2018*), somatosensory-motor and premotor cortical regions exert sharper modulation onto the DLS-MSNs than onto DMS-MSNs, which is more anatomically connected with visual, associative, and limbic prefrontal cortical areas (*Hintiryan et al., 2016*; *Hunnicutt et al., 2016*). We also observed a higher number of peaks between M1-S1 with respect to FrA (*Figure 4C*). These results suggest that the dynamics of the excitatory/inhibitory inputs during the Up states change between cortical areas and subsequently influence the striatum, opening an interesting question regarding the circuit mechanism underlying the observed cortical Up states differences.

Together with the cortical glutamatergic inputs, several additional factors may contribute to generate a functional boundary. Our classification reached ~ 90% of accuracy between DLS- and DMS-MSNs when the Up to Down state transition slopes were added (*Figure 1E*). Moreover, the Down to Up transition and transition ratio were both significantly different between DLS- and DMS-MSNs as well (*Figure 1D*). Therefore, Up states slopes are key elements to discriminate between dorsal striatal circuits too. In order to better understand the undergoing dynamics that could explain the differences in the slopes, we measured the time course of depolarized and hyperpolarized events of the MSNs during the SWO (*Figure 4D*) and compared them using the DH ratio (*Figure 4E*). Our results show more positive and negative ratio to the DMS-MSNs during the upward and downward Up states transitions slopes respectively, suggesting a different EI balance in the DLS compared to DMS. Cortical SWO propagates to both types of MSNs but also to FS and ChI (*Reig and Silberberg, 2014*). FS interneurons provide strong feedforward inhibition to MSNs (*Gittis et al., 2010*; *Szydlowski et al., 2013*; *Tepper et al., 2008*). Previous reports demonstrated the presence of a FS gradient (*Gerfen et al., 1985*; *Kita et al., 1990*; *Monteiro et al., 2018*) or diverse types of PV interneurons with different electrophysiological properties along DS (*Monteiro et al., 2018*; *Muñoz-Manchado et al., 2018*). In addition, in cortical slices with spontaneous SWO both upward and downward transition slopes are controlled by GABA$_A$ and GABA$_B$ receptor activation (*Perez-Zabalza et al., 2020*; *Sanchez-Vives et al., 2010*). Based on these evidences, and beyond the glutamatergic inputs, we hypothesize that PV interneurons may greatly influence the Up states slopes of DLS-MSNs making them different from DMS ones.

In addition, other mechanisms can also contribute to the generation of a functional boundary; for instance, a similar scenario exists for ChIs, which present a functional gradient with higher activity in the medial regions of the striatum (*Abudukeyoumu et al., 2019*; *Matamales et al., 2016*). ChIs could modulate differently the SWO in DLS- and DMS-MSNs by disynaptic inhibition (*English et al., 2012*). Under anesthesia, dopaminergic neurons of the Substantia Nigra discharge spontaneous action potentials, in tonic or burst firing mode (*Aristieta et al., 2016*; *Brown et al., 2009*). This dopaminergic activity could induce different effects in the SWO in DLS- and DMS-MSNs, either directly mediated by distinct dopaminergic projections (*Brown et al., 2009*) or indirectly by their varied impact in ChIs activity along the mediolateral axis (*Chuhma et al., 2018*). Finally, it has been recently shown that SOM corticostriatal interneurons modulate the MSNs activity from motor cortical areas (*Melzer et al., 2017*; *Rock et al., 2016*). This type of interneuron could regulate the Up states transitions slopes directly, inhibiting the MSNs in their distal dendrites. Future work will have to determine whether FS, ChI, SOM or maybe other types of interneurons and neuromodulators contribute to the generation of the sharp functional boundary between DLS and DMS.

DLS and DMS are not defined by their sensory responses

Previous studies demonstrated that MSNs in the DS respond to sensory stimulation (*Ketzef et al., 2017*; *Pidoux et al., 2011*; *Reig and Silberberg, 2014*; *Sippy et al., 2015*). MSNs in the lateral and medial regions of the DS are activated by whisker stimulation, with bigger and sharper responses in the lateral region, which receives greater density of axons from S1. On the other hand, visual responses seem restricted to more medial territories, consistent with their corticostriatal projections

(*Reig and Silberberg, 2014*). Because the detected functional border is located in between these two striatal regions, we explored whether the previously described differences in the response to visual stimulation in DMS and DLS (*Reig and Silberberg, 2014*) was also present in the MSNs recorded in our DCS striatal coordinate, and therefore could let us to discriminate between DLS- and DMS-MSNs along the whole medio-lateral axis. Tactile-whisker stimulation was discarded because MSNs from lateral and medial regions respond to this sensory modality, with no differences in onset delay (*Reig and Silberberg, 2014*). Therefore, we tested whether neurons recorded in the functional border between DLS and DMS and classified as DLS- or DMS-MSNs responded to visual stimulation. We found that the 47% of MSNs recorded in the DCS coordinate responded to visual stimulation and the 17% were also labeled as DLS-MSNs by our classifier (*Figure 3E*). Then, we compared visual responses between MSNs recorded in the DCS and DMS coordinates. We found that they differ in their responses, including their onset delay (*Figure 3F–I*): MSNs in the DMS coordinate responded 9 ms earlier than the ones in the DCS coordinate. This strongly suggests that cortical axons sending visual information to the striatum have diverse cortical origin. A previous anatomical study *Hintiryan et al., 2016* demonstrated that the striatal region in which our DCS coordinate was located receives axons from the anteromedial (AM) and anterolateral (AL) areas of the visual cortex, while the DMS one does from V1, AM, and AL. In the hierarchy of visual areas, V1 sends abundant feedforward projections to AM and AL (*Garrett et al., 2014*), which could underlie the observed differences in onset delays. Thus, bringing together our results and the previous anatomical description, we hypothesize that, while the most lateral territories of the DLS are not involved in visual processing, there is a disparity of axons from several visual areas sending different information along the DS, which does not overlap with the internal organization of the DS in DLS and DMS. The functional specialization of V1, AM, and AL cortical areas compromise different properties of the visual information (*Marshel et al., 2012*), most probably, transmitting their particular attributes to the DLS- and DMS-MSNs that they contact. Future works are required to fully understand the spectra of sensory responses along the mediolateral axis of the DS. For instance, it remains as an open question a detailed understanding of how the specific properties of somatosensory or visual stimuli, are encoded along the latero-medial axis of the striatum.

In conclusion, the functional circuitry of the striatum cannot be described based on their responses to sensory stimulation. The DS is divided in two regions as a result of the large diversity of corticostriatal and probably other afferent projections, together with differences at the level of their microcircuits. On the other hand, while sensory inputs may not determine the overall dynamics of DLS or DMS circuitry, they govern the sensory responses of the MSNs in the specific striatal coordinates on which they project.

Propagation of the cortical Up states to the striatum

SWO propagates along the cortical network (*Sanchez-Vives and McCormick, 2000*) and is transmitted to the striatum (*Reig and Silberberg, 2014*; *Wilson and Kawaguchi, 1996*) as well as to other subcortical nuclei (*Ros et al., 2009*; *Steriade et al., 1993*). Decortication or disruption of the cortical SWO impairs the striatal ones (*Kasanetz et al., 2002*; *Wilson, 1993*) and on the other hand, striatal slices are absent of rhythmic spontaneous activity (*Planert et al., 2013*).

As occurs in human slow-wave sleep (*Massimini et al., 2004*), anesthetized mice exhibit a predominant pattern of SWO propagation from rostral to caudal brain poles (*Ruiz-Mejias et al., 2011*). Here, we show how the correlation and the probability of transition of an Up state from FrA is higher to the DLS, while an Up state recorded in V1 has higher probability to propagate to the DMS (*Figure 5D–F*). These results suggest a sequential activation of DMS and DLS, similar to the one between both poles of the cortex during the SWO. As discussed before, this result describes the corticostriatal propagation of the SWO, which is different of the modulation of MSNs activity during the Up states. In order to test this hypothesis, we simultaneously recorded pairs of MSNs in DLS and DMS, in our knowledge this is the first time that double in vivo patch-clamp recordings are shown in the striatum. We found a similar probability of an Up state to appear in DLS before DMS and to appear in FrA before V1 (*Figure 6*). This description of the overall dynamics of corticostriatal transmission is based on functional, rather than anatomical connectivity, supporting a stronger coupling of caudal, sensory related cortical regions to DMS, whereas premotor and sensory-motor frontal regions are more tightly connected to DLS. Consistent with this, the sequential activation of both DS regions during a two-forced-decision-task has been recently reported, in which DMS was first

activated during the sensory stimulation period, followed by an increase in DLS activity coinciding with decision making and motor preparation/execution (*Peters et al., 2019*).

Finally, the number of peaks during Up states, the first feature selected to classify between DLS- and DMS-MSNs, were prominent in the DLS-MSNs (*Figure 1D*) as well as in S1 and M1 (*Figure 4B–C*). These results together with the anatomical descriptions (*Alloway et al., 2006*; *Hoffer et al., 2003*; *Hooks et al., 2018*) and a recent in vivo synaptic transmission experiments (*Charpier et al., 2020*), strongly suggest that the activity inside the Up state of the DLS-MSNs is controlling by sensory-motor areas. In addition, FrA send copious projections to the DLS (*Hintiryan et al., 2016*; *Hunnicutt et al., 2016*) and we found that correlations and probability of propagation of Up states to DLS were higher for FrA than S1 and M1 (*Figure 5D–F*).

Considering this results together, we suggest that, when a slow wave starts in the rostral part of the cortex, FrA projections trigger the Up state in DLS, but rarely DMS. Then, once the wave reaches somatosensory-motor areas, they will modulate the activity of DLS-MSNs, which are already in an Up state. In agreement, it was shown that the blockage of synaptic transmission in S1 by TTX application during bilateral whisker stimulation blocked whisker responses but not the Up states in DLS-MSNs (*Reig and Silberberg, 2016*), demonstrating that their Up states were not triggered by S1. Therefore, we hypothesize that during awake states, FrA could act as a gain modulator of DLS that will facilitate its response to somatosensory-motor inputs.

High-frequency oscillations

High-frequency oscillations are usually associated with wakefulness. However, they also occur during the SWO in natural sleep, under anesthesia (*Steriade et al., 1996*) and in isolated cortical slices (*Compte et al., 2008*). Especially relevant regarding the cortico-basal ganglia-thalamic loop are beta oscillations, which have been linked with the control of voluntary movements. Differences in Beta oscillations between caudate and putamen were reported in healthy monkeys at the end of a learned motor task (*Feingold et al., 2015*). Exaggerated Beta oscillations occur in Parkinson's Disease and in rats under dopamine depletion (*Brown, 2003*; *Mallet et al., 2008*; *Sharott et al., 2017*). Our results did not show differences between DLS- and DMS-MSNs for theta and gamma bands (*Figure 2—figure supplement 1*), however a difference in beta energy was detected (*Figure 2*). Possible candidates to explain the observed higher beta energy in DMS-MSNs are ChI. This type of interneurons are more active in the DMS (*Matamales et al., 2016*) and can facilitate glutamate release from presynaptic terminals to the MSNs (*Abudukeyoumu et al., 2019*). Thus, they might promote the fast glutamatergic transmission observed in DMS.

Our work adds further detail to the description of beta oscillation in healthy mice thanks to the use of NA-MEMD together with Hilbert transform (*Figure 2—figure supplement 2*), providing a new substrate for the study of aberrant beta oscillations in Parkinson disease. This result may indicate that the aberrant oscillations in Parkinson disease may be produced by the misbalance of normal striatal dynamics, as previously suggested (*McCarthy et al., 2011*).

We also analyzed the fast oscillatory activity to classify DLS- and DMS-MSNs, however this information was not useful for that purpose. Unlike other faster oscillatory bands, the ~ 1 Hz oscillation, which constitutes the main component of the SWO brain state, is described as highly reproducible within and across subjects. Based in this property, it was suggested as a method to study neuronal changes and connectivity in humans (*Massimini et al., 2004*). Our negative result using the fast oscillatory activity reinforces the idea that the ~ 1 Hz component of the SWO is a particular useful model to study functional connectivity.

Integration of the spontaneous activity in the direct and indirect MSNs along the DS

Cortical inputs innervate the DS targeting both the direct and indirect pathway MSNs (*Doig et al., 2010*; *Kress et al., 2013*; *Wall et al., 2013*). Both types of MSNs are co-activated during action initiation (*Cui et al., 2013*) and respond to tactile and visual stimulation (*Reig and Silberberg, 2014*). However, a large number of studies described differences between direct and indirect MSNs in the DLS: dMSNs have higher density of cortical and thalamic afferent synapses (*Huerta-Ocampo et al., 2014*), bigger response to whisker stimulation (*Ketzef et al., 2017*; *Reig and Silberberg, 2014*; *Sippy et al., 2015*) and based on in vivo SWO, it has been estimated that dMSNs receive stronger

synaptic input than iMSNs (*Filipović et al., 2019*), among other differences. Here, we have described changes in the activity integration between pathways in the DLS-MSNs (*Figure 7C*), which are absent in the DMS-MSNs. Despite these differences, our results show that both DLS and DMS are unified circuits that involve both pathways.

Previous in vitro (*Planert et al., 2010*) and in vivo (*Ketzef et al., 2017*; *Reig and Silberberg, 2014*) studies in the DLS showed that iMSNs have higher input resistance than dMSNs. While observed a similar trend, the main difference in the input resistance was detected between DLS-MSNs and DMS-MSNs, with bigger values in DLS. Moreover, this result was weighted by the iMSNs located in the DLS, which displayed the highest values of resistance and were statistically different than iMSNs in the DMS (*Table 1*). Interestingly, this variation between iMSNs located in both striatal regions occurred during Down states, when MSNs are mainly silent, suggesting that changes in resistance are independent of the glutamatergic inputs. It is known that dopamine alters the input resistance of MSNs in vivo (*Ketzef et al., 2017*). Therefore, distinct dopaminergic innervation of the DLS- and DMS-MSNs (*Chuhma et al., 2018*) could underlie our differences in resistance between striatal regions.

Conclusion

Human caudate and putamen have been compared to the rodent DLS and DMS, respectively (*Balleine and O'Doherty, 2010*), based in their corticostriatal connectivity and behavioral functions. Yet, a study of the circuitry that supported this division was necessary. Here, we have shown how DLS and DMS are two non-overlapping circuits isolated by a sharp functional boundary. This work provides further understanding of the corticostriatal organization and reveals the biological substrate to divide the DS in two different circuits. We have shown how DLS- and DMS-MSNs display independent spontaneous regimes during SWO brain state, that can only be explained by a combination of particular corticostriatal functional connectivity and microcircuit properties. Visual evoked responses in particular demonstrated that the differences between DLS and DMS circuits cannot be reduced to their interaction with sensory cortices. In conclusion, our results provide the required understanding to support that this functional segregation is analogous to the anatomical and functional division of the primate striatum in caudate and putamen. Considering the relevance of the mouse striatum as a model for multiple human diseases, our results indicate that research will have to consider the idiosyncrasy of the two regions of the DS.

Materials and methods

Key resources table

Reagent type (species) or resource	Designation	Source or reference	Identifiers	Additional information
Genetic reagent (*M. musculus*)	BAC-Cre Drd2-44 or STOCK Tg(Drd2-cre) ER44Gsat/Mmcd	GENSAT	RRID:MMRRC_017263-UCD	Males and females used
Genetic reagent (*M. musculus*)	Ai32 or Ai32(RCL-ChR2(H134R)/EYFP) or B6;129S-Gt(ROSA) 26Sortm32(CAG-COP4*H134R/EYFP)Hze/J	The Jackson Laboratory	Stock No: 012569	Males and females used
Genetic reagent (*M. musculus*)	C57BL/6J or C57BL/6NCrl	Charles River Laboratories	Strain Code: 027	Males and females used
Other	Cy3 conjugated streptavidin	Jackson ImmunoResearch Laboratories	Cat#: 016-160-08 Lot. #125000	1:1000
Chemical compound, drug	Ketamine, Ketamidor	Alvet Escartí S.L.	Ref. # 078100377	100 mg/ml

Continued on next page

Continued

Reagent type (species) or resource	Designation	Source or reference	Identifiers	Additional information
Chemical compound, drug	Medetomidine, Sedine	Alvet Escartí S.L.	Ref. # 005100740	10 ml
Chemical compound, drug	Sodium Pentobarbital, Dolethal	Alvet Escartí S.L.	Ref. # 015P5502	200 mg/ml, 100 ml
Software, agorithm	Spike2	Cambridge Electronic Design Limited (CED)	n/a	Version 9
Software, algorithm	Matlab	Mathworks	n/a	Version 2018
Software, algorithm	Support Vector Machine (SVM)	*Cortes and Vapnik, 1995* doi: https://doi.org/10.1007/BF00994018	n/a	https://www.scipy.org/
Software, algorithm	NA-MEMD	*Rehman and Mandic, 2010* doi: https://doi.org/10.1098/rspa.2009.0502	n/a	http://www.commsp.ee.ic.ac.uk/~mandic/research/emd.htm

Ethical permit

All the experimental procedures were conformed to the directive 2010/63/EU of the European Parliament and the RD 53/2013 Spanish regulation on the protection of animals use for scientific purposes, approved by the government of the Autonomous Community of Valencia, under the supervision of the *Consejo Superior de Investigaciones Científicas* and the Miguel Hernandez University Committee for Animal use in Laboratory.

Animal model

D2-Cre (ER44 line, GENSAT) mouse line was crossed with the Channelrhodopsin (ChR2)-YFP reporter mouse line (Ai32, the Jackson laboratory) to induce expression of ChR2 in indirect MSNs and was used to perform optogenetic differentiation of direct (dMSN) and indirect (iMSNs) MSNs (*Ketzef et al., 2017*), while performing electrophysiological recordings in the striatum (n = 36 mice). C57BL6 mice were used to perform the rest of the electrophysiological recordings of cortical neurons (n = 9).

Electrophysiological recordings

Adult mice of both sexes (47 animals, 20 males, and 27 females), between 12 and 44 weeks of age were used to perform the experiments (*Supplementary file 1B*). Anesthesia was induced by intraperitoneal injection of ketamine (75 mg/kg) and medetomidine (1 mg/kg) diluted in 0.9% NaCl. A maintaining dose of ketamine (30 mg/kg i.m.) was administrated every 2 hr, after changes in the frequency of spontaneous activity recorded by cortical LFP or reflex responses to paw pinches. Tracheotomy was performed to increase mechanical stability during recordings by decreasing breathing related movements. Mice were placed in a stereotaxic device and air enriched with oxygen was delivered through a thin tube placed 1 cm from the tracheal cannula. Core temperature was monitored and maintained at 36.5 ± 0.5°C using a feedback-controlled heating pad (FHC Inc). Craniotomies were drilled (S210, Camo) at seven sites for patch-clamp and extracellular recordings (from Bregma): AP 0 mm, L 2.5 mm (DMS); AP 0 mm, L 4 mm (DLS); AP 0 mm, L 3,25 mm (DCS); AP 2.7 mm, L 1 mm (FrA); AP 1.5 mm, L 2.0 mm (M1); AP −1.5 mm, L 3.25 mm (S1); AP −3.5 mm from Bregma, L 2.5 mm (V1) (following *Paxinos and Franklin, 2001*). When additional paired recordings were performed, the craniotomies were drilled at the following coordinates (from Bregma): AP 0 mm, L 1 mm (DMS); AP 0 mm, L 4 mm (DLS). Animals were sacrificed after recordings by injecting an overdose of sodium pentobarbital (200 mg/kg I.P.).

Whole-cell recordings

Whole-cell recordings were obtained in the DS from DLS, DMS, DCS between 2013 and 2647 μm depth. The number of striatal neurons was 126: DLS = 77, from which direct MSNs = 49, indirect MSNs = 34; DMS n = 91, from which direct MSNs = 65, indirect MSNs = 32; DCS n = 17, from which dDCS = 10, iDCS = 7. Cortical neurons (n = 26) were recorded from layer V in FrA, M1, S1 and V1 at a depth of 675–926 μm. In detail, the number of recorded neurons was: Frontal association cortex (FrA, n = 8), primary motor cortex (M1, n = 6), primary somatosensory cortex (S1, n = 6), and primary visual cortex (n = 6). Additional paired simultaneous whole-cell recordings of MSNs (n = 6 pairs) were obtained from DLS and DMS between 2039 and 2348 μm of depth, by means of two micromanipulators (Luigs and Neumann, MRE/MLE Mini 25). All of them in a perpendicular penetration angle of ∼ 30°, except for DCS cells, in which the angle was ∼20°. The exposed brain was continuously covered with 0.9% NaCl to prevent drying. Signals were amplified using MultiClamp 700B amplifier (Molecular Devices) and digitized at 20 kHz with a CED acquisition board and Spike two software (Cambridge Electronic Design).

Borosilicate patch pipettes (1B150F-4, WPI), were pulled with a Flaming/Brown micropipette puller P-1000 (Sutter Instruments) and had an initial resistance of 6–12 MΩ. Pipettes were back-filled with intracellular solution containing: 125 mM K-gluconate, 10 mM KCl, 10 mM Na-Phosphocreatine, 10 mM HEPES, 4 mM ATP-Mg and 0.3 mM GTP-Na. pH and osmolality were adjusted to ∼7.4 and ∼280 mOsm/L respectively. Biocytin (0.2–0.4%, Sigma Aldrich) was then added to the intracellular solution to perform cell reconstruction after the experiment. To perform the analysis, 100 s of spontaneous activity (no current injection, no stimulation) were used from the recording. Input resistance (*Table 1*) was measured as the slope of a linear fit between injected depolarizing and hyperpolarizing current steps and membrane potential. Also, in order to improve the quantification of the described inward membrane rectification at hyperpolarized values of the MSNs membrane potentials, mean resistance in response to the negative and positive steps delivered at Up and Down states was also analyzed (*Table 1*), as in *Reig and Silberberg, 2014*. Membrane time constant (tau) was computed as the time to reach 63% of the voltage increment in response to a current pulse. Capacitance was computed as the time constant divided by the input resistance.

Neurons were identified according to their recorded electrical properties and following morphological staining, according to the aspiny dendrites in the case of the ChI and FS interneurons. FS interneurons displayed narrow action potentials, relatively depolarized resting membrane potential, high discharge rate of action potentials, and no apparent inward rectification. Cholinergic interneurons were characterized by their depolarized membrane potential, voltage sag response to current step injections and spontaneous tonic discharge. From the whole population of recorded neurons, 2 of them were identify as FS, one in the DLS and other in the DMS, 3 ChI were recorded in the DMS. These five striatal interneurons were excluded from the data set. Neurons having a deviation by more than 10 mV from their initial resting membrane potential were excluded from analysis. Only MSNs and cortical neurons were included in the data set.

Extracellular recordings

Extracellular recordings were obtained using unipolar tungsten electrodes with impedance of 1 to 2 MΩ. The electrodes were placed in infragranular layers (∼1000 μM depth from the pia) of two cortical regions in each experiment, from FrA, M1, S1, V1 cortex with an angle between 15° and 25°. Recordings were amplified using a differential AC Amplifier model 1700 (A-M Systems) and digitized at 20 KHz with CED and Spike-2, simultaneously with the whole-cell recording.

Visual stimulation

Visual stimuli were delivered by a white LED positioned 50 mm from the contralateral eye. Duration was 15 ms and it was triggered every 5 s (0.2 Hz) during whole-cell in 17 MSNs recorded in the DCS coordinate and in 10 MSNs recorded in the DMS coordinate. The eye was covered with artificial eye drops (Viscotears, Bausch+Lomb, Germany) in order to prevent drying.

Optogenetic identification of in vivo recorded neurons

In order to identify 'on line' the specific type of MSNs belonging to the direct (dMSNs) and indirect (iMSNs) pathways, the optopatcher was used (*Katz et al., 2019*; *Katz et al., 2013*; *Ketzef et al.,*

2017; A-M systems, WA USA). Controlled pulses (SLA-1000–2, two channel universal LED driver, Mightex systems) of blue light (Fibre-coupled LED light source FCS-0470–000, 470 nm, Mightex systems) through Spike two software were delivered using an optic fibre (200 µm diameter, handmade) inserted into the patch-pipette, while recording their spontaneous activity (*Figure 7A*). One or two serial pulses with five light steps of 500 ms each were delivered every 2 s with increasing intensity from 20% to 100% of full LED power (minimal light intensity was 0.166 mW, maximal intensity was 0.83 mW measured at the tip of the fibre). Power light was measured with an energy meter console (PM100D, Thorlabs). Positive cells responded to light pulses by depolarizing the membrane potential (*Figure 7A*, upper trace), responding within 2.69 ± 1.37 ms (ranging from 0.8 to 5 ms) to light pulses by a step-like depolarization of 13.3 ± 8.28 mV (ranging from 4 to 33 mV), therefore were classified as indirect MSNs. Negative cells did not show any depolarization to light pulses (*Figure 7A*, bottom trace) and were classified as a putative direct MSNs.

Morphological reconstruction

At the end of each experiment, mice were sacrificed with a lethal dose of sodium pentobarbital and perfused with a solution containing 4% paraformaldehyde in 0.1 M phosphate buffer (PB, pH 7.4). Brains were extracted and stored in PBS solution until the cutting. Before cutting, brains were transferred into PBS containing 30% sucrose for at least 48 hr. Coronal slices (25 µm thick) containing the entire striatum from the recorded side (from AP 1.4 mm to AP −1.3 mm, following *Paxinos and Franklin, 2001*), were obtained using a digital automatic cryotome and collected on gelatine coated slides. Sections were incubated over night with Cy3-conjugated streptavidin (Jackson Immuno Research Laboratories) diluted (1:1000) in 1% BSA, 0.3% Triton-X 100 in 0.1 M PBS. Finally, the glass slides were covered with mowiol (Calbiochem) and imaged. Neurons were then reconstructed using a fluorescence microscope (DM 6000B, Leica) and a camera (DC350 FX, Leica) and then processed by ImageJ.

Extraction of up and down states

In order to isolate Up and Down states from the membrane voltage we started by smoothing the trace using a 200 ms window. Then, we extracted the Up states using a threshold consisting of the mean value of the membrane potential (Vm) plus 0.5 standard deviations. Then, we merged the parts of fragmented Up states, detected as an interval shorter than 250 ms between the transition of a prospective Up state to a prospective Down state to the transition from a prospective Down state to a prospective Up state. Finally, detected Up states shorter than 200 ms where discarded.

When studying propagation of Up states, we considered two Up states from two different cortical regions, or a cortical LFP recording and an MSN to be part of the same SWO, thus propagating from one region to the other, when their onsets were closer in time than 500 ms.

Feature extraction of Up states

In order to describe the properties of the SWO of the recorded MSNs, we computed 13 parameters (*Figure 1D*). First, we subtracted the IMFs carrying oscillations faster than 50 Hz from the MSNs membrane voltage recordings to eliminate the spikes. Then, we divided the trace into Up and Down states and calculated the different features; the mean value of the membrane potential in the Up state (Feature number 1 (1)), the standard deviation of the Up state membrane potential (2), minimum (most hyperpolarized value) membrane potential in the Up state (3) and maximum (most depolarized value) membrane potential in the up state (4). Additionally, we computed the peak to peak distance (12), which is the difference between the most depolarized and most hyperpolarized values of the membrane potential of the Up state, the maximum (6) and minimum (7) value of the derivative of the values of the membrane potential in the Up state, as well as the number of peaks in the Up state (11), understood as big, slow changes in the membrane potential inside the Up state, which created diplets or triplets during the Up state (*Figure 4A,B*). To do so, we used the *findpeaks* Matlab function on the smoothed (200 ms smooth) Up state with a minimum peak height of 0.3 standard deviations and a minimum distance between peaks of 160 ms. We also computed the length of the Up state (13), the mean amplitude of the Up state, computed as the difference in membrane potential average value between Up and Down states (5) and the speed of the transition from the Down to the Up state (8), and from the Up to the Down state (9) as well as the Slope transition ratio,

computed as the speed of transition from Down to Up states divided by the one from Up to Down states (10). In order to measure the slope speeds, we used a vector consisting in −100 to +200 ms (300 ms total) relative to the transition either to the Up or the Down state. Then, we smoothed (100 ms smooth) the selected region and computed its derivative. We delimited the slope computing the region over a threshold calculated as the mean plus 0.3 standard deviations of the derivative. Once we had delimited the transition, we fitted a lineal function to that region of the recording to compute the slope speed.

Detection of intracellular synaptic events

Intracellular synaptic currents were extracted using sharp deflections of the membrane voltage using a modification of the method presented here (*Compte et al., 2008*). In brief, we applied a Parks-McClellan low-pass differentiator filter (order 20, cut off at 200 Hz) and computed the first derivative of the intracellular membrane potential. Then, we extracted the temporal profile of depolarizing and hyperpolarizing events to the recorded cell using a threshold of the first derivative. We empirically determined a two standard deviations threshold to extract them. Next, we aligned the detected membrane deflections for both the hyperpolarizing and depolarizing events to the phase of the SWO as computed using NA-MEMD and normalized them to their respective maximum (*Figure 4E*) in order to study the profile of the recruitment of excitation and inhibition during SWO. We computed the depolarizing/hyperpolarizing ratio subtracting the hyperpolarizing normalized value to the depolarizing one at each phase point.

For our whole-cell recordings, we have used a low-chloride intracellular solution (described above), in which the reversal potential for excitation is ~ −5 mV and GABA$_A$ inhibition ~ −70 mV. The average membrane potential during the Down states of the recorded MSNs was −69.2 ± 6.48 mV for DLS-MSNs and −69.31 ± 7.68 mV for DMS-MSNs. Around these voltages, the membrane fluctuations are depolarizing and excitatory. However, during the Up states (mean voltage values: −57.24 ± 6.34 mV for DLS-MSNs and −52.95 ± 7.08 mV for DMS-MSNs), both depolarized and hyperpolarized events can be detected (*Figure 4D*). As previously discussed (*Compte et al., 2008*), this method does not extract all the EPSPs or IPSPs of the recorded cell, but it provides a major picture of the convergence of coordinated excitatory or inhibitory inputs onto the recorded cell that produced sharp deflections in their membrane potential. Therefore, this method is sufficient to study the temporal profiles of hyper/depolarizing events onto the recorded cells during SWO.

Lateromedial classification

We classified MSNs from DLS and DMS using a Support Vector Machine (SVM) (*Cortes and Vapnik, 1995*) with a linear kernel. This supervised classification method estimates a hyperplane to separate both populations. Classification was cross-validated 10 times.

In order to determine which features were more relevant for the classification of DLS- and DMS-MSNs, we used Recursive Feature Elimination. This approach organizes the features relative to their importance to the classification by recursively pruning the least relevant features starting from the initial set.

MSNs distribution along the classification boundary

Support Vector Machines (SVMs) are supervised classifiers that predict the category of a new entry based on their previous training history and are not suitable to predict new categories in novel data. In order to study the spontaneous activity of DCS-MSNs, we examined its distribution in the classification space, relative to the classification boundary instead of directly using the output of a classifier. This approach provides information, not only about whether the new data (DCS-MSNs) creates a new cluster in the classification space, but also about where is it placed along the classification axis used to discriminate between DLS- and DMS-MSNs. Hence, it provides a more informative approach to the distribution of DCS-MSNs relative to DLS- and DMS-MSNs than a direct multi-category classification (i.e. discriminate versus Hypotheses 1 and 2, see Results).

To calculate the distribution of the data along the classification boundary, we first obtained the coefficients and intersection values of the SVM used to classify the MSNs belonging to DLS and DMS. Once we obtained these parameters, we used them to project all data points to this hypervector and computed the probability density function of the new distributions (*Figure 3D*). Now, the

data was distributed along a single hypervector and we could compute the distribution of the MSNs along the classification boundary in a comprehensible manner to study the distribution of the DCS-MSNs.

SWO computation using NA-MEMD

We used Noise-assisted Multivariate Empirical Mode Decomposition (NA-MEMD) algorithm (*ur Rehman and Mandic, 2011*) together with Hilbert transform (*Huang et al., 1998*) for the analysis of high-frequency oscillations both in LFPs and MSNS membrane potential, as well as the cortico-striatal propagation of the SWO. Because neuronal oscillations are characterized by nonlinear properties, this algorithm is suited to decompose nonlinear nonstationary signals (*Alegre-Cortés et al., 2017*; *Alegre-Cortés et al., 2016*; *Hu and Liang, 2014*; *Mandic et al., 2013*). The original EMD (*Huang et al., 1998*) is a data-driven algorithm suitable for nonlinear and non-stationary signals that does not rely on any predetermined template. It decomposes a given signal into a subset of oscillatory modes called Intrinsic Mode Functions (IMFs) (*Figure 2—figure supplement 2*). Each IMF contains the oscillations of the original data in a certain frequency range. Then, Hilbert transform is applied onto each IMF in order to compute its instantaneous frequency and amplitude. The MEMD (*Rehman and Mandic, 2010*) is a multivariate extension of the original EMD to n-dimensional signals. The MEMD is computed simultaneously in all dimensions of the signal to ensure the same number of IMFs as output. In addition, new dimensions can be added to the data containing White Gaussian Noise (WGN) to increase its performance, as it has been described that WGN addition reduces mode mixing produced by signal intermittence (*Wu and Huang, 2009*), acting as a quasi-dyadic filter that enhances time frequency resolution (*Flandrin et al., 2004*; *ur Rehman and Mandic, 2011*). The application of MEMD to the desired signal together with extra White Gaussian Noise dimensions is known as NA-MEMD analysis (*ur Rehman and Mandic, 2011*). EMDs algorithms plus Hilbert Transform have been increasingly used in neuroscience during the last years as they produce an enriched Time-Frequency (T-F) Spectrum when compared to traditional T-F linear tools (*Alegre-Cortés et al., 2016*; *Hu and Liang, 2014*). In our work, we applied NA-MEMD algorithm to a multivariate signal composed by the intracellular recording, both LFPs and one extra WGN channel. By means of this analysis, we could warrant that the number of IMFs was the same in the intracellular and the LFPs recordings for a direct comparison of the SWO extracted using this method. In order to apply NA-MEMD analysis to our data, we adapted MEMD Matlab package (http://www.commsp.ee.ic.ac.uk/mandic/research/emd.htm). Standard stopping criterion was described elsewhere (*Rilling et al., 2003*). At last, we extracted the IMF carrying the SWO as the one with maximum correlation with the membrane voltage and visually confirmed it in all the recorded cells (*Figure 1C*). Once we isolated the SWO of each recording using NA-MEMD, they were stored for further analysis.

Hilbert transform

We computed the frequency of the SWO, and theta (6–10 Hz), beta (10–20 Hz) and gamma (20–80 Hz) bands as the instantaneous frequency using the Hilbert transform (*Huang et al., 1998*). For a given time series x(t), its Hilbert transform H(x)(t) is defined as:

$$d(x)(t) = \frac{1}{\pi} C \int_{-\infty}^{\infty} \frac{x(\acute{t})}{t - \acute{t}} d\acute{t}$$

where C indicates the Cauchy principal value. Hilbert transform results in a complex sequence with a real part which is the original data and an imaginary part which is a version of the original data with a 90° phase shift; this analytic signal is useful to calculate instantaneous amplitude and frequency; instantaneous amplitude is the amplitude of H(x)(t), instantaneous frequency is the time rate of change of the instantaneous phase angle.

Statistical analysis

All experimental comparisons were tested using the Wilcoxon Rank-sum test except stated otherwise. Directionality of the SWO in the cortex and in the striatum was tested using Wilcoxon signed rank test. Phase locking of different frequency bands was tested using Rayleigh test. When required,

alpha values for multiple comparisons were corrected using Holm-Bonferroni correction. Error bars presented in the graphs represent the standard deviation unless stated otherwise.

Acknowledgements

Additional information

Author contributions

Javier Alegre-Cortés, Formal analysis, Investigation, Visualization, Writing - original draft, Writing - review and editing; María Sáez, Formal analysis, Investigation, Visualization, Methodology, Writing - review and editing; Roberto Montanari, Investigation, Methodology, Writing - review and editing; Ramon Reig, Conceptualization, Resources, Data curation, Supervision, Funding acquisition, Investigation, Methodology, Writing - original draft, Project administration, Writing - review and editing

Author ORCIDs

Javier Alegre-Cortés (iD) https://orcid.org/0000-0003-0888-7542
María Sáez (iD) https://orcid.org/0000-0001-9137-6692
Roberto Montanari (iD) https://orcid.org/0000-0002-4331-8460
Ramon Reig (iD) https://orcid.org/0000-0002-6475-4181

Ethics

Animal experimentation: All experimental procedures conformed to the directive 2010/63/EU of the European Parliament and the RD 53/2013 Spanish regulation on the protection of animals use for scientific purposes, approved by the government of the Autonomous Community of Valencia, under the supervision of the Consejo Superior de Investigaciones Científicas and the Miguel Hernandez University Committee for Animal use in the Laboratory.

Decision letter and Author response
Decision letter https://doi.org/10.7554/eLife.60580.sa1
Author response https://doi.org/10.7554/eLife.60580.sa2

Additional files

Supplementary files

• Supplementary file 1. Additional data. (A) Featurization of the SWO of DCS-MSNs. Note that the number preceding the feature labels are the same as the ones showed in *Figure 3*. All values display means ± standard deviation. (B) Data set description. The three first rows are total values; the rest display the mean ± standard deviation.

• Transparent reporting form

Data availability

All data generated during and/or analysed during the current study, as well as the required code to reproduce the figures, is available on the CSIC public repository. This is the URL access https://digital.csic.es/handle/10261/229794.

The following dataset was generated:

Author(s)	Year	Dataset title	Dataset URL	Database and Identifier
Javier A-C, Sáez M, Montanari R, Reig R	2021	Medium spiny neurons activity reveals the discrete segregation of mouse dorsal striatum	https://doi.org/10.20350/digitalCSIC/13750	DIGITAL.CSIC, 10.20350/digitalCSIC/13750

References

Abudukeyoumu N, Hernandez-Flores T, Garcia-Munoz M, Arbuthnott GW. 2019. Cholinergic modulation of striatal microcircuits. *European Journal of Neuroscience* **49**:604–622. DOI: https://doi.org/10.1111/ejn.13949

Adler A, Katabi S, Finkes I, Israel Z, Prut Y, Bergman H. 2012. Temporal convergence of dynamic cell assemblies in the striato-pallidal network. *Journal of Neuroscience* **32**:2473–2484. DOI: https://doi.org/10.1523/JNEUROSCI.4830-11.2012, PMID: 22396421

Alegre-Cortés J, Soto-Sánchez C, Pizá ÁG, Albarracín AL, Farfán FD, Felice CJ, Fernández E. 2016. Time-frequency analysis of neuronal populations with instantaneous resolution based on noise-assisted multivariate empirical mode decomposition. *Journal of Neuroscience Methods* **267**:35–44. DOI: https://doi.org/10.1016/j.jneumeth.2016.03.018, PMID: 27044801

Alegre-Cortés J, Soto-Sánchez C, Albarracín AL, Farfán FD, Val-Calvo M, Ferrandez JM, Fernandez E. 2017. Toward an improvement of the analysis of neural coding. *Frontiers in Neuroinformatics* **11**:77. DOI: https://doi.org/10.3389/fninf.2017.00077, PMID: 29375359

Alloway KD, Lou L, Nwabueze-Ogbo F, Chakrabarti S. 2006. Topography of cortical projections to the dorsolateral neostriatum in rats: multiple overlapping sensorimotor pathways. *The Journal of Comparative Neurology* **499**:33–48. DOI: https://doi.org/10.1002/cne.21039, PMID: 16958106

Alloway KD, Smith JB, Beauchemin KJ, Olson ML. 2009. Bilateral projections from rat MI whisker cortex to the neostriatum, Thalamus, and claustrum: forebrain circuits for modulating whisking behavior. *The Journal of Comparative Neurology* **515**:548–564. DOI: https://doi.org/10.1002/cne.22073, PMID: 19479997

Amiri M, Frauscher B, Gotman J. 2019. Interictal coupling of HFOs and slow oscillations predicts the seizure-onset pattern in mesiotemporal lobe epilepsy. *Epilepsia* **60**:1160–1170. DOI: https://doi.org/10.1111/epi.15541, PMID: 31087662

Aristieta A, Ruiz-Ortega JA, Miguelez C, Morera-Herreras T, Ugedo L. 2016. Chronic L-DOPA administration increases the firing rate but does not reverse enhanced slow frequency oscillatory activity and synchronization in substantia nigra pars reticulata neurons from 6-hydroxydopamine-lesioned rats. *Neurobiology of Disease* **89**:88–100. DOI: https://doi.org/10.1016/j.nbd.2016.02.003, PMID: 26852950

Averbeck BB, Latham PE, Pouget A. 2006. Neural correlations, population coding and computation. *Nature Reviews Neuroscience* **7**:358–366. DOI: https://doi.org/10.1038/nrn1888, PMID: 16760916

Balleine BW, O'Doherty JP. 2010. Human and rodent homologies in action control: corticostriatal determinants of goal-directed and habitual action. *Neuropsychopharmacology* **35**:48–69. DOI: https://doi.org/10.1038/npp.2009.131, PMID: 19776734

Berke JD, Okatan M, Skurski J, Eichenbaum HB. 2004. Oscillatory entrainment of striatal neurons in freely moving rats. *Neuron* **43**:883–896. DOI: https://doi.org/10.1016/j.neuron.2004.08.035, PMID: 15363398

Brown P. 2003. Oscillatory nature of human basal ganglia activity: relationship to the pathophysiology of Parkinson's disease. *Movement Disorders* **18**:357–363. DOI: https://doi.org/10.1002/mds.10358, PMID: 12671 940

Brown MT, Henny P, Bolam JP, Magill PJ. 2009. Activity of neurochemically heterogeneous dopaminergic neurons in the substantia nigra during spontaneous and driven changes in brain state. *Journal of Neuroscience* **29**:2915–2925. DOI: https://doi.org/10.1523/JNEUROSCI.4423-08.2009, PMID: 19261887

Busche MA, Kekuš M, Adelsberger H, Noda T, Förstl H, Nelken I, Konnerth A. 2015. Rescue of long-range circuit dysfunction in Alzheimer's disease models. *Nature Neuroscience* **18**:1623–1630. DOI: https://doi.org/10.1038/nn.4137, PMID: 26457554

Charpier S, Pidoux M, Mahon S. 2020. Converging sensory and motor cortical inputs onto the same striatal neurons: an in vivo intracellular investigation. *PLOS ONE* **15**:e0228260. DOI: https://doi.org/10.1371/journal.pone.0228260, PMID: 32023274

Chuhma N, Mingote S, Yetnikoff L, Kalmbach A, Ma T, Ztaou S, Sienna AC, Tepler S, Poulin JF, Ansorge M, Awatramani R, Kang UJ, Rayport S. 2018. Dopamine neuron glutamate cotransmission evokes a delayed excitation in lateral dorsal striatal cholinergic interneurons. *eLife* **7**:e39786. DOI: https://doi.org/10.7554/eLife.39786, PMID: 30295607

Cole SR, van der Meij R, Peterson EJ, de Hemptinne C, Starr PA, Voytek B. 2017. Nonsinusoidal beta oscillations reflect cortical pathophysiology in Parkinson's Disease. *The Journal of Neuroscience* **37**:4830–4840. DOI: https://doi.org/10.1523/JNEUROSCI.2208-16.2017, PMID: 28416595

Cole SR, Voytek B. 2017. Brain oscillations and the importance of waveform shape. *Trends in Cognitive Sciences* **21**:137–149. DOI: https://doi.org/10.1016/j.tics.2016.12.008, PMID: 28063662

Compte A, Reig R, Descalzo VF, Harvey MA, Puccini GD, Sanchez-Vives MV. 2008. Spontaneous high-frequency (10-80 hz) oscillations during up states in the cerebral cortex in vitro. *Journal of Neuroscience* **28**:13828–13844. DOI: https://doi.org/10.1523/JNEUROSCI.2684-08.2008, PMID: 19091973

Cortes C, Vapnik V. 1995. Support-vector networks. *Machine Learning* **20**:273–297. DOI: https://doi.org/10.1007/BF00994018

Cowan RL, Wilson CJ. 1994. Spontaneous firing patterns and axonal projections of single corticostriatal neurons in the rat medial agranular cortex. *Journal of Neurophysiology* **71**:17–32. DOI: https://doi.org/10.1152/jn.1994.71.1.17, PMID: 8158226

Cui G, Jun SB, Jin X, Pham MD, Vogel SS, Lovinger DM, Costa RM. 2013. Concurrent activation of striatal direct and indirect pathways during action initiation. *Nature* **494**:238–242. DOI: https://doi.org/10.1038/nature11846, PMID: 23354054

Doig NM, Moss J, Bolam JP. 2010. Cortical and thalamic innervation of direct and indirect pathway medium-sized spiny neurons in mouse striatum. *Journal of Neuroscience* **30**:14610–14618. DOI: https://doi.org/10.1523/JNEUROSCI.1623-10.2010, PMID: 21048118

English DF, Ibanez-Sandoval O, Stark E, Tecuapetla F, Buzsáki G, Deisseroth K, Tepper JM, Koos T. 2012. GABAergic circuits mediate the reinforcement-related signals of striatal cholinergic interneurons. *Nature Neuroscience* **15**:123–130. DOI: https://doi.org/10.1038/nn.2984

Faure A, Haberland U, Condé F, El Massioui N. 2005. Lesion to the nigrostriatal dopamine system disrupts stimulus-response habit formation. *Journal of Neuroscience* **25**:2771–2780. DOI: https://doi.org/10.1523/JNEUROSCI.3894-04.2005, PMID: 15772337

Feingold J, Gibson DJ, DePasquale B, Graybiel AM. 2015. Bursts of beta oscillation differentiate postperformance activity in the striatum and motor cortex of monkeys performing movement tasks. *PNAS* **112**:13687–13692. DOI: https://doi.org/10.1073/pnas.1517629112, PMID: 26460033

Filipović M, Ketzef M, Reig R, Aertsen A, Silberberg G, Kumar A. 2019. Direct pathway neurons in mouse dorsolateral striatum in vivo receive stronger synaptic input than indirect pathway neurons. *Journal of Neurophysiology* **122**:2294–2303. DOI: https://doi.org/10.1152/jn.00481.2019, PMID: 31618095

Flaherty AW, Graybiel AM. 1991. Corticostriatal transformations in the primate somatosensory system projections from physiologically mapped body-part representations. *Journal of Neurophysiology* **66**:1249–1263. DOI: https://doi.org/10.1152/jn.1991.66.4.1249, PMID: 1722244

Flandrin P, Rilling G, Goncalves P. 2004. Empirical mode decomposition as a filter bank. *IEEE Signal Processing Letters* **11**:112–114. DOI: https://doi.org/10.1109/LSP.2003.821662

Garrett ME, Nauhaus I, Marshel JH, Callaway EM. 2014. Topography and areal organization of mouse visual cortex. *Journal of Neuroscience* **34**:12587–12600. DOI: https://doi.org/10.1523/JNEUROSCI.1124-14.2014, PMID: 25209296

Gerfen CR, Baimbridge KG, Miller JJ. 1985. The neostriatal mosaic: compartmental distribution of calcium-binding protein and parvalbumin in the basal ganglia of the rat and monkey. *PNAS* **82**:8780–8784. DOI: https://doi.org/10.1073/pnas.82.24.8780, PMID: 3909155

Getting PA. 1989. Emerging principles governing the operation of neural networks. *Annual Review of Neuroscience* **12**:185–204. DOI: https://doi.org/10.1146/annurev.ne.12.030189.001153, PMID: 2648949

Gittis AH, Nelson AB, Thwin MT, Palop JJ, Kreitzer AC. 2010. Distinct roles of GABAergic interneurons in the regulation of striatal output pathways. *Journal of Neuroscience* **30**:2223–2234. DOI: https://doi.org/10.1523/JNEUROSCI.4870-09.2010, PMID: 20147549

Graybiel AM. 2008. Habits, rituals, and the evaluative brain. *Annual Review of Neuroscience* **31**:359–387. DOI: https://doi.org/10.1146/annurev.neuro.29.051605.112851, PMID: 18558860

Hauber W, Schmidt WJ. 1994. Differential effects of lesions of the dorsomedial and dorsolateral caudate-putamen on reaction time performance in rats. *Behavioural Brain Research* **60**:211–215. DOI: https://doi.org/10.1016/0166-4328(94)90149-X, PMID: 8003250

Hilário MR, Costa RM. 2008. High on habits. *Frontiers in Neuroscience* **2**:208–217. DOI: https://doi.org/10.3389/neuro.01.030.2008, PMID: 19225594

Hintiryan H, Foster NN, Bowman I, Bay M, Song MY, Gou L, Yamashita S, Bienkowski MS, Zingg B, Zhu M, Yang XW, Shih JC, Toga AW, Dong HW. 2016. The mouse cortico-striatal projectome. *Nature Neuroscience* **19**:1100–1114. DOI: https://doi.org/10.1038/nn.4332, PMID: 27322419

Hoffer ZS, Hoover JE, Alloway KD. 2003. Sensorimotor corticocortical projections from rat barrel cortex have an anisotropic organization that facilitates integration of inputs from whiskers in the same row. *The Journal of Comparative Neurology* **466**:525–544. DOI: https://doi.org/10.1002/cne.10895, PMID: 14566947

Hoffer ZS, Alloway KD. 2001. Organization of corticostriatal projections from the vibrissal representations in the primary motor and somatosensory cortical Areas of rodents. *The Journal of Comparative Neurology* **439**:87–103. DOI: https://doi.org/10.1002/cne.1337

Hooks BM, Papale AE, Paletzki RF, Feroze MW, Eastwood BS, Couey JJ, Winnubst J, Chandrashekar J, Gerfen CR. 2018. Topographic precision in sensory and motor corticostriatal projections varies across cell type and cortical area. *Nature Communications* **9**:3549. DOI: https://doi.org/10.1038/s41467-018-05780-7, PMID: 30177709

Hoover JE, Hoffer ZS, Alloway KD. 2003. Projections from primary somatosensory cortex to the neostriatum: the role of somatotopic continuity in corticostriatal convergence. *Journal of Neurophysiology* **89**:1576–1587. DOI: https://doi.org/10.1152/jn.01009.2002

Hu M, Liang H. 2014. Search for information-bearing components in neural data. *PLOS ONE* **9**:e99793. DOI: https://doi.org/10.1371/journal.pone.0099793, PMID: 24932596

Huang NE, Shen Z, Long SR, Wu MC, Shih HH, Zheng Q, Yen N-C, Tung CC, Liu HH. 1998. The empirical mode decomposition and the Hilbert spectrum for nonlinear and non-stationary time series analysis. *Proceedings of the Royal Society of London. Series A: Mathematical, Physical and Engineering Sciences* **454**:903–995. DOI: https://doi.org/10.1098/rspa.1998.0193

Huerta-Ocampo I, Mena-Segovia J, Bolam JP. 2014. Convergence of cortical and thalamic input to direct and indirect pathway medium spiny neurons in the striatum. *Brain Structure and Function* **219**:1787–1800. DOI: https://doi.org/10.1007/s00429-013-0601-z, PMID: 23832596

Hunnicutt BJ, Jongbloets BC, Birdsong WT, Gertz KJ, Zhong H, Mao T. 2016. A comprehensive excitatory input map of the striatum reveals novel functional organization. *eLife* **5**:e19103. DOI: https://doi.org/10.7554/eLife.19103, PMID: 27892854

Ikemoto S. 2007. Dopamine reward circuitry: two projection systems from the ventral midbrain to the nucleus accumbens-olfactory tubercle complex. *Brain Research Reviews* **56**:27–78. DOI: https://doi.org/10.1016/j.brainresrev.2007.05.004, PMID: 17574681

Kasanetz F, Riquelme LA, Murer MG. 2002. Disruption of the two-state membrane potential of striatal neurones during cortical desynchronisation in anaesthetised rats. *The Journal of Physiology* **543**:577–589. DOI: https://doi.org/10.1113/jphysiol.2002.0024786, PMID: 12205191

Katz Y, Yizhar O, Staiger J, Lampl I. 2013. Optopatcher–an electrode holder for simultaneous intracellular patch-clamp recording and optical manipulation. *Journal of Neuroscience Methods* **214**:113–117. DOI: https://doi.org/10.1016/j.jneumeth.2013.01.017, PMID: 23370312

Katz Y, Sokoletsky M, Lampl I. 2019. In-vivo optogenetics and pharmacology in deep intracellular recordings. *Journal of Neuroscience Methods* **325**:108324. DOI: https://doi.org/10.1016/j.jneumeth.2019.108324, PMID: 31288037

Ketzef M, Spigolon G, Johansson Y, Bonito-Oliva A, Fisone G, Silberberg G. 2017. Dopamine depletion impairs bilateral sensory processing in the striatum in a Pathway-Dependent manner. *Neuron* **94**:855–865. DOI: https://doi.org/10.1016/j.neuron.2017.05.004, PMID: 28521136

Kincaid AE, Zheng T, Wilson CJ. 1998. Connectivity and convergence of single corticostriatal axons. *The Journal of Neuroscience* **18**:4722–4731. DOI: https://doi.org/10.1523/JNEUROSCI.18-12-04722.1998, PMID: 9614246

Kita H, Kosaka T, Heizmann CW. 1990. Parvalbumin-immunoreactive neurons in the rat neostriatum: a light and electron microscopic study. *Brain Research* **536**:1–15. DOI: https://doi.org/10.1016/0006-8993(90)90002-S, PMID: 2085740

Kita H, Kitai ST. 1988. Glutamate decarboxylase immunoreactive neurons in rat neostriatum: their morphological types and populations. *Brain Research* **447**:346–352. DOI: https://doi.org/10.1016/0006-8993(88)91138-9, PMID: 3390703

Kress GJ, Yamawaki N, Wokosin DL, Wickersham IR, Shepherd GM, Surmeier DJ. 2013. Convergent cortical innervation of striatal projection neurons. *Nature Neuroscience* **16**:665–667. DOI: https://doi.org/10.1038/nn.3397, PMID: 23666180

Laurent G. 1996. Dynamical representation of odors by oscillating and evolving neural assemblies. *Trends in Neurosciences* **19**:489–496. DOI: https://doi.org/10.1016/S0166-2236(96)10054-0, PMID: 8931275

Lerner TN, Shilyansky C, Davidson TJ, Evans KE, Beier KT, Zalocusky KA, Crow AK, Malenka RC, Luo L, Tomer R, Deisseroth K. 2015. Intact-Brain analyses reveal distinct information carried by SNc dopamine subcircuits. *Cell* **162**:635–647. DOI: https://doi.org/10.1016/j.cell.2015.07.014, PMID: 26232229

Levesque M, Charara A, Gagnon S, Parent A, Deschenes M. 1996. Corticostriatal projections from layer V cells in rat are collaterals of long-range corticofugal axons. *Brain Research* **709**:311–315. DOI: https://doi.org/10.1016/0006-8993(95)01333-4, PMID: 8833768

Luczak A, McNaughton BL, Harris KD. 2015. Packet-based communication in the cortex. *Nature Reviews Neuroscience* **16**:745–755. DOI: https://doi.org/10.1038/nrn4026, PMID: 26507295

Mahon S, Vautrelle N, Pezard L, Slaght SJ, Deniau JM, Chouvet G, Charpier S. 2006. Distinct patterns of striatal medium spiny neuron activity during the natural sleep-wake cycle. *Journal of Neuroscience* **26**:12587–12595. DOI: https://doi.org/10.1523/JNEUROSCI.3987-06.2006, PMID: 17135420

Mallet N, Pogosyan A, Sharott A, Csicsvari J, Bolam JP, Brown P, Magill PJ. 2008. Disrupted dopamine transmission and the emergence of exaggerated beta oscillations in subthalamic nucleus and cerebral cortex. *Journal of Neuroscience* **28**:4795–4806. DOI: https://doi.org/10.1523/JNEUROSCI.0123-08.2008, PMID: 1844 8656

Mandic DP, Rehman Nur, Wu Z, Huang NE. 2013. Empirical mode Decomposition-Based Time-Frequency analysis of multivariate signals: the power of adaptive data analysis. *IEEE Signal Processing Magazine* **30**:74–86. DOI: https://doi.org/10.1109/MSP.2013.2267931

Marshel JH, Kaye AP, Nauhaus I, Callaway EM. 2012. Anterior-posterior direction opponency in the superficial mouse lateral geniculate nucleus. *Neuron* **76**:713–720. DOI: https://doi.org/10.1016/j.neuron.2012.09.021, PMID: 23177957

Massimini M, Huber R, Ferrarelli F, Hill S, Tononi G. 2004. The sleep slow oscillation as a traveling wave. *Journal of Neuroscience* **24**:6862–6870. DOI: https://doi.org/10.1523/JNEUROSCI.1318-04.2004, PMID: 15295020

Matamales M, Götz J, Bertran-Gonzalez J. 2016. Quantitative imaging of cholinergic interneurons reveals a distinctive spatial organization and a functional gradient across the mouse striatum. *PLOS ONE* **11**:e0157682. DOI: https://doi.org/10.1371/journal.pone.0157682, PMID: 27314496

McCarthy MM, Moore-Kochlacs C, Gu X, Boyden ES, Han X, Kopell N. 2011. Striatal origin of the pathologic beta oscillations in Parkinson's disease. *PNAS* **108**:11620–11625. DOI: https://doi.org/10.1073/pnas.1107748108, PMID: 21697509

Melzer S, Gil M, Koser DE, Michael M, Huang KW, Monyer H. 2017. Distinct corticostriatal GABAergic neurons modulate striatal output neurons and motor activity. *Cell Reports* **19**:1045–1055. DOI: https://doi.org/10.1016/j.celrep.2017.04.024, PMID: 28467898

Monteiro P, Barak B, Zhou Y, McRae R, Rodrigues D, Wickersham IR, Feng G. 2018. Dichotomous parvalbumin interneuron populations in dorsolateral and dorsomedial striatum. *The Journal of Physiology* **596**:3695–3707. DOI: https://doi.org/10.1113/JP275936, PMID: 29808928

Muñoz-Manchado AB, Bengtsson Gonzales C, Zeisel A, Munguba H, Bekkouche B, Skene NG, Lönnerberg P, Ryge J, Harris KD, Linnarsson S, Hjerling-Leffler J. 2018. Diversity of interneurons in the dorsal striatum revealed by Single-Cell RNA sequencing and PatchSeq. *Cell Reports* **24**:2179–2190. DOI: https://doi.org/10.1016/j.celrep.2018.07.053, PMID: 30134177

Packard MG, Knowlton BJ. 2002. Learning and memory functions of the basal ganglia. *Annual Review of Neuroscience* **25**:563–593. DOI: https://doi.org/10.1146/annurev.neuro.25.112701.142937, PMID: 12052921

Paxinos G, Franklin K. 2001. *The Mouse Brain in Stereotaxic Coordinates*. Second Edition. San-Diego: Academic Press.

Perez-Zabalza M, Reig R, Manrique J, Jercog D, Winograd M, Parga N, Sanchez-Vives MV. 2020. Modulation of cortical slow oscillatory rhythm by GABAb$>_{Bb}>$ receptors: an in vitro experimental and computational study. *The Journal of Physiology* **598**:3439–3457. DOI: https://doi.org/10.1113/JP279476, PMID: 32406934

Peters AJ, Steinmetz NA, Harris KD, Carandini M. 2019. Striatal activity reflects cortical activity patterns. *bioRxiv*. DOI: https://doi.org/10.1101/703710

Pidoux M, Mahon S, Deniau JM, Charpier S. 2011. Integration and propagation of somatosensory responses in the corticostriatal pathway: an intracellular study in vivo. *The Journal of Physiology* **589**:263–281. DOI: https://doi.org/10.1113/jphysiol.2010.199646, PMID: 21059765

Planert H, Szydlowski SN, Hjorth JJ, Grillner S, Silberberg G. 2010. Dynamics of synaptic transmission between fast-spiking interneurons and striatal projection neurons of the direct and indirect pathways. *Journal of Neuroscience* **30**:3499–3507. DOI: https://doi.org/10.1523/JNEUROSCI.5139-09.2010, PMID: 20203210

Planert H, Berger TK, Silberberg G. 2013. Membrane properties of striatal direct and indirect pathway neurons in mouse and rat slices and their modulation by dopamine. *PLOS ONE* **8**:e57054. DOI: https://doi.org/10.1371/journal.pone.0057054, PMID: 23469183

Poulet JFA, Crochet S. 2018. The cortical states of wakefulness. *Frontiers in Systems Neuroscience* **12**:64. DOI: https://doi.org/10.3389/fnsys.2018.00064, PMID: 30670952

Rehman N, Mandic DP. 2010. Multivariate empirical mode decomposition. *Proceedings of the Royal Society A: Mathematical, Physical and Engineering Sciences* **466**:1291–1302. DOI: https://doi.org/10.1098/rspa.2009.0502

Reig R, Silberberg G. 2014. Multisensory integration in the mouse striatum. *Neuron* **83**:1200–1212. DOI: https://doi.org/10.1016/j.neuron.2014.07.033, PMID: 25155959

Reig R, Silberberg G. 2016. Distinct corticostriatal and intracortical pathways mediate bilateral sensory responses in the striatum. *Cerebral Cortex* **26**:4405–4415. DOI: https://doi.org/10.1093/cercor/bhw268, PMID: 27664965

Reiner A, Jiao Y, Del Mar N, Laverghetta AV, Lei WL. 2003. Differential morphology of pyramidal tract-type and intratelencephalically projecting-type corticostriatal neurons and their intrastriatal terminals in rats. *The Journal of Comparative Neurology* **457**:420–440. DOI: https://doi.org/10.1002/cne.10541, PMID: 12561080

Rilling G, Flandrin P, Goncalves P. 2003. On empirical mode decomposition and its algorithms. IEEE-EURASIP workshop on Nonlinear Signal and Image Processing NSIP-03.

Rock C, Zurita H, Wilson C, Apicella AJ. 2016. An inhibitory corticostriatal pathway. *eLife* **5**:e15890. DOI: https://doi.org/10.7554/eLife.15890, PMID: 27159237

Ros H, Sachdev RN, Yu Y, Sestan N, McCormick DA. 2009. Neocortical networks entrain neuronal circuits in cerebellar cortex. *Journal of Neuroscience* **29**:10309–10320. DOI: https://doi.org/10.1523/JNEUROSCI.2327-09.2009, PMID: 19692605

Ruiz-Mejias M, Ciria-Suarez L, Mattia M, Sanchez-Vives MV. 2011. Slow and fast rhythms generated in the cerebral cortex of the anesthetized mouse. *Journal of Neurophysiology* **106**:2910–2921. DOI: https://doi.org/10.1152/jn.00440.2011, PMID: 21880935

Ruiz-Mejias M, Martinez de Lagran M, Mattia M, Castano-Prat P, Perez-Mendez L, Ciria-Suarez L, Gener T, Sancristobal B, García-Ojalvo J, Gruart A, Delgado-García JM, Sanchez-Vives MV, Dierssen M. 2016. Overexpression of Dyrk1A, a down syndrome candidate, decreases excitability and impairs gamma oscillations in the prefrontal cortex. *The Journal of Neuroscience* **36**:3648–3659. DOI: https://doi.org/10.1523/JNEUROSCI.2517-15.2016, PMID: 27030752

Sáez M, Ketzef M, Alegre-Cortés J, Reig R, Silberberg G. 2018. A new Micro-holder device for local drug delivery during in vivo Whole-cell recordings. *Neuroscience* **381**:115–123. DOI: https://doi.org/10.1016/j.neuroscience.2018.04.011, PMID: 29679647

Sanchez-Vives MV, Mattia M, Compte A, Perez-Zabalza M, Winograd M, Descalzo VF, Reig R. 2010. Inhibitory modulation of cortical up states. *Journal of Neurophysiology* **104**:1314–1324. DOI: https://doi.org/10.1152/jn.00178.2010, PMID: 20554835

Sanchez-Vives MV, Massimini M, Mattia M. 2017. Shaping the default activity pattern of the cortical network. *Neuron* **94**:993–1001. DOI: https://doi.org/10.1016/j.neuron.2017.05.015, PMID: 28595056

Sanchez-Vives MV, McCormick DA. 2000. Cellular and network mechanisms of rhythmic recurrent activity in neocortex. *Nature Neuroscience* **3**:1027–1034. DOI: https://doi.org/10.1038/79848

Schultz W, Dayan P, Montague PR. 1997. A neural substrate of prediction and reward. *Science* **275**:1593–1599. DOI: https://doi.org/10.1126/science.275.5306.1593, PMID: 9054347

Shamir M, Sompolinsky H. 2004. Nonlinear population codes. *Neural Computation* **16**:1105–1136. DOI: https://doi.org/10.1162/089976604773717559, PMID: 15130244

Sharott A, Vinciati F, Nakamura KC, Magill PJ. 2017. A population of indirect pathway striatal projection neurons is selectively entrained to parkinsonian beta oscillations. *The Journal of Neuroscience* **37**:9977–9998. DOI: https://doi.org/10.1523/JNEUROSCI.0658-17.2017, PMID: 28847810

Sippy T, Lapray D, Crochet S, Petersen CC. 2015. Cell-Type-Specific sensorimotor processing in striatal projection neurons during Goal-Directed behavior. *Neuron* **88**:298–305. DOI: https://doi.org/10.1016/j.neuron.2015.08.039, PMID: 26439527

Steriade M, Contreras D, Curró Dossi R, Nuñez A. 1993. The slow (< 1 hz) oscillation in reticular thalamic and thalamocortical neurons: scenario of sleep rhythm generation in interacting thalamic and neocortical networks. *The Journal of Neuroscience* **13**:3284–3299. PMID: 8340808

Steriade M, Amzica F, Contreras D. 1996. Synchronization of fast (30-40 hz) spontaneous cortical rhythms during brain activation. *The Journal of Neuroscience* **16**:392–417. DOI: https://doi.org/10.1523/JNEUROSCI.16-01-00392.1996, PMID: 8613806

Szydlowski SN, Pollak Dorocic I, Planert H, Carlén M, Meletis K, Silberberg G. 2013. Target selectivity of feedforward inhibition by striatal fast-spiking interneurons. *Journal of Neuroscience* **33**:1678–1683. DOI: https://doi.org/10.1523/JNEUROSCI.3572-12.2013, PMID: 23345240

Tepper JM, Wilson CJ, Koós T. 2008. Feedforward and feedback inhibition in neostriatal GABAergic spiny neurons. *Brain Research Reviews* **58**:272–281. DOI: https://doi.org/10.1016/j.brainresrev.2007.10.008, PMID: 18054796

Thorn CA, Atallah H, Howe M, Graybiel AM. 2010. Differential dynamics of activity changes in dorsolateral and dorsomedial striatal loops during learning. *Neuron* **66**:781–795. DOI: https://doi.org/10.1016/j.neuron.2010.04.036, PMID: 20547134

Timofeev I, Grenier F, Bazhenov M, Sejnowski TJ, Steriade M. 2000. Origin of slow cortical oscillations in deafferented cortical slabs. *Cerebral Cortex* **10**:1185–1199. DOI: https://doi.org/10.1093/cercor/10.12.1185, PMID: 11073868

ur Rehman N, Mandic DP. 2011. Filter bank property of multivariate empirical mode decomposition. *IEEE Transactions on Signal Processing* **59**:2421–2426. DOI: https://doi.org/10.1109/TSP.2011.2106779

Wall NR, De La Parra M, Callaway EM, Kreitzer AC. 2013. Differential innervation of direct- and indirect-pathway striatal projection neurons. *Neuron* **79**:347–360. DOI: https://doi.org/10.1016/j.neuron.2013.05.014, PMID: 23810541

Wilson CJ. 1987. Morphology and synaptic connections of crossed corticostriatal neurons in the rat. *The Journal of Comparative Neurology* **263**:567–580. DOI: https://doi.org/10.1002/cne.902630408, PMID: 2822779

Wilson CJ. 1993. The generation of natural firing patterns in neostriatal neurons. *Progress in Brain Research* **99**:277–297. DOI: https://doi.org/10.1016/s0079-6123(08)61352-7, PMID: 8108553

Wilson CJ, Kawaguchi Y. 1996. The origins of two-state spontaneous membrane potential fluctuations of neostriatal spiny neurons. *The Journal of Neuroscience* **16**:2397–2410. DOI: https://doi.org/10.1523/JNEUROSCI.16-07-02397.1996, PMID: 8601819

Wu Z, Huang NE. 2009. Ensemble empirical mode decomposition: a noise-assisted data analysis method. *Advances in Adaptive Data Analysis* **01**:1–41. DOI: https://doi.org/10.1142/S1793536909000047

Yin HH, Knowlton BJ. 2006. The role of the basal ganglia in habit formation. *Nature Reviews Neuroscience* **7**:464–476. DOI: https://doi.org/10.1038/nrn1919, PMID: 16715055